

Execution and reliability of slip resistant connections for steel structures using CS and SS (SIROCO)

Stranghöner, Natalie; Afzali, Nariman; Jungbluth, Dominik ; Veljkovic, M.; Bijlaard, F.S.K.; Gresnigt, A.M.; de Vries, P.A.; Kolstein, M.H.; Nijgh, M.P.; More Authors

DOI

[10.2777/554114](https://doi.org/10.2777/554114)

Publication date

2019

Document Version

Final published version

Citation (APA)

Stranghöner, N., Afzali, N., Jungbluth, D., Veljkovic, M., Bijlaard, F. S. K., Gresnigt, A. M., de Vries, P. A., Kolstein, M. H., Nijgh, M. P., & More Authors (2019). *Execution and reliability of slip resistant connections for steel structures using CS and SS (SIROCO)*. European Union. <https://doi.org/10.2777/554114>

Important note

To cite this publication, please use the final published version (if applicable).
Please check the document version above.

Copyright

Other than for strictly personal use, it is not permitted to download, forward or distribute the text or part of it, without the consent of the author(s) and/or copyright holder(s), unless the work is under an open content license such as Creative Commons.

Takedown policy

Please contact us and provide details if you believe this document breaches copyrights.
We will remove access to the work immediately and investigate your claim.



European
Commission

Execution and reliability of slip resistant connections for steel structures using CS and SS

(SIROCO)

FINAL REPORT

Execution and reliability of slip resistant connections for steel structures using CS and SS (SIROCO)

European Commission
Directorate-General for Research and Innovation
Directorate D - Industrial Technologies
Unit D.4 — Coal and Steel
Contact Hervé Martin
E-mail RTD-PUBLICATIONS@ec.europa.eu

European Commission
B-1049 Brussels

Manuscript completed in 2019.

This document has been prepared for the European Commission however it reflects the views only of the authors, and the Commission cannot be held responsible for any use which may be made of the information contained therein.

More information on the European Union is available on the internet (<http://europa.eu>).

Luxembourg: Publications Office of the European Union, 2019

PDF

ISBN 978-92-79-98311-5

ISSN 1831-9424

doi: 10.2777/554114

KI-NA-29-527-EN-N

© European Union, 2019.

Reuse is authorised provided the source is acknowledged. The reuse policy of European Commission documents is regulated by Decision 2011/833/EU (OJ L 330, 14.12.2011, p. 39).

For any use or reproduction of photos or other material that is not under the EU copyright, permission must be sought directly from the copyright holders.

All pictures, figures and graphs © Universitaet Duisburg-Essen (UDE), RFSR-CT-2014-00024 SIROCO

European Commission

Research Fund for Coal and Steel

Execution and reliability of slip resistant connections for steel structures using CS and SS (SIROCO)

Natalie Stranghöner, Nariman Afzali, Dominik Jungbluth, Christoph Abraham
Universitaet Duisburg-Essen (UDE), Universitaetsstr. 2, DE-45141 Essen, Germany

Milan Veljkovic, Frans Bijlaard, Nol Gresnigt, Peter de Vries, Henk Kolstein, Martin Nijgh
Technische Universiteit Delft (TUD), Stevinweg 1, NL-2628 CN Delft, Netherlands,

Erik Schedin, Johan Pilhagen, Emma Jakobsen
Outokumpu Stainless AB (OSAB), Avesta Research Centre, PO Box 74, SE-774 22 Avesta, Sweden,

Anders Söderman
BUMAX vAB (BFB), Industrivagen 11, SE-693 73 Svarta, Sweden,

Ralf Glienke, Andreas Ebert
Fraunhofer Gesellschaft zur Foerderung der angewandten Forschung e. V. (FAGP), Hansastr. 27c, DE-80686
München, Germany

Nancy Baddoo, Anqi Chen
The Steel Construction Institute LBG (SCI), Buckhurst Road Silwood Park, GB-SL5 7QN Ascot, United Kingdom,

Petr Hradil, Asko Talja, Juhani Rantala, Pertti Auerkari
Teknologian Tutkimuskeskus VTT Oy (VTT), Tekniikantie 4a, FI-02044 VTT Espoo, Finland,

Jukka Säynäjäkangas, Timo Manninen
Outokumpu Stainless OY (OSOY), Tornion Tehtaat, FI-95400 Tornio, Finland,

Andrea Rudolf, Susanne Berger
Institut für Korrosionsschutz Dresden GmbH (IKS), Gostritzer Straße 65, DE-01217 Dresden, Germany,

Murray Cook, Michael Taylor, Mark Huckshold
European General Galvanizers Association LBG (EGGA), Godstone Road Maybrook House, GB-CR3 6RE Caterham
Surrey, United Kingdom.

Grant Agreement RFSR-CT-2014-00024
01.07.2014 – 30.06.2017

Final report

Directorate-General for Research and Innovation

Table of contents

1	Final summary	5
2	WP 1 – Test procedure slip factor	14
2.1	Objectives.....	14
2.2	Work undertaken.....	14
2.3	Task 1.1 – Preload measurement.....	14
2.4	Task 1.2 – Test speed.....	19
2.5	Task 1.3 – Criteria for the slip load	24
2.6	Task 1.4 – Criteria for creep tests.....	25
2.7	Task 1.5 – Preloading procedures	30
3	WP 2 – Long term effects (CS).....	35
3.1	Objectives of WP.....	35
3.2	Work undertaken.....	35
3.3	Task 2.1 – Different preload levels	36
3.4	Task 2.2 – Plastic vs. elastic preloading	40
3.5	Task 2.3 – Preload in existing structures	45
4	WP 3 – Alternative bolts and preloading methods in slip resistant connections (CS).....	50
4.1	Objectives.....	50
4.2	Work undertaken.....	50
4.3	Task 3.1 – Use of Lockbolts and H360® bolts.....	50
4.4	Task 3.2 – Use of Injection bolts.....	56
4.5	Task 3.3 – Use of Direct Tension Indicators DTI	63
5	WP 4 – Alternative surface treatments and coatings (CS).....	67
5.1	Objectives.....	67
5.2	Work undertaken.....	68
5.3	Task 4.1 – Plain CS	68
5.4	Task 4.2 – Hot dip galvanized CS.....	74
5.5	Task 4.3 – Different application and storage parameters in case of ethyl-silicate-zinc coatings.....	78
6	WP 5 – Preloading of SS bolts	84
6.1	Objectives.....	84
6.2	Work undertaken.....	84
6.3	Task 5.1 – Relaxation of SS plates and washers	84
6.4	Task 5.2 – Relaxation of SS bars and bolts.....	91
6.5	Task 5.3 – Preloading and relaxation behaviour of SS bolt assemblies.....	95
6.6	Task 5.4 – Preloading levels	103
6.7	Task 5.5 – Numerical analysis	108
6.8	Task 5.6 – Preloading methods	112
7	WP 6 – Slip-resistant connections of SS	114
7.1	Objectives.....	114
7.2	Work undertaken.....	114

7.3	Task 6.1 – Surface characterization of SS surfaces	114
7.4	Task 6.2 – Slip factors for SS surface finishes	116
7.5	Task 6.3 – Slip factors for new types of coatings on SS.....	121
7.6	Task 6.4 – Numerical study.....	124
7.7	Task 6.5 – Design rules for slip-resistant connections	129
7.8	Task 6.6 – Design examples.....	132
8	WP 7 – Guidelines and exploitation activities.....	132
8.1	Objectives.....	132
8.2	Work undertaken.....	133
8.3	Task 7.1 – Guidelines for carbon steel	133
8.4	Task 7.2 – Guidelines for stainless steel	135
8.5	Task 7.3 – Dissemination.....	136
8.6	Task 7.4 – Contribution to standardization	136
9	List of figures.....	137
10	List of tables.....	141
11	List of acronyms.....	143
12	List of references	147
	Appendix A – Design Example.....	149

1 Final summary

Objectives

Bolted preloaded slip-resistant connections are traditionally used in steel structures when slip and/or deformation have to be highly restricted and in cases where the structure is subjected to variable loading which may lead to fatigue damage. Main application fields are e.g. bridges, cranes, radio masts and tubular towers as well as truss girders for wind turbines.

The slip resistance of these connections is mainly influenced by the friction of the contact surfaces, the level of preload in the bolts and imperfections of the structural plates clamped together. The procedures to determine the slip resistance as described in EN 1993-1-8 "Design of Joints" and EN 1090-2 "Execution of steel structures and aluminium structures - Part 2 Technical requirements for steel structures" are not very clear for use in practice and urgently need improvement and clarification. The aim of SIROCO was to clarify these open questions.

Furthermore, alternative modern types of fasteners in slip-resistant connections are lock bolts, H360 bolts and injection bolts. Direct tension indicators (DTI) are promising means to assure the correct preload during tightening. For this reason, these alternative bolts and methods were considered in SIROCO as well. To determine the characteristics of the injection resin for injection bolts, similar procedures need to be followed as for determining the slip factor. It is questionable whether this is adequate for non-preloaded and preloaded injection bolts.

The friction of surfaces in slip-resistant connections is described by the slip factor μ which is given for carbon steel for some surface treatments in the execution standard for steel structures, EN 1090-2. For surface treatments which are not explicitly cited in EN 1090-2, e.g. hot-dip galvanized carbon steel plates and modern coating systems, a slip factor test is required, which is standardized in Annex G of EN 1090-2.

These existing rules are valid for carbon steel only and so comprehensive investigations were conducted on the preloading behaviour and slip resistance behaviour of preloaded bolted connections made of austenitic, duplex, lean duplex and super duplex stainless steel.

Herewith, the main technical objectives of the project were:

- to improve the cost effectiveness of slip-resistant connections made of carbon steel by considering innovative bolts and preloading methods as well as innovative coating systems and fill important gaps in understanding regarding galvanized steel connections and
- to generate new information on stainless steel connections with regard to preloading of stainless steel bolts and to the execution of slip-resistant connections made of stainless steel.

The overall study included the exploitation of design solutions targeting

- an improved test procedure for measuring the slip factor,
- innovative preloading methods and coating systems for carbon and stainless steel surfaces to increase the surface roughness,
- development of design and execution rules for preloading of stainless steel bolts and slip-resistant connections made of stainless steel.

WP 1 - Development and concretization of the test procedure of Annex G of EN 1090-2 for the determination of the slip factor

WP 1 had the main objective to improve the test procedure for the determination of slip factors, hence solving the problems caused by the lack of undefined or unclear defined rules given in the test procedure of Annex G of EN 1090-2.

In Task 1.1 a comparative study regarding the accuracy of different methods for measuring the preload in the bolts with implanted strain gauges and load cells was carried out. Both types of preload measurements can be considered as sufficiently accurate methods of measurement. However, using load cells leads to a larger clamping length of the bolts, which influences the loss of preload and, consequently, the level of the slip load.

Next to the measurement of the preload, the position of slip measurement plays an important role for the determination of the slip factor. Care has to be taken, that the slip is measured in the centre of the bolt group. Measuring the slip at the plate edges instead of the centre of the bolts might lead to much lower slip factors as the elongation of the plates is measured as well so that increased slip deformations result. The assembled test specimen shows different slip planes. The slip can be distinguished in two failure modes, which may occur from a combination of failure of these slip planes.

The presented study also demonstrates that the highest initial and actual slip factors were achieved for grit blasted (GB) and thermally aluminium sprayed (Al-SM) surface conditions, respectively.

In Task 1.2 the influence of the test speed on the results for static slip factors was investigated. The results of Task 1.2 clarify aspects of the determination of the slip factor as described in EN 1090-2. No influence of the test duration on the scatter in the results of the short term slip factor tests and no effect of the loading speed on the results of the determination of the sensitivity to creep were found. The results will mainly be of practical use as background information for users of this standard. Ambiguous formulations regarding the requirements to the test duration can be removed from future editions of EN 1090-2.

For Task 1.3, the main objective was the comparison of the different slip load – displacement behaviours of slip-resistant connections with different coating systems for the faying surfaces. Therefore, tests from Task 1.1 were evaluated together with additional tests carried out in this WP. The background is that the individual slip load for a slip-resistant connection, F_{Si} , is defined in EN 1090-2 as the load at a slip of $\delta = 0.15$ mm. This fixed criterion has to be questioned. Different surfaces (e.g. surfaces as rolled, blasted and spray-metallized or hot-dip galvanized surfaces) show different slip load - displacement behaviours. To improve the cost effectiveness of slip-resistant connections, different coating systems were investigated in accordance with the procedure prescribed in the Annex G of EN 1090-2. During the test campaign, some questions arose: Is the given criterion for the slip load F_{Si} applicable and logical? Are there differences in the slip load - displacement behaviour of varying coating systems? The evaluation of the test results show that there are differences in the coating systems and this needs to be considered for the test procedure of EN 1090-2. The slip load is significantly underestimated by considering a determination point at 0.15 mm for evaluating the critical slip load. For this reason, the slip load criterion was extended to three criterions I, II and III, which are explained in detail. The results are linked to Task 1.4 in which the long-term stability of the coating systems for the faying surfaces was tested (test duration more than one year). The results are described in detail in chapter 5.5 and 5.6.

In Task 1.5, a preloading procedure to achieve a reduced preload level on the basis of the 0.2 % remaining strain level should be developed. Existing preloading procedures (torque and combined method) were tested with the aim of specifying specific parameters (lubrication, tightening steps etc.) in order to be able to achieve guaranteed preload levels in the elastic range with sufficient reliability. Thus, tightening tests acc. to EN ISO 16047 resp. EN 14399-2 were performed for HV and HR bolts, property classes 10.9 and 8.8 of two bolt dimensions each: M24 and M36. Various lubrication types were tested: factory provided lubrication, Fuchs Lubritech Gleitmo WSP 5040, DOW Corning Molykote 1000 spray and Microgleit HV-paste LP440.

Considering an evaluation of the test results acc. to EN 14399-3 (System HR) and EN 14399-4 (System HV), a comparison between the various lubrications led to the following conclusions: In terms of HV bolting assemblies, the best results were achieved with Gleitmo WSP 5040 and Molykote 1000 spray. The k -values at $F_{p,C}$ stand out due to low scatter (0.12–0.16) and low coefficients of variation V_k . In terms of HR bolting assemblies, a distinction must be made between bolt dimension M24 and M36:

- For bolt dimension M24, every tested lubrication showed satisfactory test results, in addition to the factory provided bolting assemblies. K-class K1 and K2 are accomplished in each tested series with low coefficients of variation V_k (2.9–5.8%).
- For bolt dimension M36, k-class K2 failed in each tested series, while k-class K1 and other criteria acc. to EN 14399-3 were only partially fulfilled. In this context, better tightening test results were achieved by using Molykote 1000 spray lubrication.

When using the modified torque method according to the German Technical Annex DIN EN 1993-1-8/NA, it could be shown that $F_{p,C}^*$ is achieved mainly for M24x100 HR bolting assemblies in property classes 8.8 and 10.9. However, the required preloading level $F_{p,C}^*$ for M36x160 HR bolting assemblies in property classes 8.8 and 10.9 are only partially achieved when using Gleitmo WSP 5040 and Molykote 1000 spray lubricants, while the tested series with factory provided and Microgleit HV-paste LP440 failed completely. The modified torque method also shows inhomogeneous test results for HV bolting assemblies. The reduced preload $F_{p,C}^*$ is also only partially achieved.

The application of the modified combined method is only valid for bolting assemblies in property class 10.9. All tested series of M24x100 HR 10.9 and M24x100 HV 10.9 HV achieved the required preload $F_{p,C}^*$. Again, the required preloading level $F_{p,C}^*$ for M36x160 HR 10.9 and M36x160 HV 10.9 bolting assemblies were only partially achieved or failed completely. The best results were achieved when using Gleitmo WSP 5040 and Molykote 1000 spray lubricants.

Further evaluations should be performed for each tested series and lubricants to determine the required tightening torques and additional angle of rotations, depending on the chosen modified tightening method. Also limiting criteria must be defined to control the achieved level of preload and to avoid plastic deformations when re-use of the bolting assemblies is intended.

WP 2 - Slip factors depending on the level of preloading considering long term effects

In WP 2 slip factors depending on the preload level under consideration of long term effects were determined. The aim was to obtain sufficient theoretical and experimental evidence to improve and extend the existing rules in EN 1993-1-8 and EN 1090-2 with respect to different preload levels.

In Task 2.1 a comparative study on the influence of different levels of preload on the reliability of slip-resistant connections was carried out. For this reason, slip factor tests were carried out to investigate the influence of the bolt type (HR vs HV) and the property class (HR8.8 vs HR10.9) on the slip factor of zinc spray metallized and ASI-ZN coated surfaces. From these investigations it could be summarized that the type of the bolt (HR / HV) has no influence on the slip factor. Furthermore, the lower preload of the HR8.8 bolts results in 5 % to 15 % higher slip factors. No general conclusions can be drawn on the magnitude of the influence as this depends on the properties of the coating (system and coating thickness). The initiative was taken to investigate the potential of an experimental procedure to estimate the maximum load level for extended creep tests. For this, an approach was developed in the frame of the so-called "Step test" for estimating the load level for an extended creep test so that this passed.

Since EN 1090-2 requires a preload level, which leads to plastic deformations in the mating threads, a comparative study on the influence of preloading the bolts in the plastic range vs. preloading the bolts in the elastic range was performed in Task 2.2. The slip resistance behaviour is influenced by two main parameters: the condition of the faying surfaces and the preload level of the bolts. In Task 1.1 and 1.4, the influence of different surface conditions was investigated. All tests performed in these Tasks were preloaded to $F_{p,C}$. In Task 2.2 two smaller preload levels ($F_{p,C}^*$ and $0.9 F_{p,C}^*$) were selected in order to investigate the influence of the preload level especially on the long-term behaviour of slip resistant connections. The results show that the actual and initial static slip factor increases slightly with decreasing preload level. Only for ASI-coated surfaces, the initial static slip factor remains approximately the same but the actual static slip factor increases by decreasing preload level. By comparing the actual static slip factors μ_{act} with those calculated with the initial preload μ_{ini} and the final slip factor μ_{ect} , it can be seen that this behaviour can also be observed for the final slip factors including the extended creep tests.

In Task 2.3 a procedure to determine the preload of bolts in slip-resistant connections of existing structures was developed. The feasibility of using the strain gauge method in practice was tested in the laboratory as well as in-situ in a Dutch highway bridge (Middachterbrug) to assess the minimum required pretension force in the bolts (see Task 2.3). Statistical evaluation showed that the scatter of the calibration factors of the bolts is sufficiently small and a mean value correction is possible, which simplifies the use of the proposed method for in-situ preload force assessment. Deviations of the mechanical and geometrical properties of bolt sets are implicitly included in the statistical model. A predicted bolt force F_{pred} [kN] for M24 bolts can be calculated by a formula based on the measured in-

situ strain ϵ_{meas} [$\mu\text{m}/\text{m}$] $\cdot F_{\text{pred}} = 0,082 \cdot \epsilon_{\text{meas}}$ [kN]. If $F_{\text{pred}} > F_{\text{p,C}}$, the actual bolt preload force is in line with 95 % confidence. Finite element analysis indicated that the proper position of the strain gauge is at 0.65 d or more from both the bolt head-shank and thread-shank transition. Directly after the successful application of the method on the Middachterbrug, several bridge owners showed interest in the developed method. However, up to now no actual follow up applications are known to the authors.

WP 3 - Use of alternative bolts and preloading methods in slip-resistant connections

In WP 3 the usage of alternative bolts and preloading methods in slip-resistant connections was investigated to study whether alternative bolts or preloading methods other than HV or HR bolts can be used in slip-resistant connections with sufficient reliability. In this work package the investigation of alternative bolts or preloading methods as Lockbolts, H360® system of Alcoa Fastening Systems, injection bolts and Direct Tension Indicators (DTI) was carried out. The main focus of this WP was the determination/consideration of the loss of preload in order to examine the suitability of these bolting assemblies in slip-resistant connections over their life time.

Task 3.1 compared alternative high-strength bolting systems for preloading - Lockbolts and H360® - and their use in slip-resistant connections. The measured and analysed initial preload levels of Lockbolts and H360® are in the same range as the well-known HV-bolts. Both, HV-bolts and H360®, show nearly the same tightening factor α_A (relation of max to min preload) and the same coefficient of variation V_x . The torque method was chosen as the tightening procedure for these bolts. Due to the tensioning process of the installation procedure, Lockbolts showed less deviation (3.1 %). In contrast to HV bolts, re-tightening of Lockbolts is not possible, but in terms of compliant design and installation procedure also not necessary. Therefore, the losses of preload due to setting effects, under external fatigue loading and sustained load action on the connection have to be taken into account. Nevertheless, Lockbolts and H360® are preloadable and can be used in slip-resistant connections. For H360® it is necessary to keep in mind that the bolt head has to be held during the tightening and re-tightening processes.

One of two focus areas of Task 3.2 was to investigate non-preloaded injected bolts using various resin types. Short-term duration tests and long term duration tests were performed to validate various mechanical properties of the resins covering the following variables: curing temperature, overload behaviour, creep behaviour, effects of slotted holes, size effect of the bolt diameter, longer bolts (ratio length vs diameter of the bolts larger than 3). Based on this investigation, the ranking of possible resins was established and the most suitable resin type was determined as RenGel SW404/HY2404. As a "bi-product" of the research, a concept of reinforced resin consisting of an optimal mixture of steel shots (steel particles remained after blasting structural steel elements) was developed and patented.

In Task 3.3 the use of Direct Tension Indicators (DTI) was investigated. The results of the Task 3.3 show that the influence of the position of DTIs on the preload losses is negligible. It could also be seen that the loss of preload for M20 bolting assemblies with DTIs was relatively higher compared to M16 bolting assemblies. The extrapolated loss of preload at a service life of 50 years indicates that the highest loss of preload was achieved for M20 bolting assemblies with DTIs and clamping length ratio of 1.6 (about 16 %). For M16 bolting assemblies with DTIs and clamping length ratio of 1.7 this value was about 10 %. The loss of preload for M20/M16 bolting assemblies without any DTIs was about 8.5 %. This phenomenon can be ascribed to a high concentration of stress on a small area of protrusions which results in more embedment in this area during time and consequently to higher loss of preload in these bolting assemblies.

WP 4 - Use of alternative surface treatments and new coating systems in slip-resistant connections

In WP 4 the use of alternative surface treatments and coating systems in slip-resistant connections was investigated. The main objective was the investigation of the influence of various surface parameters on the slip factor of carbon steel and hot-dip galvanized applications.

In Task 4.1 the influence of the surface preparation and type of coating system on the slip factor and corrosion protection of carbon steel was investigated. Coatings based on an inorganic binder with zinc dust have significantly higher slip factors than binders with an organic basis. Spherical blast-cleaning

materials tend to have lower slip factors. An influence of single-use or multiple-use blast-cleaning materials on the slip factor as well as an influence of the surface preparation grade on the slip factor could not be detected.

Regarding their corrosion protection values, the systems show differences. The corrosion on the artificial damage is, in general, lowest for systems with the highest roughness ($> 100 \mu\text{m}$). The systems with blast-cleaned surface using spherical blast-cleaning material as well as the system based on epoxy resin, which was blast-cleaned using slag, show weak spots with respect to the pull-off strength (cohesion failures between substrate and priming coat, in connection with low pull-off values).

In Task 4.2 the influence of the surface preparation and type of coating system on the slip factor and on the corrosion protection in case of hot dip galvanized steel was investigated. A hot dip galvanized (HDG) coating will typically comprise a series of Fe-Zn alloy layers covered with an outer layer of zinc. This typical coating structure will produce relatively low static slip factors (0.12- 0.14). The Fe-Zn alloy layers are harder than the outer zinc layer and are often harder than the steel substrate. The results show that higher static slip factors (in the range 0.35- 0.40) for galvanized coatings will be achieved when the outer zinc layer is sufficiently removed by a light blasting procedure (sweep blasting), so that the Fe-Zn layers will control the slip behaviour. The additionally required blasting depends on the proportion of outer zinc layer within the original coating. Sweep blasting of a hot dip galvanized coating combined with the application of an alkali-zinc silicate (ASI) paint produces the highest static slip factors observed in these tests ($\mu_{\text{ini,mean}} = 0.62$). For all test series, the creep tests failed for both the upper and lower part of the specimens, so that it is necessary to perform extended creep tests in order to determine the final slip factor. However, the available extended creep test results for the HDG-ASI and HDG-ESI coated surfaces do not allow a conclusion to be drawn regarding the final slip factor for these test series.

In the frame of relaxation tests, the influence of different post treatments on the relaxation behaviour of HDG-coated surfaces was investigated. Additionally, the influence of different preload levels for the test series HDG-ESI was investigated. The extrapolated loss of preload at a service life of 50 years shows, that the highest loss of preload was achieved for the HDG-ASI test series (between 17.3 % to 23 %). It could also be shown, that the minimum loss of preload for coated surfaces was observed for HDG-SB-I (sweep blasted surface) and HDG-ref (without any post treatment). Performing the relaxation tests with different preload levels for test series HDG-ESI shows that with higher preload level the absolute preload losses are higher. However, the preload losses as a percentage of the initial preload will be higher for preloaded bolts with lower preload level.

In Task 4.3 ethyl-silicate-zinc (ESI) was tested due to the use in slip-resistant connections. The conditioning of the samples after application, especially the temperature and relative humidity, may have an effect on the slip factor and the corrosion protection. The conditions during storage were as well part of the investigations. These influences were investigated with respect to the slip factor and the corrosion protection.

Regarding their corrosion protection values, the systems show no differences with the exception of the failure pattern. The failure pattern is the weakest part of the coating system. System A (ethyl silicate (ESI) coating, new batch) shows cohesion failures in the 1st and 2nd layer and system B (ethyl silicate (ESI) stored for 12 month) shows mainly cohesion failures in the 4th layer. An influence of storage stability on the corrosion protection values could not be detected.

A final conclusion is that there is no influence on the slip factor due to the different conditioning times and storage times. The final slip factor for series A and B was evaluated from the results of the extended creep tests with $\mu = 0.42$. The loads for those tests were determined by the newly developed step test.

WP 5 - Preloading of stainless steel bolts

WP 5 dealt with the preloading of stainless steel bolting assemblies. The main objectives were to provide preloading levels and preloading methods for stainless steel connections taking into account the effect of material relaxation.

The Tasks 5.1, 5.2 and 5.5 dealt with the collection of material data on strength and relaxation behaviour of stainless steel plates, the determination of full stress-strain and stress-decay curves for at least the basic material as well as numerical analysis of preloaded stainless steel bolted connections. Room temperature creep deformation under uniaxial constant load conditions was observed for the investigated stainless steels (austenitic, ferritic, lean duplex and duplex). The amount of creep deformation increased with increasing load level and also with increasing initial loading rates. Consequently, the amount of creep deformation in preloaded stainless connections depends on the level of stress in the plates due to preloading of the bolts. For the level of preload used in this project, the susceptibility for creep deformation were (from highest to lowest): the austenitic grade, the ferritic grade, the lean duplex grade and the duplex grade. However, comparison with results from instrumented preloaded stainless steel connections, see Task 5.3, resulted in the conclusion that creep deformation in the ferritic and duplex connections was not significant with respect to the measured loss of preload. A higher loss of preload was observed for the austenitic connection which was attributed to the higher susceptibility for creep deformation at this level of preload. In general, the results indicate that the loss of preload in a preloaded stainless steel connection is mainly caused by the stress relaxation in the bolts and not by the creep deformation of the plates.

The viscoplastic deformation behaviour of the investigated stainless steels can be described by a state of the art viscoplastic constitutive law, known as the Chaboche model. The material parameters of this model were determined based on the tests carried out in Task 5.1. This model was successfully used in the finite element modeling of preloaded stainless steel connections in Tasks 5.5 and 6.4.

Room temperature stress relaxation testing was performed on stainless steel. The aim of the testing was to investigate the stress relaxation behaviour of stainless steel bolts in preloaded connections. Bars were chosen over actual bolts due to practical limitations such as availability and ease of testing. The conclusions were that the two tested duplex grades in the “annealed” state (soft and workable state) experienced less stress relaxation compared to the tested austenitic grade in the “annealed” state. Cold drawn bars experienced less stress relaxation compared to bars in the “annealed” state. The cold drawn austenitic bar showed less stress relaxation compared to the cold drawn duplex bars. Applying the test results of the bars to preloaded bolt connections, the result indicates that machined bolts are likely to have higher stress relaxation compared to cold forged bolts and that most of the stress relaxation in preloaded bolts occurs within the first hour after preloading.

As a result of Task 5.5, a plug-in for ABAQUS/CAE was developed that is able to generate and solve 2D and 3D finite element models of bolting assemblies from stainless and carbon steel including the viscoplastic behaviour during their service life. Stainless steel material properties used in the plug-in were calibrated and validated against the tensile, creep and relaxation tests from Tasks 5.1 and 5.2. Several observations were noted during the testing of model's performance: The final preload after 50 years of service life is very close to the asymptotic stress state of the viscoplastic material. Its loss compared to the initial tightening level depends strongly on the speed of preloading, but can be improved by re-tightening. Generally, slower preloading speed and longer periods before re-tightening are more beneficial.

In Task 5.3 and 5.4 tightening tests of stainless steel austenitic and austenitic-ferritic bolting assemblies (lean duplex, duplex and super duplex) were performed and accomplished according to EN 14399-2 and EN ISO 16047. In the absence of existing adequate criteria for preloaded stainless steel bolting assemblies, the evaluation of the tightening tests was referred to EN 14399-3 and, for reasons of comparability, follows the requirements and criteria of the HR system. Stainless steel bolts according to EN ISO 4014 and EN ISO 4017 were examined using Fuchs Lubritech gleitmo 1952V standard lubrication. In total, 12 series and 125 (required 80) bolting assemblies were tested and evaluated.

As a continuation of the work undertaken in Task 5.3, tightening tests of stainless steel bolts according to EN ISO 4014 and EN ISO 4017 with various lubricants as Dow Corning Molykote P-74 paste, Dow

Corning Molykote 1000 paste, Dow Corning Molykote 1000 spray and Dow Corning Molykote D-321 spray were performed to identify a suitable, alternative lubrication for stainless steel bolting assemblies. These lubrication tests identified Dow Corning Molykote 1000 spray as an alternative lubricant for Fuchs Lubritech gleitmo 1952V standard lubrication and Dow Corning Molykote D-321R spray as a promising alternative under difficult friction conditions. Additionally, tightening tests were performed with M20 EN ISO 4017 bolts with the ceramic-based lubricant Interflon HT1200 spray and paste for austenitic (property classes 8.8 and 10.9) and lean duplex (property class 10.9) bolting assemblies.

Finally, it can be summarized that preloading of austenitic and lean duplex, duplex and super duplex stainless steel bolting assemblies in property classes 8.8 and 10.9 up to specified preload levels $F_{p,C}^*$ and $F_{p,C}$ is in principle possible by choosing a suitable material pairing and lubrication. It seems, as if a preload level of $F_{p,C}^*$ can be reliably achieved with a suitable lubricant using the torque method. Although the torque method is not the best tightening method in form of reliability, it is the most common tightening procedure in daily practice of erection of steel structures. In future work, parameters for reliable tightening of stainless steel bolting assemblies using bolts acc. to EN ISO 4014/4017 should be determined for all bolt dimensions from a range of bolt suppliers.

Regarding the investigated relaxation behaviour, it can be summarized that the loss of preload is mainly due to the embedment/plastic deformation of the clamped component surfaces and stress relaxation of the bolts. The influence of creep and stress relaxation in the plate material on the loss of preload seems to be negligible as already mentioned. The overall loss of preload extrapolated to 50 years in bolted connections is in agreement with the asymptotic stress relaxation by the Hart's model found from stress relaxation testing of cold drawn bar.

The loss of preload in preloaded stainless steel bolted connections with different grades of bolts and plates is similar to preloaded carbon steel bolted connections. This shows that previous concerns about the loss of preload due to relaxation and creep seem to be unfounded.

In Task 5.6 recommendations for preloading methods for stainless steel bolts were formulated. In principle, the preloading of austenitic and lean duplex, duplex and super duplex stainless steel bolting assemblies, property classes 8.8 and 10.9 is possible by choosing a suitable material pairing and lubrication. The higher surface pressures of the EN ISO 4014/4017 systems, resulting from smaller geometrical dimensions than the HR/HV systems, are not critical up to the preload level $F_{p,C}$ when steel is used with a yield strength/0,2% proof stress larger than or equal to 355 N/mm².

Regarding the preloading levels and design specifications, it is important to note that the tightening procedure and the required preload level are well-matched. For this reason, the suitability test for preloading according to EN 14399-2 must be carried out to check if the bolting assemblies made of stainless steel are in principle suitable for preloading. Subsequently, the boundary conditions regarding the required preload level and tightening procedure as well as the tightening parameters have to be defined in each specific case, so that the test of suitability for preloading for the determination of all functional characteristics and parameters of stainless steel bolting assemblies can be successfully carried out. In addition, the inspection requirements have to be defined depending on the required target level of preloading and the individual and specific boundary conditions.

WP 6 - Slip-resistant connections made of stainless steel plates and bolts

The main objective of WP 6 was to provide design parameters (slip factors) of preloaded slip-resistant connections made of stainless steel under consideration of various surface preparations and/or coatings of the clamped plates.

The work in Task 6.1 focussed on the surface characterization of the faying surfaces in the bolted joint, rather than on the as-prepared surfaces. The result of the investigation is that a potential explanation for the differences in slip factors between various surface preparations are differences in cold welding at surface asperities.

Task 6.2 and 6.3 dealt with the determination of slip factors for typical stainless steel surface finishes as well as for new types of coatings. The behaviour of preloaded bolted assemblies made of stainless steel components was thought to be influenced by creep and relaxation more than carbon steels to

such an extent that preload losses resulting from the time-dependant behaviour would have a negative influence on the long term slip resistance and would consequently lead to reduced slip factors in comparison to those used for slip-resistant connections made of carbon steel. However, the results show that the preload losses during slip factor tests caused by viscoplastic deformation of the stainless steel material are not significantly higher than those found for preloaded bolted connections made of carbon steel components.

Grit blasting of stainless steel surfaces results in a very high surface roughness and high slip factors. For the investigated austenitic, duplex, lean duplex and ferritic stainless steel plates, slip factors of about 0.5 and higher could be achieved. The results show that the slip factors for different grades of stainless steel with Al-SM-coating with Bumax 109 and Bumax 88 bolts were greater than 0.6 and 0.7 respectively. Stainless steel plates with untreated (1D) or shot blasted surfaces lead to comparable low slip factors of about 0.16 - 0.28, which might still be enough in some practical applications.

Unlike for carbon steels, uncoated slip-resistant connections made of stainless steel plates show higher slip factors with increasing preload levels. On the other hand, increasing the preload level in Al-SM-stainless steel slip-resistant connections leads to increased slip loads but slightly decreased slip factors, comparable to the behaviour of coated carbon steel slip-resistant connections.

In Task 6.4 FE models of stainless steel slip-resistant connections have been calibrated and validated against slip factor tests. Evaluation of long term behaviour of the FE models were also carried out by comparing with bolt preload relaxation tests and extended creep tests. The validation study illustrated that the numerical models can accurately predict the viscoplastic behaviour of stainless steel slip resistant connections. A parametric study was carried out using the validated numerical models to extrapolate the test results. Stainless steel slip-resistant connections of different geometries, surface finishes (in terms of friction) and preloading levels were investigated. The results suggest that stainless steel bolting assemblies can be used for preloading as the loss of preload after 50 years are around 10% or less.

The Tasks 6.5 and 6.6 dealt with the development of design rules preparation of design examples. Design rules have been proposed for stainless steel slip resistant connections and classification of surface and slip factors determined by tests in SIROCO are provided. Two design examples are provided to illustrate how to design stainless steel slip resistant connections.

WP 7 – Exploitation activities

WP 7 covered the exploitation activities like the development of guidelines on the design and execution of slip-resistant connections made of carbon (Task 7.1) and stainless (Task 7.2) stainless steel, preparation of peer-reviewed papers at conferences and journals (Task 7.3) and contributions to standardization and regulation process (Task 7.4).

Guidelines were prepared on the design and execution of slip-resistant connections made of carbon steel. An improved slip factor test procedure is presented in detail. The design rules and slip factors were proposed and determined. An improved slip factor test procedure is recommended.

Guidelines are given on the design and execution of slip-resistant connections made of stainless steel. It is recommended that a bolt tightening qualification procedure has to be carried out for each bolting assembly to ensure the suitability for preloading, to determine the tightening parameters and confirm the reliability of the tightening method to achieve the design preload. Load cells should be used to monitor bolt preload during the slip factor test; strain gauges should be avoided.

In total 20 peer-reviewed papers have been published in journals (14 papers) and conferences (9 papers). The November-2017-issue of the journal *Steel Construction* was dedicated to SIROCO publishing in total 8 papers presenting results from SIROCO.

Amendments to EN 1993-1-4, EN 1993-1-8 and EN 1090-2 are proposed based on the results of SIROCO. The improved slip factor test procedure is recommended. Enhanced slip factors are proposed for coated carbon steel slip-resistant connections. The design rules are recommended enabling stainless steel bolts to be used in structural applications. Furthermore, amendments were proposed to Clause 2.2.2 of EN 1993-1-4 and EN 1090-2 to allow stainless steel bolts to be used in slip-resistant connections.

Conclusions

The SIROCO project has generated a comprehensive portfolio of important results which contribute to a much better understanding of slip-resistant connections and the determination of reliable slip-factors to be used in the design of steel structures. Specific improvements to the European slip factor test procedure were developed and are already partly implemented in the current revision of EN 1090-2. The other improvements may be included in a future revision to the standard.

For the first time, thorough investigations into the viscoplastic deformation and tightening behaviour of preloaded stainless steel bolting assemblies have been carried out which demonstrate that preloaded bolted connections can be used successfully in stainless steel structures which are necessary in corrosive environmental conditions as e. g. in bridges, offshore platforms, as well as special highly aesthetic architectural structures, e. g. in textile architecture (membrane structures).

2 WP 1 – Test procedure slip factor

2.1 Objectives

The main objectives of this WP are as following:

- to achieve an improved test procedure for the determination of slip factors and
- to close the lack of undefined or unclear defined rules given in the test procedure of Annex G of EN 1090-2.

In this Work Package also regulations in other countries such as USA and Japan were taken into account as well as experiences from our colleagues in those countries. Furthermore, of course, background information to the existing tightening methods and other data from literature were part of the research.

2.2 Work undertaken

The tasks undertaken in WP 1:

- 1.1. Comparative study regarding the accuracy of different methods for measuring the preload in the bolts in the slip factor tests.
- 1.2. Influence of the test speed for static tests for the slip factor tests.
- 1.3. Definition of new criteria for the determination of the slip load F_{Si} .
- 1.4. Definition of new criteria for a successful creep test and for the evaluation of the extended creep test.
- 1.5. Development of preloading procedures to achieve a reduced preload level on the basis of the 0,2% remaining strain level.

The work undertaken for Tasks 1.1 to 1.5 is summarized in Sections 5.3 - 5.7.

Exploitation of the research results of this WP

The research results of this WP were published in five journal and conference papers: (3), (12) to (15), see Chapter 2, Publications. Furthermore, they have already been partly implemented in EN 1090-2.

2.3 Task 1.1 – Preload measurement

The focus of this task was on investigating the various test parameters such as type of preload measurement, ascertaining the possible slip planes, position of slip measurement and clamping length. The results achieved in these investigations have already been partly implemented in the revision of the current draft version of EN 1090-2. Within the scope of this task, the investigations into the slip factor test procedure were carried out using the standard test specimen geometry, M20, according to EN 1090-2, Annex G [5.3-1], with HV M20 bolting assemblies according to EN 14399-4 [5.3-2] and EN 14399-6 [5.3-3]. Six surface conditions were considered, see Table 2.3-1: (1) grit-blasted (GB), (2) alkali-zinc silicate (ASI-Zn)-coating, (3) hot dip galvanized (HDG), (4) spray metallized with aluminium (SM-Al), (5) spray metallized with zinc (SM-Zn) and (6) a combination of alkali-zinc silicate and zinc spray metalized coating (ASI - Zn-SM). The test specimens were made of S355J2C+N, for each plate thickness from one batch. Three different kinds of methods for measuring the preload in the bolts and one further method in a preliminary study have been investigated: Instrumented bolts with implanted strain gauges without any adapter (SG), instrumented bolts with implanted strain gauges with a small adapter (SG + adapter), especially produced load cells (LC) and small load cells (preliminary study).

Different combinations of instrumented bolts with small adapters (with/without) and load cells resulting in three different clamping lengths have been considered in order to investigate the influence of the extension of the clamping length by the load cell and the small adapter on the determined slip factor. Figure 2.3-1 shows the bolts which have been prepared with implanted strain gauges at the University of Duisburg-Essen (UDE). For each test specimen four HV bolts M20, class 10.9 were instrumented with a strain gauge embedded in a 2 mm hole along the bolt shank. The bolts have been prepared in four different nominal lengths 75 mm, 80 mm, 110 mm and 180 mm for testing without any adapter,

with a small adapter and combined with the load cells produced by the Delft University of Technology (TUD).

Table 2.3-1: Test programme of Task 1.1, mean slip factors based on static and creep tests only ($\mu_{ini,mean}$ and $\mu_{act,mean}$) with LVDTs 1–8 (CBG position)

Series ID	Surface preparation		$\Sigma t^{(4)}$ [mm]	Bolt size (Md x l) ⁽⁵⁾ [mm]	Preload [kN]	Number of tests st/ct/ect ⁽⁶⁾	$\mu_{ini,mean}^{(7)}$ st/st+ct [-]	$\mu_{act,mean}^{(8)}$ st/st+ct [-]	V (μ_{act}) ⁽⁹⁾ st/st+ct [%]
	Sa ⁽¹⁾ / Rz ⁽²⁾ [μ m]	DFT ⁽³⁾ [μ m]							
Grit blasted surfaces (GB)									
GB-I	-	-	152	M20 x 180	$F_{p,c}/172$	4/1/-	0.80/0.79	0.87/0.86	1.9/3.0
GB-II	Sa 2½ / 80	-	83	M20 x 110	$F_{p,c}/172$	2/-/-	0.74/-	0.83/-	2.0/-
GB-III	-	-	52	M20 x 80	$F_{p,c}/172$	2/-/-	0.74/-	0.86/-	5.0/-
Alkali-zinc silicate coating (ASI)									
ASI-I	-	-	152	M20 x 180	$F_{p,c}/172$	4/1/-	0.73/0.73	0.76/0.77	0.9/2.2
ASI-II	Sa 2½ / 80	60	83	M20 x 110	$F_{p,c}/172$	2/-/-	0.72/-	0.78/-	3.5/-
ASI-III	-	-	52	M20 x 80	$F_{p,c}/172$	2/-/-	0.70/-	0.77/-	2.9/-
Hot-dip galvanized surface (HDG)									
HDG-I	-	105	152	M20 x 180	$F_{p,c}/172$	4/1/-	0.47/0.46	0.48/0.47	9.2/9.5
HDG-II	-	105	48	M20 x 75	$F_{p,c}/172$	2/-/-	0.47/-	0.51/-	14.6/-
HDG-III	-	80	48	M20 x 75	$F_{p,c}/172$	4/-/-	0.12/-	0.12/-	6.6/-
Aluminium spray metalized coating (Al-SM)									
Al-SM-I	-	-	83	M20 x 110	$F_{p,c}/172$	2/-/-	0.74/-	0.89/-	4.5/-
Al-SM-II	-	250	52	M20 x 80	$F_{p,c}/172$	4/1/-	0.73/0.73	0.93/0.92	2.7/3.9
Zinc spray metalized coating (Zn-SM)									
Zn-SM-I	Sa 3 / 100	140	83	M20 x 110	$F_{p,c}/172$	4/-/1	0.75/0.72	0.82/0.79	2.9/7.8
Zn-SM-II	-	-	52	M20 x 80	$F_{p,c}/172$	2/-/-	0.73/-	0.82/-	2.7/-
Combination of alkali-zinc silicate and zinc spray metalized coating									
ASI – Zn-SM-I	Sa 2½/100 – Sa 3/100	55 – 170	48	M20 x 75	$F_{p,c}/172$	4/1/2	0.63/0.62	0.71/0.70	3.9/5.5

¹⁾ Sa: surface preparation grade | ²⁾ Rz: roughness | ³⁾ DFT: dry film thickness (Coating thickness) | ⁴⁾ Σt : clamping length | ⁵⁾ d: bolt diameter, l: bolt length | ⁶⁾ st: static test/ct: creep-/ect: extended creep test | ⁷⁾ $\mu_{ini,mean}$: calculated slip factors as mean values considering the initial preload when the tests started | ⁸⁾ $\mu_{act,mean}$: calculated slip factors as mean values considering the actual preload at slip | ⁹⁾ V: Coefficient of variation for μ_{act}

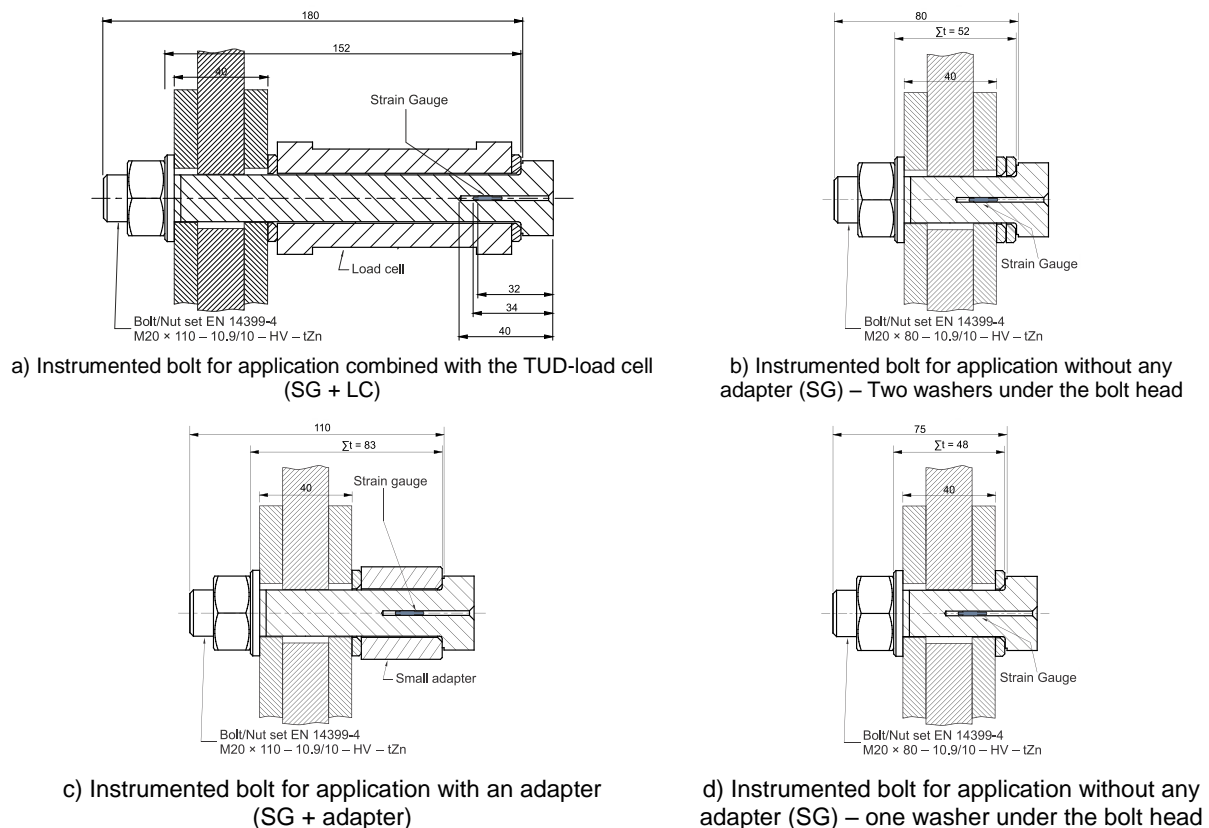


Figure 2.3-1: M20-Bolts with implanted strain gauges

The UDE bolts as well as the TUD load cells have been independently pre-checked at both testing laboratories at UDE and TUD to verify ‘common ground’ between both labs, see Figure 2.3-2. The

differences between the calibration factor of the instrumented bolts determined in UDE and the results of the TUD calibration of the bolts was less than 3 %.

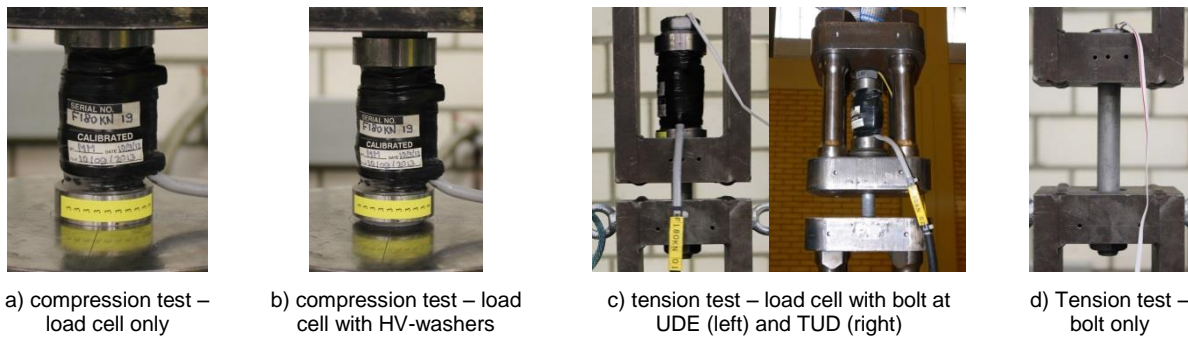


Figure 2.3-2: Calibration of bolt and load cell at TUD and UDE

Within additional, preliminary compression tests the ability to calibrate customary small load cells has been investigated with different setup configurations applying different types of washers, see Figure 2.3-3. Only the setup configuration without any additional washer showed a good agreement between the measured load of the load cell F_{KMD} and the load of the testing machine F . For all setup configurations with additional washers significant deviations (up to 35 %) were observed.

The application of these customary small load cells in slip factor tests confirmed the overestimation of the compression load, see Figure 2.3-3. The results showed that the small customary load cells were very sensitive to irregularities of the clamped parts. Consequently, the use of these load cells within slip tests would lead to a wrong estimation of the slip factor. Therefore, it is highly recommended not to use these kinds of load cells for slip factor tests.

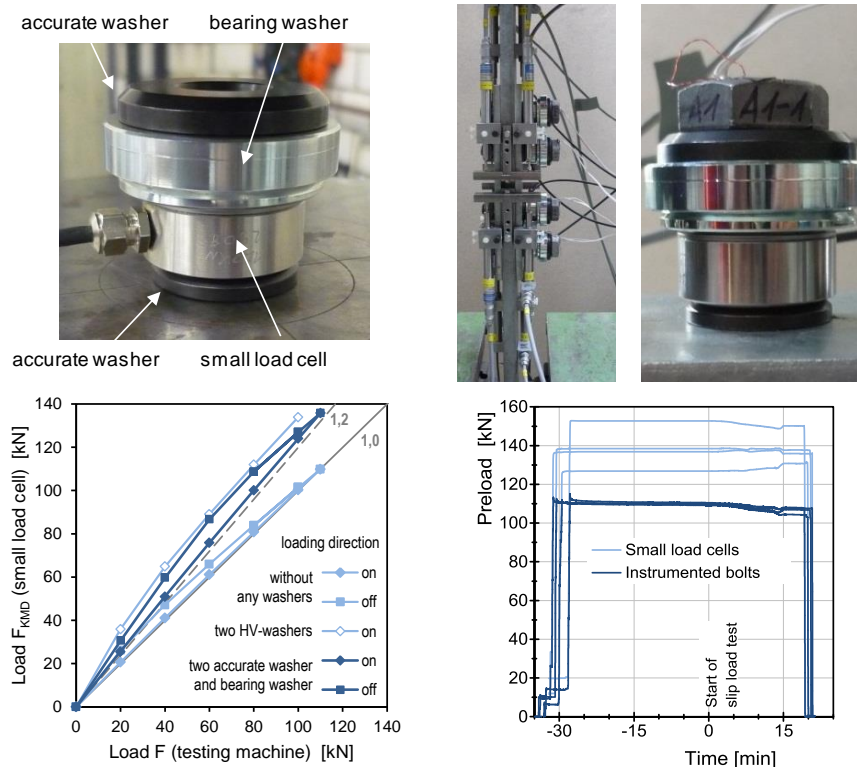


Figure 2.3-3: Results for the use of customary small load cells

The slip displacements were measured at two different positions: CBG (centre bolts group) and PE (plate edges), see Figure 2.3-4. The CBG and PE positions consisted of eight (LVDTs 1 to 8) and four (LVDTs 9 to 12) displacement transducers respectively. From Figure 2.3-5 it can be seen that the stiffness of the slip-deformation behaviour was much higher when measured with LVDTs 1-8 (CBG position) than with LVDTs 9-12 (PE position). Furthermore, large differences in the slip load resulted when the 0.15 mm slip criterion was used. Based on LVDTs 9-12, the maximum slip loads were reached far above 0.15 mm. This was caused by the fact that by using LVDTs 9-12, the elongation of the plates was implicitly measured as well. The influence of elongation could be more apparent when

the level of the slip load was higher. On the other hand, this phenomenon could be neglected when the slip takes place at the lower load level. Consequently, considering the 0.15 mm slip criterion and using a positioning of the LVDTs according to LVDTs 9-12 might lead to much lower slip factors than using the positioning for LVDTs 1-8. This has to be kept in mind when comparing results from the literature. For example, Cruz et al. [5.3-4] performed slip factor tests with positions of displacement transducers comparable to those of LVDTs 9-12. Their results fit quite well with the lower slip factors achieved with LVDTs 9-12, see Table 2.3-2, in which the mean static slip factors based on slip deformations at the PE position are summarized for the preload level $F_{p,C}$. From these investigations it could be concluded that the position of the slip measurement is of great importance. The slip measurement position has to be in the centre bolt group on both sides of the plates so that, in total, eight measurement positions are realized.

Different test setups were chosen for a comparative study to investigate the effect of the clamping length on the slip resistance behaviour of the connection, see Table 2.3-1. In the presented investigations the slip was determined at the peak before 0.15 mm slip or at the slip of 0.15 mm when no peak occurred before 0.15 mm. Evaluating the slip factor considering the initial preload in the bolts without taking into account the large clamping length might lead to an overestimation of the slip factor because the preload losses decrease and the slip load increases with increasing clamping length, see Table 2.3-1. The results show that the static slip factor slightly increases by increasing the clamping length. The difference between the static slip factors for different surface preparation with clamping length of 83 and 52 mm is negligible.

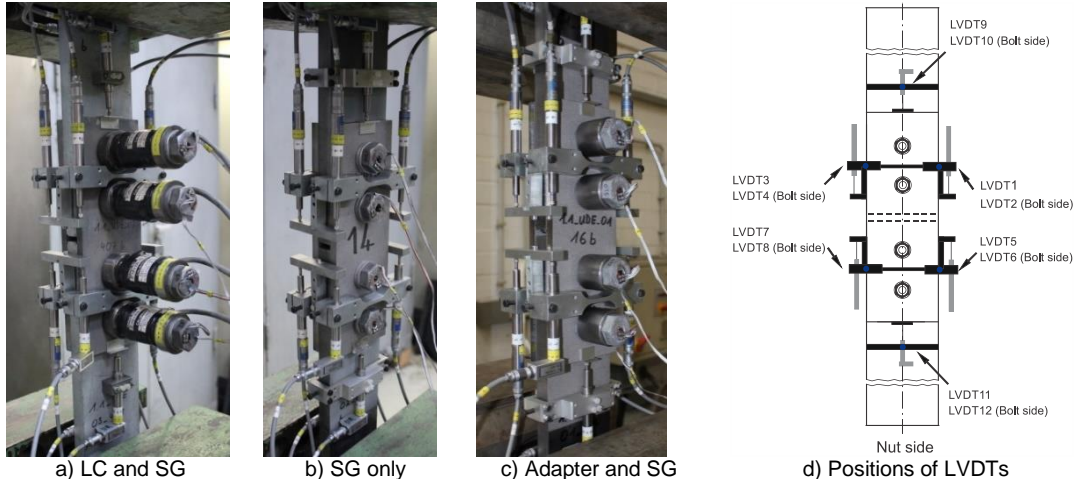


Figure 2.3-4: Test setup for comparative studies

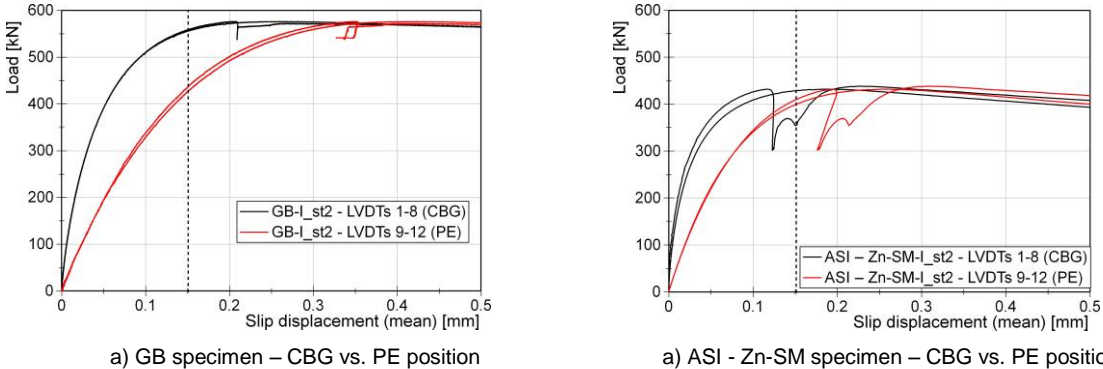


Figure 2.3-5: Influence of positioning the LVDTs (the different colours represent the upper and lower sections of the specimen)

Table 2.3-2: Mean static slip factor results based on LVDTs 9-12 (PE position)

Series ID	Surface treatment		$\Sigma t^{(4)}$ [mm]	Number of tests st/ct/ect ⁽⁵⁾	$\mu_{ini,mean}^{(6)}$ st/st+ct [-]	$\mu_{act,mean}^{(7)}$ st/st+ct [-]	$V(\mu_{act})^{(8)}$ st/st+ct [%]
	Sa ⁽¹⁾ / Rz ⁽²⁾ [μm]	DFT ⁽³⁾ [μm]					
Grit-blasted surfaces (GB)							
GB-I	Sa 2½ / 80	-	152	4/1/-	0.61/0.61	0.64/0.64	2.1/2.0
GB-II		-	83	2/-/-	0.60/-	0.64/-	1.2/-
GB-III		-	52	2/-/-	0.61/-	0.67/-	2.0/-
Cruz [5.3-4]	Sa 2½ / -	-	48	4/1/-	0.56 ⁽⁹⁾ /-	-/-	-/-
Alkali-zinc silicate coating (ASI)							
ASI-I	Sa 2½ / 80	-	152	4/1/-	0.63/0.63	0.65/0.65	1.3/1.2
ASI-II		60	83	2/-/-	0.62/-	0.66/-	2.6/-
ASI-III		-	52	2/-/-	0.61/-	0.66/-	1.7/-
Aluminium spray metallized coating (Al-SM)							
Al-SM-I	-	250	83	2/-/-	0.56/-	0.62/-	2.2/-
Al-SM-II	-	-	52	4/1/-	0.56/0.56	0.64/0.64	2.0/2.4
Zinc spray metallized coating (Zn-SM)							
Zn-SM-I	Sa 3 / 100	-	83	4/-/1	0.58/-	0.62/-	4.8/-
Zn-SM-II		140	52	2/-/-	0.58/-	0.62/-	6.2/-
Combination of alkali-zinc silicate and zinc spray metallized coating							
ASI – Zn-SM-I	Sa 2½/100 – Sa 3/100	55 – 170	48	4/1/4	0.59/0.58	0.65/0.64	2.9/3.2

¹⁾ Sa: surface treatment grade | ²⁾ Rz: roughness | ³⁾ DFT: dry film thickness (coating thickness) | ⁴⁾ Σt : clamping length | ⁵⁾ st: static test/ct: creep-/ect: extended creep test | ⁶⁾ $\mu_{ini,mean}$: calculated slip factors as mean values considering the initial preload when the tests start | ⁷⁾ $\mu_{act,mean}$: calculated slip factors as mean values considering the actual preload at slip | ⁸⁾ V: coefficient of variation for μ_{act} | ⁹⁾ reported as a nominal slip factor

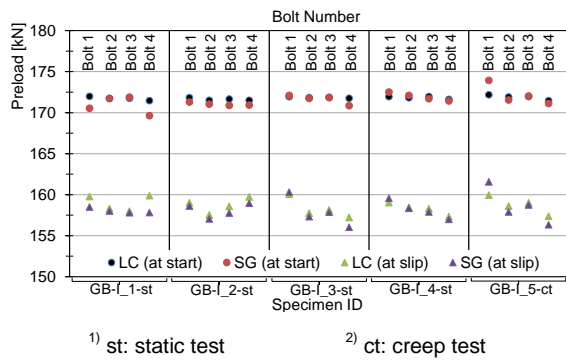


Figure 2.3-6: Comparison of preload measurements considering LC and SG for GB-I

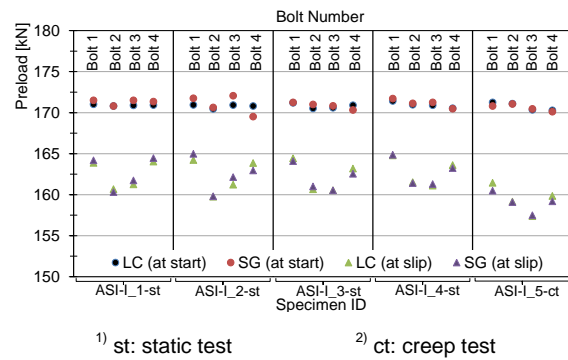


Figure 2.3-7: Comparison of preload measurements considering LC and SG for ASI-I

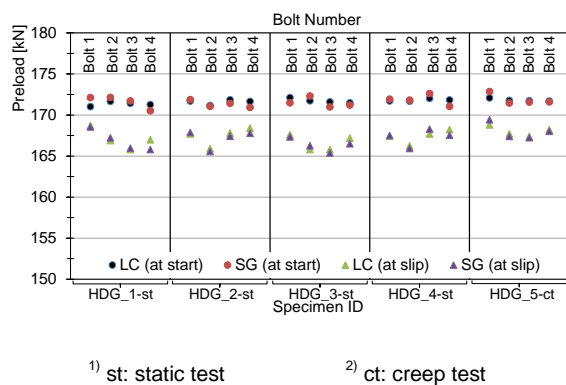


Figure 2.3-8: Comparison of preload measurements considering LC and SG for HDG-I

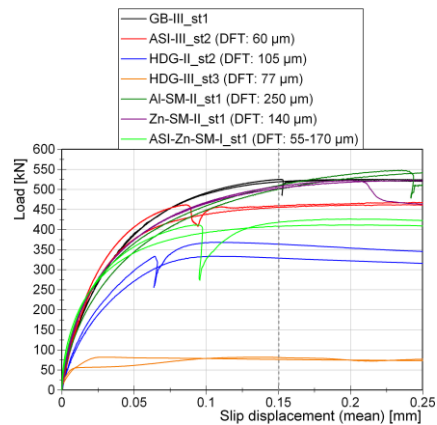


Figure 2.3-9: Influence of different surface conditions on the slip-load behaviour

Figure 2.3-6 to Figure 2.3-8 present the initial preloads at the beginning of the testing and the actual preloads at the slip in the bolts measured by SG and LC. From these diagrams the preload losses due to creep and transversal contraction could be observed as well. It can be seen that the deviations between the measurement methods SG and LC are negligible small with a maximum deviation of 1.3 %. Furthermore, the mean values of the losses of preload were detected to approximately 9 % for GB-I, 7 % for ASI-I and 3 % for HDG. As the main part of the loss of preload was caused by transversal

contraction (in static slip factor tests), the transversal contraction increased with increasing slip load too, which resulted in preload losses corresponding to the level of the slip load.

The results of the static tests and of the creep tests are summarized in Table 2.3-1 as well for the static tests only as for the combined evaluation of the static and creep tests. Table 2.3-1 shows that the highest initial and actual slip factors were achieved for GB- and Al-SM-surface conditions respectively. Figure 2.3-9 shows typical load-slip displacement curves. Approximately the same slip loads (F_{Si}) were achieved for both GB and Al-SM-surfaces. The higher actual slip factor for Al-SM can be explained by significantly higher losses of preload for AL-SM-surfaces during the tests, see Table 2.3-1.

Using LCs led to a relatively large clamping length of the bolts which influenced the loss of preload and consequently the level of the slip load. Evaluating the slip factor considering the nominal preload in the bolts without taking into account the large clamping length, might lead to an overestimation of the slip factor because the preload losses decrease and the slip load increases with increasing clamping length. Based on the results of Task 1.1, it was decided to use instrumented bolts with implanted strain gauges without small adapters for the research project.

For design purposes, preload losses have to be considered implicitly in the slip factor itself - or in the design formula for the determination of the slip resistance - one of both. Practical recommendations and specifications regarding this topic must be ensured in codes and/or test guidelines. Regarding the creep tests it can be stated that they clearly failed for all coated surfaces and extended creep tests were necessary. The creep test for grit blasted surfaces was passed and the characteristic value of the nominal slip factor could be evaluated as 0.75 (5 % fractile value with a confidence level of 75 %).

2.4 Task 1.2 – Test speed

Correction actions

The original test matrix for Task 1.2 was consisting of only two series of surface preparations: grit blasted (GB) and coated with Alkali Zinc Silicate (ASiZn). In the first bilateral meeting of UDE and TUD it was decided to add the series of zinc (Zn) spray metallized specimens (ZnSM) to the test matrix. This coating is known to be sensitive to creep. The reason for the expansion of the test matrix in Task 1.2 was the omission in the original test matrix of a series of plates with a coating that is known to be creep sensitive. Especially for creep sensitive coatings, it is important to investigate the influence of the test duration on the results of a short term slip test as for these coatings the initial test sequence should guarantee a correct conclusion of the creep test.

The total number of tests to be performed by TUD in Task 1.2 increased from 40 to 60. An overview of the test specimens and surface conditions is presented in Table 2.4-1.

Objectives

In Task 1.2 of the SIROCO project a comparative study about the influence of the duration of short term slip factor tests has been performed. It was anticipated that the test duration may have influence on:

1. The slip factor for non-creep sensitive surfaces.
2. The results of a creep test.
3. The spread in the results of short term slip factor tests.

Beside a literature study short term slip factor tests were carried out using different loading speeds. The test results were used to determine the influence of the test duration on (1) the short term slip factor and (2) the conclusion of creep sensitivity during a creep test.

First, to determine the slip factor according to Annex G of EN 1090-2, a series of 4 short term tests was conducted. In these tests, the load was gradually increased until a critical slip value of the connection was reached. The results of the short term tests were used to define the load level of a following creep test. The results of this creep test indicated if the coating was creep sensitive. These creep test results were essential for the determination of slip factors for different coatings. If a test passed, the slip factor was calculated based on the combined results of the short term tests and the creep test. However, if the a creep test failed, time consuming extended creep tests had to be carried

out. The results of a creep test were depending on the load level at which the test was performed. This load level was defined as the average of the results of the short term tests.

As time is essential for creep effects, the results of the short term tests were potentially influenced by the duration of these tests. For this reason, time limits were specified wherein the short term tests were to be executed. This is currently implemented in EN 1090-2, Annex G by the following statement: 'tests shall be carried out at normal speed (duration of test approximately 10 min to 15 min)'. The meaning of 'normal speed' is not further defined or explained in the standard. In practice, the specification of the duration of short term slip tests raises questions and leads to confusion:

- The specimens that have to be used for slip factor tests should have 2 identical friction grip connections. It is not clear what is meant exactly by the test duration; does this refer to the time that it takes to load one side of the specimen up to the critical slip or to the time that it takes to make both connections slip?
- The method of loading a specimen is not prescribed in detail, that means the user is free to choose between stress- and strain-controlled loading. In addition, a combination of both methods is possible.
- The parameters of the load control method must be determined by performing initial tests on dummy specimens. Labs may use their expertise with similar coating systems to choose an initial loading speed. This can result in a test duration that complies with the requirements, but most likely will be outside the time limit of 10-15 minutes. The formulation of the test duration suggests that within this time limit the influence of the load speed on the slip factor is negligible. However, it is not clear what to do with results of tests that took a few minutes shorter than 10 or longer than 15 minutes.

This lack of clarity can lead to different interpretations and consequently to differences in the way slip factor tests may be executed in practice. For this reason, more knowledge about the influence of the mentioned aspects is desirable.

Experimental tests

Experiments on double lap shear connections cf. Annex G of EN 1090-2 have been carried out using HV bolts M20 x 180 of class 10.9. The steel plates used for all experiments were grade S355J2C+N. An overview of the test specimens and surface conditions is presented in Table 2.4-1. For each of the GB, ASiZn and ZnSM series also steel plates were produced for 8 additional specimens thus a total of 28 (16+4+8) specimens was available for each series. The additional specimens were produced in case of erroneous tests, to be able to vary with the slip factor setups and to be able to perform verification tests.

Table 2.4-1: Test specimens and surface conditions for slip tests in Task 1.2

Series ID	Surface preparation		Clamp length Σt [mm]	Clamp length ratio $\Sigma t/d^{(2)}$ [-]	Number of tests in task 1.2	
	Coating material	Coating thickness ⁽¹⁾			Static test	Creep test
Grit blasted surfaces, Sa 2 ½ (R _z = 80 µm)						
GB	-	-	152	7.5	16	4
Grit blasted surfaces, Sa 2 ½ (R _z = 80 µm) + ASiZn coating						
ASiZn	Alkali-zinc silicate	60 µm	152	7.5	16	4
Grit blasted surfaces, Sa 3 (R _z : 100 µm) + ZnSM coating (after coating: R _z = 85 µm)						
ZnSM	Zinc spray metallized	140 µm	152	7.5	16	4
Level of preload: F _{p,C} = 172 kN (M20) ⁽¹⁾ Nominal dry film thickness (DFT). ⁽²⁾ d = 20 mm						

The preload was applied using a pneumatic torquing device. For the tests in Task 1.2 the preload in the bolts was measured concurrently with implanted strain gauges (produced at UDE) and load cells (produced by TUD). By measuring with both load cells and strain gauges the tests in Task 1.2 also gave input to Task 1.1 (study of different methods for measuring the preload during slip factor tests). The preload in each of the bolts was measured continuously from the beginning of the tightening

procedure until the end of the slip factor test. Due to creep sensitive coatings or surface treatments the preload may drop fast during the first minutes after initial application to $F_{p,C}$. However, from a practical point of view, it is impossible to have a guaranteed fixed time span between the application of the preload and the beginning of the slip factor test. A varying time limit could mean that the preload level at the beginning of the slip factor test may vary between specimens. To avoid this, a waiting period of at least 30 minutes between the end of preloading and the beginning of the slip factor test was maintained. When the loss of preload over the waiting period reached more than 5 % of $F_{p,C}$ all bolts of the specimen were retightened. Retightening was necessary for all ZnSM specimens. None of the GB and ASiZn specimens needed to be retightened.

Another aspect that influenced the results of the slip factor tests was the clamping length of the bolts. Larger clamping lengths led to a reduction of the preload losses during the tests and consequently resulted in higher slip factors. The length of the used load cells in Task 1.2 was resulting in a clamping length of the bolts of (4+100+4+40+4=) 152 mm which is significantly more than the 'standard' clamping length of (4+40+4=) 48 mm in tests for M20 bolts acc. to EN 1090-2, Annex G. This means the achieved slip factors in Task 1.2 were higher than comparable slip factors from experiments carried out with standard bolts. Because the objective of Task 1.2 was to determine the influence of the test duration on slip factor test results, the ratios between the slip factors achieved from the various test durations were of interest. However, the clamping length was not relevant for this. Additionally, a method was described (and validated) to adjust slip factors by experiments with longer bolts. In all other work packages of the SIROCO project the 'standard' clamping length (48 mm for M20) was used. 4 tests of each surface with HV 10.9 bolts with a clamping length of 48 mm were conducted on specimens in Task 1.2 as reference tests for experiments in task 2.1 (influence of preload level and bolt type on slip factors). Furthermore, 2 specimens of each series (GB, ASiZn and ZnSM) from Task 1.2 were used as reference tests with HR 8.8 and HR 10.9 bolts in Task 2.1. Some of these additional specimens were used to gain more general insight in the behaviour of high strength friction grip bolts (HSFG) connections.

Additional tests were performed on two GB specimens with single bolts using compressive and tensile loading. These tests were conducted to investigate if there is any difference in the results depending of the load orientation. This investigation was motivated by the American standard RCSC 2014 [5.4-1] that states that short term friction coefficients may be determined using compressive rather than tensile loading. During the slip factor tests the following two phenomena influenced the preload losses:

1. Settling of the bolting assembly components and the properties of the coating system caused initial preload losses (losses directly after the required preload level were reached).
2. Losses during the execution of slip factor tests were caused by:
 - elastic lateral contraction of the steel plates (the specimen was loaded in tension),
 - flattening of the asperities of the steel surface during the slip process,
 - coating was flattened/compacted by mutual displacements of centre and lap plates.

The initial preload losses and the preload losses during the load application were determined for all specimens. The losses that were caused by the elastic behaviour of the plates (lateral contraction) were an order of magnitude smaller than the losses by other causes. But the coating system and the clamping length of the bolts were of major influence on the losses. The measurements confirmed the reproducibility of the measurement system over time.

The duration of a test was defined as the time that it takes from the beginning of a test until the loading of a specimen up to the level at which the slip criterion was reached in both connections. For each slip factor test two results for the test duration were achieved. Strain-controlled loading was used for short term slip factor tests and stress-controlled loading was used for creep tests and extended creep tests. To examine the influence of the test duration on slip factors all three series were tested by four test durations of short term tests:

- about 5 minutes (loading speed 0.01 mm/s),
- about 10 minutes (loading speed 0.005 mm/s),
- about 20 minutes (loading speed 0.0025 mm/s),
- about 45-60 minutes (loading speed 0.001 mm/s).

The first three durations were based on the same scale as the time limit in EN 1090-2, Annex G is prescribed (10 to 15 minutes). The last duration was significantly longer but still short compared to the duration of a standard 3 h creep test.

The slip load (F_{slip}) was defined as the maximum load that could be applied on a specimen or the load when a certain 'slip' occurred between the centre and the lap plates before the maximum load was reached. The slip is defined as the displacement between a location on the centre plates and a location on the lap plates. EN 1090-2 clearly states that these locations should be the point in between the bolts (at the centre of the bolt group - CBG position) on centre and lap plates. In the evaluation of the results of the short term tests the slip criterion as described in EN 1090-2 was used:

- 0.15 mm displacement between the centre plates and the lap plates measured at the CBG position.

In various research studies on slip factors of steel plates and coatings systems the slip at the CBG position was not used, but the displacement between the edge of the lap plates and a point on the centre plates near to it (this position is referred to as the PE (plate edge) position). Using the slip at the PE position is beneficial from a practical point of view, as only 4 linear variable differential transformers (LVDTs) were needed to determine the slip compared to 8 at the CBG position.

In all short term slip factor tests as well as creep tests in the SIROCO project the slip at both the CBG and PE positions were measured. The data gathered could be used in other work packages of this project to define an alternative slip criterion that is to be used when slip measurements are recorded at the PE position.

Creep tests

The intention of a creep test is to investigate the creep sensitivity of a coating. The load level for the creep test was set to 90 % of the mean value of the short term tests results based on the CBG position criteria. For the creep tests stress-controlled loading was used. The loading speed [kN/s] for the creep tests was derived from the loading speed that was achieved in the associated short term tests in the same load duration group. The current version of EN 1090-2, Annex G prescribes a test duration of 3 hours for a creep test. All creep tests in the SIROCO project were executed over a time period of at least 12 hours. The test results (load level - slip-time relation) for this extended time period were used as input for Task 1.4 (in this task research was done to formulate alternative criteria to determine the creep sensitivity).

Conclusion

In Task 1.2 of the SIROCO project a comparative study about the influence of the duration of short term slip factor tests has been performed. It was anticipated that the test duration could be of influence on:

1. The slip factor for non-creep sensitive surfaces.
2. The results of a creep test.
3. The spread in the results of short term slip factor tests.

The following conclusions can be drawn from the test results:

1. When the CBG position criterion is used to determine slip factors, there is a tendency of a slightly higher slip factor at longer test durations for grit blasted specimens. For zinc spray metalized surfaces an opposite effect and for alkali-zinc coated surfaces no effect occurred.
2. For variations in the test durations of ± 5 minutes compared to the 10-15 minutes time limit given in EN 1090-2, the influence of the test duration on the slip factor is ± 1.5 % compared to the slip factor that was achieved at a test duration of 12.5 minutes.
3. No effects of the test duration on the spread in the results of short term slip factor tests occurred.
4. No effects of the loading speed on the determination of the sensitivity to creep occurred.
5. Based on the achieved results the slip factor tests should be determined as follows:
 - Displacement controlled load application,
 - Test duration "between 10 and 15 minutes".
6. Based on the variation in slip factors occurred in practice, it is impossible to specify a certain loading speed at which slip factor tests should be carried out. When slip factor tests will be performed on a new coating system or surface treatment, the correct loading speed (mm/s) of the used test rig has to be estimated by performing an initial test on the coating system. Unless the

load duration of this initial test is outside a time limit ranging from 5 to 20 minutes, the results of the initial test can be used as part of the series of 4 short term tests.

Results

The results of the slip factor tests in Task 1.2 are summarized in Table 2.4-2 and Figure 2.4-1.

Table 2.4-2: Results of Task 1.2 - influence of the test duration on the slip factor

Speed [mm/s]	Surface preparation		Σt^4 [mm]	Bolt type	Bolt size (Md x L) ⁵⁾ [mm]	Test duration [min]	Number of tests	$\mu_{ini,mean}^7$	$\mu_{act,mean}^8$	$V(\mu_{act})^9$
	Sa ¹⁾ / Rz ²⁾ [μ]	DFT ³⁾ [μ]						st/st+ct	st/st+ct	st/st+ct
								[-]	[-]	[%]
Grit blasted surfaces (GB)										
0.01			152		M20 x 180	5	8/2	0.72/0.72	0.79/0.80	2/2
0.005			48		M20 x 80	10	4/-	0.67/-	0.81/-	2/-
0.005	Sa 2½ / 80	-	152	HV10.9	M20 x 180	11	6/2	0.77/0.78	0.84/0.85	1/2
0.0025			152		M20 x 180	24	4/-	0.79/-	0.85/-	3/-
0.001			152		M20 x 180	64	4/-	0.82/-	0.88/-	1/-
Alkali-zinc silicate coating (ASiZN)										
0.01			152		M20 x 180	5	6/2	0.70/-	0.76/-	1/-
0.005			48		M20 x 80	9	4/2	0.68/-	0.75/-	1/-
0.005	Sa 2½ / 80	60	152	HV10.9	M20 x 180	10	6/2	0.71/-	0.76/-	3/-
0.0025			152		M20 x 180	19	6/-	0.70/-	0.76/-	2/-
0.001			152		M20 x 180	49	6/2	0.72/-	0.78/-	1/-
Zinc spray metalized coating (ZN-SM)										
0.01			152		M20 x 180	6	6/2	0.76/-	0.82/-	2/-
0.005			48		M20 x 80	10	4/-	0.74/-	0.83/-	4/-
0.005	Sa 3 / 100	140	152	HV10.9	M20 x 180	11	6/2	0.76/-	0.83/-	3/-
0.0025			152		M20 x 180	20	4/-	0.72/-	0.78/-	3/-
0.001			152		M20 x 180	45	4/-	0.69/-	0.75/-	2/-
0.0005			152		M20 x 180	95	4/-	0.69/-	0.74/-	1/-

¹⁾ Sa: surface preparation grade | ²⁾ Rz: roughness | ³⁾ DFT: dry film thickness (Coating thickness) | ⁴⁾ Σt : clamp length ⁵⁾ d: bolt diameter, l: bolt length | ⁶⁾ st: static test/ct: creep test | ⁷⁾ $\mu_{ini,mean}$: calculated slip factors as mean values based on the initial preload when the tests started | ⁸⁾ $\mu_{act,mean}$: calculated slip factors as mean values based on the actual preload at slip (friction coefficients) | ⁹⁾ V: Coefficient of variation for μ_{act} | * Nominal level of preload: $F_{p,C} = 172$ kN

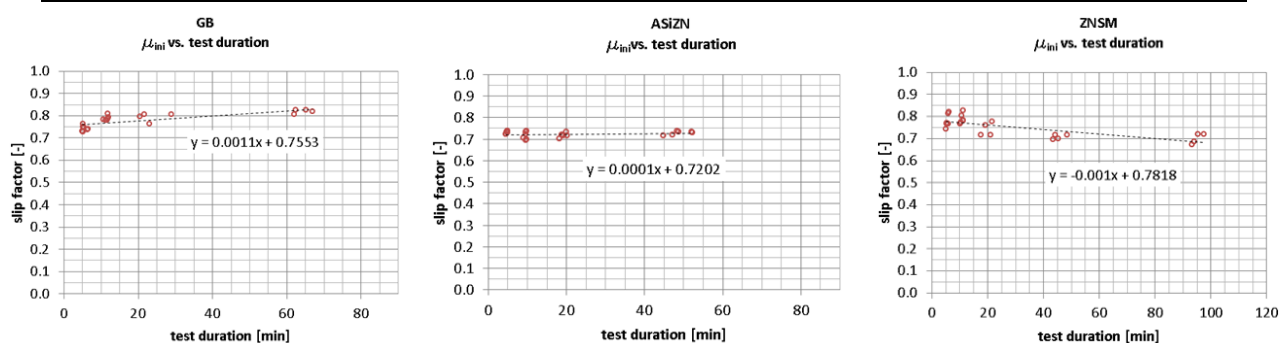


Figure 2.4-1: Graphical representation of the experimental results of Task 1.2

2.5 Task 1.3 – Criteria for the slip load

Introduction

The individual slip load F_{Si} for slip-resistant connections is defined as the load at a displacement of $\delta = 0.15 \text{ mm}$ acc. to EN 1090-2, Annex G. The results of Task 1.1 showed that the slip load F_{Si} should not always be taken at a fix value of $\delta = 0.15 \text{ mm}$, like it is recommended in EN 1090-2, Annex G, due to different slip load-displacement behaviours which have been detected for various coatings. A first idea was to take the maximum load as the slip load what could be assumed in case of a decreasing slip load-displacement curve after reaching a maximum value. Subsequently, the displacement δ had to be determined at the point of the maximum slip load. The displacement directly affected the extended creep test procedure (see Task 1.4). It was representing the point of failure of the connection at long term loads. Up to now, EN 1090-2, Annex G mentions the value of $\delta = 0.3 \text{ mm}$ as a failure criterion for extended creep tests within a life of the structure of 50 years. Existing test results show that a slip load-displacement behaviour differs from the size of the specimen and the coating system of the faying surfaces. For this reason, the slip-load evaluation criterion at a fixed value is questionable. Concerning a dependable slip load displacement criterion, a reliability analysis had to be performed taking into account the consequences for the design of steel constructions.

Objectives

In Task 1.3 no experimental tests were performed. A comparison of the load-displacement behaviour of slip-resistant connections with different systems of the faying surfaces was done. As an example, the characteristic curves are shown in Figure 2.5-1.

Results

The applied coating system as preparation for the faying surfaces of slip-resistant connections has an influence onto the individual slip load-displacement behaviour (see Figure 2.5-1). The fixed criterion with $\delta = 0.15 \text{ mm}$ for the evaluation of the slip load could underestimate the performance/slip load F_{Si} of the tested coating systems, e.g. for Al-SM and Zn-SM. For the Al-SM coating the mean slip load at $\delta = 0.15 \text{ mm}$ ($\delta = 150 \mu\text{m}$) was $F_{Sm,150\mu\text{m}} = 504.3 \text{ kN}$ and the evaluated slip load at the maximum was $F_{Sm,max} = 551.9 \text{ kN}$. This slip occurred between 0.25 mm and 0.35 mm at slip load tests. The used results in task 1.3 which were achieved from Task 1.1 are summarized in Table 2.5-1. In the current draft of prEN 1090-2:2017, a change of the evaluation of the slip load to either a slip value of $\delta = 0.15 \text{ mm}$ or the peak before has already been accepted as a result of SIROCO, see Figure 2.5-2.

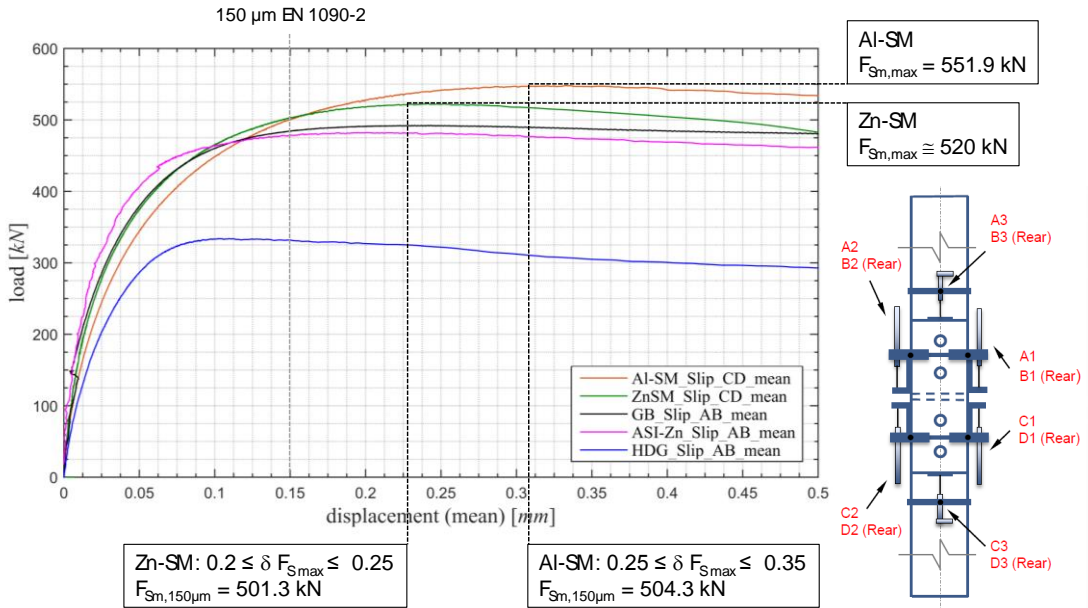


Figure 2.5-1: Influence of the coating system on the faying surfaces from specimens in Task 1.1 (LVDTs A3, B3, C3, D3 were not used for calculation of the mean displacement)

Table 2.5-1: Compared results for Task 1.3, achieved from Task 1.1

Coating system (# results)	Clamping length Σt	$F_{S_m,150\ \mu m}$ (min. / mean / max.)	$F_{S_m,max}$ (min. / mean / max.)	$\mu_{start,150\ \mu m,5\%}$ (min. / mean / max.)
	[mm]	[kN]	[kN]	[-]
Al-SM (8)	52 mm	487.5 / 504.3 / 528.8	536.2 / 551.9 / 572.2	0.71 / 0.73 / 0.76 ($V_x = 2.5\%$)
Zn-SM (4)	52 mm	485.3 / 501.2 / 508.8	493.6 / 512.0 / 522.7	0.71 / 0.73 / 0.75 ($V_x = 2.1\%$)
GB (4)	52 mm	484.5 / 507.4 / 525.3	492.4 / 513.1 / 525.6	0.71 / 0.74 / 0.77 ($V_x = 3.7\%$)
ASi-Zn (4)	52 mm	455.7 / 469.0 / 479.9	461.9 / 473.3 / 482.2	0.68 / 0.70 / 0.71 ($V_x = 2.4\%$)
HDG (8)	152 mm	278.2 / 323.6 / 355.8	290.9 / 326.0 / 355.8	0.40 / 0.47 / 0.52 ($V_x = 9.0\%$)

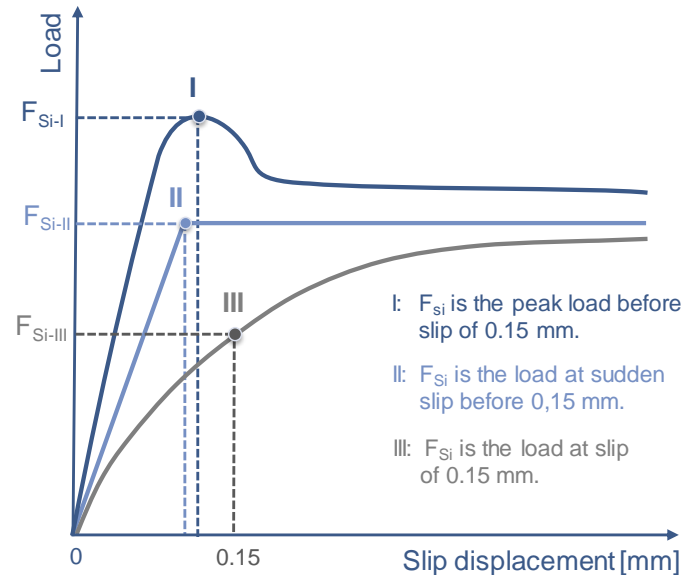


Figure 2.5-2: Criteria for the evaluation of the slip load

Conclusion

The maximum allowable displacement will be kept with $\delta = 0.15$ mm for slip loads (see Figure 2.5-2, curve III). For accepting the real physical failure of the slip-resistant connection (maximum of slip load curve) as the slip load further investigations need to be performed, because no decrease of load may occur. In this case no maximum exists that defines the slip load. However, the main result of Task 1.3 is that the slip load should not be taken from a fix displacement value.

2.6 Task 1.4 – Criteria for creep tests

There is a close link to Task 1.3 in which the slip load tests of Task 1.1 were evaluated regarding their different load-displacement behaviour comparing the slip load at $\delta = 150\ \mu m$ and at the maximum load $F_{S_m,max}$. Task 1.1 is the basis of the test campaign in this Task, which investigates the creep sensitivity of different coatings for the faying surfaces of slip-resistant connections acc. to EN 1993-1-8 and test procedure acc. to EN 1090-2, Annex G. The mean values of the slip load F_{S_m} from the quasi-static slip load tests of Task 1.1 were needed for determining relative load levels for the extended creep tests (EXCT, acc. to EN 1090-2, Annex G.5) and for the step-tests, presented in Table 2.6-1.

All tests have been performed. During the project it came out that an increase of the observation time for the Extended Creep Tests (EXCT) over the project duration was necessary for a final and verified evaluation of the creep of the coating systems in the slip-resistant connections. Therefore, it was necessary to plan, calculate, manufacture, erect and calibrate autarkic test rigs that work without any electrical power to avoid bottlenecks at the hydraulic and electrical test machines. The new developed test rigs are presented in Figure 2.6-7.

Explanation for Table 2.6-1: To investigate a new creep criterion and to revise the procedure of defining a sufficient load level for the mostly necessary EXCT the following tests were carried out:

1. *long-term* step tests
2. *short-term* step tests (later denoted as “step tests”)

3. extended creep tests with different load levels that will not pass
4. extended creep tests with load levels that passes the criterion of EN 1090-2, Annex G.5

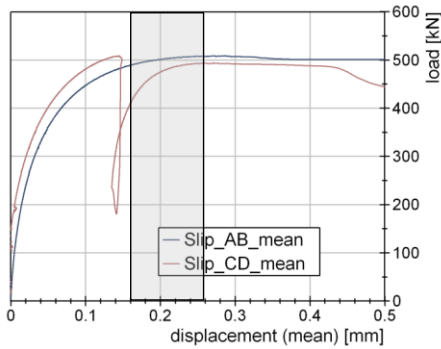
The step tests have been performed for two variations of time per load step, “long-term” (three days per load level/step for approximately six steps) and “short-term” (90 min per load level/step). The step tests should give a load level at which an EXCT could pass the test. To verify the results of the step tests a minimum of two EXCTs was necessary. The first EXCTs were performed at the load level at which the step tests showed a failure in connection. Although, a failure criterion could not be quantified, it was possible to evaluate a qualitative criterion at that the connection seams to fail, e.g. reaching a maximum displacement, complete slip (approximately the hole clearance) or a displacement per time criterion. Afterwards, an EXCT had to be performed with a reduced load level that would pass the criterion of EN 1090-2, Annex G.5 (limit of $\delta = 300 \mu\text{m}$ of linear extrapolated displacements). This test was not restricted to minimum test duration. This issue was also investigated in this task. Therefore, one EXCT had to observe over the remaining project duration, to exclude long-term creep effects (tertiary creep). Each test had instrumented bolts with strain gauges (BTM6C) like in Task 1.1 and each test was equipped with eight LVDTs (Company HBM Type: WI/5 mm) and additionally four EXCTs in the autarkic test rigs. At first the slip load tests (coating system Zn-SM) from Task 1.1 had to be evaluated, see Figure 2.6-1.

The grey areas around a displacement of $\delta > 0.15 \dots 0.2 \text{ mm}$ show the displacement where the slipping between inner and outer plates occurred. Based on the mean value of the individual slip loads F_{Si} ($\delta = 150 \mu\text{m}$) the load levels for the step tests were calculated. With these loads the first step test with long-term steps with a minimum of three days per step was performed. The specimen size, preparation and coating were from the same batch as in Task 1.1. The results of the “long-term” step test for the Zn-SM specimen are given in Figure 2.6-2.

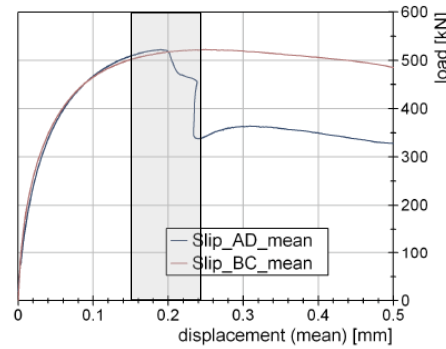
Table 2.6-1: Overview of test campaign in Task 1.4

Coating	Tests and test limitation	Comment
ASi-Zn	<ol style="list-style-type: none"> 1. step test - long-term 2. EXCT 90 % of F_{Sm} 3. EXCT 80 % of F_{Sm} 4. step test - short-term 5. step test - short-term 	<ul style="list-style-type: none"> - did not work, no slip occurred: max. $\delta \cong 0.17 \text{ mm}$ - done, not passed the EN 1090-2, Annex G.5 - failed - in progress (~ 1000 d) → passed - did not work, no slip occurred until test load of 80 % F_{Sm} - slip/high creep rate at 90 %
HDG	<ol style="list-style-type: none"> 1. step test - long-term 2. EXCT 80 % of F_{Sm} 3. EXCT 75 % of F_{Sm} 4. step test - short-term 5. slip load test 	<ul style="list-style-type: none"> - did not work, no slip occurred: max. $\delta \cong 0.07 \text{ mm}$ - done, not passed the EN 1090-2, Annex G.5 - failed - in progress (~ 500 d) → passed - ok, failed at 80 % - acc. to EN 1090-2, Annex G
Zn-SM	<ol style="list-style-type: none"> 1. step test - long-term 2. EXCT 80 % of F_{Sm} 3. EXCT 75 % of F_{Sm} 4. step test - short-term 5. EXCT 70 % of F_{Sm} 6. EXCT 65 % of F_{Sm} 7. EXCT 60 % of F_{Sm} 	<ul style="list-style-type: none"> - slip/high creep rate at 80 % - done, not passed the EN 1090-2, Annex G.5 - failed - done, not passed the EN 1090-2, Annex G.5 - failed - slip/high creep rate at 70 % - done, not passed the EN 1090-2, Annex G.5 - failed - finished (ca. 318 d) – load limit → test failed - in progress (ca. 450 d) → passed
Al-SM	<ol style="list-style-type: none"> 1. step test - long-term 2. step test - short-term of $F_{Sm,150\mu\text{m}}$ 3. step test - short-term of $F_{Sm,max}$ 4. EXCT 90 % of $F_{Sm,max}$ 5. EXCT 80 % of F_{Sm} 	<ul style="list-style-type: none"> - did not work, no slip occurred: max. $\delta = 0.07 \text{ mm}$ - max. $\delta = 0.16 \text{ mm}$ - done, slip/high creep rate at 90 % of $F_{Sm,max}$ (551.9 kN) - done, not passed the EN 1090-2, Annex G.5 - failed - in progress (~ 670 d) → passed
ASi-Zn - alkali-zinc silicate coating GB - grit-blasted (Sa2½) HDG - hot dip galvanized Zn-SM - zinc spray metallized Al-SM - aluminium spray metallized EXCT - extended creep test F_{Sm} - mean slip load at a mean displacement of $\delta = 150 \mu\text{m}$ $F_{Sm,max}$ - maximum slip load (see Figure 2.5-1, p. 24)		

Zn-SM slip load test _ UDE _41



Zn-SM slip load test _ UDE _40



previous tests in SIROCO (UDE)

specimen	$F_{S,150\mu m}$ [kN]	LVDT-position
40_st	507,5	AB_mean
	503,4	CD_mean
41_st	508,8	AB_mean
	485,3	CD_mean
mean	501,3	

$\Sigma = 52 \text{ mm}$
 $l_{k/d} = 2,6$
 2 tests $F_{Sm} = 501,2 \text{ kN}$
 4 results $\mu_{mean,start} = 0,73$

Figure 2.6-1: Slip load tests of Zn-SM from Task 1.1

During the test with a load of 80 % of $F_{Sm} = 401 \text{ kN}$ there was a high increase of displacement δ . This increase seemed to be the load level of failure though a quantitative criterion could not be given. At next, an extended creep test at 80 % of F_{Sm} had to be performed, see Figure 2.6-3 left. This was assumed as the load at that the specimen would not pass the test. Because the criterion in EN 1090-2, Annex G.5 for passing this test is an extrapolated displacement $\delta < 0.3 \text{ mm}$ up to 50 years or the life-time of the structure the test failed. Due to that the test was repeated with 75 % of F_{Sm} , see Figure 2.6-3 right.

The 75 % F_{Sm} load level tests ended (failed) after 1000 min (16.7 h) but in the *long-term* step test a degressive displacement curve occurred for this load level. This leads to the assumption that a load level of 75 % could pass the extended creep test procedure. Nearly the same behaviour was also observed during the test campaign regarding the other coating systems: ASi-Zn, HDG and Al-SM. As an example, the *long-term step test* of a hot dip galvanized specimen is shown in Figure 2.6-4 (left). The results did not show a slip in the connection, but the 90 % EXCT failed after a few minutes. To solve this issue the duration of the steps had been adapted and reduced to 90 min per step. The results were qualitative plausible, so the adaption was successful. Thus the time could be reduced from 3 days to 90 min per step and the results get more reasonable. The results of the (*short-term*) *step-test* for the Zn-SM coating are shown in Figure 2.6-4 (right).

Zn-SM: step-test long-term (steps of $F_{Sm} = 501,3 \text{ kN}$)

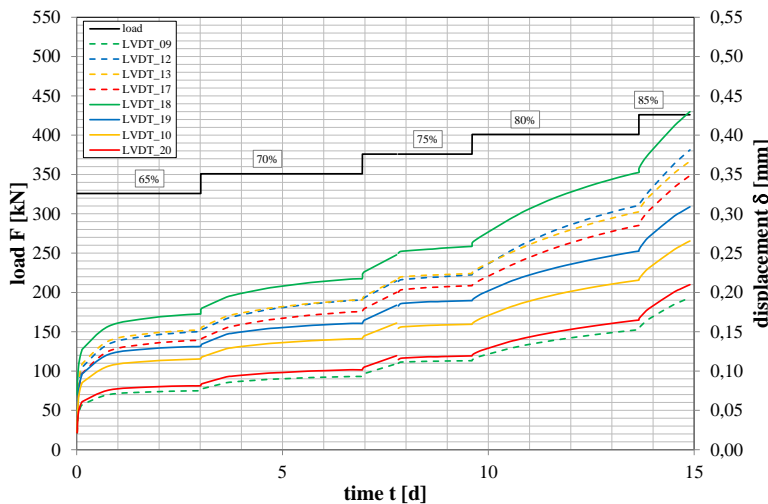


Figure 2.6-2: Results of long-term step test for Zn-SM specimen



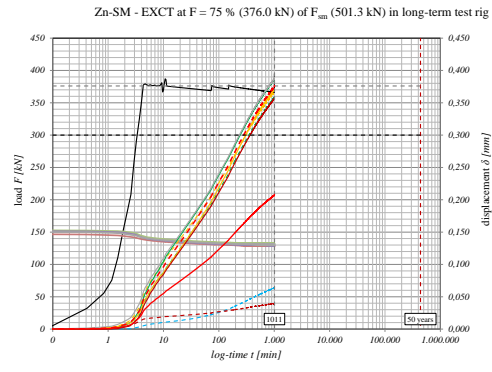
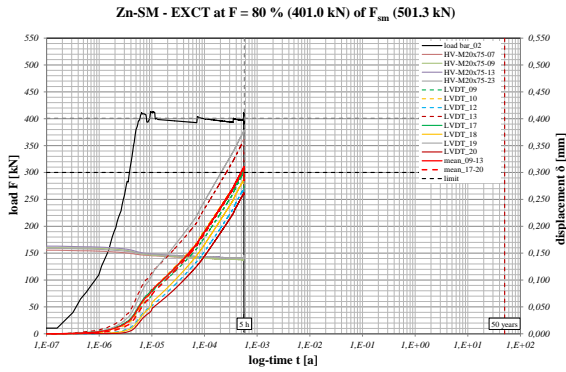


Figure 2.6-3: Load-time-displacement diagram of an EXC (top: 80 % of the load, bottom: 75 % of the load)

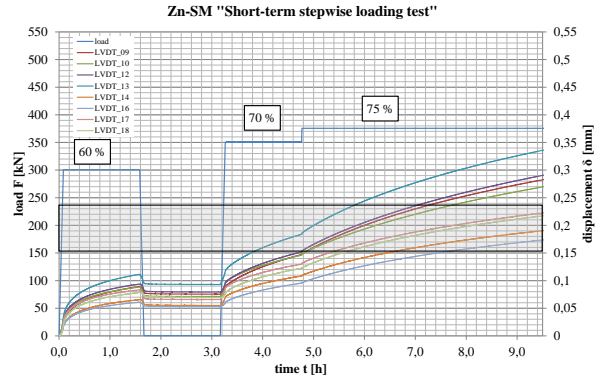
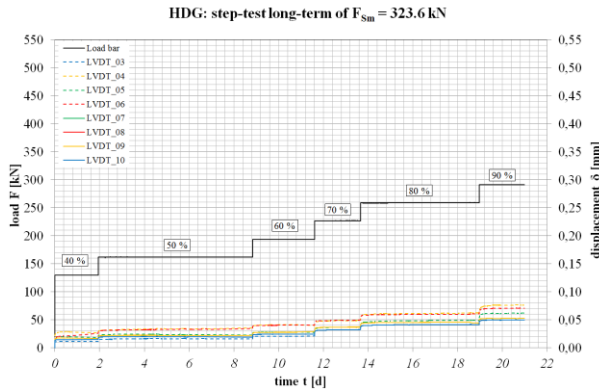


Figure 2.6-4: Long-term step test of HDG specimen (left); Short-term step-test of Zn-SM specimen (right)

It started with a step of 60 % of F_{Sm} , $F = 300$ kN continued with a 65 % step which unfortunately was without load due to an programming error of the test machine. However, it could be shown that the failure area of displacement of about $\delta > 0.15 \dots 0.2$ mm (grey area) was reached during the quasi-static slip load tests, see Figure 2.6-1. (This comparison was made after the performance of the long-term step tests of the other coating systems Al-SM and ASi-Zn that have shown the same less displacement like the HDG tests, see Figure 2.6-4.) Therefore, 70 % of the mean slip load F_{Sm} was the limit that could not be hold permanently in the EXCTs. To prove this idea two tests at load levels of 70 % and 65 % were performed, see Figure 2.6-5.

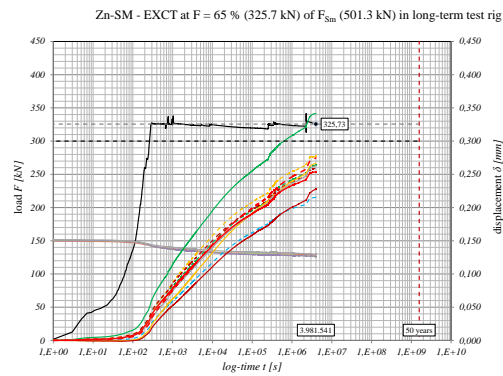
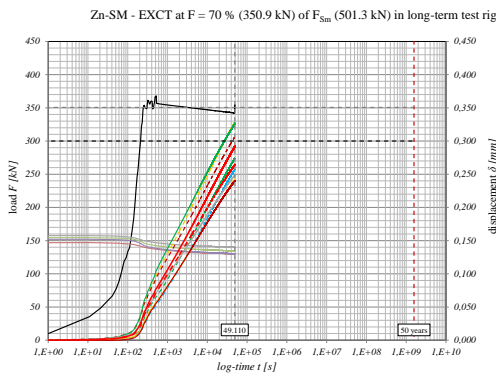


Figure 2.6-5: Extended creep test with 70 % and 65 % load for Zn-SM specimens

In the long-term step-test at 70 % of F_{Sm} no displacements up to $\delta < 0.3$ mm occurred (failure criterion of EN 1090-2, Annex G.5). Due to this it was assumed as the load, which would pass the EXCT. However, both specimen showed a high slope of displacement and the linear extrapolation exceeded the limit of 0.3 mm within 50 years. The connections did not pass the EXCT. Due to this, further tests had been performed with a load level of 60 %, see Figure 2.6-6.

The procedure of *long-term* and *short-term* step tests with steps of relative load levels from F_{Sm} given from Task 1.1 was performed for each coating system. It could be shown that the *long-term* variant did not work well for defining a load level for the first extended creep test. No displacements comparable to the slip load test were achieved. No slipping occurred at a load level of 90 % for the HDG *long-term step test*, see e.g. Figure 2.6-4, although the related extended creep test with a load level of 80 % failed, see Table 2.6-1. Therefore, the duration of each load step was reduced from 3 days to 90 min, including also positive economical and practical effects on the test procedure. The *short-term* step test could be a new adaption of the current procedure of EN 1090-2, Annex G and could replace the *creep test*.

As a main result of Task 1.4 the investigations show an alternative possibility for the current test procedure for determining slip factors μ for new coating systems for the faying surfaces of slip-resistant connections. The *short-term* step tests could substitute the actual *creep tests*. This *creep test* is only a ~ 3 h test at 90 % of the load and gives no answers for the mostly necessary extended creep test. As a result of the step tests a first load level for the extremely time-consuming extended creep tests could be estimated quite quickly so that the specimen would pass the tests.

Further interesting results of this project are the long-term stability or the creep behaviour of the investigated coatings for slip-resistant connections under permanent loading. This was possible because of the erection of autarkic test rigs that were especially built for this project, see Figure 2.6-7.

The results of the specimens tested in these test rigs are summarized in Figure 2.6-8.

Figure 2.6-8 shows the observations for the investigated coating systems (ASi-Zn - alkali-zinc silicate coating, HDG - hot dip galvanized, Zn-SM - zinc spray metallized and Al-SM - aluminium spray metallized).

Zn-SM: extended creep test with 60 % (300.8 kN) of F_{Sm} (501.3 kN)

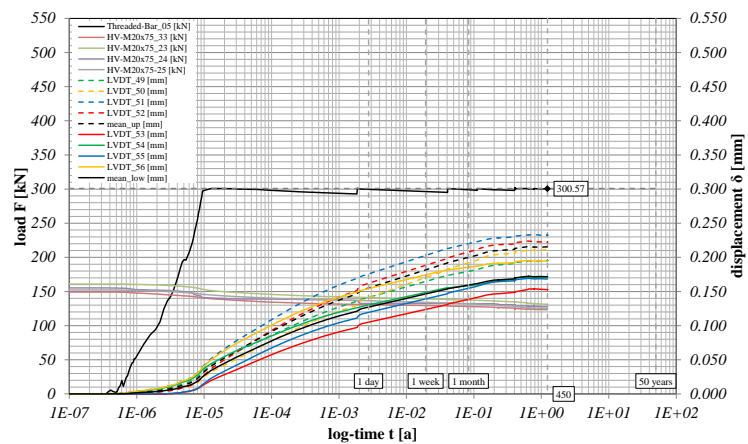


Figure 2.6-6: Extended creep test with 60 % for Zn-SM specimen (450 d test duration)

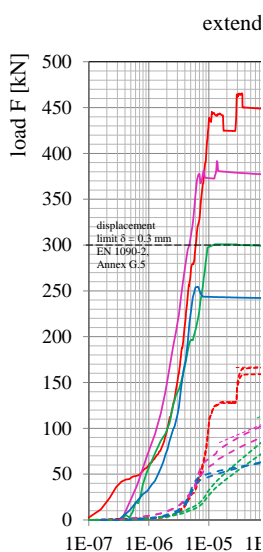


Figure 2.6-8: Summary of the observations of the creep behaviour for the coating systems

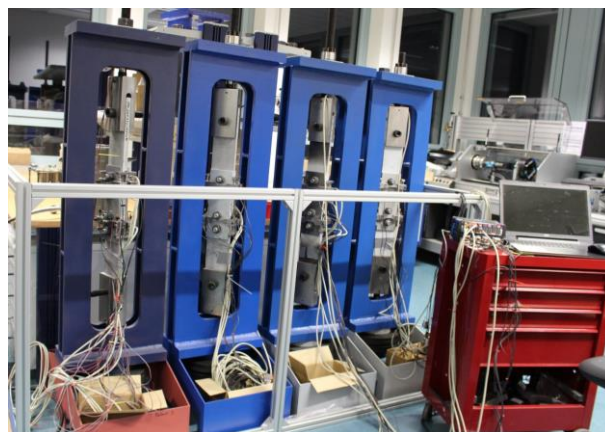


Figure 2.6-7: Autarkic test rigs for the investigations of the creep behaviour for the coating systems

2.7 Task 1.5 – Preloading procedures

The target development of tightening procedures for slip-resistant connections where the preload level is based on the 0.2 % remaining strain level of the bolt material instead of the ultimate stress level is related to the required experimental tightening tests. To achieve guaranteed preload levels in the elastic range with sufficient reliability, specific parameters (lubrication, tightening steps etc.) must be investigated in detail. Acc. to the Technical annex, and because the main influencing parameter in the tightening process is the lubrication of the nut, various lubrication types were tested (see Figure 2.7-1).

In a first step, evaluation of the performed tightening tests focused on the criteria of EN 14399-3 [5.7-1] and EN 14399-4 [5.3-2] to gain information regarding the complex basic preloading behaviour of the delivered bolting assemblies and to allow comparisons between the effectivity of the lubricants used and the resulting effects on tightening parameters, like torque, friction, and preload. On this basis, and considering the 0.2 % remaining strain level as an alternative preloading level, in-depth analysis of the achieved torques and angles of rotation at different preload levels ($F_{p,C}^* = 0.7 \cdot f_{yb} \cdot A_s$ and $F_{p,C} = 0.7 \cdot f_{ub} \cdot A_s$) is presented, including statistical evaluation. More on this subject, further discussion of preloading procedures (modified torque method and modified combined method) are provided in Deliverable report D1.5 – Task 1.5 “Preloading procedures to achieve a reduced preloading level in the elastic range of the bolt material with sufficient reliability”.



Figure 2.7-1: Task 1.5 – Types of lubrication

Test matrix and procedure

Experimental tightening tests of bolting assemblies were performed at the Institute for Metal and Lightweight Structures, University of Duisburg-Essen (UDE). The test programme is given in Table 2.7-1. The test matrix for tightening tests shows the bolt type (HR and HV), bolt dimension, strength classes of the bolts, and the lubrication used. For each series, 10 bolting assemblies were tested and evaluated.

In total, 24 series and 240 bolting assemblies were tested at UDE using the Institute’s tightening torque testing machine, divided into 160 assemblies for System HR (property class 8.8 and 10.9), and 80 assemblies for System HV (property class 10.9). All tightening tests were performed according to EN 14399-2 [5.7-2] and EN ISO 16047 [5.7-3].

Table 2.7-1: Task 1.5 – Test matrix for System HR and HV bolting assemblies

Lubrication	System HR / EN 14399-3:2015				System HV / EN 14399-4:2015	
	M24 8.8	M24 10.9	M36 8.8	M36 10.9	M24 10.9	M36 10.9
Factory provided	10/10	10/10	10/10	10/10	10/10	10/10
Gleitmo WSP 5040	10/10	10/10	10/10	10/10	10/10	10/10
Molykote 1000 spray	10/10	10/10	10/10	10/10	10/10	10/10
Microgleit HV-paste LP440	10/10	10/10	10/10	10/10	10/10	10/10

Concluded tightening tests

240 / 240 tests required acc. Technical Annex

Suitability for preloading and evaluation criteria

The suitability for preloading of high-strength structural bolting assemblies and the tightening test procedure are typically regulated by EN 14399-2 “High-strength structural bolting assemblies for

preloading – Part 2: Suitability for preloading” and valid for System HR (EN 14399-3) and System HV (EN 14399-4).

Figure 2.7-2 schematically visualizes a typical bolt force-angle of rotation curve and bolt force-tightening torque curve and defines relevant tightening and evaluation values. Furthermore, the determination of the k-value is graphically displayed.

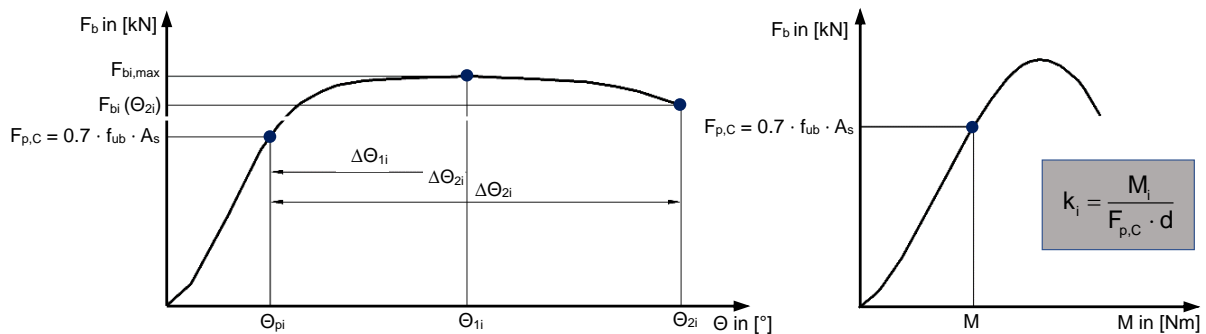


Figure 2.7-2: Tightening curves and criteria of evaluation acc. EN 14399-2 [5.7-2]

The criteria of evaluation of high-strength structural bolting assemblies for preloading, according to EN 14399-3:2015-04 and EN 14399-4:2015-04 are:

- $F_{bi,max} \geq 0.9 \cdot f_{ub} \cdot A_s$ in kN as *maximum individual value of bolt force during tightening*, where f_{ub} is the nominal tensile strength (R_m) and A_s is the nominal stress area of the bolt, ensuring that high bolt force levels can be sufficiently achieved.
- $F_{p,C} = 0.7 \cdot f_{ub} \cdot A_s$ in kN as specified preload level.
- The angle difference $\Delta\Theta_{1i}$, defined as $(\Theta_{1i} - \Theta_{pi})$, and corresponding to the point at which the maximum bolt force $F_{bi,max}$ has been reached.
- The angle difference $\Delta\Theta_{2i}$, defined as $(\Theta_{2i} - \Theta_{pi})$, and corresponding to the point at which the test has been stopped.
- Individual values of the k-factor (k_i) for k-class K1: $0.10 \leq k_i \leq 0.16$.
- Mean value of the k-factor (k_m) and the coefficient of variation of the k-factor (V_k) for k-class K2: $0.10 \leq k_m \leq 0.23$ and $V_k \leq 0.06$, see the following equations:

$$k_m = \frac{\sum_{i=1}^n k_i}{n}, \quad V_k = \frac{s_k}{k_m}, \quad s_k = \sqrt{\frac{\sum (k_i - k_m)^2}{n-1}}.$$

- Additionally in the frame of this research $F_{p,C}^* = 0.7 \cdot f_{yb} \cdot A_s$ as alternate preloading in the context of quantitative improvement of serviceability, where f_{yb} is the nominal yield strength, acc. to DIN EN 1993-1-8/NA:2010-10.

Main results and evaluation of tightening tests

Table 2.7-2 shows a summary of the evaluation of the tested M24/M36 System HR and HV bolting assemblies after finishing tightening tests for Task 1.5.

Table 2.7-2: Summary of the evaluation of tightening tests acc. to EN 14399-3 and EN 14399-4

Tested series	n [-]	$F_{p,C}^*$	$F_{p,C}$	$F_{bl,max}$	$\Delta\theta_{1,min}$	$\Delta\theta_{2,min}$	k-values	k-class K1	k-class K2		Fracture
							[-]	$0.10 \leq k_1 \leq 0.16$	$0.10 \leq k_m \leq 0.23$	$V_k \leq 0.06$	
System HR: M24x100 8.8											
Factory provided	10	100%	100%	100%	100%	100%	0.12 – 0.14	100%	0,130	0,029	0%
Gleitmo WSP 5040	10	100%	100%	100%	100%	100%	0.13 – 0.15	100%	0,141	0,045	0%
Molykote 1000 spray	10	100%	100%	100%	100%	100%	0.12 – 0.14	100%	0,128	0,047	0%
Microgleit HV-paste LP440	10	100%	100%	100%	100%	100%	0.14 – 0.16	100%	0,148	0,058	40%
System HR: M24x100 10.9											
Factory provided	10	100%	100%	100%	100%	100%	0.12 – 0.14	100%	0,129	0,053	0%
Gleitmo WSP 5040	10	100%	100%	100%	100%	100%	0.13 – 0.15	100%	0,136	0,043	0%
Molykote 1000 spray	10	100%	100%	100%	100%	100%	0.12 – 0.14	100%	0,127	0,044	0%
Microgleit HV-paste LP440	10	100%	100%	100%	100%	100%	0.13 – 0.15	100%	0,139	0,052	0%
System HR: M36x160 8.8											
Factory provided	10	100%	70%	0%	20%	30%	0.12 – 0.14	0%	0,287	0,147	30%
Gleitmo WSP 5040	10	100%	100%	30%	80%	90%	0.15 – 0.18	50%	0,166	0,067	30%
Molykote 1000 spray	10	100%	100%	90%	100%	100%	0.14 – 0.17	40%	0,161	0,066	0%
Microgleit HV-paste LP440	10	100%	100%	10%	100%	100%	0.21 – 0.25	0%	0,227	0,069	50%
System HR: M36x160 10.9											
Factory provided	10	100%	100%	0%	40%	0%	0.22 – 0.37	0%	0,267	0,157	20%
Gleitmo WSP 5040	10	100%	100%	40%	60%	80%	0.14 – 0.19	80%	0,153	0,099	20%
Molykote 1000 spray	10	100%	100%	80%	90%	100%	0.14 – 0.17	90%	0,151	0,069	10%
Microgleit HV-paste LP440	10	100%	100%	20%	90%	100%	0.17 – 0.23	0%	0,199	0,094	50%
System HV: M24x100 10.9											
Factory provided	10	100%	100%	0%	100%	100%	0.14 – 0.17	40%	0,158	0,085	10%
Gleitmo WSP 5040	10	100%	100%	80%	100%	100%	0.14 – 0.16	80%	0,152	0,042	0%
Molykote 1000 spray	10	100%	100%	80%	70%	100%	0.14 – 0.16	90%	0,146	0,057	0%
Microgleit HV-paste LP440	10	100%	100%	80%	100%	100%	0.16 – 0.21	10%	0,180	0,086	0%
System HV: M36x160 10.9											
Factory provided	10	100%	100%	30%	100%	90%	0.13 – 0.22	10%	0,184	0,125	40%
Gleitmo WSP 5040	10	100%	100%	100%	100%	100%	0.13 – 0.15	100%	0,140	0,035	0%
Molykote 1000 spray	10	100%	100%	100%	100%	100%	0.12 – 0.16	90%	0,134	0,087	0%
Microgleit HV-paste LP440	10	100%	100%	100%	100%	100%	0.16 – 0.22	0%	0,192	0,096	0%

Considering the evaluation results acc. to EN 14399-3 (System HR) and EN 14399-4 (System HV), a comparison between the various lubrications led to the following conclusions:

- All three lubrications and factory provided series reached the specified preload of $F_{p,C}^* = 0.7 \cdot f_{yb} \cdot A_s$, as well as $F_{p,C} = 0.7 \cdot f_{ub} \cdot A_s$ with the exception of HR M36 8.8 series, where only 7 of 10 bolts achieved both preloading levels.
- In terms of HV bolting assemblies, best results were achieved with Gleitmo WSP 5040 and Molykote 1000 spray. The k-values at $F_{p,C}$ stood out due to low scatterings (0.12 - 0.16) and low coefficients of variation V_k . Gleitmo WSP 5040 and Molykote 1000 spray significantly decreased the frictions μ_{tot} and μ_{th} and led to k-values in a narrow range (e.g. 0.14 - 0.16 for M24x100 10.9 series). k-class K2 was accomplished (with the exception of HV M36x160 10.9 series and Molykote 1000 due to coefficient of variation $V_k = 8.7 \% > 6 \%$).
- In terms of HR bolting assemblies, a distinction must be made between bolt dimension M24 and M36:

For bolt dimension M24, every tested lubrication showed satisfactory test results, in addition to the factory provided bolting assemblies. The k-classes K1 and K2 were accomplished in each tested series with low coefficients of variation V_k (2.9 - 5.8 %). Bolt fracture occurred only in one series, and only when turning off the hexagon nut after the end of the test procedure.

For bolt dimension M36, k-class K2 failed in each tested series, while k-class K1 and other criteria acc. to EN 14399-3:2015-04 were only partially accomplished. Bolt fracture occurred in nearly all tested HR M36 series. However, it must be emphasized that the M36 HR bolting assemblies were delivered from another manufacturer as k-class K0. In this context, better tightening test results were achieved by using Molykote 1000 spray lubrication.

Furthermore, Figure 2.7-3 shows exemplarily the tightening curves of HR M24x100 8.8 series comparing factory provided lubrication (black) and Molykote 1000 spray (yellow), characterised by slightly reduced scattering. In addition, Figure 2.7-4 presents the tightening curves of HR M36x160 10.9 series comparing factory provided lubrication and Gleitmo WSP 5040 lubrication. The positive effects of alternative lubrication are a significant improvement of ductility.

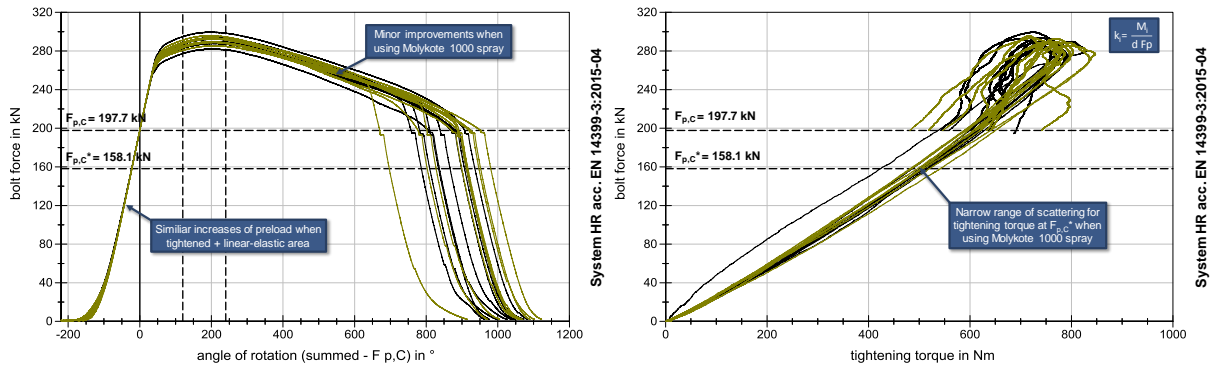


Figure 2.7-3: Comparison between HR M24x100 8.8 – factory provided (black) and Molykote 1000 (yellow)

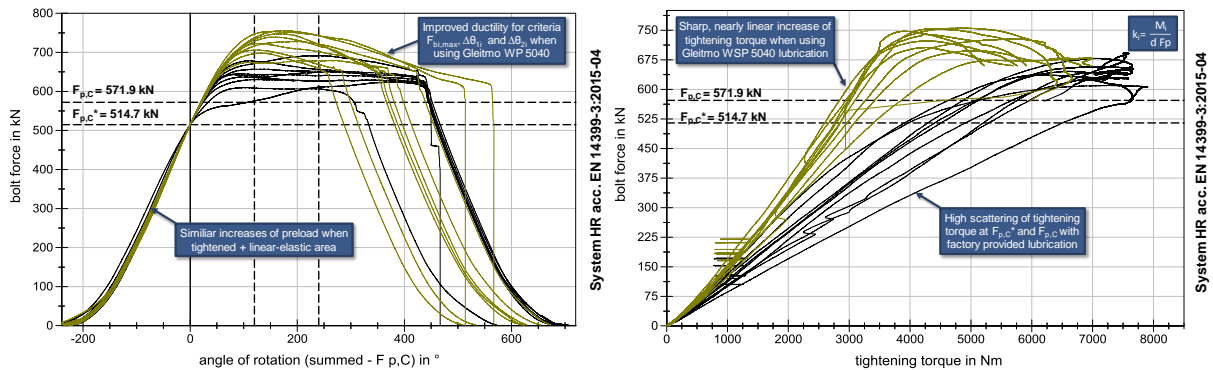


Figure 2.7-4: Comparison between HR M36x160 10.9 – factory provided (black) and Molykote 1000 (yellow)

Recommendation of tightening methods to achieve a reduced preloading level in the elastic range of the bolt material with sufficient reliability

The evaluation of the tightening tests for preloading procedures to achieve a reduced preloading level in the elastic range of the bolt material with sufficient reliability was based on the German modified torque method and the modified combined method according to DIN EN 1993-1-8/NA [5.7-4]. The target level of preloading for these tightening methods was $F_{p,C}^* = 0.7 \cdot f_{yb} \cdot A_s$. It is to note that the required tightening torques, and additional angle of rotations must be determined experimentally for each specific lubrication in a tightening test. The scattering of tightening parameters must be considered as well as the maximum preload level to avoid overtightening of the bolting assemblies, especially when a re-use of the bolting assemblies is intended. Table 2.7-3 shows the summary of the evaluation of the modified torque method and modified combined method acc. to DIN EN 1993-1-8/NA for all tested carbon steel HR/HV bolting assemblies. Additionally, Figure 2.7-5 summarizes the achieved preloads of HR bolting assemblies in property class 8.8 and 10.9.

Table 2.7-3: Summary of the evaluation of the modified torque method and modified combined method acc. to DIN EN 1993-1-8/NA for all tested carbon steel HR/HV bolting assemblies

Tested series	Modified torque method acc. DIN EN 1993-1-8/NA					Modified combined method acc. DIN EN 1993-1-8/NA					
	$F_{p,C}^*$ achieved?	Minimum achieved bolt force	Maximum achieved bolt force	range	Vk [%]	$F_{p,C}^*$ achieved?	Minimum achieved bolt force	Maximum achieved bolt force	range	Vk [%]	
System HR: M24x100 8.8		$M_A = 600 \text{ Nm acc. Table NA.A.1}$					not valid for strength class 8.8				
Factory provided	100%	180,2	201,6	21,4	3,13	-	-	-	-	-	
Gleitmo WSP 5040	90%	156,4	190,6	34,2	5,52	-	-	-	-	-	
Molykote 1000 spray	100%	178,8	214,9	36,1	5,20	-	-	-	-	-	
Microgleit HV-paste LP440	80%	151	182,9	31,9	5,73	-	-	-	-	-	
System HR: M24x100 10.9		$M_A = 800 \text{ Nm acc. Table NA.A.2}$					$M_{A,MKV} = 600 \text{ Nm} + \vartheta_{MKV} = 60^\circ$				
Factory provided	100%	235,2	275,8	40,6	5,62	100%	278,4	304,6	26,2	3,42	
Gleitmo WSP 5040	100%	222,9	261,3	38,4	4,69	100%	268,0	296,1	28,1	2,89	
Molykote 1000 spray	100%	236,7	281,9	45,2	4,64	100%	285,1	309,3	24,2	2,19	
Microgleit HV-paste LP440	90%	221,0	255,9	34,9	4,71	100%	270,2	300,9	30,7	3,42	
System HR: M36x160 8.8		$M_A = 2100 \text{ Nm acc. Table NA.A.1}$					not valid for strength class 8.8				
Factory provided	0%	197,7	260,3	62,6	9,69	-	-	-	-	-	
Gleitmo WSP 5040	10%	303,1	370,7	67,6	6,11	-	-	-	-	-	
Molykote 1000 spray	30%	318,7	396,4	77,7	7,08	-	-	-	-	-	
Microgleit HV-paste LP440	0%	225,9	278,3	52,4	6,95	-	-	-	-	-	
System HR: M36x160 10.9		$M_A = 2800 \text{ Nm acc. Table NA.A.2}$					$M_{A,MKV} = 2100 \text{ Nm} + \vartheta_{MKV} = 60^\circ$				
Factory provided	0%	236,0	408,0	172,0	15,30	0%	355,8	483,0	127,2	9,60	
Gleitmo WSP 5040	40%	427,1	563,4	136,3	8,34	90%	498,7	572,9	74,2	3,97	
Molykote 1000 spray	40%	463,6	575,6	112,0	7,24	100%	535,3	608,8	73,5	4,57	
Microgleit HV-paste LP440	0%	339,5	448,6	109,1	9,42	0%	433,4	510,7	77,3	5,22	
System HV: M24x100 10.9		$M_A = 800 \text{ Nm acc. Table NA.A.2}$					$M_{A,MKV} = 600 \text{ Nm} + \vartheta_{MKV} = 60^\circ$				
Factory provided	30%	186,3	241,5	55,2	10,28	100%	244,7	287,9	43,2	5,71	
Gleitmo WSP 5040	10%	190,7	230,2	39,5	5,07	100%	244,4	270,5	26,1	3,00	
Molykote 1000 spray	60%	200,8	244,3	43,5	6,19	100%	259,4	291,7	32,3	4,34	
Microgleit HV-paste LP440	0%	178,6	205,8	27,2	5,26	100%	240,7	265,9	25,2	3,32	
System HV: M36x160 10.9		$M_A = 2800 \text{ Nm acc. Table NA.A.2}$					$M_{A,MKV} = 2100 \text{ Nm} + \vartheta_{MKV} = 60^\circ$				
Factory provided	10%	385,9	583,2	197,3	13,93	30%	485,9	619,3	133,4	7,84	
Gleitmo WSP 5040	100%	530,3	594,4	64,1	4,46	100%	571,4	613,0	41,6	2,28	
Molykote 1000 spray	90%	478,0	671,1	193,1	10,02	100%	555,2	665,4	110,2	5,77	
Microgleit HV-paste LP440	0%	368,4	465,2	96,8	7,52	50%	471,2	558,4	87,2	5,46	

M24 8.8: $F_{p,C}^* = 158,1 \text{ kN}$ M24 10.9: $F_{p,C}^* = 222,4 \text{ kN}$ M36 8.8: $F_{p,C}^* = 366,0 \text{ kN}$ M36 10.9: $F_{p,C}^* = 514,7 \text{ kN}$

When using the modified torque method according to DIN EN 1993-1-8/NA, it could be shown that $F_{p,C}^*$ was achieved mainly for M24x100 HR bolting assemblies in strength class 8.8 and 10.9. However, the required preloading level $F_{p,C}^*$ for M36x160 HR bolting assemblies in strength class 8.8 and 10.9 was only partially achieved when using Gleitmo WSP 5040 and Molykote 1000 spray lubricants, and the factory provided and Microgleit HV-paste LP440 tested series failed completely. The modified torque method also showed inhomogeneous test results for HV bolting assemblies, the reduced preload $F_{p,C}^*$ was also only partially achieved. The application of the modified combined method was only valid for bolting assemblies in strength class 10.9 and all tested series of M24x100 HR 10.9 and M24x100 HV 10.9 HV achieved the required preload $F_{p,C}^*$. However, the required preloading level $F_{p,C}^*$ for M36x160 HR 10.9 and M36x160 HV 10.9 bolting assemblies was again only partially achieved or failed completely. The best results were achieved when using Gleitmo WSP 5040 and Molykote 1000 spray lubricants.

Nevertheless, adjusted tightening torques and angles of rotation can be determined to achieve reduced preload level $F_{p,C}^*$ with suitable reliability for tightening in the elastic range depending on the tightening method. Additionally, limiting criteria must be defined to control the achieved level of preload to avoid overtightening and plastic deformations when a re-use of the bolting assemblies is intended.

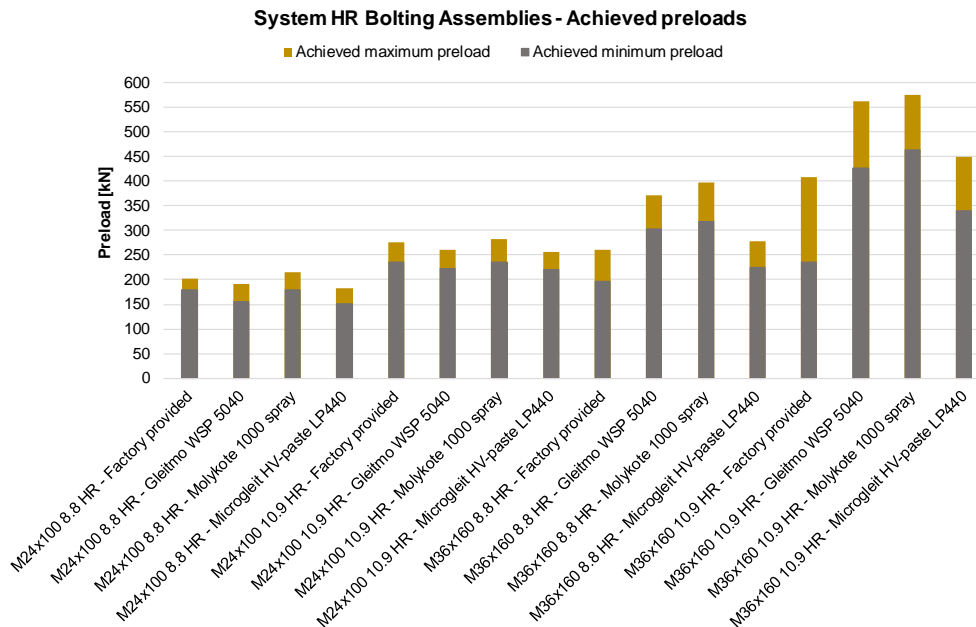


Figure 2.7-5: Achieved preloads of HR bolting assemblies in property class 8.8 and 10.9

3 WP 2 – Long term effects (CS)

3.1 Objectives of WP

In EN 1993-1-8 for preloaded connections the preload is related to the ultimate tensile stress of the bolt material. In EN 1090-2 rules are given how to perform the tightening of the bolts dependent on the chosen tightening method in order to reach the intended preload in the bolts of slip-resistant connections. In these rules attention is paid to the fact that after performing the tightening the preload in the bolts will decrease due to deformations in the threads of the bolts and nuts. This effect is compensated by a certain "overload" when using the torque method and when using the turn of the nut method or the combined method, this compensation is not necessary. The effect of creep caused by compressing the applied surface treatment such as galvanising or paint is of course investigated in the procedure of determining the slip-factor.

However, when the preload will be related to the equivalent yield stress level of the bolt material, only the torque-based tightening methods can be used. Then the reliability of the slip-resistance of the connection relies not only on the reliability of the friction coefficient but also on the reliability of the level of preload in the bolts.

The work programme aims at obtaining sufficient theoretical and experimental evidence to improve and extend the existing rules in EN 1993-1-8 and in EN 1090-2.

3.2 Work undertaken

The tasks undertaken in WP 2:

- 2.1 Comparative study on the influence of different levels of preload on the reliability of slip-resistant connections.
- 2.2 Comparative study on the influence of bolts preloaded in the plastic range vs. bolts preloaded in the elastic range only.
- 2.3 Development of a procedure how to determine the pre-load of bolts in slip-resistant connections of existing structures.

The work undertaken for Tasks 2.1 to 2.3 is summarized in Sections 6.3 - 6.5.

Exploitation of the research results of this WP

The research results of this WP were published in seven journal and conference papers: (3), (4), (12) to (16), see Chapter 2, Publications.

3.3 Task 2.1 – Different preload levels

Work undertaken

Slip factor tests were carried out to investigate the influence of the bolt type (HR vs HV) and the bolt class (HR 8.8 vs HR 10.9) on the slip factor of zinc spray metallized and alkali silicate zinc coated surfaces. For both creep sensitive coatings, the short term slip factor tests and extended creep tests were carried out. Extended creep test rigs have been developed and built for this purpose. The practical problems, which the extended creep tests to determine the long-term slip factors typically encountered, have enabled to use an initiative investigation an experimental procedure to estimate the load level for extended creep tests. The tests with short stepwise loading was merely done in addition to the tests mentioned in the Technical Annex for Task 2.1.

Introduction

In HSFG connection bolts of class 10.9 and also bolts of class 8.8 can be used. The high preload force in 10.9 bolts potentially leads to more creep of coatings and also more ‘flattening’ of the plate surfaces compared to the preload in bolts 8.8, which influences the slip factor. For this reason, EN 1090-2 [5.3-1] allows slip factors of surfaces and coating systems that were determined by tests on specimens which were preloaded with bolt classes 10.9 could be used to calculate the design slip resistance of connections preloaded with bolt class 8.8. The other way around this is not allowed.

It is unclear if and to what extent slip factors determined by tests with 10.9 bolts change when 8.8 bolts are used. If there is any of the preload, it is somehow vague that this should apply only to the short term slip factor, or also to the sensitivity of the creep/long term slip factor. Bolt class 8.8 is only available as HR bolts, while class 10.9 is available as HV and HR ones. In the frame of this work package slip factor tests were carried out on carbon steel plates with 2 different coating systems with variation of the considered bolt types (HR and HV) and classes (8.8 and 10.9).

Study performed

A comparative study was performed to assess the influence of the bolt preload ($F_{p,C,HR8.8} = 138$ kN vs $F_{p,C,HR10.9} = 172$ kN) on the slip factor of zinc spray metallized (ZnSM) and alkali zinc silicate coated (ASi) surfaces. Both ZnSM and ASi series are known as creep sensitive coatings. Therefore, investigations on the influence of the preload level extended creep tests are necessary. It was anticipated that:

- higher levels of preloading in bolts would have a negative influence on the slip factor;
- the influence of the preload level on the short term slip factors would be different from influence on the long-term slip factors.

In addition to the original objectives, slip tests were performed on grit blasted, ASiZn and ZnSM surfaces to investigate the influence of the clamp length (48 mm vs 152 mm) on the result of slip factor tests.

Methods and Materials

All experiments have been carried out on double lap shear connections cf. Annex G of EN 1090-2 [5.3-1] using M20 bolts. The steel plates used for all experiments were grade S355J2C+N. An overview of the test specimen and surface conditions is presented in Table 3.3-1.

Extended Creep Tests

The main goal of the research is to compare the long-term slip factor for 2 creep sensitive coatings (ZnSM and ASiZn) preloaded with class 8.8 and 10.9 bolts. To make this comparison, the maximum load that can be transferred without exceeding the 0.3 mm in 50 years criterion has to be determined. The idea was to find this load by performing extended creep tests on the plates.

Table 3.3-1: Test specimens and surface conditions

Series ID	Surface preparation		Clamp length Σt [mm]	Clamp length ratio $\Sigma t/d^2$ [-]	Number of tests in this task		
	Coating material	coating thickness ¹⁾			Static test	Creep test	Extended creep test
Grit-blasted Sa 2 ½ (R _z : 84 µm) + ASi-Zn coating							
ASiZn	alkali-zinc silicate	55 µm	48	2.4	8	2	6
Grit-blasted Sa 3 (R _z : 100 µm) + Zn-SM coating (R _z after coating 85 µm)							
Zn-SM	Zinc spray metallized	165 µm	48	2.4	8	2	6
Level of preload F _{p,c} = 172 kN (M20) ¹⁾ Nominal dry film thickness (DFT) ²⁾ d = 20 mm							

An extended creep test is a 'Proof Loading' procedure which is used for proving that the long-term slip is less than or equal to 0.3 mm over a period of 50 years. It is not a test for determining the load that leads to a predefined slip over time. By performing a series of extended creep tests on a surface, one can find an indication of the maximum load that can be transferred. However, it is not practically feasible to determine the long term slip factors precisely.

As there was no knowledge of the long-term slip factors for the various combinations of coatings and preloads, a 'trial and error' approach was followed to estimate the slip factors in which initially 0.75 F_{Sm} (75% of the average of the short-term slip tests) was applied as load in the extended creep tests.

Result short-term slip factor tests

In Table 3.3-2 the results of the short-term (quasi-static) slip factor tests are summarized, evaluated by considering the initial preload when the tests started ($\mu_{init,mean}$) and the actual preload at slip ($\mu_{act,mean}$). Table 3.3-2 also shows the influence of the clamp length of the bolts on the results of a slip factor test.

Table 3.3-2: Results quasi static slip factor tests

specimen batch	surface treatment / R _z ²⁾	film thickness (average)	Σt	bolt class	F _{p,c}	number of test results (n)	slip factor $\mu_{act,mean}$ ³⁾	slip factor $\mu_{init,mean}$ ⁴⁾	ratio	ratio
									$\mu_{init,mean}$ at $\Sigma t=152$ vs $\Sigma t=48$ mm	$\mu_{init,mean}$ at F _{p,c} =138 vs F _{p,c} =172 kN
	[µm]	[µm]	[mm]		[kN]		[-]	[-]	[-]	[-]
Grit blasted surfaces (GB)										
wp1.2	Sa 1) 2½ / 80	-	152	HV10.9	172	6	0,84	0,79	1,14	
			48			4	0,81	0,69		
			48	HR10.9	2	0,80	0,70	1,05		
				HR 8.8	4	0,85	0,74			
Alkali-zinc silicate coating (ASiZn)										
wp1.2	Sa 2½ / 80	62	152	HV10.9	172	24	0,76	0,72	1,07	
wp2.1	Sa 2½ / 84	55	48	HR10.9		4	0,76	0,68	1,06	
				HR 8.8	138	8	0,78	0,69		
				HR 8.8	138	8	0,84	0,73		
Zinc spray metalized coating (ZnSM)										
wp1.2	Sa 3 / 104	140	152	HV10.9	172	6	0,83	0,79	1,08	
			48			4	0,82	0,73		
wp2.1	Sa 3 / 100	165	48	HR10.9		8	0,73	0,65	1,21	
				HR 8.8	138	8	0,91	0,79		

¹⁾ Sa: surface preparation grade | ²⁾ R_z: roughness steel surface | ³⁾ $\mu_{ini,mean}$: slip factor (mean values) considering the initial preload when the tests started | ⁴⁾ $\mu_{act,mean}$: slip factor (mean values) considering the actual preload at slip

Results extended creep tests

The influence of preload on long-term slip factor is shown in Table 3.3-3.

Table 3.3-3: Influence of preload on long term slip factor

specimen batch	parameters				load at 0.15 mm slip				slip factors	
	surface treatment Rz	film thickness	clamp length (CL)	bolt class	$F_{P,c,nom}$	$F_{s,m}$	$\mu_{init,mean}$	$\mu_{nom,exc}$	ratio slip factors at $F_{P,c,nom}=138$ kN vs $F_{P,c,nom}=172$ kN	
	[μ m]	[μ m]	[mm]		[kN]	[kN]	[-]	[-]	$\mu_{init,mean}$	$\mu_{nom,exc}$
wp1.2	Grit blasted (GB)									
	80	-	48	HR10.9	172	483	0.70	-	1.05	-
				HR 8.8	138	415	0.74	-		
	Alkali-zinc silicate coating (ASiZn)									
85	85	48	HR10.9	172	470	0.69	0.59	1.06	1.10	
			HR 8.8	138	405	0.73	0.65			
Zinc spray metalized coating (ZnSM)										
wp2.1	100	165	48	HR10.9	172	442	0.65	0.42	1.21	1.14
				HR 8.8	138	439	0.79	0.48		

Short stepwise loading procedure

Searching about long-term slip factor of new coating systems could be time consuming. Series of extended creep tests have to be performed to determine the maximum load level for which the slip after 50 years is still below the threshold value of 0.3 mm. The process described in EN 1090-2 [5.3-1] Annex G, in which the load is increased stepwisely until the (on the log timescale linearly) extrapolated slip exceeds 0.3 mm before $t = 50$ years, typically takes weeks. After this procedure 3 additional extended creep tests on the load level that was found are necessary to prove the slip factor. In these tests the load level is directly brought to the required level and should be kept constant over the entire test period.

The SSWL test protocol is introduced in the project to develop a means to a quick estimation of the maximum load level that can be achieved in extended creep tests. In an SSWL test the load on the specimen is kept constant over periods of 1.5 h. The initial loading is set to 60 % of the mean slip load that was found in the short term slip factor tests of the coating ($F_{s,m}$) and the load is raised with 5 % of $F_{s,m}$ until a slip of 0.3 mm at CBG is reached.

During each load step the development of the slip speed is evaluated. The slip speed appears to be not constant over the 1.5 h periods; it is therefore calculated over 3 intervals of 25 minutes:

- 10 – 35 minutes
- 35 – 60 minutes
- 60 – 85 minutes

The hypothesis is that there is a ‘critical SSWL test slip speed’, independent of the coating system that can be used to estimate the long duration slip load level for creep sensitive coatings. The hypothesis can be tested by combining the results of extended creep tests and the SSWL tests. This way the SSWL slip speed can be determined that is associated with the load level at which the extended creep test still passes. This can be seen as the *critical SSWL slip speed*. Load levels with lower SSWL slip speed would pass the ECT test, load levels while with higher slip speed would not.

Figure 3.3-1 gives an example of the result of a SSWL test and the way it is combined with the results of the extended creep tests to find the critical SSWL slip speed. The graph shows that after the initial load application ($0 - 60\%F_{s,m}$) the specimens show high slip speeds. In subsequent loading steps (in which there is a $5\%F_{s,m}$ increase of the load) the slip speed first reduces until a minimum is reached. From a certain load level on, the slip speed increases with increasing load. The critical SSWL slip speed for the series is defined as the slip speed at the load level that the extended creep test for the series still (just) passes. Figure 3.3-1 shows how the results of SSWL and extended creep tests were combined to find the critical slip speed for the ZnSM-10.9 series ($0.1 - 0.15 \mu\text{m}/\text{min}$).

Figure 3.3-2 illustrates intended use of SSWL test result for new coatings: the (generic) critical SSWL slip rate ($0.12 \mu\text{m}/\text{min}$) is used to get an indication of the maximum load level that will pass (slip <

0.3 mm over 50 years) during extended creep tests on the coating. SSWL testing is not intended to be a replacement for extended creep tests.

Further researches are needed to proof the value of SSWL tests to estimate critical load levels for long-term loadings and/or use SSWL tests to estimate the influence of the preload on the long-term slip behaviour.

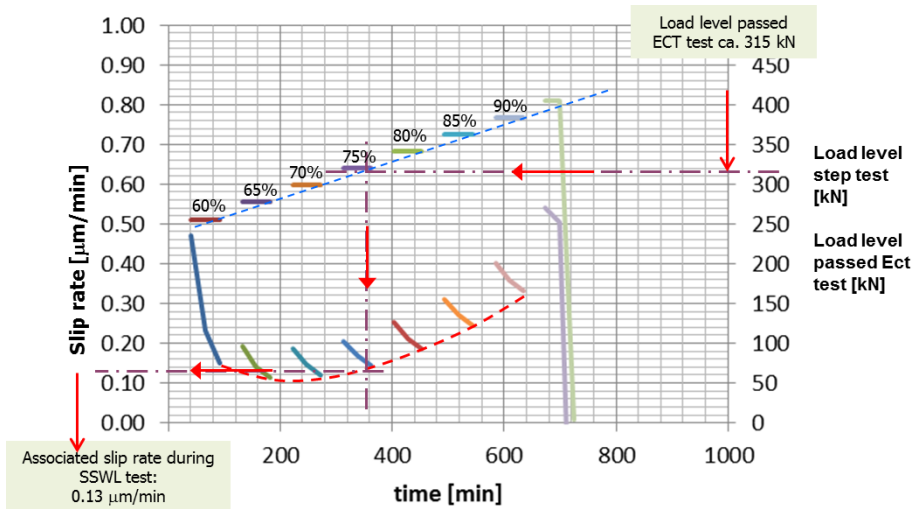


Figure 3.3-1: Combined results of SSWL and extended creep test

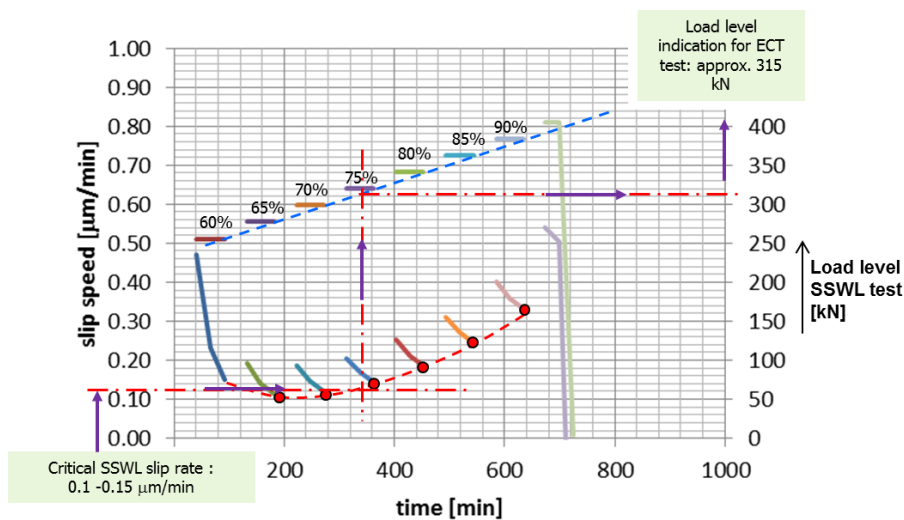


Figure 3.3-2: Illustration of intended use of SSWL test result for new coatings

Conclusions

In Task 2.1 a comparative study was performed to the influence of the bolt preload ($F_{p,C,HR8.8} = 138 \text{ kN}$ vs $F_{p,C,HR10.9} = 172 \text{ kN}$) on the slip factor of Zinc spray metallized (ZnSM) and Alkali Silica Zinc coated (ASiZn) surfaces. From this study it can be concluded that:

1. The type of the bolt (HR / HV) that is used in slip factor tests has no influence on slip factor;
2. Slip factors determined according to EN1090-2 depend on the preload level during the test. On both, the short term slip factor and the long term slip factor, a positive influence of the lower preload of bolt class 8.8 (preloaded to 138 kN) compared to 10.9 (preloaded to 172 kN) was observed. The following influences were found:

Grit blasted (S355, Rz = 80 µm):	+5%
ASiZn (S355, Rz=85 µm, DFT=85 µm):	+6% / +10% (short / long)
ZnSM (S355, Rz=100 µm, Ct=165 µm):	+21% / +14%

3. No general conclusions can be drawn on the magnitude of the influence, this is depending on the properties of the coating (system, coating thickness);
4. In a limited study, no further negative influence on the slip factor was found for preload levels above 172 kN;
5. Experiments with the Short StepWise Loading (SSWL) protocol to estimate the load level, which can be used to determine the slip factor for creep sensitive coatings in extended creep tests, is promising. More research is needed to proof the value of the proposed procedure.

3.4 Task 2.2 – Plastic vs. elastic preloading

EN 1090-2 [5.3-1] defines a preload level of $F_{p,C} = 0.7 f_{ub} A_s$ up to now. Preloading up to $F_{p,C}$ yields to plastic deformation in the bolt resp. in the thread combination of bolt and nut. For some reasons (e.g. reuse of the bolt), it might be useful to offer a second preload level, where the bolt is preloaded up to the elastic range only. $F_{p,C}^* = 0.7 f_{yb} A_s$ is such a reasonable second preload level. Currently available standards do not address the influence of a lower preload level on the slip resistance behaviour of the bolted connections. In Task 1.1 and 1.4, the influence of different surface conditions was investigated. All tests performed in these tasks were preloaded to $F_{p,C}$ level. In the present task two smaller preload levels ($F_{p,C}^*$ and $0.9 F_{p,C}^*$) were selected, in order to investigate the influence of the preload level especially on the long-term behaviour of slip resistant connections.

Experimental Investigations

In order to investigate the influence of different surface conditions and preload levels, three different surface conditions were considered, see Table 3.4-1: (1) alkali-zinc silicate (ASI-Zn)-coating, (2) spray metallized with zinc (SM-Zn) and (3) a combination of zinc metalized-alkali-zinc silicate coating (ASI – Zn-SM). The results of this task were compared with the results of Task 1.1 and 1.4 to investigate the influence of different preload levels on the determination of the slip factor. All static, creep and extended tests with preload level $F_{p,C}$ were covered by Task 1.1 and Task 1.4 and the results presented in this task, too. All specimens were made of steel S355J2+N. The test specimen geometry was chosen for the test specimen with M20 bolts as shown in Figure 3.4-1 (a). For each test specimen four M20 HV bolts class 10.9 were instrumented with a strain gauge, see Figure 3.4-1 (b). Three different levels of preloads ($F_{p,C}$, $F_{p,C}^*$ and $0.9 F_{p,C}^*$) were chosen. Herein, $F_{p,C}^*$ is defined as $F_{p,C}^* = 0.7 f_{yb} A_s = 160$ kN (with f_{yb} : nominal yield strength of the bolt and A_s : tensile stress area of the bolt) and $0.9 F_{p,C}^* = 144$ kN. $F_{p,C}$ is defined as $F_{p,C} = 0.7 f_{ub} A_s = 172$ kN (with f_{ub} : nominal tensile strength of the bolt and A_s : tensile stress area of the bolt). The slip displacements were measured in two different positions: CBG (centre bolts group) and PE (plate edges) positions. CBG and PE positions consist of 8 (LVDTs 1-8) and 4 (LVDTs 9-12) displacement transducers respectively, as shown in, see Figure 3.4-1 (c). In the present investigation, the slip factors were evaluated based on the measured slip displacement in CBG position. Figure 3.4-1 (d) shows the test setup used for the comparative study to investigate the influence of different preload levels. The slip load F_{Si} was determined at 0.15 mm slip or at the highest peak before. The mean values of the static slip factors by considering the initial preload when the tests started ($\mu_{ini,mean}$) as well as the actual preload at slip ($\mu_{act,mean}$) and the characteristic values ($\mu_{5\%}$ for a passed creep test and μ_{ect} based on a passed extended creep test) are presented in Table 3.4-1.

The influence of different preload levels for the ASI-surface condition is shown in Figure 3.4-2. The results show that the slip load increases slightly with increasing preload. However, only a minor difference can be observed for the actual slip factor. The actual static slip factor for the specimens with preload level of $0.9 F_{p,C}^*$ ($\mu_{act,mean} = 0.79$) is slightly higher than the $\mu_{act,mean}$ value obtained from the specimens with $F_{p,C}$ ($\mu_{act,mean} = 0.77$), see Table 3.4-1. The initial static slip factor was approximately the same for the specimens with the preload levels of $0.9 F_{p,C}^*$ ($\mu_{ini,mean} = 0.69$) and $F_{p,C}$ ($\mu_{ini,mean} = 0.70$).

Table 3.4-1: Mean slip factors based on static and creep tests only ($\mu_{ini,mean}$ and $\mu_{act,mean}$) as well as final slip factors calculated as 5% fractile or determined in the extended creep test ($\mu_{5\%}$ or μ_{ect})

Series ID	Surface preparation	$\Sigma t^{(4)}$ [mm]	Preload [kN]	Number of tests	$\mu_{ini,mean}^{(6)}$	$\mu_{act,mean}^{(7)}$	$V(\mu_{act})^{(8)}$	Final slip factor [-]
-----------	---------------------	-----------------------	--------------	-----------------	------------------------	------------------------	----------------------	-----------------------

	Sa ¹⁾ / Rz ²⁾ [µm]	DFT ³⁾ [µm]	st/(sp)ct/ect ⁵⁾			st/st+ct [-]	st/st+ct [-]	st/st+ct [%]	µ _{5%} ⁹⁾ / µ _{ect} ¹¹⁾
Alkali-zinc silicate coating (ASI)									
ASI-III	Sa 2½ / 80	60	52/48 ⁷⁾	F _{p,C}	2/(3)/2	0.70/-	0.77/-	2.9/-	-/0.56
ASI-IV			48	F _{p,C} *	4/1/3	0.69/-	0.79/-	1.1/-	-/0.63
Zinc spray metalized coating (Zn-SM)									
Zn-SM-II	Sa 3 / 100	140	52/48 ⁷⁾	F _{p,C}	2/(2)/4	0.73/-	0.82/-	2.7/-	-/0.44
Zn-SM-III		48	F _{p,C} *	4/-/4	0.74/-	0.83/-	2.2/-	-/0.48	
Zn-SM-IV		164	48	0.9 F _{p,C} *	4/-/3	0.80/-	0.92/-	1.3/-	-/0.48
Combination of alkali-zinc silicate and zinc spray metalized coating									
ASI – Zn-SM-I	Sa 2½/100	55 – 170	48	F _{p,C}	4/1/4	0.63/-	0.71/-	3.9/-	-/0.44
ASI – Zn-SM-II	Sa 3/100		48	0.9 F _{p,C} *	4/1/3	0.69/-	0.77/-	3.7/-	-/0.55

¹⁾ Sa: surface treatment grade | ²⁾ Rz: roughness | ³⁾ DFT: dry film thickness (coating thickness) | ⁴⁾ Σt: clamping length | ⁵⁾ st: static test/ sp: step test / ct: creep-/ect: extended creep test | ⁶⁾ µ_{ini,mean}: calculated slip factors as mean values considering the initial preload when the tests started | ⁷⁾ µ_{act,mean}: calculated slip factors as mean values considering the actual preload at slip | ⁸⁾ V: coefficient of variation for µ_{act} | ⁹⁾ µ_{5%}: slip factors as 5 % fractile calculated on the basis of the static tests and the creep test passed | ¹⁰⁾ µ_{ect}: slip factor resulting from the extended creep test passed

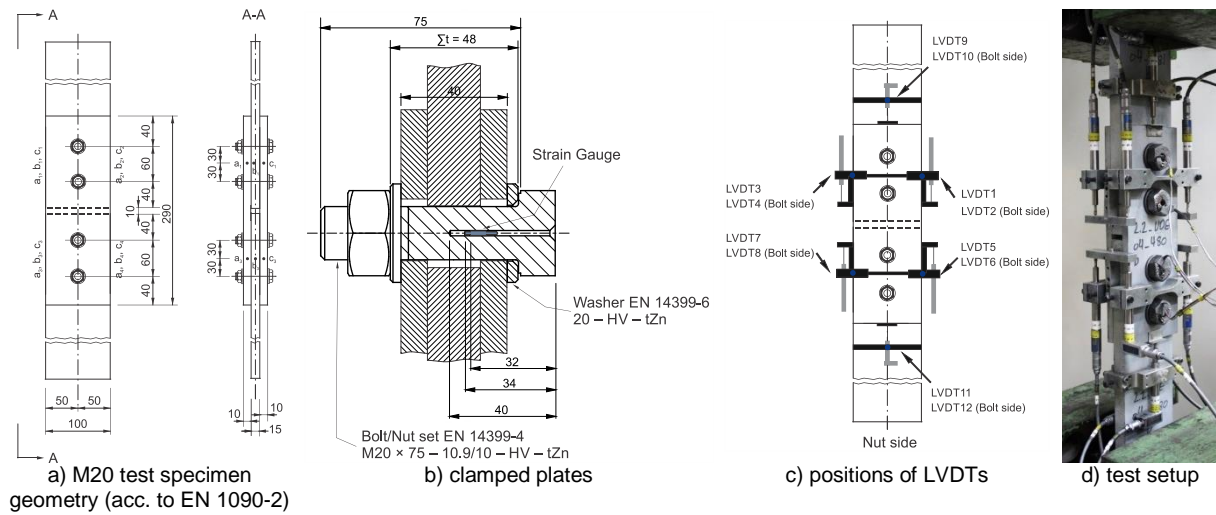


Figure 3.4-1: Test setup, test specimen geometry, positions of displacement transducers (LVDTs) as well as clamped plates of a bolted connection with bolts with implanted strain gauge

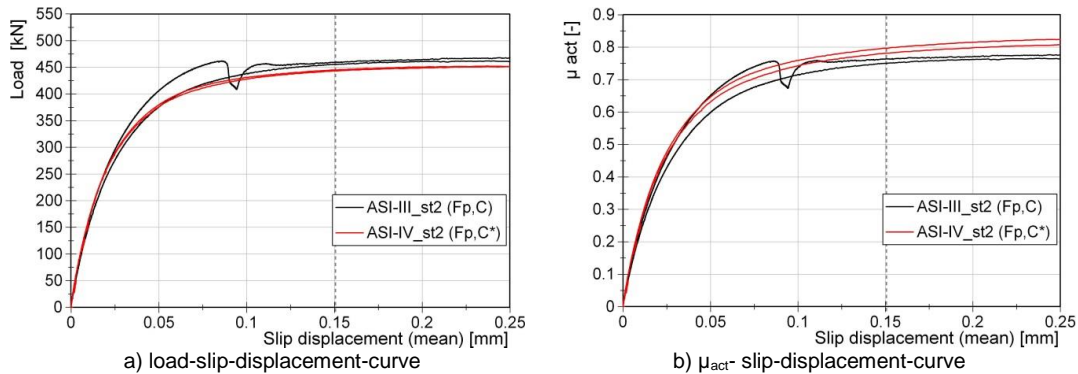


Figure 3.4-2: Influence of different preload levels for ASI-surface condition

It can also be seen in Figure 3.4-3 and Figure 3.4-4 that the highest actual static slip factor is achieved for Zn-SM-IV with a preload level of $0.9 F_{p,C}^*$ ($\mu_{act,mean} = 0.92$) in comparison to Zn-SM-III with a preload level of $F_{p,C}^*$ ($\mu_{act,mean} = 0.83$) and Zn-SM-II with a preload level of $F_{p,C}$ ($\mu_{act,mean} = 0.82$). Table 3.4-1 shows that in this case, the initial static slip factors are following the same principle.

Figure 3.4-5 also confirms this phenomenon. The results show that in the ASI-Zn-SM series, $\mu_{act,mean}$ ($0.9 F_{p,C}^*$) = 0.77 is higher than $\mu_{act,mean}$ ($F_{p,C}$) = 0.71. These behaviours confirm that a higher static slip factor can be achieved by a lower preload level (lower surface pressure), see Figure 3.4-6. For all coated test series the creep tests were failed for both, upper and lower parts of the specimens, and performing extended creep tests was necessary to determine the final slip factor, see Figure 3.4-7.

Figure 3.4-8 shows the long-term test-rigs that were designed and erected at the Institute for Metal and Lightweight Structures of the University of Duisburg-Essen. Each test rig was made of a stiff steel

frame, which consists of three positions for extended creep test specimens, for more details see Deliverable 2.2.

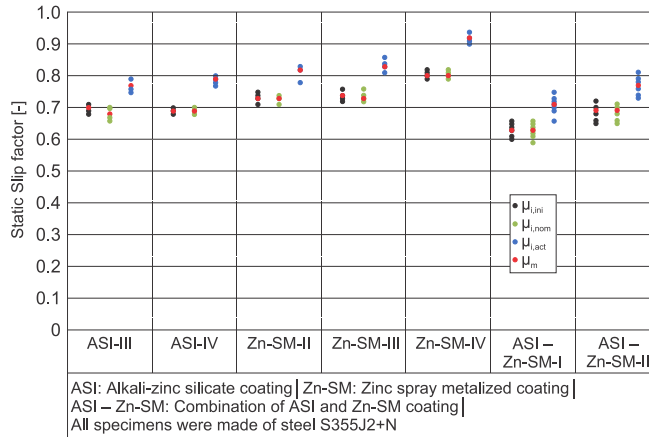


Figure 3.4-3: Influence of different preload level on the static slip factors

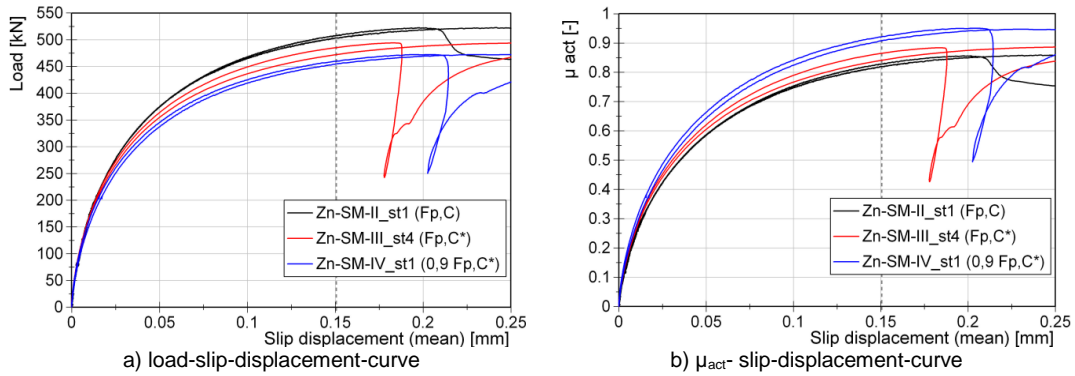


Figure 3.4-4: Influence of different preload levels for Zn-SM-surface condition

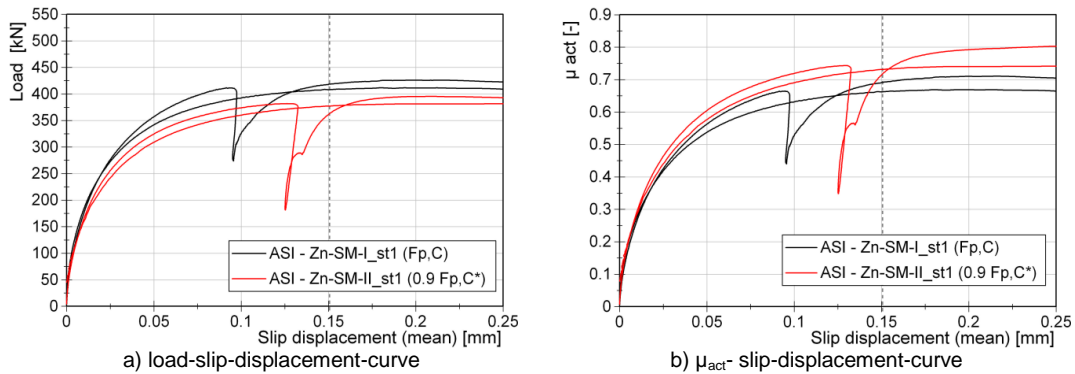


Figure 3.4-5: Influence of different preload levels for ASI-Zn-SM-surface condition

In Task 1.4, for ASI coated surfaces with preload level of $F_{p,C}$, the extended creep test was performed for more than 707 days with a load level of $0.8 F_{Sm}$, see Figure 3.4-9 (a). The results show that the slip is less than 0.3 mm when extrapolated to 50 years. Herewith, it is considered as passed extended creep test. As shown in Figure 3.4-9 (b), for the ASI-surface conditions the slip displacement – log time curves are presented based on the results of creep and extended creep tests at 0.8, 0.85 and 0.9 F_{Sm} . The duration of the creep test is short in comparison to the extended creep test and it is not possible to consider these tests as passed extended creep tests. For this reason, to consider this load level as appropriate load level for extended creep test, an extended creep test with a constant load level of $0.9 F_{Sm}$ was performed. The result shows that the slip is less than 0.3 mm for this load level when extrapolated to 50 years and the tests are considered as passed extended creep tests so that the nominal slip factors can be calculated as $\mu_{ect,ASI}(F_{p,C}) = 0.66$ and $\mu_{ect,ASI}(F_{p,C}^*) = 0.63$.

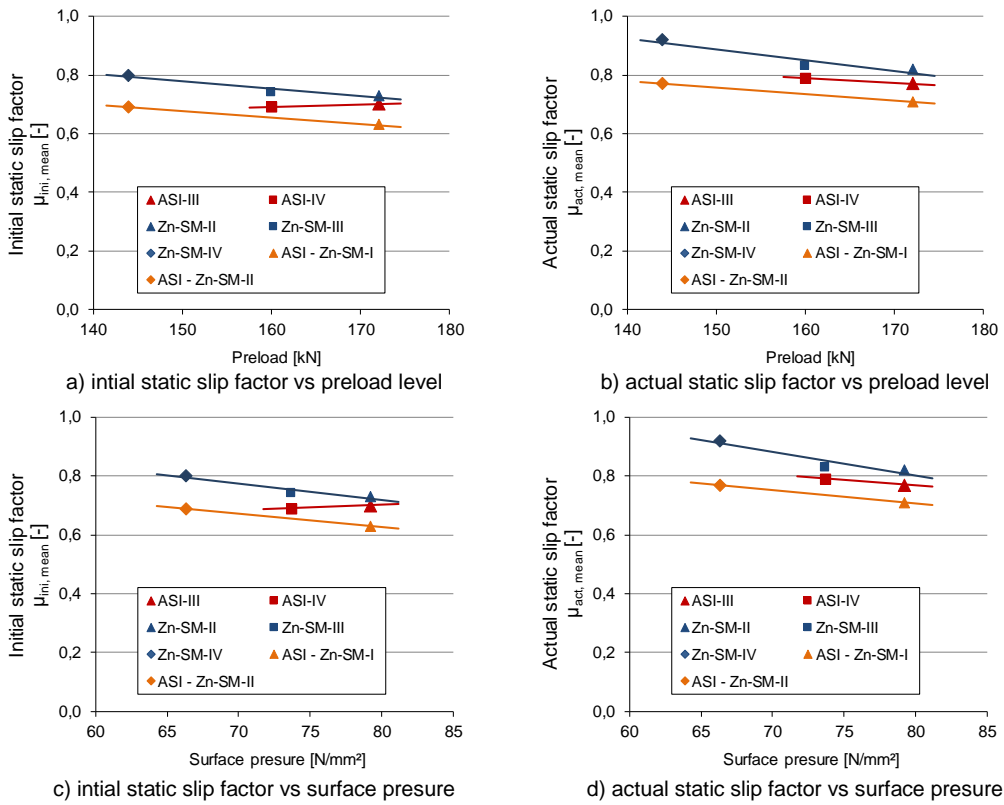


Figure 3.4-6: Influence of different preload levels and surface pressures

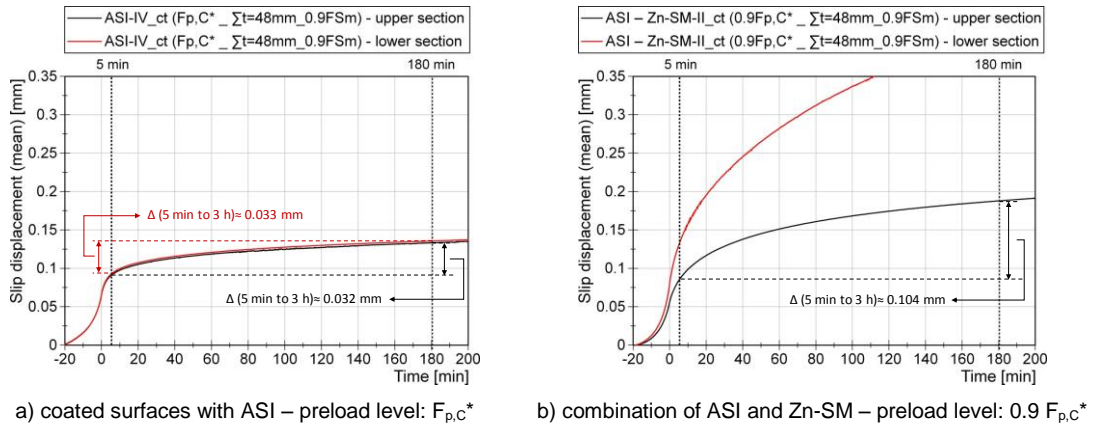


Figure 3.4-7: Exemplary results of creep tests considering different coating surfaces

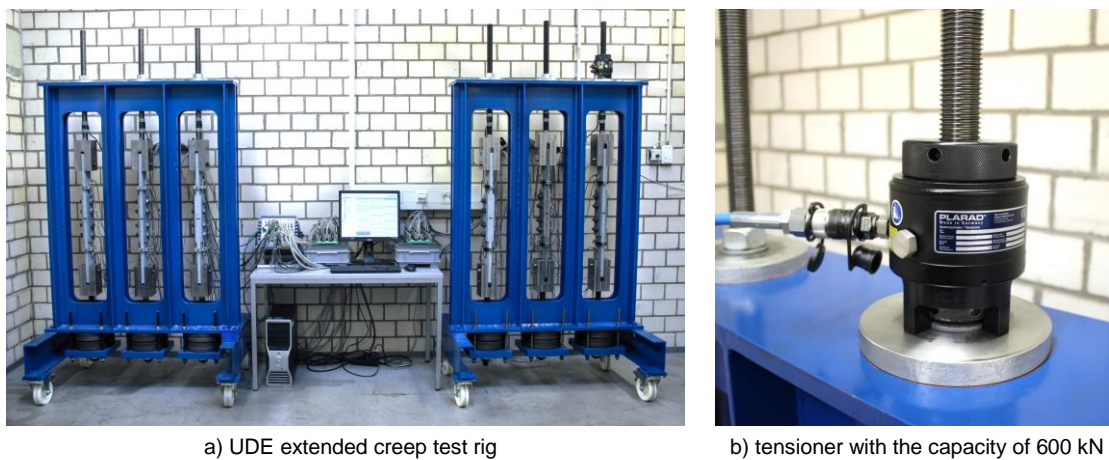


Figure 3.4-8: Test rig for extended creep tests

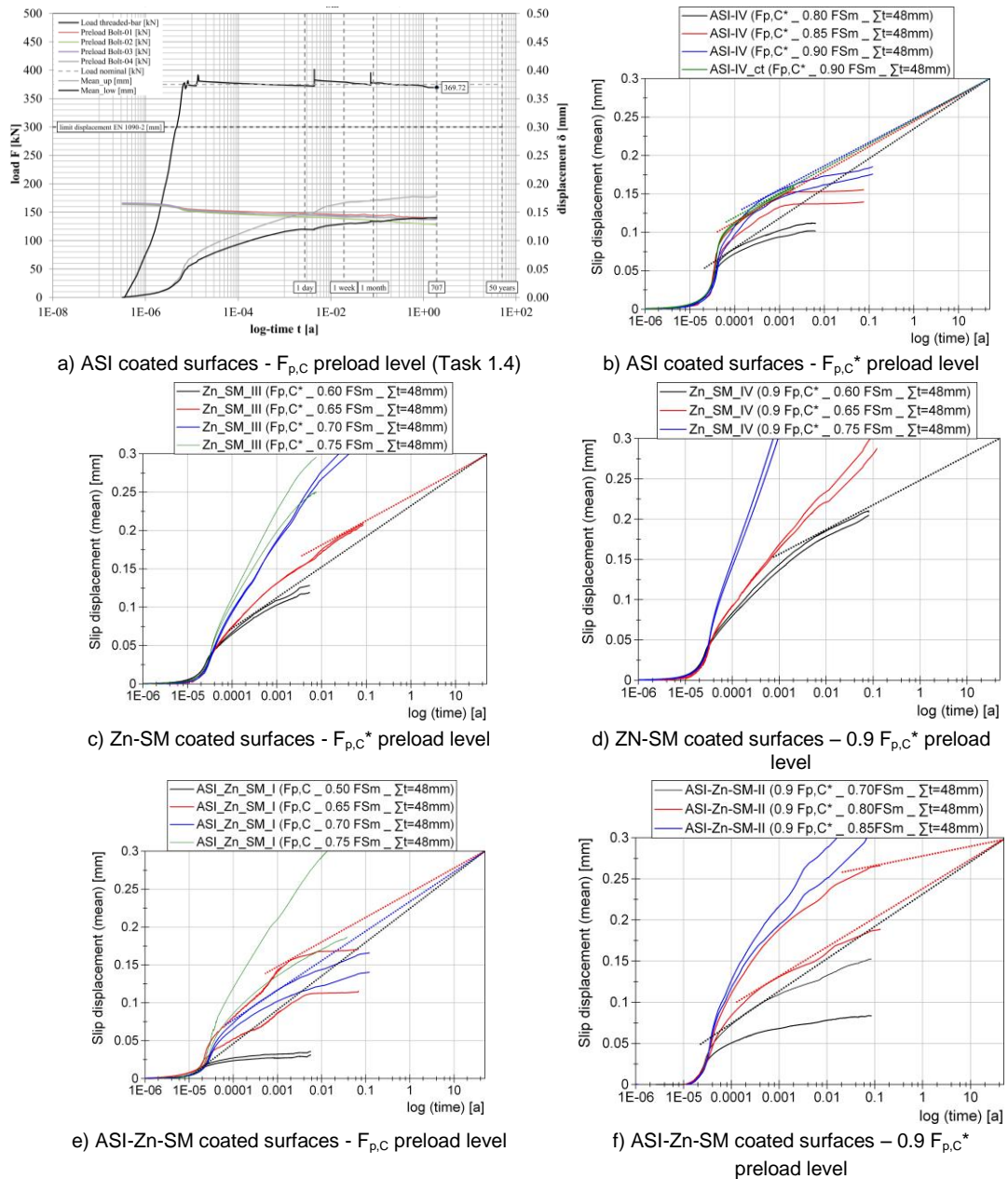


Figure 3.4-9: Results of the extended creep tests for different test series (each colour represents the upper/lower section of the specimen)

In general, almost all coated surfaces can be considered as creep sensitive surfaces. However, the ASI-coated surfaces show a relatively good slip resistance behaviour with high loading levels under the long-term extended creep test.

Seven extended creep tests were performed for the Zn-SM-surface condition with two different preload levels of $F_{p,C}^*$ and $0.9 F_{p,C}^*$, see Figure 3.4-9 (c) and (d). The extrapolated displacement – log time curves of the extended creep tests show that for a constant load level of $0.65 F_{Sm}$ for Zn-SM-III and for a constant load level of $0.60 F_{Sm}$ for Zn-SM-IV, the slip is less than 0.3 mm when extrapolated to 50 years. Herewith, they are considered as passed.

The extended creep tests were also performed for Zn-SM-surface condition with preload level of $F_{p,C}$ in Task 1.4 and the test was passed with load level of $0.60 F_{Sm}$. The nominal slip factor for Zn-SM-III and IV (with preload levels of $F_{p,C}$, $F_{p,C}^*$ and $0.9 F_{p,C}^*$) based on $0.60 F_{Sm}$, $0.65 F_{Sm}$ and $0.60 F_{Sm}$ can be calculated as $\mu_{ect,Zn-SM}(F_{p,C}) = 0.44$, $\mu_{ect,Zn-SM}(F_{p,C}^*) = 0.48$ and $\mu_{ect,Zn-SM}(0.9 F_{p,C}^*) = 0.48$ respectively.

The extended creep test for ASI - Zn-SM-I with a preload level of $F_{p,C}$ and $0.70 F_{Sm}$ was passed for both parts of the test specimen, see Figure 3.4-9 (e). The result also shows that the extended creep test for ASI - Zn-SM-II with a preload level of $0.9 F_{p,C}^*$ and $0.80 F_{Sm}$ is clearly passed, see Figure 3.4-9 (f). The nominal slip factor for ASI - Zn-SM with preload levels of $F_{p,C}$ and $0.9 F_{p,C}^*$ can be calculated as $\mu_{ect,ASI-Zn-SM}(F_{p,C}) = 0.44$ and $\mu_{ect,ASI-Zn-SM}(0.9 F_{p,C}^*) = 0.55$ respectively.

Conclusion

It becomes obvious that actual and initial static slip factors increase slightly with decreasing preload level. Only by ASI-coated surfaces, the initial static slip factor remains approximately the same but the actual static slip factor increases by decreasing preload level. By comparing the actual static slip factors μ_{act} with those calculated with the initial preload μ_{ini} and the final slip factor μ_{ect} , this behaviour can also be observed for the final slip factors including the extended creep tests.

3.5 Task 2.3 – Preload in existing structures

Introduction

The feasibility of using the strain gauge method in practice has been tested both in a laboratory and in-situ in a Dutch highway bridge (Middachterbrug) to assess the minimum required pretension force in the bolts. Statistical evaluation has shown that the spread in the calibration factors of the bolts is sufficiently small and mean value correction is possible, which simplifies the use of the proposed method for in-situ preload force assessment. Deviations of the mechanical and geometrical properties of bolt sets are implicitly included in the statistical model. Predicted bolt force F_{pred} [kN] for M24 bolt can be calculated by the formula below based on the measured in-situ strain ϵ_{meas} [$\mu\text{m}/\text{m}$] $\cdot F_{pred} = 0.082 \epsilon_{meas}$ [kN]. If $F_{pred} > F_{p,C}$ the actual bolt preload force is satisfactory with 95 % confidence. Finite element analysis has indicated that the proper position of the strain gauge is at 0.65 d or more from the both the bolt head-shank and thread-shank transition.

A literature study was conducted to review the available methods to determine the actual preload in preloaded bolts. Based on the literature study and innovations in the field of installation of strain gauges suitable for bolts, experiments were carried out in the laboratory and in-situ to determine the actual preload level using the Strain Gauge Method. The experimental results were used to determine the reliability of the strain gauge method as a predictor of preload level in bolts in existing structures.

Objectives

Preloaded bolts are used in connections in which the relative displacements between plates must be prevented when exposed to load reversals or vibrations. The behaviour of such connections depends on the magnitude of the preload. If the force is lower than the minimum prescribed preload, slip occurs leading to excessive deformations or fatigue failure of the connection, whereas if the preload is too high bolt failure may occur. The preload level is decreasing in time, e.g. as a result of coating and bolt creep, and thus it is necessary to know the preload of the bolts at each point in time during the service life of a connection in order to predict the (residual) connection lifetime. The purpose of this work was to investigate the feasibility of determining the actual preload force in bolts of existing connections with minimum costs and measurement efforts.

The actual bolt preload can be measured using several principles and corresponding methods. The work of Wang et al. (2013) [6.5-1] describes methods based on the principles of acoustoelastic effects, piezo active sensing and piezo impedance. Wang et al. (2013) conclude that acoustoelastic methods provide inadequate results, originating from environmental noise, the thickness of the bonding layer and microstructure effects. The practical applicability of the piezo active sensing method cannot be guaranteed in all cases: the applicability depends on whether or not the surface asperities are deformed plastically to the extent that the surface contact is said to be saturated (Liu et al., 2014) [6.5-2]. The piezo impedance method is not developed to such an extent yet that it is ready to be used in practice [6.5-1].

One of the most common ways to estimate preload level is to measure axial strain along the bolt by a strain gauge, and to perform calibration afterward. Strain gauges are often embedded in bolts. However, the installation procedure of the strain gauge into the bolt requires special (vacuum) treatment to prevent air inclusions in the adhesive. This procedure limited wider practical application of the Strain Gauge Method for the preload level assessment in existing bolted connections.

Estimation of preload level in a connection for a new structure can be done using a wider range of methods. An example is the use of permanent mounted transducer systems, which requires the use of factory-instrumented bolts and works based on the time-of-flight principle. Another way of measuring

preload in a newly built structure is the use of instrumented washers; special systems are already available that prevent measuring errors as a result of bolt eccentricity.

Strain Gauge Method

A new type of adhesive suitable for installation of strain gauges (CN adhesive) recently has become available on the market. This adhesive does not require vacuum treatment and cures in the presence of water, which is supplied from the upper part of the strain gauge itself. As a result of a less complicated installation process, the use of the strain gauge method has become more practical to use. Recently, Mohammadi et al. (2017) [6.5-3] have successfully used a similar strain gauge system in their experiments. The strain gauge method used for assessment of the preloading forces is based on measurements of the total strain difference due to complete unloading of the bolt. Influence of the ambient temperature is compensated by using a full Wheatstone bridge. The relationship between the strain measurements and stress/force levels depends on scattering in the Young's Modulus E and effective area A of the bolts. The spread in E and A is experimentally established by the calibration in order to provide minimum strain level to assure a required preload force in a given bolt.

Implementation of the strain gauge method using CN adhesive was initially tested in the laboratory, with execution top-down, bottom-up and sideways and with or without initial bolt preload to resemble situations as in practice. Only handheld tools were used to duplicate circumstances on site. To facilitate the installation procedure, a specially manufactured hexagonal (Figure 3.5-1) was used in order to drill Ø2 mm holes (total drill depth 40 mm) through the bolt head into the bolt shank ensuring (1) centric placement and (2) parallel orientation of the strain gauge with respect to the bolt axis. Hereafter, any remaining contamination (e.g. dust) within the hole was removed using solvent and tissue. Insertion of the strain gauge into the bolt hole is preceded by injection of the CN adhesive using a syringe. Curing of the CN adhesive was done for 24 hours after installation of the strain gauge at ambient temperature.

The initial laboratory tests were carried out using M24 bolts of grade 10.9, with a clamping length of 50 mm. Strain gauges of type BTMC-3-D20-006LE were used in combination with CN adhesive. After installation, calibration of the strain gauges was carried out using a Skidmore Wilhelm instrument (Figure 3.5-2).

Each bolt was loaded three times to the minimally required preload level ($F_{p,C} = 247$ [kN]) in order to establish calibration curves (i.e. to relate a change in strain to a change in force). Any temperature influence on the measurements was corrected for by the use of a full Wheatstone bridge.

After the initial laboratory tests, the strain gauge method as used in the laboratory was introduced in practice to determine the actual preload level of HSFG bolts in the Middachterbrug (1974) in the Netherlands. The Middachterbrug is a bridge in the A348 highway; the Dutch Ministry of Infrastructure and the Environment was interested in the current state of its asset because the structure is nearing its design lifetime of 50 years.

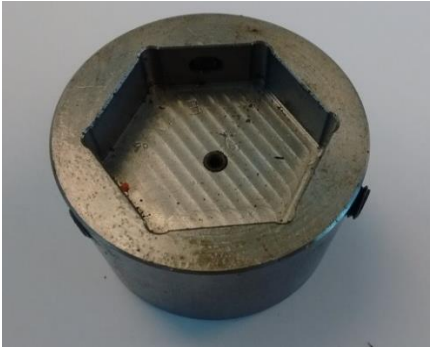


Figure 3.5-1: Hexagonal die used to (1) centre and (2) keep the drill parallel to the bolt axis. **Figure 3.5-2:** Strain gauge installed in bolt and connected to terminal. Bolt is placed in Skidmore-Wilhelm instrument.

The strain gauge method was implemented to determine the actual preload force within the bolts in a bottom flange connection. The connection consists of two cover plates ($t = 26$ mm) and an intermediary beam flange ($t = 32$ mm), providing a total clamping length of 92 mm (including 2 washers). The connection consists of 84 bolts (M24 grade 10.9 bolts, $L = 120$ mm), of which 16 are

instrumented with strain gauges (4 per quarter of the connection). The location of the instrumented bolts was chosen such that insight was obtained in (1) differences in actual preload in bolts in the same row, and (2) the influence of (un)tightening a bolt on the neighbouring bolts. In order to assess the spread within the actual bolt preload, bolts with the same relative position within each of the four quadrants were selected.

After successful installation of the strain gauges, the bolts were untightened and removed one-by-one. A new HSFG bolt was installed and preloaded (using the combined method) immediately after removal of each bolt in order not to compromise the structural safety of the bridge. The removed bolts were taken to the laboratory, where calibration was performed using a Universal Testing Machine (UTM).

Load/Strain Measurements

Calibration factors (CF), obtained using curve fitting of the load-strain diagram, are presented in Table 3.5-2.

Table 3.5-1 for all instrumented bolts. Additionally, the actual calibration factor (CF) as well as the corresponding actual bolt preload before untightening to bolt failure force and strain at actual preload level and bolt failure force for all Instrumented bolts in the beam flange friction grip connection in the Middachterbrug are presented in Table 3.5-2.

Table 3.5-1: Calibration factors

	Bolt position + Condition (loaded vs. unloaded) during installation of strain gauge	Actual calibration factor (CF) [kN/ $\mu\epsilon$]			Spread [%]
		Loading Cycle 1	Loading Cycle 2	Loading Cycle 3	
Laboratory	Web, unloaded	0.0833	0.0836	0.0837	0.3
	Web, unloaded, drilled using drilling oil	0.0917	0.0894	0.0892	1.8
	Web, loaded	0.0847	0.0845	0.0848	0.2
	Flange, unloaded	0.0868	0.0869	0.0867	0.1

Discussion

Both for the laboratory and in-situ experiments, a linear relationship between bolt force and the measured strain was found by calibration. The idea of measuring the bolt preload using the strain gauge method is not to calibrate every bolt, since this is rather laborious and time-consuming. Therefore, the feasibility of the strain gauge method to determine the actual preload in a bolt is assessed based on nominal properties, such as the nominal area and Young's Modulus.

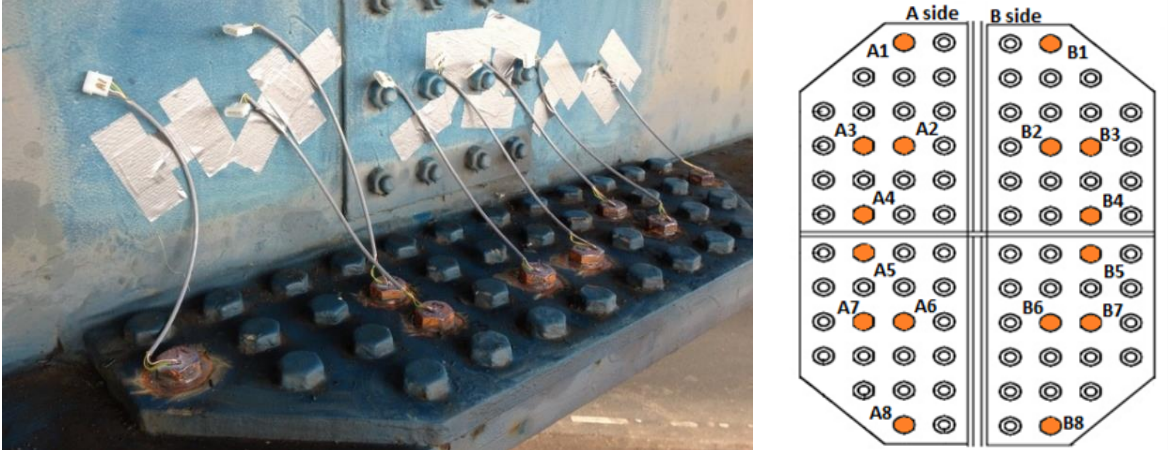


Figure 3.5-3: Instrumented bolts in the beam flange friction grip connection in the Middachterbrug (1974)

Table 3.5-2: Actual preload levels obtained in the testing programme

Middachterbrug	Bolt ID	Actual calibration factor (CF) [kN/μ€]	Corresponding actual bolt preload before untightening [kN] / Bolt failure force [%]	Strain at actual preload level [μ€]	Bolt Failure Force [kN]
	A1	0.0889	280 / 75	3239	376
	A2	0.0985	335 / 86	3346	388
	A3*	-	-	-	-
	A4	0.0917	346 / 95	3579	364
	A5	0.0917	330 / 86	3502	385
	A6	0.0919	331 / 84	3625	394
	A7	0.0908	189	2104	-
	A8	0.0914	344 / 87	3754	395
	B1	0.0897	315 / 86	3466	365
	B2	0.0899	305 / 83	3385	368
	B3	0.0899	315 / 84	3531	373
	B4	0.0895	310 / 88	3537	351***
	B5*	-	-	-	363
	B6	0.0876	323 / 83	3676	387
	B7	0.0898	277 / 72	3074	385
	B8**	-	-	-	343***
	Average	0.0887 incl. lab. experiments	318 / 84	3371	376

The bolt force is related to the strain gauge measurements via $F = CF \cdot \varepsilon$
*: Strain gauges gave unreliable readings
**: Bolt was untightened before attaching strain gauge to terminal
***: Failure force is lower than nominal failure load (353 [kN])

The laboratory and in-situ measurements are used in the analysis, since the combination gives a broader spectrum of data. The goal is to achieve a reliable prediction of the “calibration factor” based only on nominal material properties (e.g. $E = 210$ GPa), i.e. via the following equations.

$$F = (CF)_{act} \cdot \varepsilon = (EA)_{act} \cdot \varepsilon \quad (6.5-1)$$

$$(CF)_{nom} = (EA)_{nom} = E \cdot \frac{1}{4} \pi d^2 \quad (6.5-2)$$

$$(CF)_{prediction} = \eta \cdot (CF)_{nom} \quad (6.5-3)$$

E	Young’s Modulus (actual or nominal) [F/L ²]
A	Bolt area (actual or nominal) [L ²]
ε	Bolt strain [–]
η	Mean value correction factor [–]

The average actual calibration factor $(CF)_{act,\mu}$ (Table 3.5-2.

Table 3.5-1) and nominal calibration factor $(CF)_{nom}$ are related by $\eta = 0.933$ [–]. The mean value of the actual calibration factor is $(CF)_{act,\mu}$ [kN/μ€], whereas the standard deviation is $\sigma = 0.003491$ [kN/μ€]. The magnitude of the actual calibration factor with a 95 % exceedance probability for 25 measurements, leading to $n - 1 = 24$, is determined by equation (6.5-4) under the assumption that the actual calibration factor is normally distributed.

$$(CF)_{ch} = (CF)_{act,\mu} - 1.711 \cdot \sigma \quad (6.5-4)$$

With: $(CF)_{ch}$	Characteristic calibration factor (95% exceedance prob.) [F · L/L]
$(CF)_{act,\mu}$	Mean observed calibration factor [F · L/L]
σ	Standard deviation [F · L/L]

From the test results it is found that $(CF)_{ch} = 0.0827$ [kN/μ€], which means that the characteristic calibration factor is 7.2 % smaller than the average calibration factor. Hence, to have 95 % certainty of a given minimum bolt preload, it is necessary to prove that the bolt strain in practice is $1/\eta \cdot [(CF)_{act,\mu}/(CF)_{ch}] = 1/0.933 \cdot 1/0.933 = 15$ % higher than the corresponding nominal bolt strain. Differences in Young’s Modulus E nominal bolt area A may lead to changes between the actual preload and the preload predicted by the strain gauge method. However, by conducting more tests on bolts from different batches the influence of spread in E and A is implicitly taken into account through the resulting standard deviation σ. Using the statistical method described, η and σ can also be derived

for different bolt sizes (diameters). For larger bolt sizes, the effect of deviation in actual bolt diameter reduces relatively because of the greater nominal bolt area.

In contrast to the expectations, no measurable effects were observed in neighbouring bolts as a result of either untightening of the old bolt or preloading of the new bolt.

The depth of the strain gauge is of importance because of the disturbance length over which the strain is not constant over the cross section, since the bolt preload is distributed from the bolt head to the bolt shank. The centre of the strain gauge is positioned 30 mm below the top of the head of the bolt, meaning that it is embedded in the shank at a depth of 15 mm in case of an M24 bolt. For this particular geometry, finite element analysis has indicated that the bolt strain at the centreline of the bolt reaches a constant value after $0.625 d = 15 \text{ mm}$ below the bolt head-washer interface, confirming that the strain gauge method worked well based on nominal bolt properties as discussed above. A similar disturbance length ($0.58 d$) is found for the influence of the threads. Figure 3.5-4 presents the longitudinal bolt strain as a function of position along the bolt axis. Based on the above, it is suggested to demand a minimum distance of $0.65 d$ between the strain gauge and the thread-shank and shank-head transition if calibration is not carried out. In case calibration is carried out, the calibration factors will compensate for the non-uniform stress and strain distribution across the bolt cross section.

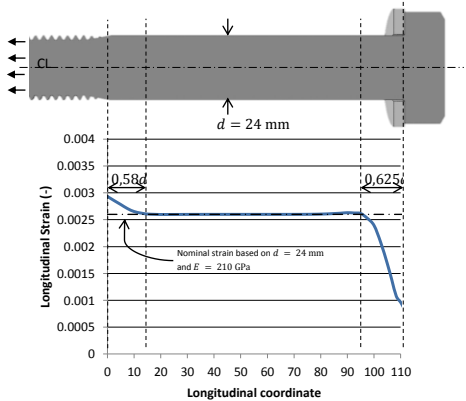


Figure 3.5-4: Longitudinal strain distribution along the bolt centreline (CL) for $F_{p,C} = 247 \text{ kN}$

The actual preload levels in the bolt in the Middachterbrug (on average 308 kN after 40 years of service) are rather high compared to the required preload of $F_{p,C} = 254 \text{ kN}$. The way the bridge was assembled is not well documented, and it is only known that a tightening torque of 1100 [Nm] and a k-factor of 0.18 were prescribed based on contemporary Dutch guidelines [6.5-4]. This k-factor is said to be valid for lubricated bolts with metric ISO threads, whereas currently the Dutch Ministry of Infrastructure and the Environment (Rijkswaterstaat) prescribes a k-value of 0.12 for bolts in identical condition and 0.15 for bolts as-delivered from the manufacturer [6.5-5]. Hence, it can be concluded that the k-value assumed in the 1970s was significantly higher, and that it is likely that a higher bolt preload was obtained as a result of the lower true k-factor during installation and tightening. A k-factor of 0.135 is derived based on the assumption that the initial preload was 110 % of the remaining average actual preload, which is in between the courant k-values belonging to lubricated and as-delivered bolts today.

Evidence of the high initial preload in the bolts from the Middachterbrug can be seen through the condition of the bolt fracture surface. The bolts have been loaded to failure in uniaxial tension, meaning no torsional stress was introduced in the bolts. As opposed to the fracture surface predicted by Kulak et al. (2001) [6.5-6] for bolts loaded in uniaxial tension, 63 % of the bolts showed a fracture surface belonging to failure as a result of torqued tensioning. Since the investigations by Kulak et al. (2001) were conducted on new bolts, it can be concluded that the (over)tightening of the bolts during erection of the Middachterbrug has led to internal damage and consequently led to a change in fracture mechanism.

Conclusion

The feasibility of the strain gauge method in practice has been tested both in laboratory and in-situ in a Dutch highway bridge (Middachterbrug) to address the minimum required pretension force in the bolts. All strain gauges were calibrated in order to derive the calibration factors (i.e. the factors relating the

strain to bolt force), which have been compared to the nominal calibration factors based on an assumption for Young's Modulus E and nominal bolt diameter d . Statistical evaluation has shown that the spread in the calibration factor is sufficiently small (COV 4.6 %) and mean value correction is less than 10 % which simplifies the use of the strain gauge method for in-situ preload force assessment. Deviations of the mechanical and geometrical properties are implicitly included in the statistical model. Predicted bolt force F_{pred} [kN] for M24 bolt can be calculated by the formula below based on the measured in-situ strain ϵ_{meas} [$\mu\text{m}/\text{m}$].

$$F_{pred} = 0.082 \cdot \epsilon_{meas} \text{ [kN]}$$

If $F_{pred} > F_{p,C}$ the actual bolt preload force is satisfactory with 95 % confidence.

Finite element analysis has indicated that the proper position of the strain gauge is 0.65 d from both the bolt head-shank and thread-shank transition.

Impact of the research results

Directly after successful application of the method on the Middachterbrug several bridge owners showed interest in the developed method. However, thus far no actual follow up applications are known to the authors.

4 WP 3 – Alternative bolts and preloading methods in slip resistant connections (CS)

4.1 Objectives

The main objectives of this WP were as following:

- The investigation whether alternative bolts or preloading methods than HV or HR bolts can be used in slip-resistant connections with sufficient reliability.

The most promising alternatives are

- Lock Bolts, which are already widely used in mechanical engineering so far,
- H360® system of Alcoa Fastening Systems,
- Injection Bolts, further development and optimization of connections with injection bolts to achieve slip and creep resistant bolted connections considering various influencing parameters and
- Direct Tension Indicators, so called DTIs. The use of DTIs is an alternative preloading method.

The main focus in this WP was on the loss of preload using the alternative bolts resp. method due to the fact that for slip-resistant connections it must be sure that the preload will be constant over the life time.

4.2 Work undertaken

The tasks undertaken in WP 3:

- 3.1. Use of lock bolts and H360 bolts.
- 3.2. Use of injection bolts.
- 3.3. Use of Direct Tension Indicators DTI.

The work undertaken for Tasks 3.1 to 3.3 is summarized in Sections 7.3 - 7.5.

Exploitation of the research results of this WP

The research results of this WP were published in two journal papers: (5) (Task 3.2) and (6) (Task 3.1), see Chapter 2, Publications. A publication regarding Task 3.3 is in preparation.

4.3 Task 3.1 – Use of Lockbolts and H360® bolts

These both bolting systems are preloadable high-strength friction grip bolting solutions and compared to HV-bolts, acc. to EN 14399-4 a promising alternative. Main objective is the investigation of the preloading procedure and the comparison of the achievable and remaining preload $F_{p,C}$ to conventional HV-Bolts. In this task, the potential of the installation (initial) preload ($F_{p,C,ini}$) of the bolted assemblies using Lockbolts, H360® and as the well-known reference HV-Bolts (EN 14399-4) have been investigated. The tightening tests have been performed with specimens according to EN 1090-2,

Annex G, Figure G.1, Type a) with M20 bolts of the same clamping length. In these bolted assemblies, with two connections in a joint, the tightening procedure follows the standard EN 1090-2 (tightening from the most rigid part of the joint to the least rigid part). The alternative bolts are shown in Figure 4.3-1.

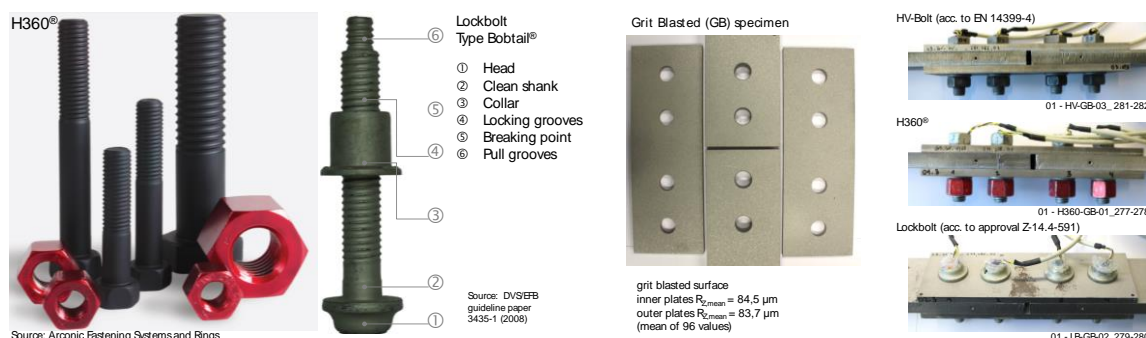


Figure 4.3-1: Alternative high-strength bolting systems, H360® and Bobtail Lockbolts for preloaded joints and preloaded specimen (acc. to EN 1090-2, Annex G, Figure G.1, Type a)

For tightening tests and with regard to further slip load tests, the best practice is to use uncoated grit-blasted steel plates, because the loss of preload due to setting effects is negligible. A comparison of the initial preload $F_{p,C,ini}$ between the three types of bolts was carried out within this investigation of grit-blasted specimen and for a further use in slip-resistant connections with coated plates (specimens in Figure 4.3-1). When using this type of specimen for the tests, four bolts per specimen were used. As a result, four values were achieved per specimen for evaluating the initial preload $F_{p,C,ini}$. Three different surface conditions as mentioned in the technical annex were investigated: Grit-blasted (GB), Hot-dip galvanizing (HDG) and Aluminium spray metallized (AI-SM). The test matrix is given in Table 4.3-1.

There are 42 preload values for Lockbolts, 71 for H360® and 47 preload values from HV bolts that are the reference basis to compare and evaluate the ability to preload. As a result, the different preload-time-behaviours of the setting/installation process of the three bolting systems can be compared directly to each other. A characteristic preload-time curve of each bolting system is shown in Figure 4.3-2. The initial preload $F_{p,C,ini}$ is the maximum load during the second tightening step for HV-Bolts and H360®. For Lockbolts it is determined 2 s after the peak. The peak is not representative for the value of $F_{p,C,ini}$ because of the longitudinal tensioning (tightening-) procedure. The drop is caused by springback effects and the achievable preload is determined afterwards when removing the tool. For the HV bolts and the H360® the “Turn-of-Nut Method” was used for preloading. HV bolts are tightened acc. to EN 1090-2, 8.5.3 Torque Method. The preloading procedure of the H360® based on it. The tightening torque is given by the manufacturer with 610 Nm for M20 bolts. The preloading-time-curves of the three bolt systems are compared in Figure 4.3-2.

Table 4.3-1: Test matrix with specimen acc. EN 1090-2 (4 bolts [preload values] per test)

Series ID	Bolt type	Steel grade	Surface preparation	Slip load test	Step test	Extended creep test (ECT)
01	“HV-Bolt” EN 14399-4-HV-M20x75-10.9/10-tZn-k1	S355J2+N	GB ¹⁾	3	-	-
02			HDG ²⁾	2	1	1
03			AI-SM ³⁾	2	1	2
04	“LB”		GB ¹⁾	2	-	-
05	Bobtail lockbolt		HDG ²⁾	4	1	-
06	M20-G40 J45/46 (Grade 10.9)		AI-SM ³⁾	3	1	1
07	“H360®”		GB ¹⁾	3	-	-
08	M360H-DT20x80D1		HDG ²⁾	4	1	1
09	(Grade 10.9)		AI-SM ³⁾	4	1	1
			Σ:	27	6	6

¹⁾ Grit blasted surface Sa 2 ½ (Roughness Rz = 80 µm) | ²⁾ Hot dip galvanized steel plates ³⁾ Aluminium spray metallized coating on grit blasted Sa 2 ½ (measurement of dry film thickness: mean $m_x = 132 \mu\text{m}$, $s_x = 55.7 \mu\text{m}$, $n = 576$, mean roughness Rz = 106.5 µm, $s_x = 14.7$, $n = 336$)

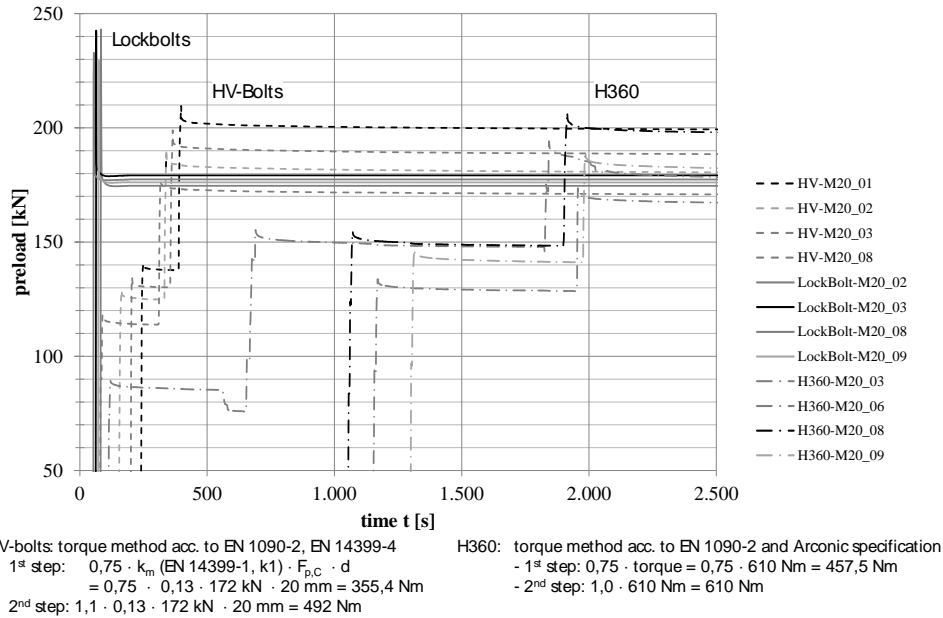


Figure 4.3-2: Preload-time diagram of the tightening process of Lockbolts, H360® and HV-Bolts

Lockbolts show specific and different preload-time behaviour during the tightening process compared to HV bolts and H360®. The tightening process of Lockbolts in comparison to HV-bolts differs fundamentally (details see deliverable of Task 3.1). The overall test results of the preload-time behaviour and installation preload are explained in the deliverable of Task 3.1 in detail. Table 4.3-2 summarises the evaluation of preloading/tightening processes.

Table 4.3-2: Results for the preloads obtained over all tests includes different faying surfaces

	HV-M20x75-tzn-k1	H360®-M20-G40 J45	Bobtail Lockbolt-M20-G40 J45/46
mean $F_{p,C,ini}$ (s_x) [kN]	192.8 (15.4)	182.7 (17.7)	187.8 (6.9)
$V_x F_{p,C}$	8.0 %	9.7 %	3.7 %
lower 5% quantile [kN]	167.5	153.1	176.6
min / max [kN]	148.3 / 225.8	143.1 / 226.3	174.7 / 200.3
α_A (max/min)	1.52	1.6	1.15
amount of tests n	47	71	42

The scatter of the preload of Lockbolts $V_x = 3.7 \%$ is compared to H360® with $V_x = 9.7 \%$ quite low. The tightening factor α_A acc. to VDI 2230 [7.3-1] reflects this value. A value of $\alpha_A = 1.4 - 1.6$ is recommended for HV bolts that are preloaded with the torque method. The value for Lockbolts is smaller with $\alpha_A = 1.15$. That value is comparable to a hydraulic frictionless and torsion-free tightening process with $\alpha_A = 1.1 - 1.4$ as it is given in VDI 2230.

Figure 4.3-3 shows the test setup with the test machine and measurement equipment. The slip load tests were carried out in accordance with the Annex G of EN 1090-2. The characteristic slip load-displacement curves for each bolting system and the different preparations of the faying surfaces are compared in Figure 4.3-4. The evaluation of the performed slip load tests is summarised in Table 4.3-3.

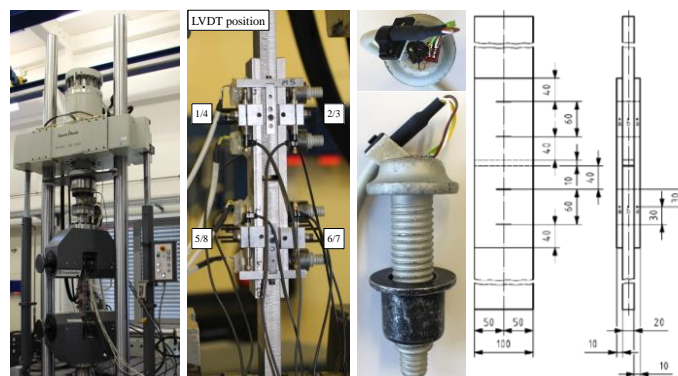


Figure 4.3-3: Test setup for experimental investigation according to EN 1090-2, Annex G, specimen type a)

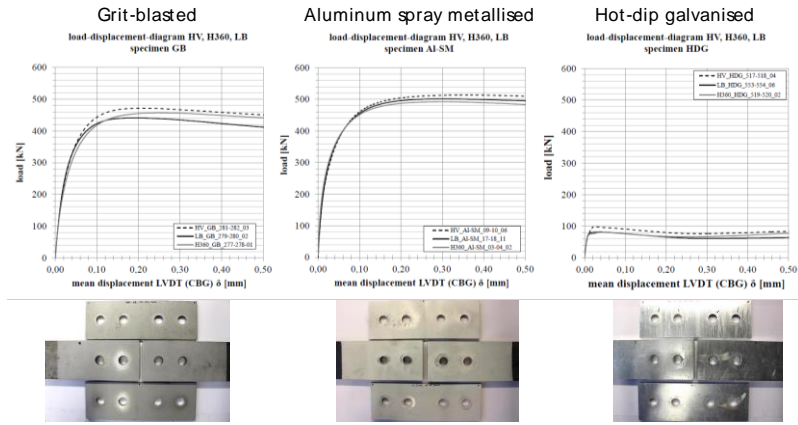


Figure 4.3-4: Characteristic slip load – displacement curves of Lockbolts, H360® and HV bolts with different prepared faying surfaces (grit-blasted – GB, aluminium spray metallised AI-SM, hot-dip galvanised – HDG)

Table 4.3-3: Results of the slip load tests

	GB			AI-SM			HDG		
	HV	H360®	LB	HV	H360®	LB	HV	H360®	LB
	$F_{Si,max}$	$F_{Si,max}$	$F_{Si,max}$	$F_{Si,max}$	$F_{Si,max}$	$F_{Si,max}$	$F_{Si,max}$	$F_{Si,max}$	$F_{Si,max}$
	[kN]	[kN]	[kN]	[kN]	[kN]	[kN]	[kN]	[kN]	[kN]
$F_{S1,max}$	467.9	430.7	440.9	506.9	465.6	506.8	94.0 ¹⁾	80.8 ¹⁾	81.8 ¹⁾
$F_{S2,max}$	471.3	457.0	474.9	507.8	480.4	529.4	95.1 ¹⁾	86.1 ¹⁾	89.6 ¹⁾
$F_{S3,max}$	483.5	473.2	480.0	513.1	488.6	501.5	98.3 ¹⁾	122.0 ²⁾	90.1 ¹⁾
$F_{S4,max}$	487.3	511.7	495.1	524.1	489.8	528.6	120.6 ¹⁾	123.7 ²⁾	92.7 ¹⁾
$F_{S5,max}$	512.7	519.3			492.0	525.3		133.6 ²⁾	155.3 ²⁾
$F_{S6,max}$	562.0	523.0			493.3	545.0		139.4 ²⁾	157.4 ²⁾
$F_{S7,max}$					518.0			169.4 ²⁾	198.1 ²⁾
$F_{S8,max}$					521.1			174.1 ²⁾	208.4 ²⁾
$F_{Sm,max}$	497.5	485.8	472.7	513.0	493.6	522.8	102.0 ¹⁾	83.5 ¹⁾	88.5 ¹⁾
V_X	7.1%	7.8%	4.8%	1.5%	3.7%	3.1%	12.3% ¹⁾	4.5% ¹⁾	5.3% ¹⁾
							$F_{Sm,max}$	143.7 ²⁾	179.8 ²⁾
							V_X	15.8% ²⁾	15.2% ²⁾
	GB			AI-SM			HDG		
$F_{Sm,max}(V_X)$	$F_{Sm,max} = 486.9 \text{ kN (6.8 \%)}$			$F_{Sm,max} = 507.6 \text{ kN (4.0 \%)}$			¹⁾ $F_{Sm,max} = 92.9 \text{ kN (11.2 \%)}$ ²⁾ $F_{Sm,max} = 158.1 \text{ kN (18.8 \%)}$		
¹⁾ $v = 0.01 \text{ mm/s (} F_{Si} \sim 1.5 \text{ min)}$ ²⁾ $v = 0.003 \text{ mm/s (} F_{Si} \sim 8 \text{ min)}$									

The results show for GB and AI-SM surfaces nearly the same slip load between the three fasteners. That indicates the possibility to use these bolts in slip-resistant connection. Further results are presented in the deliverable of Task 3.1.

Torque/clamp force test with H360® to proof the ability to preload for a use in slip-resistant connections

For the performance of the torque/clamp force tests a Schatz Analyse horizontal test bench was used. Aim of the torque/clamp force tests was the determination of the characteristic torque/clamp load behaviour of the H360® system during installation. Figure 4.3-5 shows on the left side a schematic drawing of an installed H360® and test bench. The torque/clamp force tests were performed in accordance with EN ISO 16047 [7.3-2].

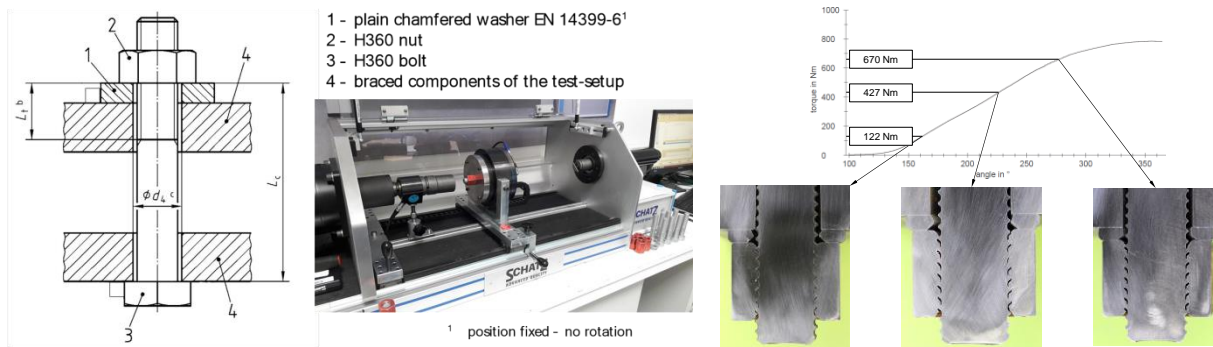


Figure 4.3-5: Left: Test bench for torque/clamp force testing acc. to DIN EN ISO 16047:2013-01, right: Forming effect of the nut by tightening up to the nominal torque H360@ size M20

The H360® set used for the tests consisted of a H360® bolt (grade 10.9) with a nominal diameter of 20 mm (M360H-DT20x100D1) and a special H360® nut (R20RX). The H360® system contained no washers. For each test an unused plain chamfered washer acc. to EN 14399-6 was placed under the nut. The hexagon H360® bolt head was fixed to the test rig to avoid turning during the tightening procedure. To determine the bearing surface and friction coefficient μ_b in the contact area between the nut and the washer, the washer was also fixed to the test rig. Due to the non-standard thread geometry the determination of the friction coefficient for the thread μ_{th} was impossible. The torque was applied continuously by turning the nut with a rotation speed of 5 rpm. In a first step the mechanism of the H360® system was tightened in the torque/clamp force testing machine to evaluate the forming effect of the nut. The nut is made of a softer material compared to the bolt. This shall provide that the material of the nut forms into the grooves (thread) of the bolt. The results and cross-sections at three different torque steps are shown in Figure 4.3-5 (right). This effect of forming the nut into the grooves of the bolt shall provide that the nut does not loosen under vibration loads. By the cold forming process of the nut the material will be strengthened and the friction between nut and bolt will increase. This increasing friction can reduce the ability to preload the bolt up to a defined preload $F_{p,C}$. The preload $F_{p,C}$ is besides the slip factor μ a necessary parameter to design slip-resistant connections. Therefore, torque/clamp force tests were performed to evaluate the ability to preload. The investigation of the torque/clamp force behaviour of the H360® system was divided into two sections (Table 4.3-4).

The first test section is explained in a shortened form (more details are in deliverable of Task 3.1). Torque/clamp force test will provide the following parameters:

- preload $F_{p,Ck}$ for the specified tightening torque T_{H360} and its scatter $\Delta F_{p,Ck}$ (tightening factor α_A),
- maximum preload tightening torques and angles of rotation, effective diameter D_b of the plane bearing surface.

The following points of analysis in Table 4.3-5 will be used for evaluating the ability to preload. An explanation of these points of analysis is summarised in Figure 4.3-6 - left.

Table 4.3-4: Description of test sections

Test section	Description of test procedure
I	Torque/clamp force test to evaluate the ability to preload H360® bolting system
II	Torque/clamp force test for stepwise tightening → details in deliverable Task 3.1

Table 4.3-5: Description of points of analysis

Step	Points of analysis	Step	Points of analysis
#1	$0,75F_p = 152,3 \text{ kN} - F_p$ according to DIN 898-1	#5	torque Arconic $T_{H360} = 610 \text{ Nm}$
#2	preload national $F_{p,C} = 160 \text{ kNs}$	#6	yield point (thread deformation nut)
#3	preload international $F_{p,C} = 172 \text{ kN}$	#7	3 % decrease of the max. preload
#4	preload Arconic $F_{p,C,H360} = 179 \text{ kN}$	#8	rotation to loose after waiting time

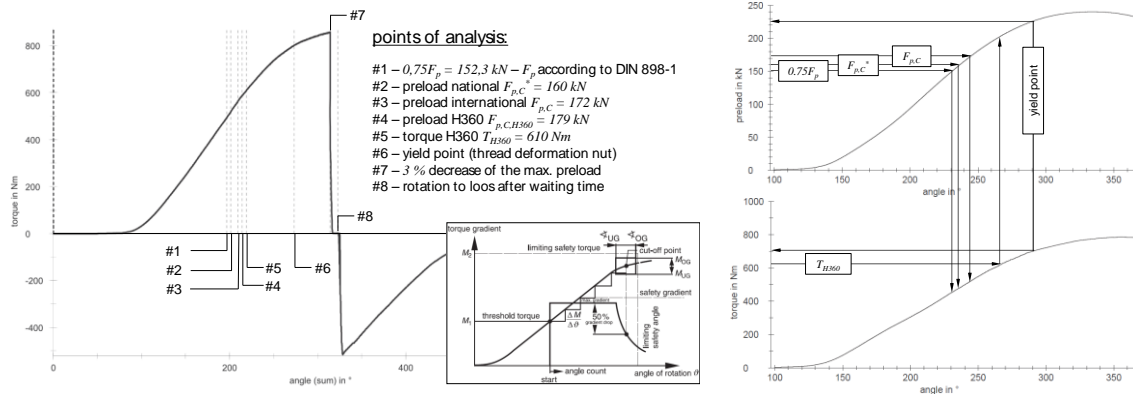


Figure 4.3-6: left - points of analysis for torque/clamp force test, right – evaluation points

There are different points of the tightening curve which have to be evaluated. Figure 4.3-6 (right) shows a continuous tightening curve. In the upper chart the preload is plotted over the angle. The three loads of interest are marked ($0.75 \cdot F_p$, $F_{p,C}^*$ and $F_{p,C}$). The torque, which belongs to the preload is determined in the lower chart, as shown in Figure 4.3-6 - right. Another evaluation point is the torque, which is given by ARCONIC. In this case the preload is taken from the point where the torque T_{H360} is reached. The last evaluation point is the yield point at which the yield strength of the thread of the nut is reached and the deformation begins. In test section I H360® bolts were tested with washers acc. to EN 14399-6 from manufacturer FUCHS. The results are given in Table 4.3-6. For the calculation it is necessary that the area of the thread remains the same and the thread of the H360® has to be deformed to be secured against vibration.

As mentioned before, it is necessary to deform the thread of the nut. The required torque to reach the yield point T_{yield} is given in Table 4.3-6. The yield torque goes from 826 Nm up to 1064 Nm and is much higher than the torque, which is given by ARCONIC ($T_{H360} = 610 \text{ Nm}$). As a conclusion the torque for the H360® must be defined by further tests to ensure that the vibration resistance is given. For the estimation of the scatter of the preload the tightening factor is calculated acc. to VDI 2230 – Part 1. The tightening factor for the torque T_{H360} is $\alpha_A = 1.32$ and comparable with the tightening factor of HV bolts with $\alpha_A = 1.4 - 1.6$. But as mentioned before, the torque is not high enough to deform the thread of the nut and that's why the tightening factor has to be calculated again with a new defined torque, which is high enough. According to EN ISO 16047 the friction coefficients are evaluated at $0.75 \cdot F_p$. The coefficient of friction for the bearing surface $\mu_{b, 0.75F_p}$ is 0.079. The coefficient of friction for the thread μ_{th} cannot be determined for H360®, because the nut deforms during the tightening. The necessary torque to reach the preload level of $F_{p,C}^*$ is compared to HV bolts much higher than the defined torque in DIN EN 1993-1-8/NA of $M_A = 450 \text{ Nm}$.

Table 4.3-6: Results of torque/clamp load tests with washers from company FUCHS

No.	$T_{0.75 F_p}$ [Nm]	$\mu_{b, 0.75F_p}$ [-]	T_{F_p,C^*} [Nm]	μ_{b, F_p,C^*} [-]	$T_{F_p,C}$ [Nm]	$\mu_{b, F_p,C}$ [-]	$F_{p,C,H360}$ [kN]	$\mu_{b, F_p,C,H360}$ [-]	T_{yield} [Nm]	F_{yield} [kN]
1	476.93	0.075	504.15	0.08	548.07	0.08	187.76	0.08	825.66	226.52
2	561.66	0.070	589.93	0.07	632.1	0.07	166.04	0.07	911.59	228.98
3	546.11	0.079	572.98	0.08	617.00	0.08	170.05	0.08	892.17	232.27
4	646.18	0.100	680.85	0.10	740.42	0.10	142.54	0.10	1064.04	229.33
5	588.47	0.078	621.18	0.08	675.12	0.08	157.30	0.08	969.96	224.09
6	628.88	0.077	661.58	0.08	717.13	0.08	147.34	0.08	978.81	218.83
7	533.73	0.072	560.35	0.07	604.17	0.07	173.50	0.07	858.56	229.75
8	566.34	0.075	594.26	0.08	638.34	0.08	164.51	0.08	951.39	232.35
9	489.41	0.075	515.22	0.08	556.02	0.08	186.53	0.08	874.11	237.13
10	568.30	0.087	597.83	0.09	644.57	0.09	163.34	0.09	982.03	231.87
mean	560.60	0.079	589.83	0.08	637.29	0.08	165.89	0.08	930.83	229.11
s_x	53.60	0.009	56.33	0.01	62.00	0.01	14.72	0.01	71.48	5.06
V_x	9.56	10.98	9.55	11.11	9.73	12.09	8.87	12.24	7.68	2.21

4.4 Task 3.2 – Use of Injection bolts

Correction actions

The 105 tests were originally planned according to TA, which includes 75 tests on non-preloaded connections and 30 on preloaded connections.

During the research, the decisions have been made to reduce number of variables related to structural behaviour but increase number of material tests investigating material properties of various alternative resins. There are two major reasons that justify these decisions.

Firstly, material properties of the resin are the dominating part in connections and very limited investigation has been conducted into alternative resins than the traditional Araldite resin. Curing temperature and resin loading delay influence strongly the resin characteristic in the connection. These aspects resulted in a large scatter of test results which have imposed needs for additional tests, otherwise the basis for conclusions would be insignificant. Further it was decided to study the behaviour of long bolts, large bolts and the fatigue behaviour. All these tests were planned in the original test program, but because of sensitive of results additional measuring devices are included in experiments.

Secondly, structural behaviour of connections using injected bolts in connections of steel to steel members or connections between steel and concrete in composite structures are possible to predict by FEA. The most recent results [7.4-1] show that the advanced FEA has to be based on reliable material data and prediction of structural behaviour is then obtained with very good accuracy. Therefore, due attention is focused on thorough investigation of material properties rather than on pretension bolts. Additionally, effects of the resin creep negatively influence behaviour of a connection therefore experiments of pre-tensioned bolts are completely omitted, on expense of additional tests of creep of various resins. No comparative study has ever been made before which would provide insight into various resins performance by using a same type of test set-up. In addition to Araldite resin, 4 more resin types are investigated, see Table 4.4-1

The number of perform test is shown in Table 4.4-1 comparing with plans presented in the TA.

Work undertaken

Research was conducted to further develop and optimize double shear connections with injection bolts to investigate if it is possible to achieve slip- and creep-resistant bolted connection. Various influencing parameters were studied, such as the type of resin, the curing condition of the resin, the geometrical and mechanical characteristics of the connection and the type of loading. The experimental results indicate the stiffness and creep behaviour injected bolted connections for 5 epoxy resins, as well as the fatigue behaviour and effects of different l/d ratios of injected bolted connections [7.4-2], [7.4-3], [7.4-4].

Table 4.4-1: Summary of test planned and performed

Test description	Number of tests		Investigated parameter
	Planned	Performed	
Creep behaviour	20	24	Variety of load duration
Impact load	20	8	Standard and oversize hole
Bolt length	5	8	Effect on bearing strength
Bolt diameter and hole clearance	10	4	M20 M36
Resin type	20	43	RenGel SW404 + HY2404 (Araldite) Edilon Dex-R2k, Edilon Dex-G20, Sikadur 30 Sika Injection 451
Total	75	84	

Injection bolts may be used in shear connections as an alternative to fitted bolts, rivets or preloaded high-strength friction bolts. Injection bolts are bolts in which the cavity produced by the clearance between the bolt and the wall of the hole is completely filled with a two-component resin, as illustrated in Figure 4.4-1. Filling of the clearance is carried out through a small hole in the head of the bolt.

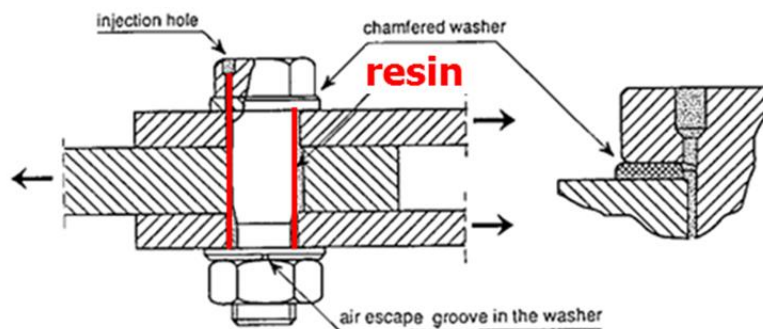


Figure 4.4-1: Injection bolt in a double lap joint

The current regulations are provided in EN 1993-1-8 [7.4-5] and EN 1090-2 [5.3-1], the design rules of a connection with injected bolts and execution rules on the detailing, respectively. The washers must fulfil the requirements of EN 1090-2, Annex K.

EN 1090-2, Annex K, prescribes that a two-component epoxy resin with a pot life of at least 15 min but a type of resin is not further defined. Current practice is the two-component epoxy resin Araldite SW404 with HY2404 hardener, now available as RenGel SW404 with Ren HY2404 [7.4-6] is used.

Test programme within SIROCO

An experimental plan was carried out with different influencing parameters such as type of resin, the curing condition of the resin, the geometrical and mechanical characteristics of the connection and type of loading. Due to the many influencing parameters, the experimental plan was divided into several stages and each stage concerns only a few influencing parameters.

The main parameters considered in the experiments are listed in Table 4.4-2.

Selection of resins

Short-duration tests – force for 0.15 mm slip criterion

Five resins were selected as candidates for use in injection bolts to examine the feasibility and effectiveness of the injection. RenGel SW404 + HY2404 (Araldite) is the initial resin recommended in ECCS publication No. 79 [7.4-7] and the possible alternative resins are Edilon Dex-R2k, Edilon Dex-G20, Sikadur 30 and Sika Injection 451. The curing temperature under ambient conditions was approx. 24 °C and the curing time was 72 h. After curing, short-term tests were performed on standard specimens with M20 bolts, according to the guidelines in EN 1090 - Annex K, to determine the tensile force needed to achieve a displacement of 0.15 mm at the centre of the bolt group (CBG). This specimen had a top and bottom connection with two non-preloaded M20x80 injection bolts per connection. The bolts were placed in a normal hole of 22 mm dia. The specimen including instrumentation, test machine and test procedure are shown in Figure 4.4-2.

Table 4.4-2: Experimental parameters for double shear connections with injection bolts

Bolt	Type	Non-preloaded / Preloaded
	Size	M20 / M36
	Hole and clearance	Normal round hole 2 mm/3 mm / Slotted hole 4 mm/6 mm
	Shank	40 mm / 80 mm / 100 mm
Resin type	Initial	RenGel SW404 + HY2404 (Araldite)
	Alternative	Edilon Dex-R2K/Edilon Dex-G20/Sikadur 30/Sika Injection 451
Curing	Time	6 / 24 / 48 / >72 h
	Temperature	8 / 16 / 24 °C / ambient temperature (~20 °C)
Test load	Short duration	Constant/Step load
	Long duration	Constant/Step load
	Fatigue load	Constant amplitude with different load level

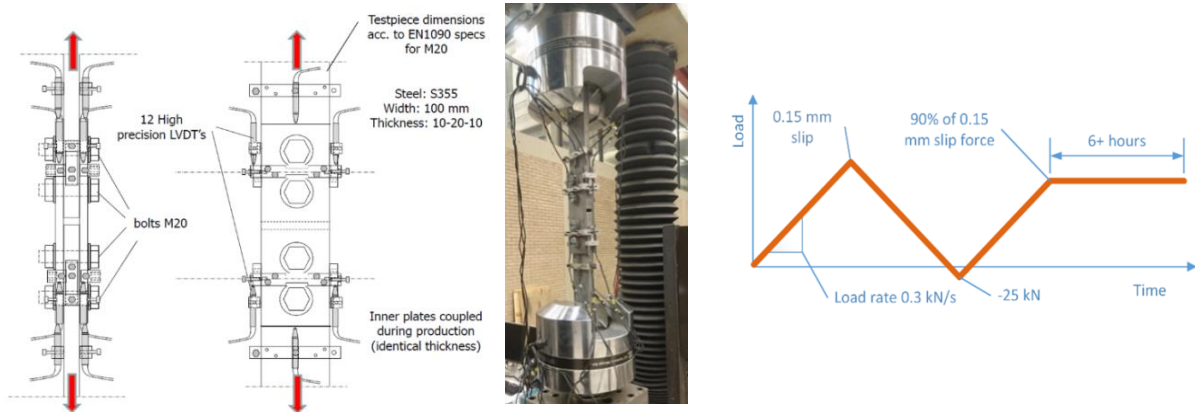


Figure 4.4-2: Specimen with instrumentation, test machine and test procedure

The short-term test results, see Figure 4.4-3, lead to following conclusions :

- Edilon Dex-R2k, Edilon Dex-G20 and Sikadur 30, used separately show good performance regarding resin injection. For the Sika injection 451, the cavity in the bolt hole was not filled properly and therefore, Sika Injection 451 was not included in the further research.
- RenGel (Araldite), recommended in [7.4-7], achieved the highest tensile force at the slip of 0.15 mm, i.e. 215 kN at CBG, and show the best time-dependent behaviour of all of the resins tested.
- Edilon Dex-R2K shows the tensile force at the slip value of 0.15 mm at CBG is 183 kN.
- For Edilon Dex-G20 and Sikadur 30 show the tensile force at the slip value of 0.15 mm at CBG of 170 kN, and 171 kN, respectively. However, both resins of have significant creep behaviour.

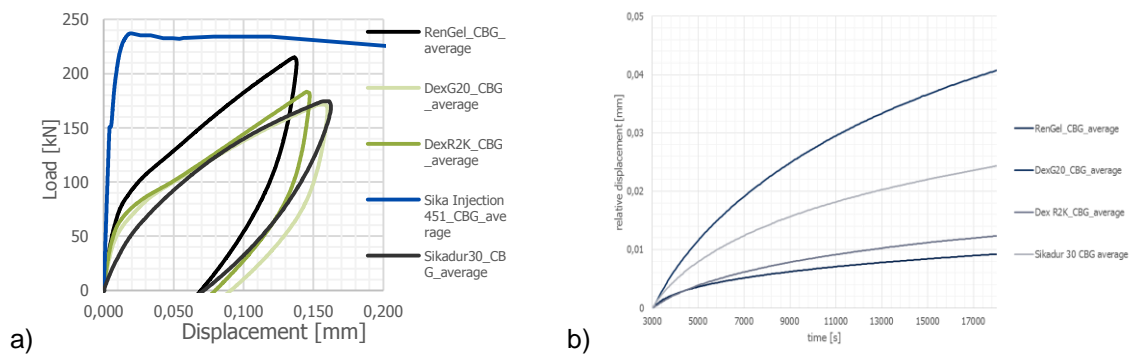


Figure 4.4-3: Initial test results: a) load–displacement curves, b) displacement–time curves

Short-duration tests – influence of curing temperature and overload behaviour

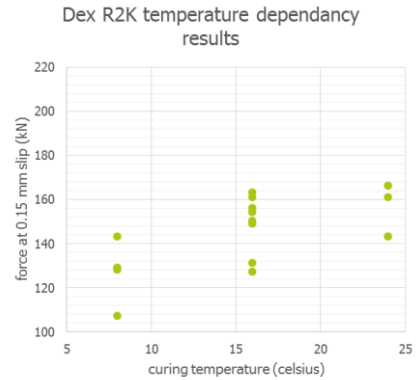
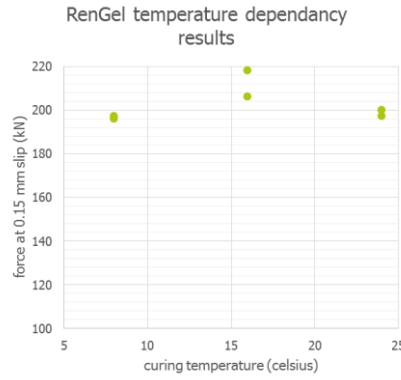
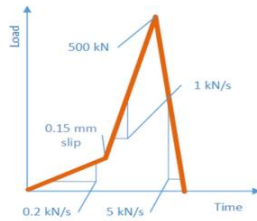
The strength and stiffness properties under different temperature conditions (8, 16 and 24 °C) were investigated in step 2. The curing time in all tests was 48 h. In addition to the EN 1090-2 load procedure, an additional overload step with increased load rate was applied up to the maximum load of the specimen see Figure 4.4-4. The following results were obtained and decisions taken:

- For the curing temperature in the range 8–24 °C, rather small temperature dependency can be neglected for the RenGel and the Edilon Dex-R2K resins, see Figure 4.4-4.b) and c).
- The Edilon Dex-G20 and Sikadur 30 resins cannot be used as alternatives due to their low strength values and large creep behaviour, so these resins were not considered in the subsequent tests.
- The benchmark value of 0.15 mm slip at CBG can be taken as 200 kN for the RenGel resin and 160 kN for the Edilon Dex-R2K resin.
- In order to reduce the effects of the friction between plates in subsequent tests, a torque value of 30 Nm was used for pre-tightening.
- The overload behaviour of the RenGel and the Edilon Dex-R2k connections remain quasi-linear far beyond the 0.15 mm slip criterion of EN 1090 (see Figure 4.4-4d).

a)

b)

c)



d)

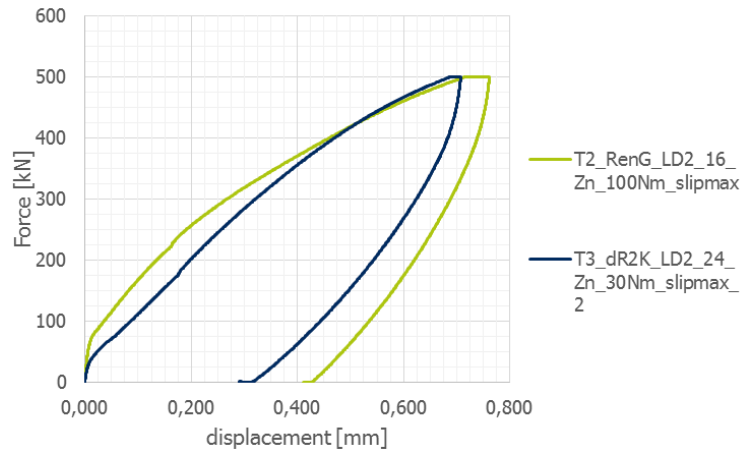


Figure 4.4-4: a) load procedure, b) & c) curing temperature results, d) overload behaviour

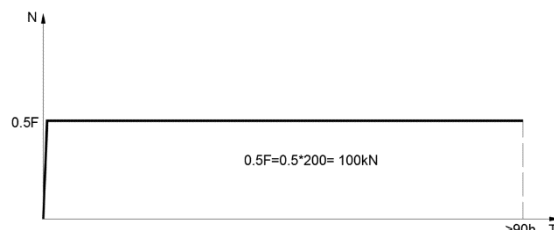
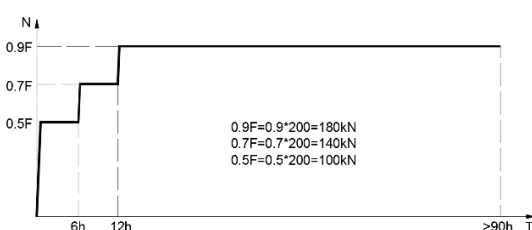
Short-duration tests – creep behaviour for at least 90 h

The strength and stiffness properties under a constant load applied for at least 90h were investigated in the 3rd step for the two resins, after the 2nd step of testing.

The curing time was 6h or 24h and the two loading types were used, see Figure 4.4-5. The F value in this figure stands for the benchmark force at the slip of 0.15 mm at CBG obtained in the 2nd step. The following results were obtained:

- RenGel (Araldite) exhibited a good, stable bearing capacity during a loading period of at least 135 h. The resin showed only a very slight creep behaviour, at the first hours of the loading.
- The curing time of RenGel (Araldite) and Edilon Dex-R2K, 6 and 24 h respectively, did not affect the creep behaviour.
- Edilon Dex-R2K exhibited an unstable bearing capacity.

Considerable difference was found between the different specimens. Edilon Dex-R2K may be used an alternative to RenGel (Araldite), but this type of resin has a larger displacement.



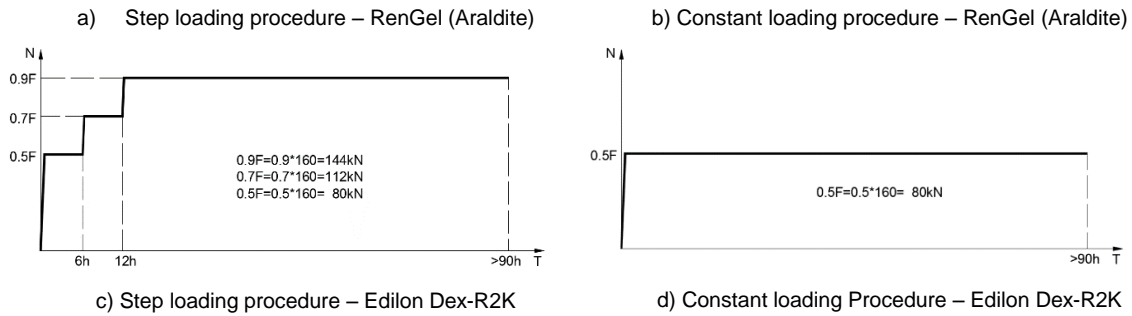


Figure 4.4-5: loading procedures for Edilon Dex-R2K and RenGel (Araldite)

Long-duration tests – effect of using slotted holes

Based on the results obtained in the short-term tests, two types of resin were selected for the long-term tests: RenGel (Araldite) and Edilon Dex-R2k. A standard specimen with M20 bolts was used. This specimen has one non-preloaded M20 injection bolt per connection. The bolts were placed in a normal 22 mm dia. round hole or a 24 or 26 mm slotted hole. The specimens were loaded in a string, each including four specimens. In each string, two specimens had the normal round holes with 2 mm clearance, one specimen had the slotted holes with 4 mm clearance and one specimen had the slotted holes with 6 mm clearance. The loading procedures applied are shown in Figure 4.4-6. The F value stands for the 0.15 mm connection slip for both resins as obtained in the short-duration tests. For the specimens with one connection, the F value is 100 kN for the RenGel specimens and 80 kN for the Edilon Dex-R2K specimens.

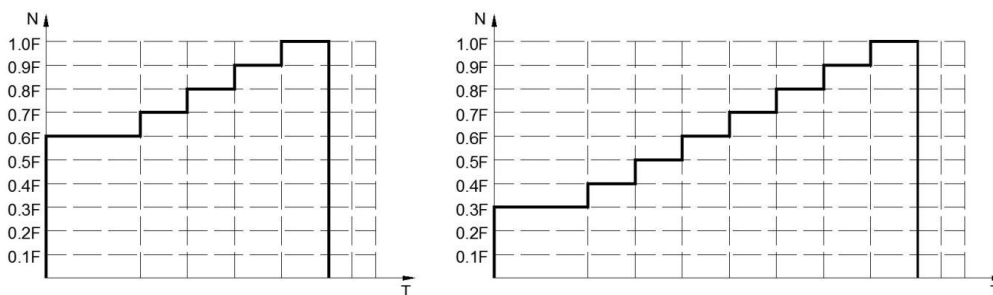


Figure 4.4-6: Loading procedures for long-duration tests – effect of using slotted holes

The following results have been obtained:

- RenGel (Araldite) has shown a good and stable bearing resistance during a loading period of 70 days (Figure 4.4-7) at a maximum load level of 70 % of the benchmark force value of 0.15 mm slip at CBG of the plate as obtained in 2nd step. The displacements of the specimens with a normal round hole with 2 mm was approx. 0.15 mm. The displacements of the specimens with a slotted hole with 4 or 6 mm clearance showed a higher value, 0.20 mm and 0.25 mm respectively.
- Edilon Dex-R2K showed an unstable bearing capacity, see Figure 4.4-8. Considerable difference was even found between the two connections of the same specimens. The effect of slotted holes could not be distinguished because of the large scatter of the results

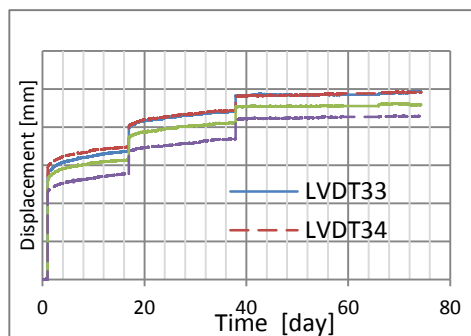


Figure 4.4-7: Long-term test results for a RenGel specimen with slotted holes with 6 mm clearance – $F_{max} = 70$ kN

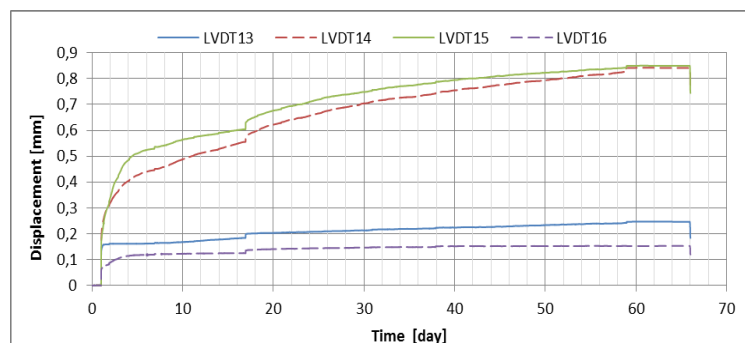


Figure 4.4-8: Long-term test results for a Dex-R2K specimen with normal round holes with 2 mm clearance – $F_{max} = 56$ kN

Large bolt tests

The specimen of the double shear connection has two non-preloaded M36 injection bolts with 3 mm clearance per side of the connection. The same plate thickness, as for the specimens in the M20 bolt tests, was used. The other plate dimensions were increased depending on the bolt size. RenGel resin was used in this test series. After curing for at least 24 h, short-term tensile testing according to the guidelines in EN 1090 - Annex K, was performed to determine the tensile force needed to achieve a displacement of 0.15 mm at the centre of the bolt group (CBG). The following results were obtained:

- The slip load was approximately the same for the M36 and M20 specimens (see Figure 4.4-9a).
- The bearing stress of the connection with the M36 bolts was 40 % lower than that of the connection with M20 bolts (see Figure 4.4-9b).

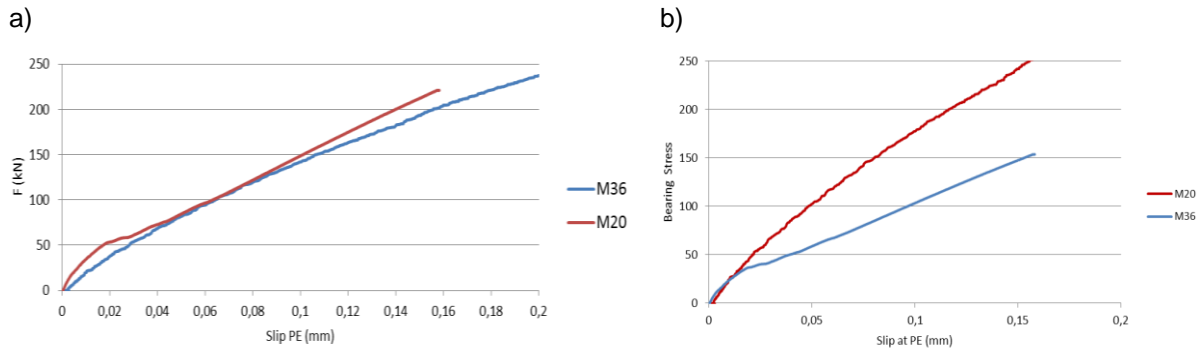


Figure 4.4-9: Large bolt test results: a) load–displacement curves, b) stress–displacement curves

Long bolt tests

- In the case of relatively long bolts (diameter of bolt small in comparison to thickness of plates), the bending deformation of the bolt may cause a very uneven bearing stress distribution. These uneven bearing stresses will result in additional creep deformation.
- Tests were carried out on connections with $L/D = 3$ and 4 using RenGel resin; M20 bolts were used and the plate package length was 60 and 80 mm respectively. The loading procedure according to EN 1090-2 was applied (see Figure 4.4-10a) and the following results were obtained (see Figure 4.4-10c):
- More research on bolt length effect is necessary to evaluate the effective width method of EN 1993-1-8, due to the scattering of results.

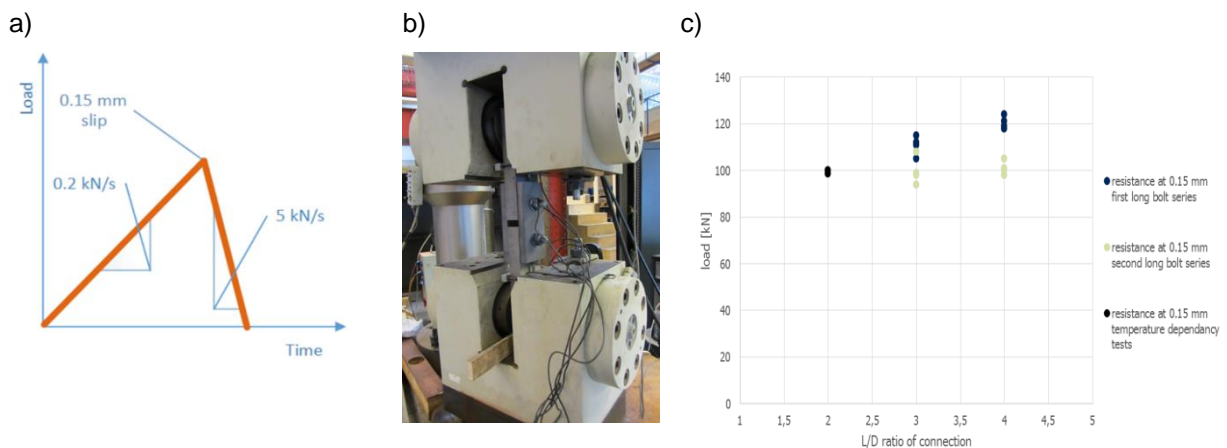


Figure 4.4-10: Long bolt tests: a) loading procedure, b) specimen in test rig, c) test results

Concluding remarks

The main conclusions are:

- Pot life and viscosity are the most important parameters of a resin.
- No correlation between mechanical properties and the performance for injected bolts exist.
- Edilon Dex G 20, Sika 30 and Sika injection 451 are not suitable for injected bolted connections.
- Edilon Dex R2K shows large scattering of results and lower strength compare to RenGel SW404/HY2404.
- The curing temperature was important for RenGel SW404/HY2404, but not for Edilon Dex R2K.
- An analytical analysis shows maximum connection resistance for the bolt l/d ratio of 3 but experimental results show a slightly increasing resistance for l/d ratios between 3 and 4.
- A bearing stress of 175 MPa is a safe recommendation for the long-term limit without exceeding deformation limits.
- The long-term tests showed that 60 % of the initial slip is due to deformation mechanisms other than compression of the resin.
- The use of oversized holes reduces the bearing resistance as a result of lower initial stiffness and increased slip as a result of a longer creep length.
- Connections with M36 bolts have the same initial stiffness as M20 connections and a reduced creep deformation at equal loads as a result of a lower bearing resistance.

Impact of the research results

During the SIROCO research, reinforced resin [7.4-8] was developed and patented. Reinforcing the resin is achieved by inserting spherical steel shots into the connection prior to injecting conventional epoxy resin, see Figure 4.4-11. The steel skeleton provides an increase connection stiffness (+71 %) and decreased creep deformation (-35 %). Preliminary investigation has shown that the Young's modulus of the reinforced resin is in the range 10-15 GPa, whereas for the resin itself this is approx. 4.2 GPa.

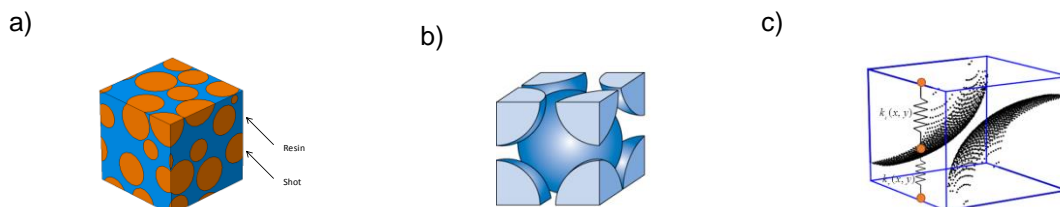


Figure 4.4-11: a) Reinforced resin with spherical steel particles (shots) and b) unit cell with body-centred cubic arrangement for c) derivation of an analytical material model for the reinforced resin

4.5 Task 3.3 – Use of Direct Tension Indicators DTI

The Direct Tension Indicator (DTI) method specified in EN 1090-2 [5.3-1] is one of several methods for tightening preloaded bolting assemblies to ensure the proper preload level ($F_{p,c}$) of a bolt. The most common types of direct tension indicators are produced with hollow bumps/protrusions on one side of the washer which must bear against the unturned element. These protrusions are plastically flattened by preloading the DTI, whereas the preloading force is applied by tightening the bolting assembly either by rotation of the nut or bolt. The gap developed by the bumps can be measured with a feeler gauge, see Figure 4.5-1.



Figure 4.5-1: Use of a feeler gauge to check the gap

When the feeler gauge no longer fits in the gap, it can be considered as feeler gauge refusal. When the number of feeler gauge refusals n_{refusal} at the gaps is more than half the number of the protrusions, the bolt has reached the proper preload level. Table 4.5-1 summarises the thicknesses of feeler gauges depending on a chosen assembly configuration that have to be used during the tightening procedure.

Table 4.5-1: Proper thickness of the feeler gauge

Assembly configurations	Thickness of feeler gauge
When DTI is faced non-rotated component	0.40 mm
When DTI is faced rotated component	0.25 mm

In this task, the Institute for Metal and Lightweight Structures of the University Duisburg-Essen investigated preloaded bolted connections using DTIs in HV bolting assemblies under the bolt and under the nut. The experimental investigations consisted of three different steps: in the first step, compression tests were performed to verify the mechanical performance of DTIs individually. In the second step, tightening and tensile tests were performed with a combination of DTIs and HV bolting assemblies (acc. to EN 14399-4) to verify the suitability of using DTIs in an assembly. Finally, relaxation tests were conducted on preloaded bolted connections using DTIs to investigate the potential preload losses.

The compression tests were performed in two steps and the local displacement was measured continually by a displacement transducer (LVDT). The test is presented in detail in the deliverable D3.3 of Task 3.3. In total, six compression tests (three M16 and three M20) were performed to verify the mechanical performance. Figure 4.5-2 shows the test setup of the compression test and a gap - compression load diagram for each DTI individually. As it can be seen, all DTIs fulfilled the requirements for the compression test, see Figure 4.5-2. At the end, in order to find the maximum loading F_{max} , the compression load was increased to close all gaps. When all gaps were closed, the compression load was recorded as the maximum loading, see Table 4.5-2.

The suitability tests for preloading with DTIs were carried out on the basis of EN 14399-2, EN 14399-4 and EN 14399-9 [7.5-1]. The investigated bolting assemblies contained bolts and nuts acc. to EN 14399-4 system HV M20x115 and M16x65, property class 10.9 with plain chamfered washers acc. to EN 14399-6 and nut face washers as well as bolt face washers acc. to EN 14399-9.

To pass the suitability test, every tested bolting assembly had to exceed $\Delta\Theta_{2i,\text{min}}$ by at least 10 %, fulfil the criterion of the individual maximum bolt force $F_{\text{bi,max}} \geq 0.9 \cdot f_{\text{ub}} \cdot A_{\text{s}}$ and achieve the nominal minimum preload $F_{\text{p,C}}$ by reaching the minimum number of feeler gauge refusals. In total, seven suitability tests (three M16-N, two M20-N and two M20-B) were conducted. Exemplary tightening curves of the tested M16x55 HV 10.9 bolting assemblies with DTIs under the nut are shown in Figure 4.5-3. It can be seen that the criterion of individual maximum bolt force $F_{\text{bi,max}}$ was not achieved. This deficit varies between 1.4 % and 7.6 % depending on a test sample. For this reason, the suitability tests failed for every tested M16 bolting assembly, even though the minimum angle of rotation of $1.1 \cdot \Delta\Theta_{2i,\text{min}}$ and the nominal minimum preload level $F_{\text{p,C}}$ were exceeded in all cases.

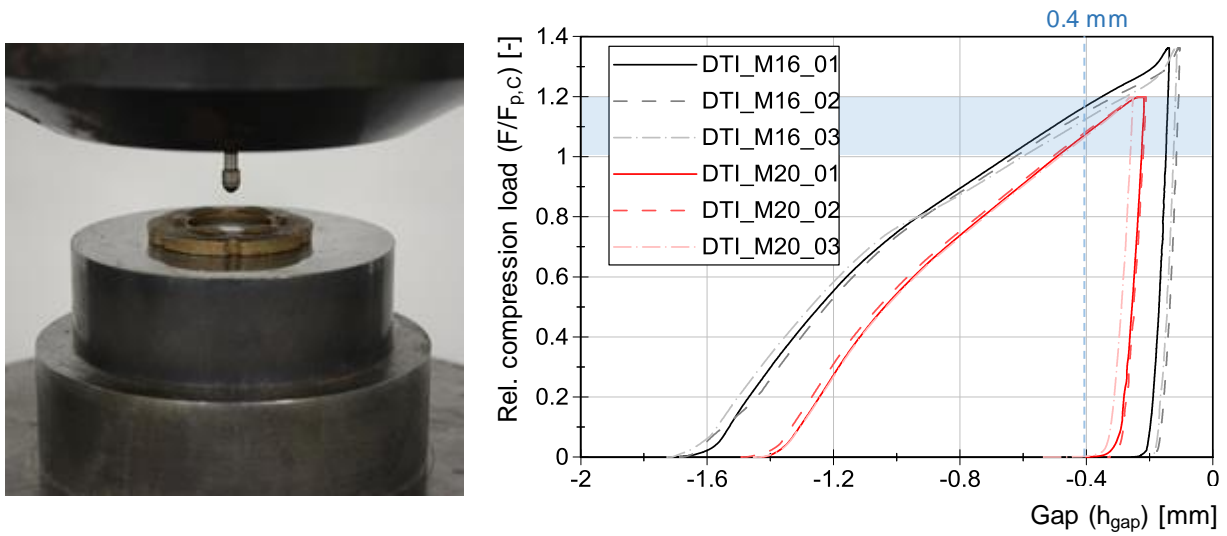


Figure 4.5-2: Compression test acc. to EN 14399-9 and gap - compression load diagram for each DTI

Table 4.5-2: Results of compression tests

Test ID	Test duration	Load at 0.4 mm	Testing rate	Maximum load	Relative load at 0.4 mm
	t [s]	$F_{0.4}$ [kN]	v_F [kN/s]	F_{max} [kN]	$F_{0.4} / F_{p,c}$ [-]
DTI – M16 – H10					
DTI-M16-01	30	128.6	4	150	1.17
DTI-M16-02	30	126.3	4	150	1.15
DTI-M16-03	30	124.0	4	150	1.13
DTI – M20 – H10					
DTI-M20-01	29	185.3	6	206	1.08
DTI-M20-02	29	186.7	6	206	1.09
DTI-M20-03	29	184.1	6	206	1.07

M20x115 HV 10.9 bolting assemblies were tested with DTIs in configuration under the nut and under the bolt head. The results showed that both bolting assemblies with DTIs under the nut fulfilled the normative determined criteria and therefore passed the suitability tests. However, the nominal preload level $F_{p,c}$ by reaching the minimum number of feeler gauge refusals could not be achieved for both tested M20 bolting assemblies with DTIs under the bolt head. That consequently led to failed suitability tests for both bolting assemblies. Detailed results of the suitability tests are presented in the deliverable D3.3 of Task 3.3.

The main focus of the experimental investigations in Task 3.3 lied on relaxation tests. These were conducted on preloaded bolted connections (M20 and M16 HV) with and without DTIs. Two different configurations acc. to EN 14399-9 were selected to investigate the influence of positioning of DTIs on the achieved preload level and preload losses. In addition, different clamping lengths were considered in order to investigate the influence of the clamping length on the relaxation behaviour of bolted connections for each bolt dimension. The clamping lengths were selected in such a way that the calculated clamping length ratios were the same for different bolt dimensions with and without DTIs. The clamping length ratios can be categorised in three different groups: series with clamping length ratio of about 1.5, 2.5 and 4.5. In total, twelve test series were investigated, each containing two types of specimens - eight-bolt-/ and one-bolt-specimens. For the eight-bolt-specimens, the DTIs were placed under the bolt heads in the first row and under the nuts in the second row. For all one-bolt-specimens, the DTIs were placed under the nut. The test specimens contained S355 carbon steel plates according to EN 10025-2 [7.5-2] in the “as received” surface condition, see Figure 4.5-4. The roughness R_z of the faying surfaces was measured acc. to EN ISO 4287 [7.5-3] and varied from 6 μm to 12 μm . The preload in the bolting assemblies during the relaxation tests was measured with implanted strain gauges.

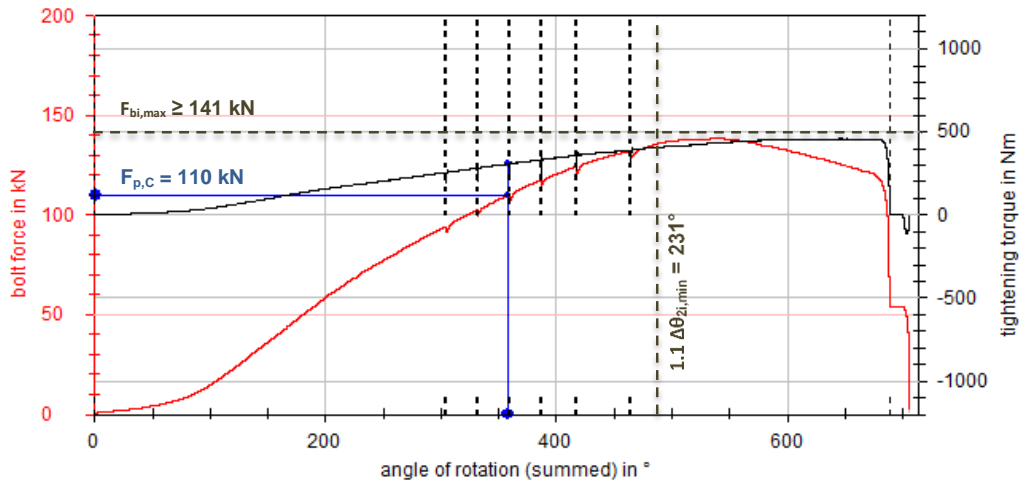


Figure 4.5-3: Tightening curves of test specimen M16-HN-2



Figure 4.5-4: Test specimen geometry for the relaxation tests of the bolted connections (test specimens for M16 and M20 bolts)

Tightening of the bolted connections with DTIs was carried out in multiple steps until the number of feeler gauge refusals n_{refusal} at the gaps exceeded half the number of total protrusions. In both combinations (DTI under the bolt head and DTI under the nut), the preload was applied by turning the nut. Test series without DTIs were tightened to an aimed preload level of $F_{p,C} = 0.7 \cdot f_{ub} \cdot A_s$ acc. to EN 1090-2. Herewith, the preload level for M20 and M16 HV 10.9 bolts yielded to about 172 kN and 110 kN respectively. The preload was measured continuously during the tests for all test series, see Figure 4.5-5.



Figure 4.5-5: Exemplary test setup for M16 bolted connection without DTIs (left) and for M20 bolted connection with DTIs (right)

After tightening of the bolts, a considerable drop in the measured preload curve between the maximum peak and the first seconds after tightening can be observed. This instant drop is not entirely related to the relaxation behaviour of the bolting assemblies. However, this phenomenon is explained by turning back of the nut and elastic recovery of the bolt threads when the wrench is removed; it is the so-called overshoot effect. For this reason, this overshoot has to be extracted. By removing the

first three seconds and by considering the linear behaviour of the loss of preload in a logarithmic scale, it is possible to derive the exact starting point of the relaxation test. The results in Figure 4.5-6 show that for M16 bolted connections with DTIs under the nut and refusals measured with a 0.25 mm feeler gauge, $F_{p,C}$ was achieved in all cases. For M20, the preload level $F_{p,C}$ was achieved in most of the cases. However, the achieved preload level for bolting assemblies with DTIs under the bolt head was always lower and in many cases $F_{p,C}$ was not even reached.

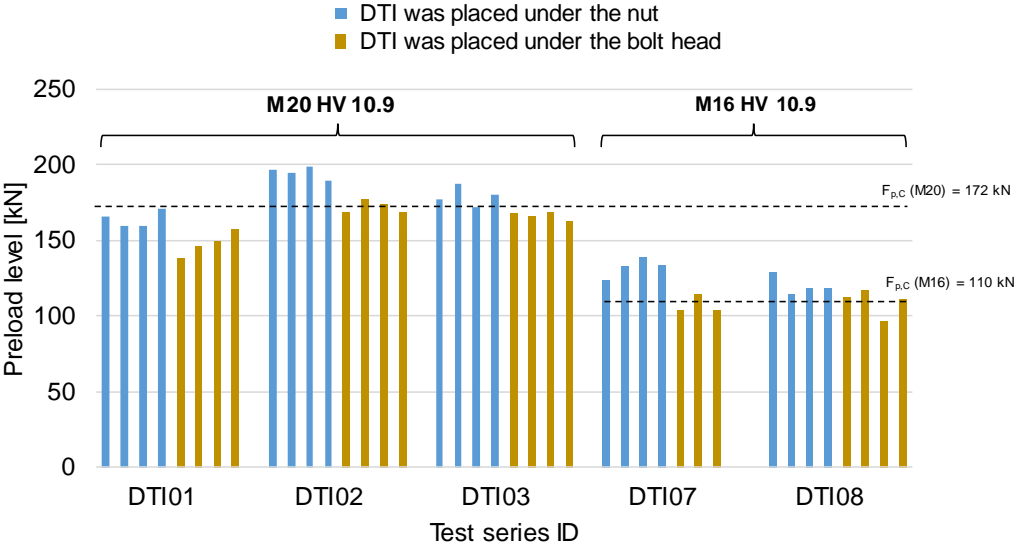
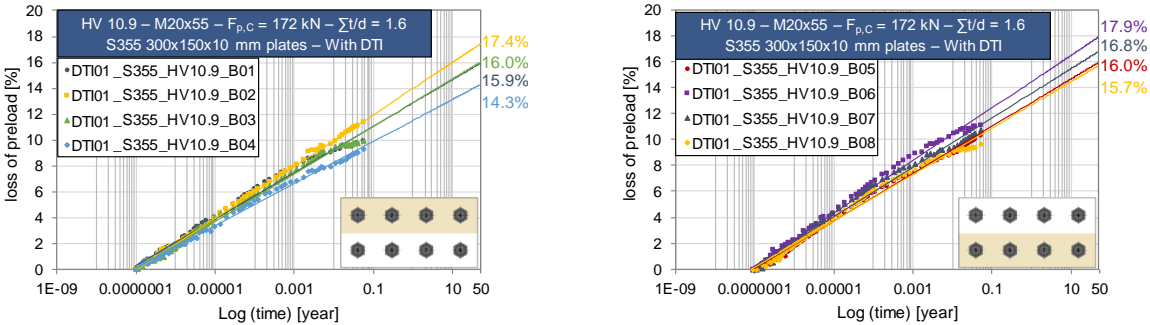


Figure 4.5-6: The achieved preload level for different DTIs bolted assemblies configurations (under the bolt head and under the nut) – results of eight-bolts-specimens

The resulting preload losses of the bolting assemblies after testing were extrapolated to 50 years, see Figure 4.5-7. As mentioned above, in order to have a rational evaluation of the measurements, the first three seconds of the measurements were not taken into account.

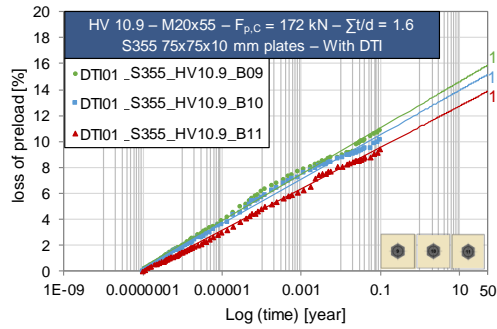
The results show that the loss of preload starts immediately after tightening of the bolts and gradually continues as time elapses. As it can be seen from Figure 4.5-7 (e) and (f) the highest rate of loss of preload is at the beginning of the test and after that the rate decreased during the passage of time. The present relaxation experiments show that the influence of positioning of the DTIs on the relaxation behaviour of the bolted connection is negligible. That means whether the DTIs are placed under the bolt head or under the nut, the same amount of loss of preload can be expected. The highest loss of preload for M20 bolting assemblies with DTIs (clamping length ratio of 1.6) was observed by about 16 % which is higher in comparison to the loss of preload resulting for M16 bolting assemblies with DTIs with a similar clamping length ratio (1.7) of about 10 %, see Figure 4.5-8. The loss of preload for M20/M16 bolting assemblies without any DTIs was about 8.5 %. This phenomenon can be ascribed to a high concentration of stress on a small area of protrusions. That results in more embedment in this area during time and consequently to higher loss of preload in these bolting assemblies.

Complete results of relaxation tests are presented in the deliverable D3.3 of Task 3.3.

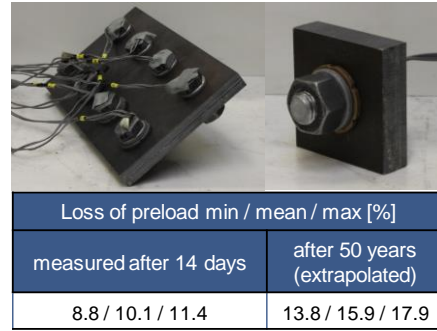


a) preload losses-log (time) diagrams for eight-bolts specimens - first row

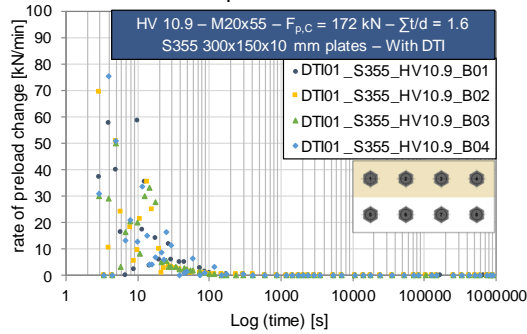
b) preload losses-log (time) diagrams for eight-bolts specimens - second row



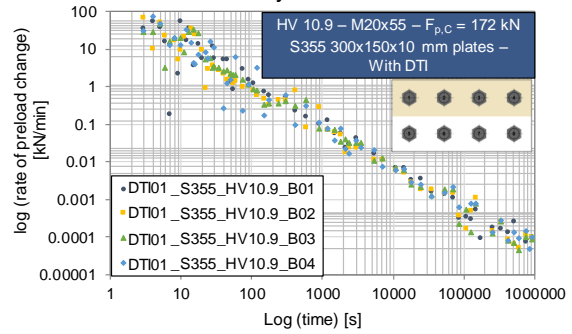
c) preload losses-log (time) diagrams for one-bolt specimens



d) loss of preload measured/extrapolated after 14 days/ 50 years



e) log (rate of loss of preload) – time diagrams for eight-bolts specimens - first row



f) log (rate of loss of preload) – log (time) diagrams for eight-bolts specimens - first row

Figure 4.5-7: Exemplary preload losses and rate of loss of preload for DTI01 test series

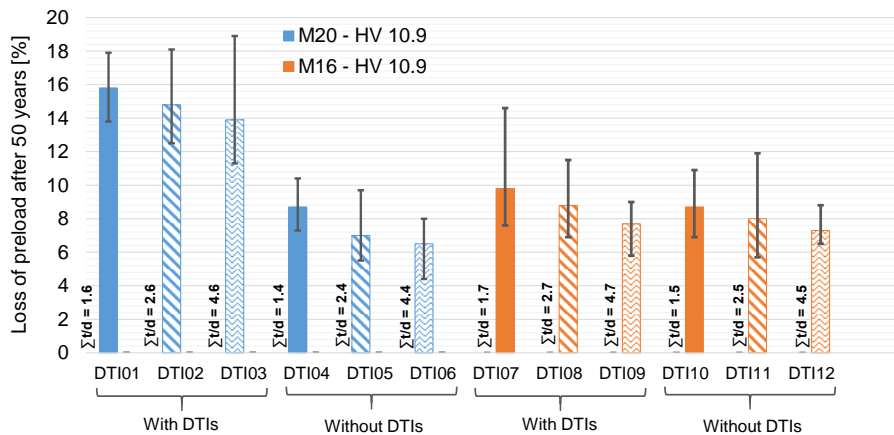


Figure 4.5-8: Extrapolated loss of preload at a service life of 50 years

5 WP 4 – Alternative surface treatments and coatings (CS)

5.1 Objectives

The main objectives of the WP are the investigation of the influence of various surface parameters on the slip factor of carbon steel and hot-dip galvanized steel applications.

(1) Carbon Steel applications

- Influence of surface preparation and blasting material (chill casting, slag, steel casting)
- Influence of coating material type or coating system
- Influence of application conditions, conditioning period and stability in storage

(2) Hot-dip galvanized steel applications

- Influence of steel composition (particularly the content of silicon)
- Influence of surface preparation and post treatment
- Determination of level of preload loss

(3) Investigation of the corrosion protection of carbon steel applications:

- a. Stress application by salt spray test according to ISO 9227 (NSS)
- b. Stress application by continuous condensation according to ISO 6270-1
- c. Determination of adhesive strength by cross-cut (ISO 2409) or pull-off test (ISO 4624)
- d. Visual evaluation after the end of the stress application with regard to corrosion protection properties
- e. Measurement of corrosion and delamination around a scribe

5.2 Work undertaken

The tasks undertaken in WP 4:

- 4.1. Influence of surface preparation and type of coating system on the slip factor and on the corrosion protection in case of carbon steel.
- 4.2. Influence of the surface preparation and type of coating system on the slip factor in case of hot dip galvanized steel.
- 4.3. Influence of the application and storage parameter on the slip factor and corrosion protection in case of ethyl-silicate-zinc coatings.

The work undertaken for Tasks 4.1 to 4.3 is summarized in Sections 8.3 - 8.5.

5.3 Task 4.1 – Plain CS

Coating systems for friction-grip joints usually consist merely of a primer. Too high film thicknesses lead to higher losses of preload due to creeping of the coating and shall not be carried out. Film thicknesses that are too low have negative effects on corrosion protection, since roughness peaks are not covered sufficiently. It is expected that the slip factor is influenced by the condition of the steel surface or the roughness, respectively. In accordance with EN 1090-2 [5.3-1] by reference to ISO 12944-4 [8.3-1] blast-cleaning until reaching roughness degree “medium” is recommended for sufficient adhesive strength of the coating on the substrate. For the examinations regarding the influence of different surface preparations five variations have been selected, which differ in regard to the type of blast-cleaning material, the preparation grade as well as the roughness. These five variations, on the one hand, have been coated with a primer based on ethyl silicate (ESI) and, on the other hand, with a coating based on epoxy resin (EP) (see Table 5.3-1 and Figure 5.3-1).

For the investigations, the coatings on the specimens have been applied under the same conditions in compliance with the coating manufacturer’s processing instructions by means of pneumatic spraying. Subsequently, the coatings have been conditioned for 7 days under standard climate (23 °C and 50 % relative humidity).

Table 5.3-1: Coating systems with different surface preparations

No.	Preparation of surface	Roughness	Blasting material	Primer A	Primer B
1	abrasive blast cleaning Sa 3	Rz. 80 µm grit	chill casting	ESI	EP
2	abrasive blast cleaning Sa 3	Rz. 80 µm grit	slag	ESI	EP
3	abrasive blast cleaning Sa 2 ½	Rz. 80 µm grit	chill casting	ESI	EP
4	abrasive blast cleaning Sa 3	Rz. >100 µm grit	chill casting	ESI	EP
5	abrasive blast cleaning Sa 3	Rz. 80 µm shot	steel casting	ESI	EP

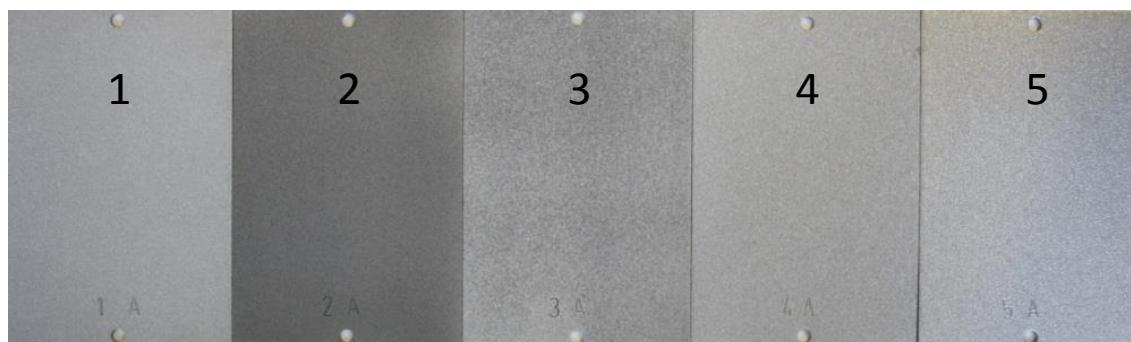


Figure 5.3-1: Blast-cleaned surface of variations

Slip-resistant behaviour

All slip factor tests were carried out according to EN 1090-2 (short term slip factor tests and creep tests). The steel plates of grade S355J2C+N were used for all experiments in Task 4.1. All plates were cut from plates of the same batch and individually marked (numbered). The material properties of the steel plates are presented in Table 5.3-2. All slip factor tests were performed in accordance with WP 1 and 2.

Table 5.3-2: Material properties of steel plates in Task 4.1

steel grade	specimen part	width	thickness	Rp0.2	Rm	A5	HB
		[mm]	[mm]	[N/mm ²]	[N/mm ²]	%	
S355J2C+N	centre	100	20	380	499	24%	-
	lap		10	395	530	30%	-

In Task 4.1, the influence of the surface preparation on the slip factor was investigated on 2 coating systems: ethyl silicate zinc and epoxy. Five surface treatments were used to clean/roughen the surface of the steel plates.

Table 5.3-3: Test matrix ethyl silicate zinc series (series A)

parameters							number of tests		
batch	surface preparation	roughness	film thickness	clamp length (CL)	bolt class	F _{P,c}	quasi static	creep test	SSWL test
		[μm]	[μm]	[mm]		[kN]		[-]	[-]
Coating: Interzinc 22 (2K-Etyl-silicate-zinc)									
A1	Sa 3, grit, chill casting	82	87	48	HR 10.9	172	8	2	2
A2	Sa 3, grit, slag	70	82				8	2	2
A3	Sa 2.5, grit, chill casting	79	84				8	2	2
A4	Sa 3, grit, chill casting	101	86				8	2	2
A5	Sa 3, shot, steel casting	67	84				8	2	2

Details on the surface roughness and coating thickness can be found in the deliverable of Task 4.1. Displacement (stroke) controlled loading was applied for all short term slip factor tests that were performed. Test rig displacement rates used for ethyl silicate zinc and epoxy was 0.003 mm/s and 0.0015 mm/s respectively.

Table 5.3-4: Test matrix epoxy series (series B)

parameters							number of tests		
batch	surface preparation	roughness	film thickness	clamp length (CL)	bolt class	F _{P,c}	quasi static	creep test	SSWL test
		[μm]	[μm]	[mm]		[kN]		[-]	[-]
Coating: SikaCor Zink R Papid (Epoxy)									
B1	Sa 3, grit, chill casting	82	75	48	HR 10.9	172	8	2	2
B2	Sa 3, grit, slag	72	77				8	2	2
B3	Sa 2.5, grit, chill casting	75	?				8	2	2
B4	Sa 3, grit, chill casting	103	81				8	2	2
B5	Sa 3, shot, steel casting	66	82				8	2	2

The slip load (F_{slip}) is defined as the maximum load that can be applied on the specimen or the load when a certain 'slip' occurs between the inner and cover plates before the maximum load is reached.

The slip is the displacement between the point in between the bolts (at the centre of the bolt group – CBG position) on inner and cover plates. To determine the slip factor in the short term tests the slip criterion, as described in EN 1090-2, was used: 0.15 mm displacement between the inner plates and the cover plates measured at the CBG position.

Due to setting effects and/or creep the preparation time of a specimen for a slip factor test and/or the duration of the test could have an influence on the bolt preload during the test. The changes in the preload level can directly influence the slip load. To be able to analyse these effects, the slip factor for each specimen was calculated in 3 different ways. μ_{nom}: based on the nominal bolt preload (slip factor

according to EN 1990-2), μ_{ini} : based on the preload in the bolts at the start of the slip factor test and μ_{act} : based on the preload in the bolts when the slip criterion is reached.

The preload in the bolts was applied using an air driven torque wrench. The bolts were initially preloaded to $F_{p,C} = 172$ kN. The preload was applied in a fixed order: Bolt2-Bolt3-Bolt4-Bolt1. Typically, the $F_{p,C}$ in all 4 bolts was reached within 3 minutes, see Figure 5.3-2.

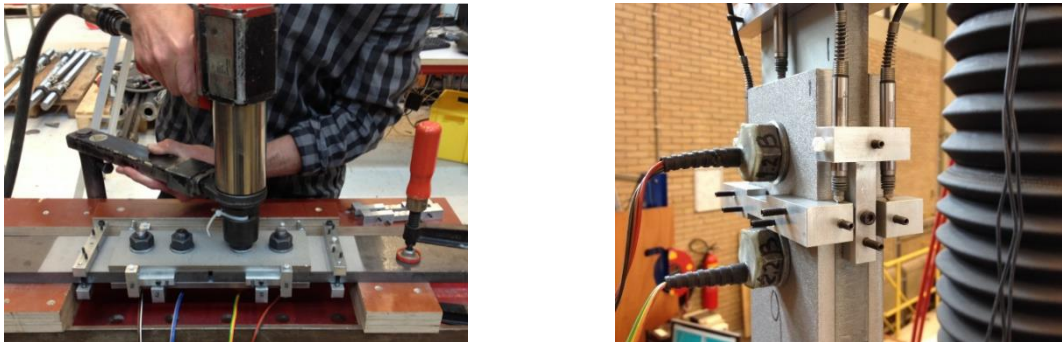
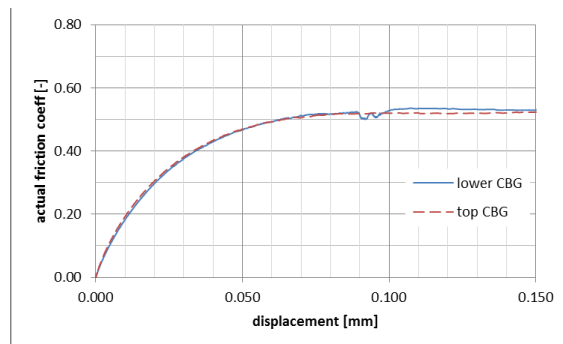
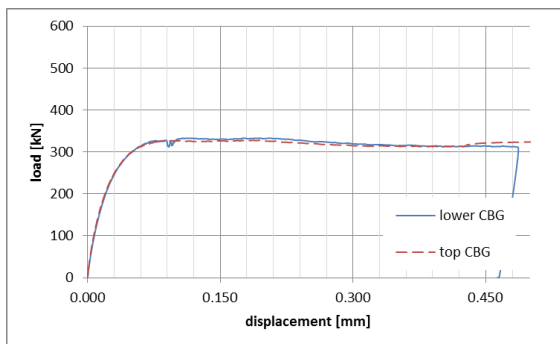


Figure 5.3-2: Application of pretension using air driven torque tool; mounting of LVDT brackets on cover plates

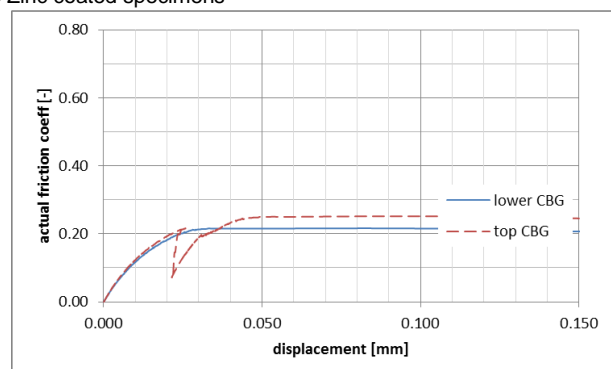
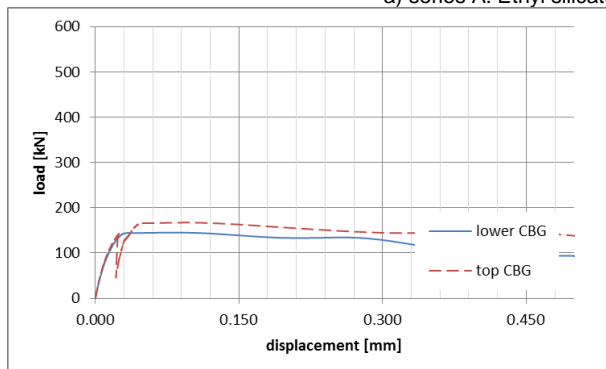
Figure 5.3-3 shows typical load - slip displacement diagrams that are obtained for all series. The slip in the ethyl silicate zinc coated specimens is progressing smoothly over both connections. The slip behaviour of the Epoxy differs from this. This coating suddenly slips.

In Table 5.3-5 the results of the slip factor tests for series A and B are summarized. The influence of the surface roughness for both series is very small. Short term slip factors in the order of magnitude of 0.5 are obtained for the A series. The slip factor of all variations of the Epoxy coating is limited to approximately 0.2.

The results of the creep tests indicate that all series are sensitive to creep, see Table 5.3-6. Sudden complete slip through occurred during some of the creep tests. The slip during the 3 hours creep tests on the A series seems a serious indication of creep sensitivity (slip in the order of magnitude between 25 and 50 μm are observed, where this is limited to 2 μm for non creep sensitive surfaces). Both extended creep tests carried out on series A1 and A5 with $0.85 F_{S,m}$ passed. It is likely that all B series would have passed the ECT on $0.9 F_{S,m}$. It is very unlikely that extended creep tests would have indicated the influence of the surface preparation of the B series on the long term slip factors.



a) series A: Ethyl silicate Zinc coated specimens



b) series A: epoxy resin coated specimens

Figure 5.3-3: Typical load – slip displacement diagram for series A and B

Table 5.3-5: Results of slip factor tests series A: Ethyl Silicate Zinc coating

a) series A: Ethyl Silicate Zinc coating

test results short term tests							test results including creep test				characteristic value acc. to Annex G	
series	test duration [min]		μ_{act}		μ_{ini}		μ_{act}		μ_{ini}		μ_k	
	mean	COV	mean	COV	mean	COV	mean	COV	mean	COV	actual	Fp,init
A1	11	11%	0.54	1%	0.49	2%	0.52	5%	0.48	5%	-	-
A2	12	16%	0.53	2%	0.48	2%	0.52	4%	0.47	4%	-	-
A3	11	14%	0.53	2%	0.48	2%	0.52	3%	0.47	4%	-	-
A4	11	19%	0.55	1%	0.49	1%	0.54	4%	0.48	4%	-	-
A5	12	34%	0.52	3%	0.47	2%	0.51	4%	0.46	5%	-	-

(b) series B: Epoxy coating

test results short term tests							test results including creep test				characteristic value acc. to Annex G	
series	test duration [min]		μ_{act}		μ_{ini}		μ_{act}		μ_{ini}		μ_k	
	mean	COV	mean	COV	mean	COV	mean	COV	mean	COV	actual	Fp,init
B1	11	33%	0.24	8%	0.23	8%	0.23	8%	0.23	8%	-	-
B2	12	33%	0.23	9%	0.22	9%	0.24	11%	0.23	11%	-	-
B3	11	34%	0.20	7%	0.20	7%	0.21	10%	0.21	9%	-	-
B4	11	33%	0.22	6%	0.22	5%	0.22	6%	0.21	6%	-	-
B5	16	36%	0.18	10%	0.18	10%	0.19	12%	0.18	11%	-	-

Table 5.3-6: Results of creep tests

a) series A: Ethyl Silicate Zinc coating

test results creep tests				
series	Fcreep test	slip top	slip lower	comment
	kN	[μm]	[μm]	
A1	301	35	54	
A2	297	1883	40	slip through
A3	297	26	37	
A4	306	34	1880	slip through
A5	289	39	26	

b) series B: Epoxy coating

test results creep tests				
series	Fcreep test	slip top	slip lower	comment
	kN	[μm]	[μm]	
B1	143	1938	1913	complete slip through
B2	137	9	10	
B3	124	6	6	
B4	135	9	11	
B5	110	8	8	

The results show that the influence of the surface preparation on the short term slip factor of both tested primers is small. The static slip factors for primer A (ethyl silicate + zinc dust) vary between 0.52 and 0.54 (average values). For primer B (epoxy with zinc dust) values between 0.18 and 0.24 were found. Creep tests show that both primers are sensitive to creep.

Investigations in regard to corrosion protection

The characterization of the corrosion protection effect of a coating system can be performed by means of different examinations in regard to corrosion protection. On the one hand, the detection of weak spots in the coating system is of interest; on the other hand, information on barrier effects can be supplied. The duration of stress application was scheduled for 2.160 hours in neutral salt spray in accordance with ISO 9227 [8.3-2] as well as for 1.200 hours in condensating-water constant climate in accordance with ISO 6270-1 [8.3-3].

Ethyl silicate coatings with zinc-dust can tend towards blistering due to their porosity when over coated with further coatings. In order to avoid blistering in practice so-called bonding agents are applied in thin films. They provide that the pores remain open longer and entrapped gas can escape. Therefore, the variations of system B have been prepared with an additional film.

Prior to the stress application, parameters for the adhesive strength were determined on the reference test specimens by means of the cross-cut test (ISO 2409 [8.3-4]) as well as the pull-off strength and the failure pattern were determined with the sandwich method (ISO 4624 [8.3-5]).

The results of the cross-cut test show differences between coatings based on organic and inorganic binders. Cross-cuts of coatings with inorganic (silica based) binders often do not correspond to the characteristic value 1 due to their hardness and brittleness. This was also the case for the examined coating system A, the failure of which always occurred within the coating. The examined coating system B based on organic binder, in contrast, showed very good cross-cut values, see Table 5.3-7 and Table 5.3-8.

Table 5.3-7: Results corrosion protection tests series A

	A1	A2	A3	A4	A5
Reverence samples					
DFT [μm]	236 \pm 7	237 \pm 9	232 \pm 17	242 \pm 16	236 \pm 10
Cross-cut	5	5	5	5	5
Pull-off strength [MPa]	7,7	9,2	11,9	7,1	8,1
Failure pattern*	100 B	100 B	100 B	90 B, 10 C	10 A/B, 90 B
Assessment after 2.160 hours neutral salt spray test					
DFT [μm]	244 \pm 11	233 \pm 14	240 \pm 17	238 \pm 11	237 \pm 14
Cross-cut	5	5	5	5	5
Pull-off strength [MPa]	12,3	12,6	10,8	16,0	9,5
Failure pattern*	100 C	100 C	30 B, 70 C	100 C	50 A/B, 50 C
Corrosion at the scratch [mm]	1,4 \pm 0,5	1,8 \pm 0,5	1,9 \pm 0,6	1,0 \pm 0,5	1,5 \pm 0,2
Assessment after 1.200 hours continuous condensation					
DFT [μm]	237 \pm 10	226 \pm 15	228 \pm 12	233 \pm 14	234 \pm 13
Cross-cut	5	5	5	5	5
Pull-off strength [MPa]	5,2	7,6	8,6	9,2	6,8
Failure pattern*	50 B, 50 B/C	10 B, 90 B/C	30 B, 70 B/C	100 B/C	100 B/C

The best results are obtained for the variant with the highest roughness ($R_z > 100 \mu\text{m}$) - System 4A and 4B. The film thickness as well as the coating system have been characterised by means of metallographic cross-sections and light-microscope images (see Figure 5.3-4).

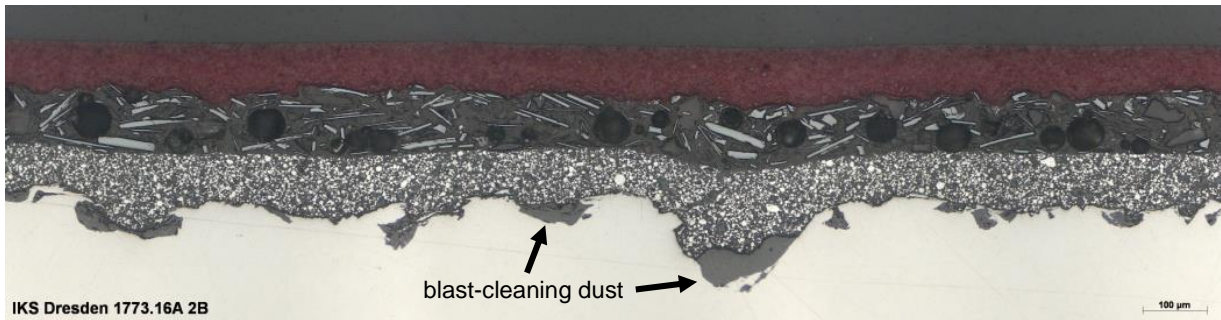
The different roughness profile is clearly visible in the cross-section images. Surfaces blast-cleaned with chilled-iron grit show a typical roughened profile (a). In case of blast-cleaning using slag (b), residue of the blast-cleaning material can remain on the surface. This blast-cleaning dust is partially enclosed in the surface and cannot be blown off even by means of pressurized air. Visually the surface gains a dark shade. Slags are single-use blast-cleaning material and are used in practice e.g. on construction sites. They are not expensive and the wasted blast-cleaning material can easily be disposed of.

Table 5.3-8: Results corrosion protection tests series B

	B1	B2	B3	B4	B5
Reverence samples					
DFT [μm]	246 \pm 13	252 \pm 8	254 \pm 8	253 \pm 10	253 \pm 16
Cross-cut	1	1	1	1	2
Pull-off strength [MPa]	16,2	17,0	18,6	18,8	18,9
Failure pattern*	70 C, 30 D	60 C, 40 D	60 C, 30 D	50 C, 50 D	50 C, 50 D
Assessment after 2.160 hours neutral salt spray test					
DFT [μm]	234 \pm 9	249 \pm 8	239 \pm 7	243 \pm 8	242 \pm 8
Cross-cut	1	from 1 to 5	0-1	1-2	1-2
Pull-off strength [MPa]	19,0	from 1,8 to 18,2	19,0	23,1	16,7
Failure pattern*	100 C	100 A/B and 100 C	100 C	100 C	from 50 A/B to 100 C
Corrosion at the scratch [mm]	2,6 \pm 0,8	3,1 \pm 0,7	3,4 \pm 0,8	1,9 \pm 0,7	2,6 \pm 0,6
Assessment after 1.200 hours continuous condensation					
DFT [μm]	239 \pm 5	241 \pm 9	235 \pm 9	238 \pm 6	233 \pm 9
Cross-cut	1	from 1 to 3	1	1	from 1 to 5
Pull-off strength [MPa]	16,4	13,1	17,0	19,2	19,6
Failure pattern*	100 C	100 A/B and 100 C	100 C	100 C	100 C
*meaning for evaluation:	A/B ... adhesion failure between substrate (steel) and 1 st layer B ... cohesion failure in the 1 st layer B/C ... adhesion failure between 1 st layer and 2 nd layer C ... cohesion failure in the 2 nd layer D ... cohesion failure in the 3 th layer				



a) Roughness profile of chill casting



b) Roughness profile of slag



c) Roughness profile of steel casting

Figure 5.3-4: Metallographic cross-sections of different roughness profiles

Blast-cleaning with spherical blast-cleaning material leads to less roughening of the surface and to solidification of the surface. For low-alloy steels blast-cleaning with grit blast-cleaning material is normally recommended in order to achieve sufficient roughness. A correlation of the results from the examinations in regard to corrosion protection and the results of the slip factor tests could not be determined.

5.4 Task 4.2 – Hot dip galvanized CS

The application of hot dip galvanized steel is an efficient method of corrosion protection. Previously reported friction coefficients in hot dip galvanized plates show large variations, e.g. from 0.15 to 0.5. In practice, the results in the use of the lower values in design. It is understood that the causes of the variations are the thickness and structure of the coating which can vary dependent on factors such as the chemical composition of the steel (some promote a stronger reaction between zinc and iron than other compositions), the thermal mass of the steel component and other process variables. The extent to which a softer, outer zinc-phase is present on the coating surface is reported to be the main determinant of slip-resistance although if small amounts of slip can be tolerated, this phase will experience a 'cold welding' upon loading. However, when small amounts of initial slip cannot be tolerated this layer can be easily removed by abrasive sweep blast cleaning or other techniques to modify the surface. In this task, the influence of surface preparation and post treatment on slip-resistant behaviour of the connection and level of loss of preload were investigated.

Slip factor tests

Seven slip factor test series (static and creep tests), see Table 5.4-1, have been conducted to investigate the influence of different post treatments on the slip-resistant behaviour of galvanized surfaces.

Table 5.4-1: Test programme, mean slip factors based on static and creep tests only ($\mu_{ini,mean}$ and $\mu_{act,mean}$) as well as final slip factors calculated as 5 % fractile or determined in the extended creep test ($\mu_{5\%}$ or μ_{ect})

Series ID	Steel grade	Final surface condition					Number of tests	$\mu_{ini,mean}^{5)}$ st/st+ct	$\mu_{act,mean}^{6)}$ st/st+ct	V ($\mu_{act}^{7)}$) st/st+ct	Final slip factor [-]				
		Main coating		Rz ¹⁾ [μ m]	t ²⁾ [μ m]	Additional coating									
		Type	Post treatment			Type						DFT ³⁾ [μ m]	st/ct/ect ⁴⁾		
Task 1.1	HDG-II	S355 ¹⁰⁾			-	105				2/-/2	0.47/-	0.51/-	14.6/-	-/0.35	
	HDG-III		no post treatment	-	80			4/-/-	0.12/-	0.12/-	6.6/-	-/-			
	HDG-Ref			-	71			4/-/-	0.14/-	0.14/-	11.6/-	-/-			
	HDG_NG-I		needle gun at an angle of 45°	30	60-70			4/1/-	0.23/-	0.24/-	6.2/-	-/-			
	HDG_NG-II		needle gun at an angle of 90°	40	60-70	-	-	4/1/-	0.20/-	0.21/-	3.7/-	-/-			
Task 4.2	HDG_SB-I	S355 ¹¹⁾	Hot dip galvanized	sweep blasted at an angle of 30° with particle size 0.2 - 0.5 mm	30	60-70					4/1/-	0.35/-	0.36/-	11.9/-	-/-
	HDG_SB-II			sweep blasted at an angle of 30° with particle size 0.5 - 1.0 mm	50	60-70			4/1/-	0.39/-	0.41/-	11.8/-	-/-		
	HDG-ASI			sweep blasted at an angle of 30° with particle size 0.2 - 0.5 mm	30	120-130	ASI ¹²⁾	60	4/1/1	0.62/-	0.70/-	5.1/-	-/-		
	HDG-ESI			sweep blasted at an angle of 30° with particle size 0.2 - 0.5 mm	30	120-130	ESI ¹³⁾	70	4/1/1	0.47/-	0.52/-	4.3/-	-/-		

¹⁾ surface roughness | ²⁾ average HDG coating thickness | ³⁾ dry film thickness (total coating thickness) | ⁴⁾ st: static test/ct: creep-ect: extended creep test | ⁵⁾ $\mu_{ini,mean}$: calculated slip factors as mean values considering the initial preload when the tests start | ⁶⁾ $\mu_{act,mean}$: calculated slip factors as mean values considering the actual preload at slip | ⁷⁾ V: coefficient of variation for $\mu_{act,mean}$ | ⁸⁾ $\mu_{5\%}$: slip factors as 5 % fractile calculated based on the static tests and the passed creep test | ⁹⁾ μ_{ect} : slip factor resulting from the extended creep test passed | ¹⁰⁾ moderately reactive steel (S355J2C+N) | ¹¹⁾ low-reactive steel chemistry for galvanizing | ¹²⁾ alkali-zinc silicate (ASI) coating | ¹³⁾ ethyl-zinc silicate (ESI) coating. | All bolts were preloaded to $F_{p,C} = 172$ kN.

The test specimen geometry was chosen for the test specimen with M20 bolts as shown in Figure 5.4-1 (a) according to EN 1090-2, Annex G. For each test specimen four M20 HV bolts class 10.9 were instrumented with a strain gauge, see Figure 5.4-1 (b). In the presented investigation, the slip factors are evaluated based on the measured slip displacement in CBG position, see Figure 5.4-1 (b) and (c). The slip load F_{Si} was determined at 0.15 mm slip or at the highest peak before.

The faying surfaces of two test series were treated with needle gun with 9 bar air pressure and two different angles to the coated surfaces (45° and 90°). Two test series were sweep blasted with air pressure of 2.5 bar at an angle of 30° to the zinc surface but with two different particle sizes. Two more series were also sweep blasted using an identical blasting procedure as for series HDG_SB-I and then coated with alkali-zinc silicate (ASI) coating (HDG-ASI) and ethyl-zinc silicate (ESI) coating (HDG-ESI). All post treatments were conducted at Institute for Corrosion Protection (IKS) Dresden GmbH. One test series was tested without any further surface treatment, as a reference. The results of this task are compared with the results of HDG-test specimens which were tested in Task 1.1 (HDG-II, HDG-III).

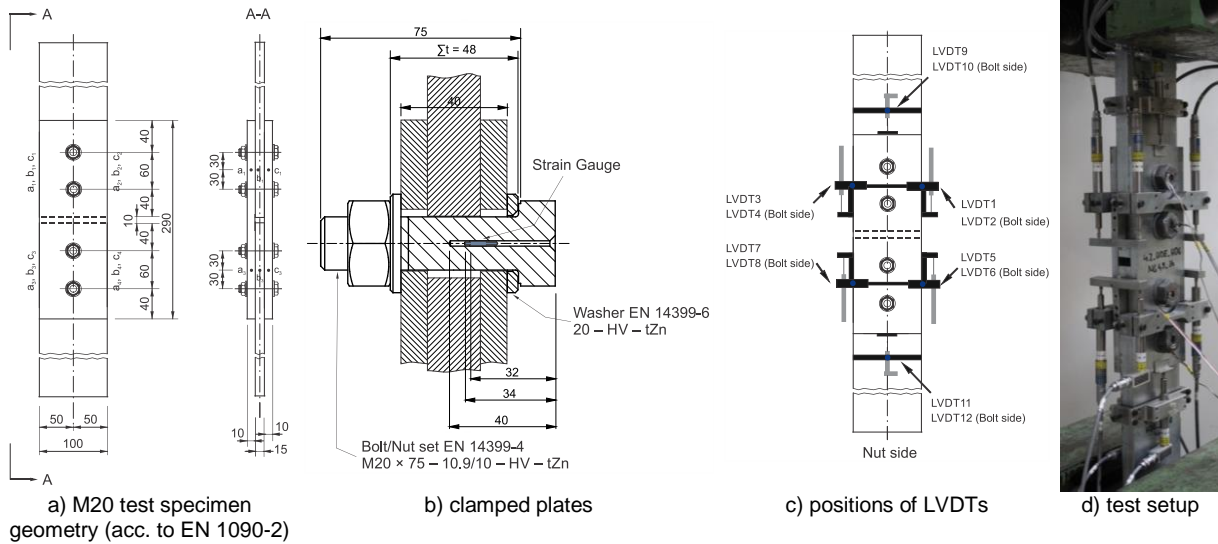


Figure 5.4-1: Test setup, test specimen geometry, positions of displacement transducers (LVDTs) as well as clamped plates of a bolted connection with bolts with implanted strain gauge

Table 5.4-1 also presents the calculated slip factors as mean values considering the nominal preload in the bolts $\mu_{nom,mean}$, the initial preload when the tests started $\mu_{ini,mean}$ and the actual preload at slip $\mu_{act,mean}$. The final slip factors are also presented as 5 % fractile if no extended creep test is necessary or after the extended creep test. Figure 5.4-2 (a) shows typical load-slip displacement curves that resulted from the static slip factor tests for all different test series. Each test presented by two graphs, which represent the behaviour of the upper and lower part of the connection.

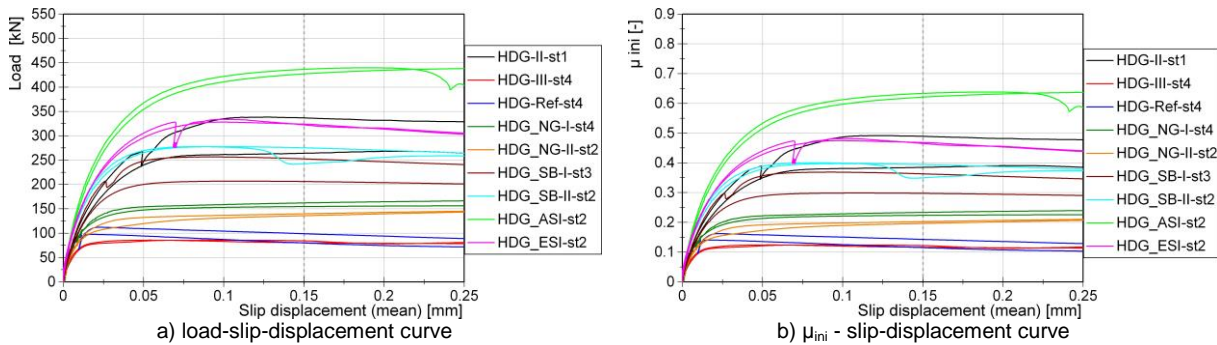


Figure 5.4-2: Influence of different surface treatment/preparation on the slip-load behaviour and initial slip factors
Using needle gun shows slightly improved slip-resistance behaviour of the galvanized specimens, see Figure 5.4-2 (b) and Figure 5.4-3. The results show that the sweep blasted surfaces achieved higher static slip factors compared to needle gun treated surfaces. Figure 5.4-3 shows that better results can be achieved by using a more effective for sweep blasting of the surfaces. The results show that the highest static slip factor for test specimens is achieved for the sweep blasted and coated with ASI-coating (HDG-ASI) test series followed by the sweep blasted test series with ESI coating (HDG-ESI).

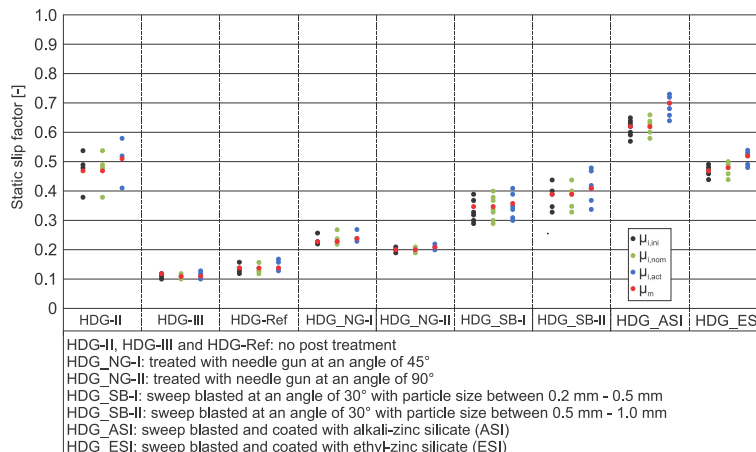


Figure 5.4-3: Influence of different post treatments on the static slip factors

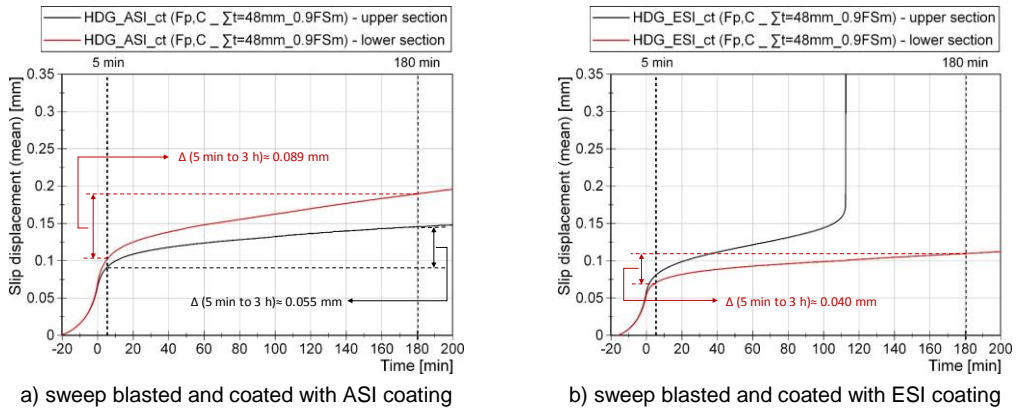


Figure 5.4-4: Results of creep tests considering different post treatment for galvanized specimens

For all test series the creep tests failed for both upper and lower part of the specimens, thus it is necessary to perform extended creep tests to determine the final slip factor, see Figure 5.4-4. For HDG_ASI and HDG_ESI coated surfaces one extended creep test was performed with a lower constant load level of $0.8 F_{Sm} = 341.4 \text{ kN}$ and $0.83 F_{Sm} = 272.4 \text{ kN}$ respectively. As it can be seen in Figure 5.4-5, the tests cannot be considered as a passed extended creep test. The available extended creep test results for the HDG_ASI and HDG_ESI coated surfaces do not allow a conclusion regarding the final slip factor for these test series. Extended creep tests were not carried out for the other HDG test series in this task.

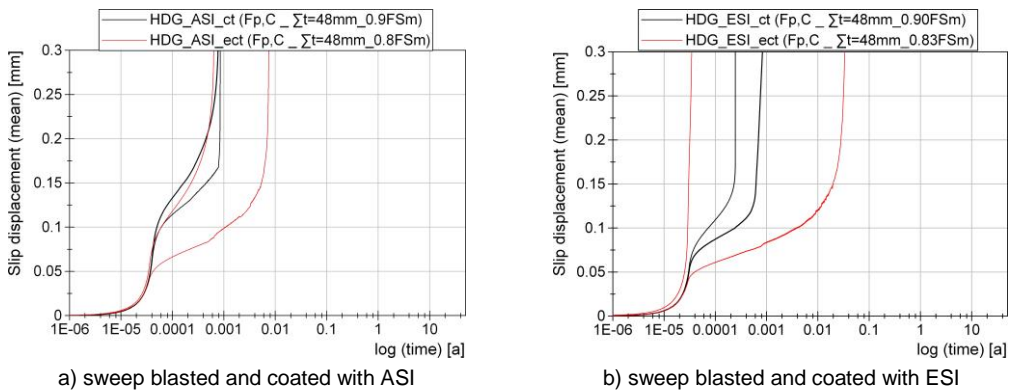


Figure 5.4-5: Evaluating the slip displacement – log time curves

Relaxation tests

The level of preload has an important influence on the resulting slip factor (the higher the preload the higher the slip factor). Hot dip galvanized steel in some surface conditions has a tendency to creep. This leads to a loss of preload. For this reason, some relaxation tests were performed in order to investigate the relaxation behaviour of HDG-coated surfaces. The relaxation tests were performed using two bolted carbon steel plates (made of S355 identical to that used for slip factor tests) of the dimensions approx. 300 mm x 150 mm with eight preloaded bolts and 75 mm x 75 mm with one preloaded bolt, see Figure 5.4-6.

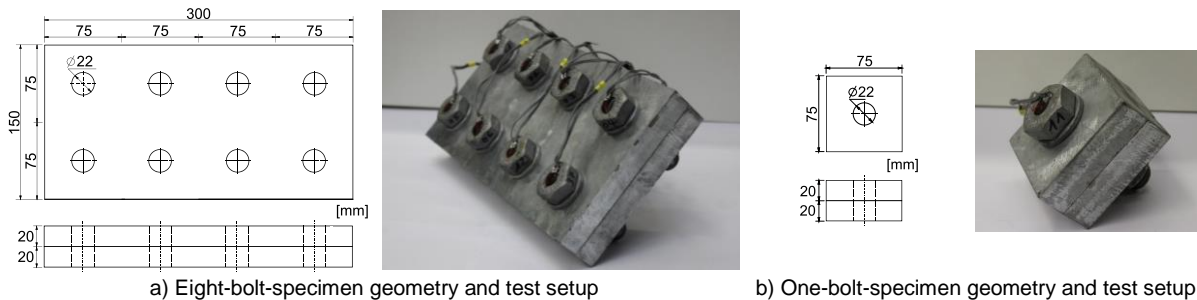


Figure 5.4-6: Test specimen geometry for the relaxation tests of the bolted connections

All bolts were equipped with implanted strain gauges to measure the change of preload in the bolts during the whole test time, see Figure 5.4-6. In comparison to the tests performed in Task 3.3 (the test results for test specimens without DTIs), identical plate thicknesses were chosen.

The resulting preload losses of the bolting assemblies after testing were extrapolated to 50 years, see Table 5.4-2. In order to have a rational evaluation of the measurements, the first three seconds of the measurements were not taken into account, see more information in Deliverable 4.2.

Table 5.4-2: Relaxation test matrix/results

Ser. ID	Type of specimen	No. of tests	Clamped plates				F_p ³⁾ [kN]	Loss of preload		
			Post treatment		Additional coating			measured after		
			Type	DFT ¹⁾ [μm]	Type	DFT ²⁾ [μm]		days – min / mean / max [%]	after 50 years (extrapolated) min / mean / max [%]	
DTI05 ⁴⁾	8 bolt	First row	4	–	–	–	–	14 – 4.0 / 5.1 / 6.5	6.0 / 7.7 / 9.7	
		Sec. row	–	–	–	–	–	–	–	
	1 bolt	–	4	–	–	–	–	35 – 9.4 / 10.1 / 10.8	5.5 / 6.2 / 7.1	
HDG-Ref	8 bolt	First row	4	–	71	–	–	20 – 6.9 / 7.2 / 7.4	10.5 / 11.2 / 11.7	
		Sec. row	4	–	–	–	–	20 – 5.7 / 6.1 / 6.4	9.3 / 9.7 / 10.1	
HDG_SB-I	8 bolt	First row	4	sweep blasted at an angle of 30° with particle size 0.2 - 0.5 mm	60-70	–	–	$F_{p,C}$	20 – 6.8 / 7.1 / 7.4	10.3 / 10.8 / 11.3
		Sec. row	4						20 – 5.3 / 6.0 / 7.9	8.0 / 9.3 / 12.0
	1 bolt	–	3						20 – 5.2 / 6.3 / 7.2	7.9 / 9.5 / 10.8
HDG_ASI	8 bolt	First row	4	sweep blasted at an angle of 30° with particle size 0.2 - 0.5 mm	60-70	ASI ⁵⁾	60	$F_{p,C}$	25 – 13.2 / 14.2 / 15.3	19.6 / 21.2 / 23.0
		Sec. row	4						25 – 11.7 / 13.7 / 14.8	17.3 / 20.5 / 22.2
	1 bolt	–	3						25 – 12.7 / 13.3 / 14.4	19.1 / 20.0 / 21.5
HDG_ESI	8 bolt	First row	4	sweep blasted at an angle of 30° with particle size 0.2 - 0.5 mm	60-70	ESI ⁶⁾	70	$F_{p,C}$	25 – 9.1 / 9.6 / 10.0	13.8 / 14.4 / 14.9
		Sec. row	4						25 – 8.5 / 8.9 / 9.4	13.0 / 13.4 / 14.0
	1 bolt	–	2						25 – 10.2 / 10.5 / 10.8	14.9 / 15.6 / 16.2
	8 bolt	First row	4	$F_{p,1}$					55 – 9.6 / 9.9 / 10.3	13.6 / 14.2 / 14.5
		Sec. row	4						55 – 12.1 / 12.4 / 12.8	17.1 / 17.4 / 18.0

¹⁾ dry film thickness (Zn/Coating thickness) | ²⁾ dry film thickness (additional coating thickness) | ³⁾ preload level ($F_{p,C} = 0.7 \cdot f_{ub} \cdot A_s = 172$ kN, $F_{p,1} = 0.8 \cdot f_{ub} \cdot A_s = 197$ kN, $F_{p,2} = 0.6 \cdot f_{ub} \cdot A_s = 123$ kN) | ⁴⁾ the results from Task 3.3 | ⁵⁾ alkali-zinc silicate (ASI) coating | ⁶⁾ ethyl-zinc silicate (ESI) coating

Figure 5.4-7 shows the exemplary preload losses-log (time) diagrams for HDG-Ref test series. The results show that the highest loss of preload was observed for HDG_ASI test series by about 20.6 %, see Figure 5.4-8. It can also be seen that the minimum amounts of loss of preload for coated surfaces were observed for HDG_SB-I and HDG-Ref test series. As expected the lowest loss of preload was observed for uncoated test series from Task 3.3.

The loss of preload starts immediately after tightening of the bolts and gradually continues as time elapses. As it can be seen from Figure 5.4-9, the highest rate of loss of preload is at the beginning of the test and after that the rate decreases with the passing of time. Figure 5.4-8 shows that for the HDG_ESI specimens there is a tendency towards a higher loss of preload in percent for a lower level of preload. However, the results show that by applying a higher preload the amount of loss of preload in kN is higher.

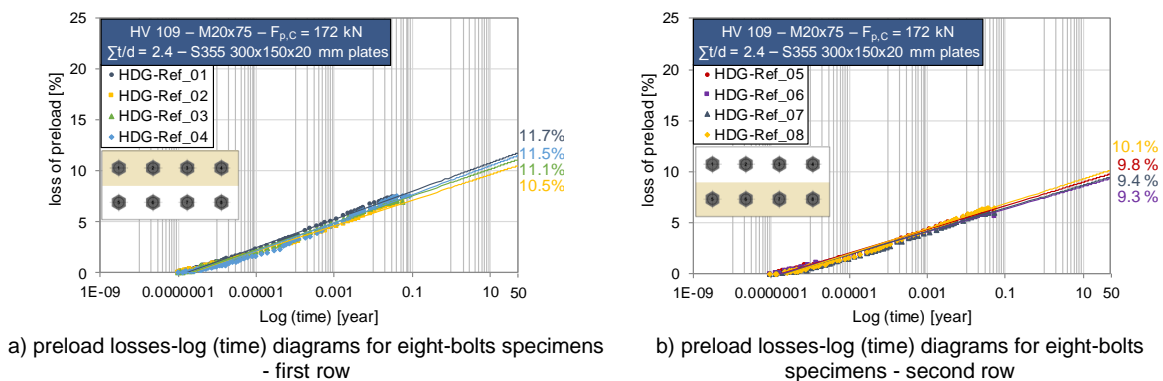


Figure 5.4-7: Preload losses for HDG-Ref (preload level: $F_{p,C} = 0.7 \cdot f_{ub} \cdot A_s = 172$ kN)

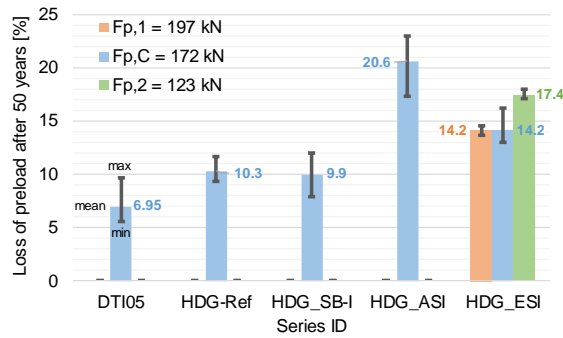


Figure 5.4-8: Extrapolated loss of preload at a service life of 50 years

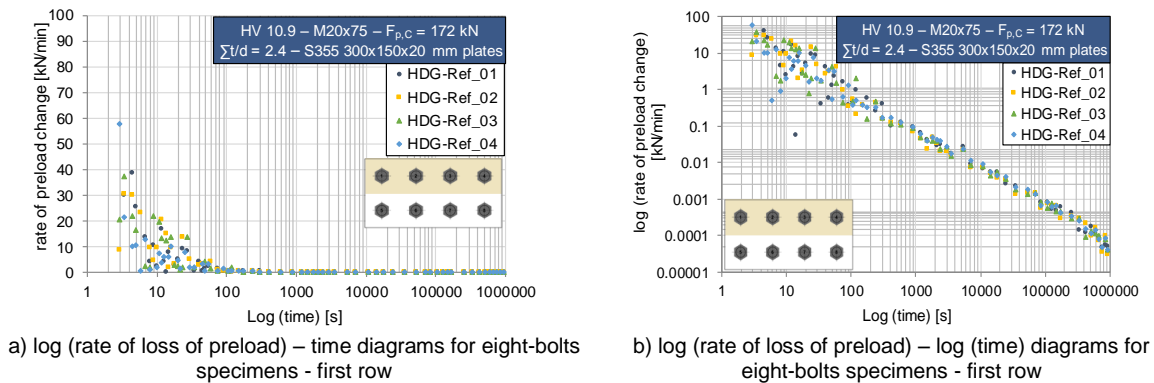


Figure 5.4-9: Rate of loss of preload for HDG-Ref (preload level $F_{p,C} = 172$ kN)

Conclusion

These results show that higher static slip factors (in the range 0.35 - 0.40) for galvanized coatings will be achieved when the outer zinc layer is sufficiently removed by a light blasting procedure (sweep blasting), so that the Fe-Zn layers will control the slip behaviour. Sweep blasting of a hot dip galvanized coating combined with the application of an alkali-zinc silicate (ASI) paint produces the highest static slip factors observed in these tests ($\mu_{ini,mean} = 0.62$). The extrapolated loss of preload at a service life of 50 years shows that having additional coating like ESI- and ASI-coating on hot dip galvanized surfaces, increase the amount of loss preload significantly.

5.5 Task 4.3 – Different application and storage parameters in case of ethyl-silicate-zinc coatings

In practice, the hardening conditions and storage parameters can be very different. The storage stability is the period of time during which the coating material remains ready for use while being stored in a closed original container under standard conditions (specified by the manufacturer). The conditioning of the samples after application, especially the temperature and relative humidity, and the storage stability has an effect on the slip factor and the corrosion protection. In Task 4.3, these influences will be investigated. For this, test specimens with a coating material based on ethyl silicate have been prepared (Table 5.5-1). One part of the test specimens has been conditioned for 7 days (System B, C) and another one has been conditioned for 3 weeks (System A). In order to maintain the hardening conditions constant, the test specimens have been stored in the climate cabinet at 23 °C and 60 % relative humidity. Simultaneously, test specimens coated with ethyl silicate have been prepared. The ethyl silicate had already been stored for 12 month in the Institute for Corrosion Protection (IKS) (System B in Table 5.5-2). By means of these test specimens the influence of the storage stability was examined by using an expired ESI batch (“old”). Furthermore, coating systems have been prepared on which investigations in regard to corrosion protection were carried out. On the one hand, the detection of weak spots in the coating system is of interest; on the other hand, information on barrier effects can be supplied. The duration of stress application was scheduled for 2.160 hours in neutral salt spray in acc. with ISO 9227 [8.3-2] as well as for 1.200 hours in condensation-water constant climate in acc. with ISO 6270-1 [8.3-3].

Table 5.5-1: Coating systems for examinations in regard to corrosion protection

System	Description	Coating structure		Nominal dry film thickness [μm]	Total dry film thickness [μm]
A	ethyl silicate (ESI) new batch	50 μm Interzinc 22 30 μm Intergard 269 80 μm Intergard 345 80 μm Interthane 990	ESI primer EP coupling agent EP intermediate coat PUR top coat	240	247 ± 11
B	ethyl silicate (ESI) stored for 12 month				249 ± 10
C	ethyl silicate (ESI) new batch				241 ± 8

Table 5.5-2: Test matrix

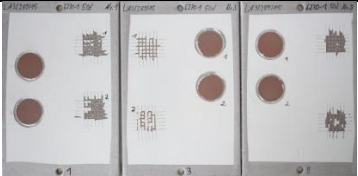

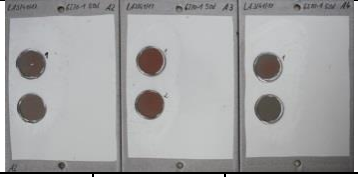

system	coating	conditioning [week(s)]	batch	∑t clamp length [mm]	notation	static tests	creep (step) test	ECT ¹⁾
A	ESI	3	new	48 mm	A-ESI-3-n	4	1	1
B	ESI	1	old	48 mm	B-ESI-1-o	4	1	2
C	ESI	1	new	48 mm	C-ESI-1-n	4	1	-


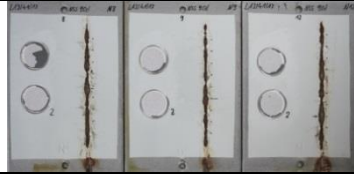
¹⁾ ECT – Extended Creep Test | Bolting System: Bolt dimensions: HV-M20x75, 10.9, k-class K1, Test specimen acc. to EN 1090-2 Annex G “M20” | tightening on defined preload in two steps: 1. step 100 kN 5min setting, 2. step F_{p,c} = 172 kN | test velocities: Slip Load Test: v = 0.004 mm/s, Step Test: v = 1 kN/s, Extended Creep Test: v = 1 kN/s

Before the salt spray test an artificial damage is introduced on the test specimens down to the steel substrate in order to evaluate the behaviour of the coating system around the scratch. The scratch ran parallel to one of the longitudinal sides of the test specimen at a distance of 30 mm to the edge of the test specimen. The width of the scratch was 0.5 mm. A scratching tool with a profile based on Clemen was used. Prior to the stress application, parameters for the adhesive strength were determined on the reference test specimens. The pull-off strength and the failure pattern were determined with the sandwich method (ISO 4624 [8.3-5]). For the determination of the pull-off strength test cylinders (Ø 20 mm) are adhered to test panels. With the sandwich method two test cylinders each are installed coaxial by means of a centring device. After hardening of the adhesive (cyanoacrylate), using a tensile tester, the pull-off strength information on the failure pattern and, thus, on the weakest part of the coating system is given.

Adhesion failure, cohesion failure or mixed failure can occur (see Table 5.5-3). Regarding their corrosion protection values the systems show no differences with the exception of the failure pattern. The failure pattern is the weakest part of the coating system. System A shows cohesion failures in the 2nd layer, system B shows cohesion failures in the 1st and 2nd layer and system C shows mainly cohesion failures in the 4th layer. A negative influence of storage stability on the corrosion protection values could not be detected.

Table 5.5-3: Results of corrosion protection tests for System A and N

	Assessment after 1.200 hours continuous condensation			Assessment after 2.160 hours neutral salt spray test		
System A (ESI new batch)						
Film thickness ISO 2808 [8.5-1] [μm]	244 ± 15	248 ± 10	246 ± 18	247 ± 9	245 ± 10	253 ± 7
Visual evaluation	no visual changes			no visual changes		
Pull-off strength [MPa]	11,8	10,7	10,8	18,2	12,2	17,9
Failure pattern	cohesion failure in the 2 nd layer			cohesion failure in the 2 nd layer		
Corrosion at the scratch [mm]	-			1,9 ± 1,0	1,7 ± 0,4	2,1 ± 0,6
Delamination at the scratch [mm]	-			2,3 ± 0,8	2,2 ± 0,4	2,4 ± 0,6
	Assessment after 1.200 hours continuous condensation			Assessment after 2.160 hours neutral salt spray test		
System B (ESI stored for 12 month)						
Film thickness ISO 2808 [μm]	247 ± 13	247 ± 11	252 ± 8	249 ± 10	252 ± 10	242 ± 12

Visual evaluation	no visual changes			no visual changes		
Pull-off strength [MPa]	6,9	8,5	8,7	9,4	11,1	7,7
Failure pattern	cohesion failure in the 2 nd layer			cohesion failure in the 1 st and 2 nd layer		
Corrosion at the scratch [mm]	-			< 0,5	< 0,5	0,7 ± 0,3
Delamination at the scratch [mm]	-			1,9 ± 0,9	1,9 ± 0,8	1,6 ± 0,8
	Assessment after 1.200 hours continuous condensation			Assessment after 2.160 hours neutral salt spray test		
System C (ESI new batch)						
Film thickness ISO 2808 [µm]	242 ± 8	246 ± 12	247 ± 5	236 ± 5	236 ± 9	240 ± 10
Visual evaluation	no visual changes			no visual changes		
Pull-off strength [MPa]	8,5	9,9	10,8	8,3	10,5	9,6
Failure pattern	cohesion failure in the 1 st and 4 th layer	cohesion failure in the 4 th layer		cohesion failure in the 1 st and 4 th layer	cohesion failure in the 4 th layer	
Corrosion at the scratch [mm]	-			1,4 ± 0,5	1,3 ± 0,5	1,4 ± 0,7
Delamination at the scratch [mm]	-			1,4 ± 0,5	1,3 ± 0,5	1,4 ± 0,7

Slip load tests for three test series were performed to evaluate the coating system ESI for a use in slip-resistant connections, according to the test procedure to determine the slip factor acc. to EN 1090-2, Annex G [5.3-1]. Table 5.5-2 summarizes the performed tests. Specimens with ESI system A has been conditioned for 3 weeks while systems B and C have been conditioned for 1 week by using an expired batch for System B. The tests were performed in the same way as prescribed in Task 1.1 and evaluated with the new criterion of the slip load prescribed in Task 1.3. The test matrix also required some extended creep tests (ECT) to ensure the slip factor under sustained loads. Therefore, the new invented step test (prescribed in Task 1.4) was performed to define a first load level for the ECT. The specimen is shown in Figure 5.5-1.

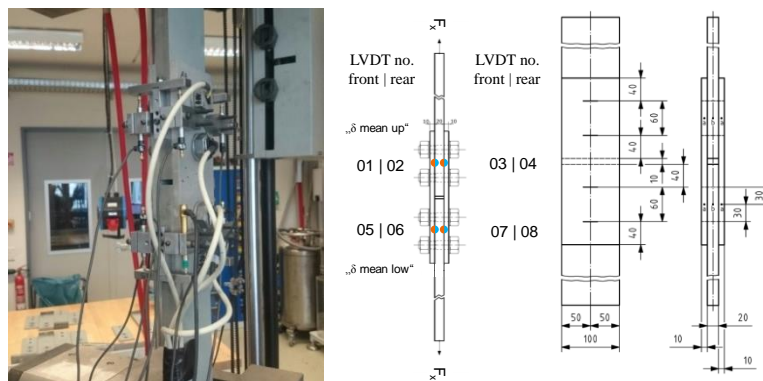


Figure 5.5-1: M20-test specimen according to Annex G of EN 1090-2 [5.3-1] and LVDT position

For measuring of the displacement, four LVDTs were mounted in the upper and lower part of the connection (see Figure 5.5-1). The evaluation of the slip load F_{Si} is based on these displacement measurements while taking four values to the mean value. The mean value of the displacement of the upper connection is based on LVDT No. 01, 02, 03 and 04. Figure 5.5-2 shows the slip load-displacement curves for the test series A-ESI-3-n. The faying surfaces of the specimens before and after testing is shown in Figure 5.5-2. Around the holes the pressure contact areas, which result from the preload of the bolts and which are responsible for the transmission of the acting shear load by friction, are visible. The evaluation of the slip load tests is given in Table 5.5-4.

The resulting mean slip factor $\mu_{start, F_{S-max}}$ for the series A is 0.52. The ongoing procedure is the step test. The load-time-displacement behaviour is shown in Figure 5.5-3 (left) for the step test of A-ESI-3-n.

The load-time-displacement behaviour shows an increase of the displacement (right ordinate) while incrementally increasing the test load in steps of 5 % of F_{Sm} from Table 5.5-4 (left ordinate). The whole procedure is explained in detail in Task 1.4. The highlighted grey area shows the displacement area in which the slip load tests (curves displayed in Figure 5.5-2) failed.

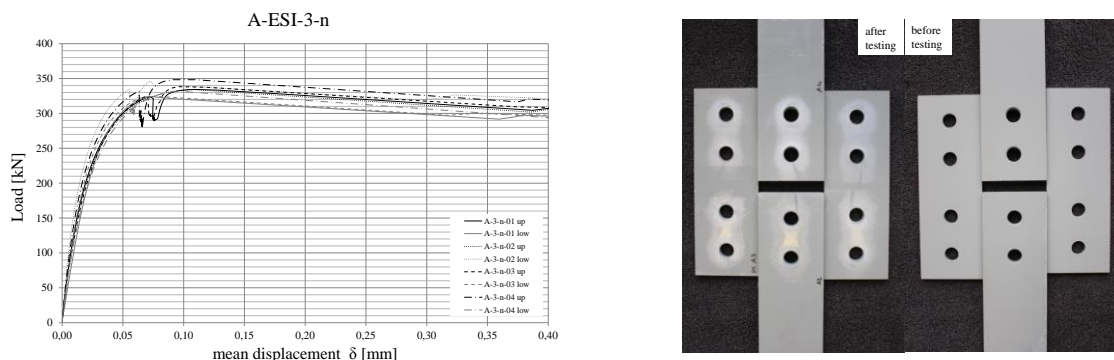


Figure 5.5-2: Left: Slip load-displacement curves of test series A-ESI-3-n, Right: Faying surfaces of specimen with the coating system A-ESI-3-n

Choosing the load level below the “failure area” for an extended creep test (ECT) would mean, that the test would fulfil the requirements of EN 1090-2, Annex G.5. By applying a load level of $0.90 \cdot F_{Sm}$ the displacement measurements would reach the highlighted grey area. This indicates the failure of the step test and for an extended creep a load level below this 90 % has to be chosen. In this case the load level was $0.8 \cdot F_{Sm} = 0.8 \cdot 335.5 \text{ kN}$. A mixed up number was corrected after testing, more specifically, during the evaluation process. That means that the chosen load for the ECT shown in Figure 5.5-3 (right) corresponds to 81.3 % of F_{Sm} . The result of the ECT shows that the presented slip factor in Table 5.5-4 $\mu_{start, Fs-max} = 0.52$ has to be reduced by the factor 0.81. The remaining slip factor for this coating system A-ESI-n is $0.81 \cdot 0.52 = 0.42$. The Figure 5.5-4 shows the slip load-displacement curves of the test series B-ESI-1-o (left) and C-ESI-1-n (right). Both diagrams of Figure 5.5-4 show the same slip load-displacement behaviour as A-ESI-3-n curves. That indicates a similar performance of the coating systems in slip-resistant connections. The evaluation of the test data is summarized in Table 5.5-5. As a result, all three tested ESI coating systems have the same slip factor out of the slip factor tests. For the series B-ESI-1-o curves of the step test are shown in Figure 5.5-5 (left).

The grey failure area is taken from the slip load tests. In case of an ECT with a load level below/near this area, the “limit load” of the specimen can be found to pass the test. In this case 80 % of F_{Sm} seems most reasonable. The load-log time-displacement curve of the ECT-80 % is shown in Figure 5.5-5 (right). The failure criterion acc. to EN 1090-2, Annex G.5 is given with a displacement of 0.3 mm within 50 years or the lifetime of the structure. It shall be shown that the measured displacements in Figure 5.5-5 (right) will not exceed this 0.3 mm criterion (right ordinate). To verify these results, a second ECT with 85 % of F_{Sm} was performed. Figure 5.5-6 (left) shows the load-log-time-displacement curves. Figure 5.5-6 (right) shows the load-displacement behaviour of the three tested systems.

The 85 % ECT in Figure 5.5-6 (left) can be considered as failed, because of the increasing displacements (dashed lines) of the upper part of the connection. This part of the connection will exceed the 0.3 mm criterion with the 50 years.

Table 5.5-4: Results on slip load test of test series A-ESI-3-n

specimen	part	$F_{p,C,start 01}$	$F_{p,C,start 02}$	$F_{p,C,slip01}$	$F_{p,C,slip02}$	$F_{Si,max}$	$\mu_{start, Fs-max}$	$\mu_{actual, Fs-max}$
		[kN]	[kN]	[kN]	[kN]	[kN]	[-]	[-]
A-3-n-01	up	160.4	161,2	151.9	145.5	334.4	0.52	0.56
	low	164.5	159.0	147.3	151.9	324.1	0.50	0.54
A-3-n-02	up	161.4	160.7	147.9	142.5	334.3	0.52	0.58
	low	161.6	160.2	143.5	134.4	346.4	0.54	0.62
A-3-n-03	up	163.7	162.6	156.7	150.4	338.7	0.52	0.55
	low	158.1	163.5	136.6	147.0	324.8	0.51	0.57
A-3-n-04	up	163.5	161.2	152.7	147.3	348.9	0.54	0.58
	low	159.5	163.0	138.7	145.9	332.2	0.51	0.58
	x	161.6	161.4	146.9	145.6	335.5	0.52	0.57

Table 5.5-4: Results on slip load test of test series A-ESI-3-n

specimen	part	$F_{p,C,start_01}$	$F_{p,C,start_02}$	$F_{p,C,slip01}$	$F_{p,C,slip02}$	$F_{Si,max}$	$\mu_{start,Fs-max}$	$\mu_{actual,Fs-max}$
		[kN]	[kN]	[kN]	[kN]	[kN]	-	-
	Vx	1.37%	0.95%	4.75%	3.70%	2.68%	2.55%	4.31%

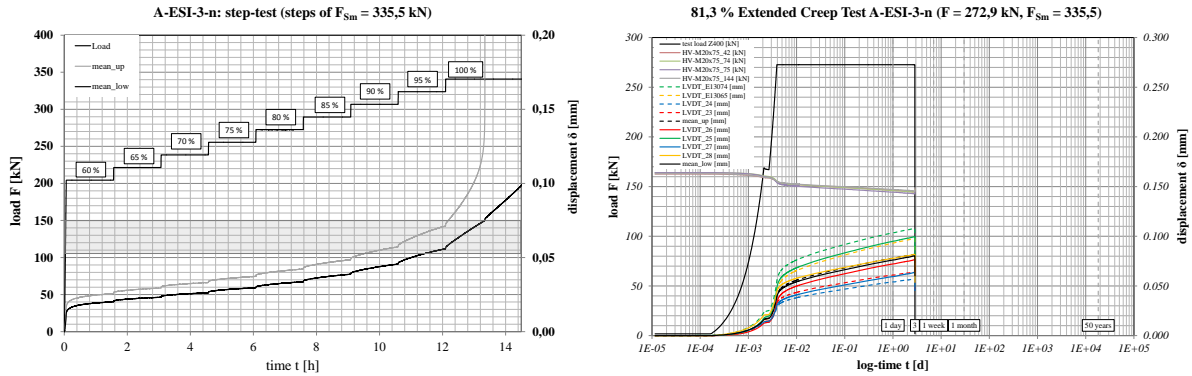


Figure 5.5-3: Left: Load-time-displacement curve of the step test of specimen with A-ESI-3-n, Right: Extended creep test (ECT) with 81.3 % load of F_{Sm} for the specimen A-ESI-3-n

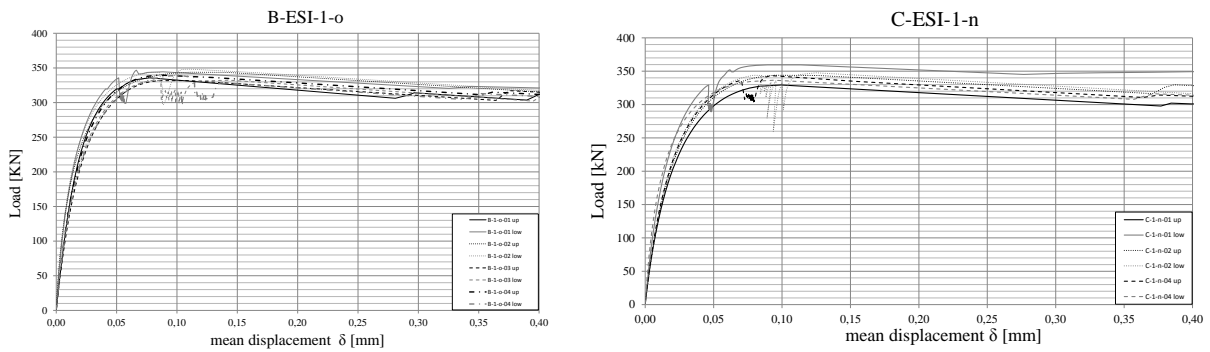


Figure 5.5-4: Slip load-displacement curves of the test series B-ESI-1-o and C-ESI-1-n

Table 5.5-5: Results of slip load test of test series B-ESI-1-o and C-ESI-1-n

specimen	part	$F_{p,C,start_01}$	$F_{p,C,start_02}$	$F_{p,C,slip_01}$	$F_{p,C,slip_02}$	$F_{Si,max}$	$\mu_{start,Fs-max}$	$\mu_{actual,Fs-max}$
		[kN]	[kN]	[kN]	[kN]	[kN]	-	-
B-1-o-01	up	161.9	160.1	147.8	144.9	335.9	0.52	0.57
	low	163.1	169.8	147.5	158.8	346.8	0.52	0.57
B-1-o-02	up	160.7	161.2	147.8	142.1	344.2	0.53	0.59
	low	165.5	162.0	145.2	147.8	348.4	0.53	0.59
B-1-o-03	up	162.1	160.9	150.6	145.8	332.5	0.51	0.56
	low	164.4	162.3	145.7	150.2	332.6	0.51	0.56
B-1-o-04	up	163.0	168.1	148.1	151.9	340.0	0.51	0.57
	low	166.7	164.1	148.9	147.1	329.0	0.50	0.56
	x	163.4	163.6	147.7	148.6	338.7	0.52	0.57
	Vx	1.22%	2.18%	1.14%	3.45%	2.14%	2.34%	2.59%
C-1-n-01	up	163.0	163.0	151.4	149.2	329.3	0.51	0.55
	low	164.7	167.3	146.3	142.2	359.9	0.54	0.62
C-1-n-02	up	162.7	162.2	147.7	144.1	344.7	0.53	0.59
	low	162.5	164.6	144.9	152.3	347.7	0.53	0.58
C-1-n-03	up	161.0	160.9	147.6	144.1	335.4	0.52	0.57
	low	161.6	159.8	138.4	142.5	328.4	0.51	0.58
C-1-n-04	up	162.4	163.0	150.6	147.9	343.9	0.53	0.58
	low	162.8	161.8	149.5	152.3	336.6	0.52	0.56
	x	162.6	162.8	147.0	146.8	340.7	0.52	0.58
	Vx	0.68%	1.43%	2.81%	2.85%	3.07%	2.29%	3.94%

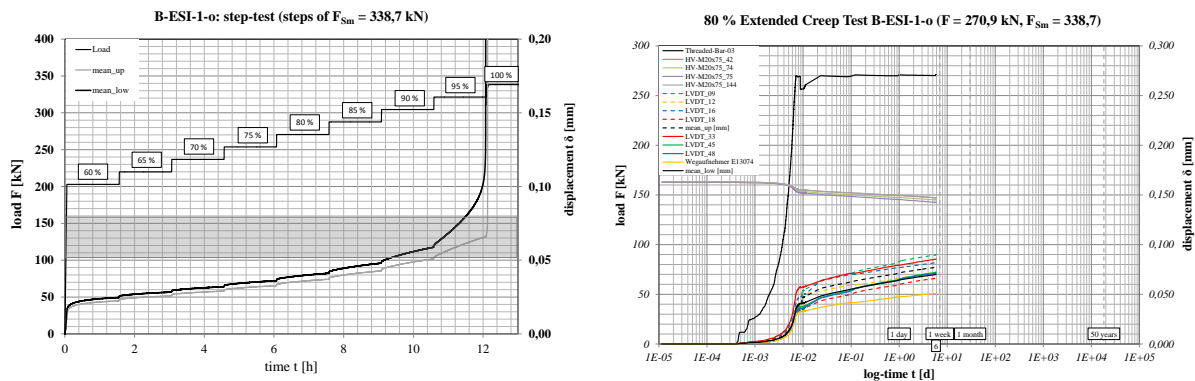


Figure 5.5-5: Left: Load-time-displacement curve of step test (B-ESI-1-o), Right: Load-log-time-displacement of the extended creep test (ECT) with 80 % load of F_{Sm} (B-ESI-1-o)

The three coating systems behave in a similar way during the slip load tests plotted in the slip load-mean displacement diagram in Figure 5.5-6 (right). The failure of the slip-resistant connections occurs at a displacement between $\delta = 0.06 \text{ mm} \dots 0.07 \text{ mm}$.

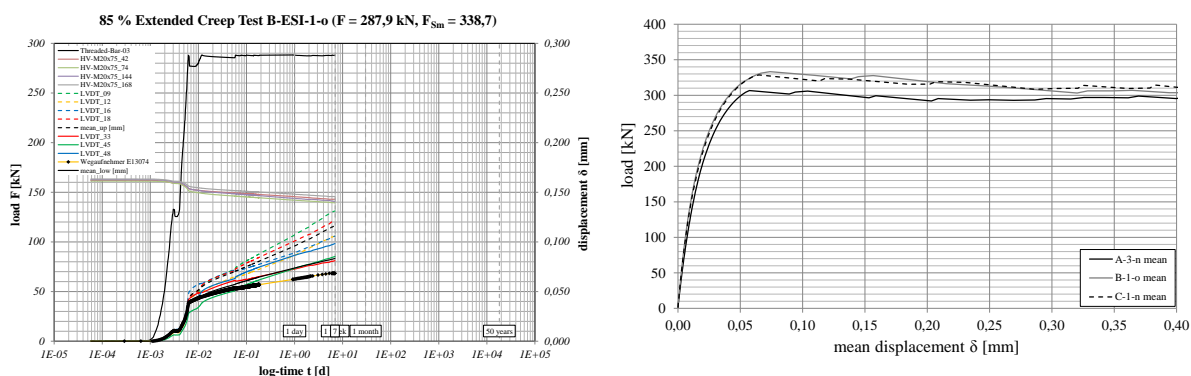


Figure 5.5-6: Left: Load-log time-displacement of the extended creep test (ECT) with 85 % load of F_{Sm} for specimen B-ESI-1-o, Right: Comparison of the slip load-mean displacement curves of the three test series A-ESI-3-n, B-ESI-1-o and C-ESI-1-n

Conclusion

On the basis of the conducted tests, it can be concluded that different conditioning times and storage times have no influence on the slip factor. The final slip factor for series A and B was evaluated from the results of the extended creep tests with $\mu = 0.42$. The load for those tests was determined by the new invented step test (Task 1.4).

Regarding their corrosion protection values the systems show no differences with the exception of the failure pattern. The failure pattern is the weakest part of the coating system. System A shows cohesion failures in the 2nd layer, system B shows cohesion failure in the 1st and 2nd layer and system C shows mainly cohesion failures in the 4th layer. A negative influence of storage stability on the corrosion protection values could not be detected.

6 WP 5 – Preloading of SS bolts

6.1 Objectives

The main objective of this work package is to provide

- preloading levels and
- preloading methods

For stainless steel connections taking into account the effect of material relaxation in bolt assemblies. For this reason, the relaxation of bolts and plates as isolated elements will be studied as well as the relaxation behaviour of the whole assembly to clearly separate the base material behaviour from other effects resulting from the assemblies (such as friction of the threads and so on).

The characteristics of creep of selected stainless steel grades at room temperature will be determined using a combination of tensile tests and creep tests. The test results will be used to define an

appropriate mathematical model for the creep deformation of stainless steel materials for numerical simulation preloaded bolt connections.

6.2 Work undertaken

The tasks undertaken in WP 5:

- 5.1. Material data on the strength and relaxation behaviour of stainless steel plates.
- 5.2. Material data on the strength and relaxation behaviour of stainless steel bolts (as isolated elements).
- 5.3. Basic preloading behaviour of stainless steel bolts assemblies and relaxation of preloaded stainless steel bolted connection assemblies.
- 5.4. Determination of recommended preloading levels.
- 5.5. Numerical analysis of preloaded stainless steel bolted connection assemblies.
- 5.6. Determination of recommended preloading methods.

The work undertaken for Tasks 5.1 to 5.6 is summarized in Sections 9.3 - 9.8.

Exploitation of the research results of this WP

The research results of this WP were published in nine journal and conference papers: (7) to (11), (16), (18) to (20), see Chapter 2, Publications. One journal paper is submitted and accepted for publication: (2), see Chapter 2, Publications.

6.3 Task 5.1 – Relaxation of SS plates and washers

Introduction

Room temperature creep deformation under uniaxial constant load conditions was observed for the investigated stainless steels (austenitic, ferritic, lean duplex and duplex). The amount of creep deformation increased with increasing load level and likely also with increasing initial loading rates. Consequently, the amount of creep deformation in preloaded stainless steel connections therefore depends on the level of stress in the plates due to the preloading of the bolts. For the level of preload used in this project, the susceptibility for creep deformation was (from highest to lowest): the austenitic grade, the ferritic grade, the lean duplex grade and the duplex grade. However, comparison with results from instrumented preloaded stainless steel connections (see Task 5.3) resulted in the conclusion that creep deformation in the ferritic and duplex connections was not significant in regard to the measured loss of preload. A higher loss of preload was observed for the austenitic connection which was attributed to the higher susceptibility for creep deformation at this level of preload. In general, the results indicate that the loss of preload in a preloaded stainless steel connection is mainly caused by the stress relaxation in the bolts and not by the creep deformation of the plates. The viscoplastic deformation behaviour of the investigated stainless steels could be described by state of the art viscoplastic constitutive known as the Chaboche model. The material parameters of this model were determined based on the tests carried out in Task 5.1. This model was successfully used in the finite element modelling of preloaded stainless steel connections in Tasks 5.5 and 6.4.

The tested stainless steel materials were hot-rolled and annealed sheet of EN 1.4404 (austenitic), hot-rolled and annealed sheet of EN 1.4003 (ferritic), hot-rolled and annealed plate of EN 1.4162 (lean duplex) and hot rolled and annealed plate of EN 1.4462 (duplex). The plate thicknesses were 8.0 mm for the austenitic, the ferritic and the duplex. The lean duplex plate thickness was 8.6 mm.

Experimental technique for tensile testing and the results

The testing systems consisted of electromechanical servo controlled machines where the strain was measured by external extensometers. For the austenitic and ferritic grade, the tensile specimens had a parallel length of 75 mm and corresponds to type 1 in the annex B of EN ISO 6892-1:2009 and tested according to the tensile test standard EN ISO 6892-1:2009, method A224. For the two duplex grades, the specimens used were flat specimens with cross-section of $12.5 \times \text{thickness mm}^2$ and 110 mm parallel length in compliance with EN ISO 6892-1:2009 and tested according to the tensile test standard EN ISO 6892-1:2009, method B11. The mean mechanical properties of the tested materials

are summarized in Table 6.3-1. Three tensile tests per type. The tested materials had continuous yielding behaviour.

Table 6.3-1: Mean mechanical properties of the investigated materials.

Grade, EN	Direction	R _{p0.2} , MPa	R _{p1.0} , MPa	R _m , MPa	A5, %
1.4003	Transversal	352	369	486	27.7
	Longitudinal	304	329	456	30.5
1.4404	Transversal	293	333	596	51.1
	Longitudinal	280	315	583	52.7
1.4162	Transversal	568	609	731	41.0
	Longitudinal	509	569	705	40.7
1.4462	Transversal	692	742	858	31.3
	Longitudinal	619	671	797	36.5

In addition to basic characterization of test materials, tensile tests were also used to investigate the rate-dependent and rate-independent strength of these materials. In these tests, different loading rates in the range from 10⁻⁷ 1/s to 10⁻² 1/s were used.

Experimental technique for creep testing

For the short term (12.5 hour) room temperature uniaxial creep testing of the austenitic and ferritic sheets, the testing was carried using the same tensile testing machine as for the tensile tests. For the long-term constant load creep tests an in-house built lever-arm testing rig was used. Strain was measured using strain gages for the long-term creep tests. The type of strain gages was selected to minimize the influence of minor temperature variation in the laboratory. Austenitic and ferritic stainless steels have different coefficient of thermal expansion. Therefore, different strain gages had to be used for different test materials. The strain gages were used in a quarter bridge configuration. For the room temperature creep testing of the duplex plates, an electromechanical servo controlled machine was used for both the short and long-term testing. Table 6.3-2 shows the used load levels and times for the room temperature constant load creep tests. The creep tests were carried out in the longitudinal direction.

Table 6.3-2: Loading levels used for room temperature constant load creep tests.

Grade, EN	Time, h	Nominal Stress, xR _{p0.2} ^a	Repeats
1.4003 &	12.5	0.300	3
	12.5	0.475	3
1.4404	12.5, 150	0.650	3
	12.5, 150	0.825	3
	12.5, 150	1.000	3
	12.5	1.200	3
1.4162 &	12	0.500	3
	20, 100, 150	0.650	6
1.4462	12, 20, 100, 160	0.825	8
	12, 20, 150	1.000	7
	20	1.200	3

^a Longitudinal direction

The initial loading rate for the 12.5 h creep test for the austenitic and ferritic sheets was 50 MPa/s. For the test piece geometry used, this loading rate corresponds to the strain rate of 2.5x10⁻⁴ 1/s, which is the same loading rate which was used in the tensile tests. For the two duplex plates three types of initial loading rates were used: 2 MPa/s up to 10 MPa from the specified initial stress and 0.5 MPa/s thereafter, constant crosshead speed with resulting strain rate of 10⁻⁵ 1/s and 10⁻⁴ 1/s.

Experimental technique for short-term stress relaxation testing with repeated reloading

The original testing plan outlined in the Technical Annex included short term creep tests with staircase loading for grade 1.4003 and 1.4404 materials. The purpose of these tests was to investigate material response in the case that the bolts are retightened once or several times during the execution procedure or during the service life. Once the results of the short term constant load creep tests were analysed, it was, however, concluded that a repeated relaxation test would a better way of observing the material response under repeated loading. Therefore, creep tests with staircase loading were replaced by an equal number of repeated relaxation tests of grade 1.4003 and 1.4404 materials. The short-term stress relaxation tests with repeated reloading were carried out using the same tensile testing machine and the same test piece geometry as the short-term constant load creep tests. Two different loading rates were used. The loading phase was done out under position control and the relaxation periods under strain control. The duration of one relaxation period was 3 hours and one test included four repeated relaxations. Figure 6.3-1 shows an example. Continuous 12-hour relaxation tests were also carried out for comparison purposes. The load levels and loading rates used are summarized in Table 6.3-3.

The results of repeated relaxation tests showed clearly that the amount of stress relaxation decreases in each subsequent relaxation period and that the amount of stress relaxation increases with the speed of loading. Therefore, the results suggest that repeated retightening of bolts can be used to reduce the loss preload. It would also be beneficial to do preloading slowly.

Table 6.3-3: Load levels and loading rates used in the repeated relaxation tests. Continuous 12-hour relaxation tests also were conducted for comparison purposes.

Steel grade	Nominal Stress (x $R_{p0.2}$)	Loading rate (MPa/s)	Test type	Repeats
1.4003	0.825	0.5	4 x 3h	2
	0.825	5.0	4 x 3h	2
1.4404	0.825	0.5	4 x 3h	2
	0.825	5.0	4 x 3h	2
1.4003	0.825	0.5	12h	2
1.4404	0.825	0.5	12h	2

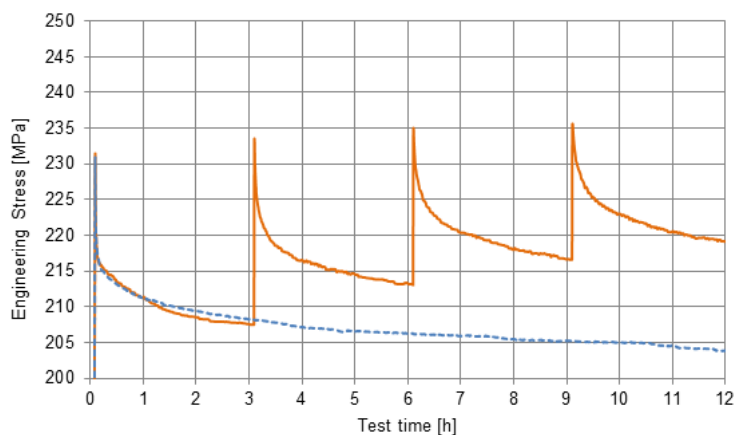


Figure 6.3-1: Repeated 4 x 3 h relaxation test for grade 1.4404 plate material. The stress relaxation curve measured on continuous 12h loading is shown as reference. The loading speed was 0.5 MPa/s and the load level corresponds to the 82.5 % of the 0.2 % proof stress of the material.

Measured room temperature creep

Figure 6.3-2 shows the uniaxial tensile creep results for the investigated stainless steels at room temperature condition. The inelastic strain was defined as the total strain minus the elastic strain (Hooke's law). The immediate plastic strain that occurs during the loading stage is included in the inelastic strain. Therefore, the creep strain is always smaller than the inelastic strain. The inelastic strain after 0.5 hour of testing is showed. At the $0.50 \times R_{p0.2}$ creep load, creep deformation was observed for all the tested stainless steel grades. After 2.5 h of testing, the inelastic strain became constant indicating that the creep rate was below the resolution of the testing systems.

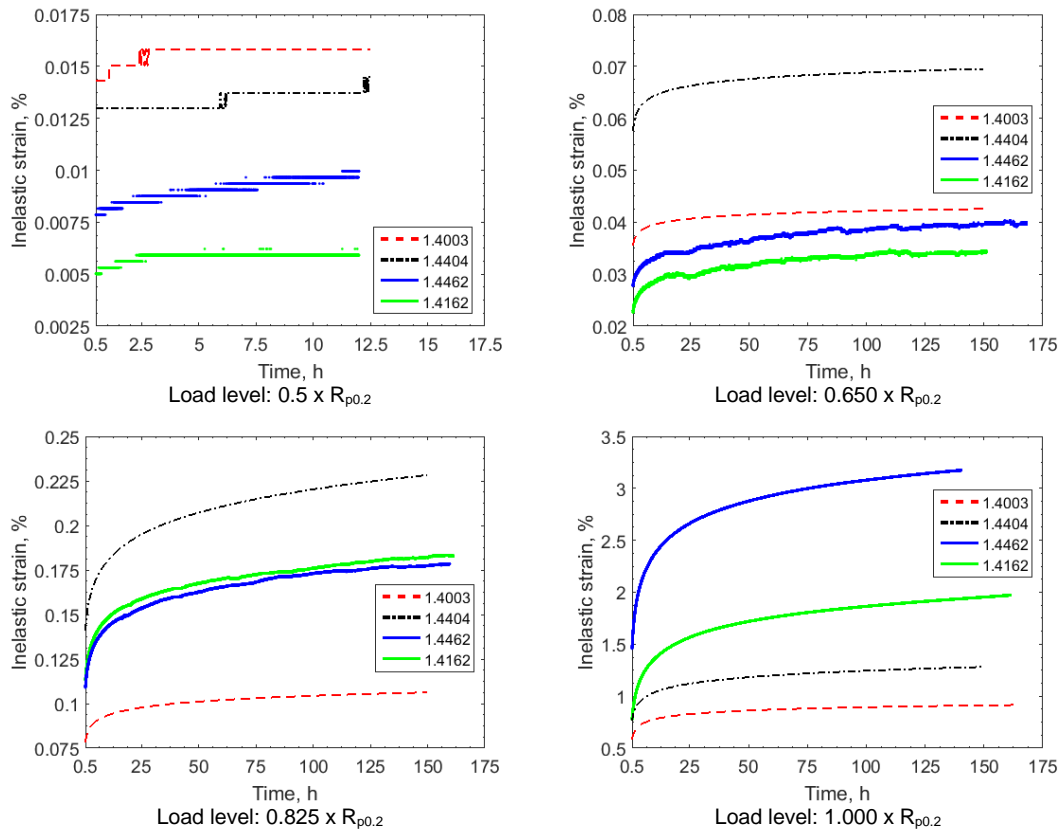


Figure 6.3-2: Uniaxial tensile creep results at room temperature condition.

The ferritic grade, except at the $0.50 \times R_{p0.2}$ load level, exhibit lower inelastic strain than the austenitic. The two duplex grades exhibited the lowest amount of inelastic strain for the two lowest load levels. At the $0.825 \times R_{p0.2}$ load level the two duplex grades showed increased inelastic strain compared to the austenitic and ferritic grades. At the $1.00 \times R_{p0.2}$ load level the two duplex grades exhibited the highest inelastic strain. One part of the explanation was likely that the duplex grades had higher proof strength compared to the austenitic and ferritic grades (recall Table 6.3-1). This resulted in higher amount of strain during the initial loading which consequently resulted in larger contribution of plastic strain to the inelastic strain due to the continuous yielding behaviour of stainless steel. The mean contribution of plastic strain to the inelastic strain at the $1.00 \times R_{p0.2}$ load level was 33 % for the duplex grades where the 1.4462 had the highest contribution of plastic strain in the initial loading stage.

The “waviness” of the two duplex grades at the 0.65 and the $0.825 \times R_{p0.2}$ load levels were due to changes in the ambient temperature during testing (as no climate chamber was available so no control over the ambient temperature was possible). For the austenitic and ferritic steels the temperature dependent part of the measurement signal was removed by processing of measurement data.

For austenitic stainless steel, it has been reported [9.3-1, 9.3-2] that the creep at room temperature can be described by the following phenomenological equation:

$$\varepsilon(t) = \alpha \ln(t) + \beta \quad (9.3-1)$$

where α and β is a function of the applied stress and t is the time. This is usually referred to as logarithmic creep behaviour. The time derivative of equation (9.3-1) is:

$$\dot{\varepsilon}(t) = \alpha t^{-1} = m t^k \quad (9.3-2)$$

To investigate if the tested duplex plates had logarithmic creep behaviour the creep rate was determined. If the coefficient k was found to be -1 then the creep was logarithmic. If $k \neq -1$ then the creep is usually defined as power-law creep [9.3-3].

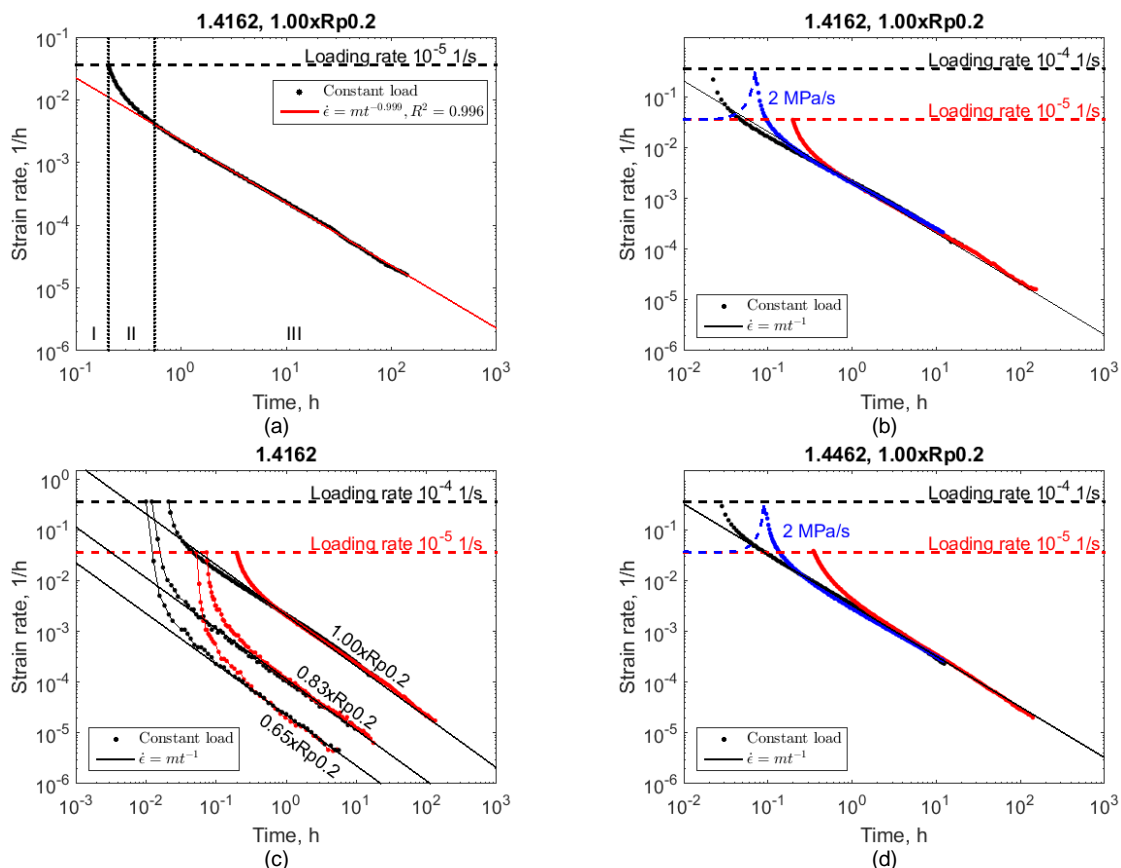


Figure 6.3-3: The creep rate, a) logarithmic creep behaviour in region III, b) influence of the initial loading rate, c) influence of the load level, d) similar creep behaviour for 1.4462.

Figure 6.3-3 (a) shows the strain rate during the uniaxial tensile creep testing of the lean duplex grade at the $1.00xR_{p0.2}$ load level. Three distinct regions could be found: the first region (I) was the initial loading which in this case was constant strain rate of 10^{-5} 1/s, the second region (II) was the initial creep region where the creep rate rapidly decreases and the third region (III) was the creep rate region where the creep rate could be described by equation (9.3-2). Apparently, equation (9.3-2) does not describe the initial creep behaviour.

The logarithmic creep rate region was independent of the initial loading rate as seen in Figure 6.3-3 (b) which shows the creep rate for the three different initial loading rates. The initial loading rate determines the strain at the specified load and the maximum creep rate obtained during testing. Figure 6.3-3 (c) shows the influence of the load level on the creep rate. The rapid decrease in creep rate during the initial creep region (II) was observed to depend on the load level where a high load level had lower creep rate drop which resulted in an elevated logarithmic creep rate (higher m value) which results in higher amount of inelastic strain. The 1.4462 duplex plate had similar creep behaviour as the 1.4162, see Figure 6.3-3 (d). The creep behaviour for the austenitic and ferritic grade in the present work was also found to be logarithmic.

The Chaboche model

And extensive literature study was conducted as part of Task 5.1 in the SIROCO project. In the literature study, available information on creep and stress relaxation behaviour of stainless steel at room temperature was reviewed. Several characteristic features in the room temperature creep and stress relaxation of different stainless steels were identified. Additionally, the present state of the art in computational viscoplasticity was reviewed. The capability of different models in describing the creep and stress relaxation behaviour of stainless steel at room temperature was assessed. Based on the assessment, a model referred henceforth as the Chaboche model was chosen as the constitutive model for modelling the room temperature creep and stress relaxation of all stainless steel grades studied in the present work. The Chaboche model is widely used both in academia and in industry for modelling cyclic plasticity. Furthermore, this model has also been successfully used for modelling room temperature stress relaxation of AISI 316 type austenitic stainless steel [9.3-4, 9.3-5, 9.3-6].

The Chaboche model is a unified model. The immediate and time dependent plastic deformations are treated as one inelastic strain component. Time-independent plasticity is obtained as a limiting case. The model uses two internal state variables for describing the material hardening behaviour. One internal state variable is a tensorial back-stress α used for describing kinematic hardening of the material. The other state variable R accounts for isotropic hardening. Parametrized evolution laws are given for each internal variable. The back-stress is described as a sum of three components $\alpha^{(i)}$:

$$\alpha = \sum_{i=1}^3 \alpha^{(i)} \quad (9.3-3)$$

Parametrized evolution laws are given for each internal variable. The evolution of kinematic hardening components is described by:

$$\dot{\alpha}^{(i)} = \frac{2}{3} C_i \dot{\epsilon}^p - \gamma_i \alpha^{(i)} \dot{\epsilon}^p \quad (9.3-4)$$

where $\dot{\epsilon}^p$ is the rate of plastic strain tensor and $\dot{\epsilon}^p$ is the equivalent plastic strain rate. C_i and γ_i are material parameters. The scalar isotropic hardening component R follows the evolution law:

$$\dot{R} = b(Q - R) \dot{\epsilon}^p \quad (9.3-5)$$

The rate of equivalent plastic strain is given by the power law viscosity function:

$$\dot{\epsilon}_p = \left\langle \frac{\|\sigma - \alpha\|_{VM} - R - k}{D} \right\rangle^n \quad (9.3-6)$$

where D , k and n are material parameters. The norm $\|\cdot\|_{VM}$ denotes the Von Mises yield function. The McCauley brackets $\langle \cdot \rangle$ guarantee that there exists an elastic limit below which no inelastic deformation occurs. The elastic limit is also the threshold for the onset of creep deformation and the limit at which stress relaxation ceases. The model is described in more detail in the deliverable 5.2.

A numerical method was developed for identifying the parameters of the Chaboche model based on the results of extensive materials testing carried out in Task 5.1. The identified material parameters are summarized in Table 6.3-4.

Table 6.3-4: Chaboche model parameters for the plate materials.

Grade	D	n	C ₁	γ ₁	C ₂	γ ₂	C ₃	γ ₃	Q	b	k
	[MPa]	[-]	[MPa]	[-]	[MPa]	[-]	[MPa]	[-]	[MPa]	[-]	[MPa]
1.4404	110	15.0	45949	591.4	617031	6765.3	1434	2.5	380	2.5	73
1.4003	130	11.0	623733	5855.1	17430	558.6	1680	10.8	104	10.8	106
1.4462	313	24.3	947349	11334.6	252038	1222.1	2971	60.0	723	2.8	106
1.4162	329	30.2	483769	4875.7	102445	975.3	6766	180.8	649	3.5	109

Exploitation and impact of the research results

Room temperature creep deformation under uniaxial constant load was observed for the investigated stainless steels. The amount of creep deformation increased with increasing load level and likely also with increasing initial loading rates. At load levels around $0.5x_{R_{p0.2}}$ the two duplex grades had the least susceptibility for creep but at around load levels of $1.0 x R_{p0.2}$ they had the highest susceptibility for creep. This indicates that in general, higher 0.2 % proof strength gives higher resistance to room temperature creep. But the actual creep behaviour at absolute loads close to and above the proof strength seems to greatly depend on the yielding behaviour. The ferritic 1.4003 had in overall the least susceptibility for creep.

However, the amount of creep deformation in the plates of preloaded stainless steel connections then greatly depends on the level of stress in the plates due to the preloading of the bolts. The preloading force in the bolt can be considered independent of the plate material. Therefore, level of stress in the plate is less significant for plates materials with higher yield strength. It has been estimated that for the preload ($F_{p,c}$) used in this project, the maximum through-thickness load levels were $0.71 x R_{p0.2}$ for the austenitic plates, $0.66 x R_{p0.2}$ for the ferritic plates, $0.49 x R_{p0.2}$ for the lean duplex plates and $0.40 x R_{p0.2}$ for the duplex plates. The approximate creep deformation after equivalent time (normalized to the

austenitic sheet, i.e. 1.0) would then be 2/7 for the ferritic sheet, 1/25 for the lean duplex plate and <1/25 for the duplex plate, recall Figure 6.3-2. Thus, for the used preload in this project, the susceptibility for creep were (from highest to lowest): the austenitic, the ferritic, the lean duplex and the duplex material.

In Task 5.3, instrumented preloaded connections of stainless steels were used for measuring the loss of preload in such connection. Table 6.3-5 shows 30 min of measured loss of preload for reused Bumax 109 bolts in preloaded connections together with extrapolation to 50 years. There was no significant difference in loss of preload between ferritic and duplex stainless steel connections while the austenitic stainless steel connection had a higher loss of preload. The higher loss of preload for the austenitic connection would then be explained by the higher susceptibility for creep at the used preload. When using new bolts, the extrapolated loss increased to 8 % indicating that it is the stress relaxation in the bolt (see Task 5.2) that mainly contributes to the loss of preload in a stainless steel preloaded connection and not the creep deformation in the plates. This hypothesis is further strengthened when comparing with the structural carbon steel set-up (S355 with reused HV 10.9 bolts) as the S355 steel is usual regarded as creep resistant at room temperature conditions.

Table 6.3-5: Measured and extrapolated loss of preload (mean values) from instrumented preloaded connections (reused bolts) (Task 5.3).

Grade, EN	30 min, %	50 years, %
1.4404 (austenitic)	2.0	5.7
1.4003 (ferritic)	1.1	2.5
1.4162 (lean duplex)	1.0	2.5
1.4462 (duplex)	0.9	2.5
S355 (HV10.9 bolt)	0.9	2.5

The higher loss of preload for the austenitic plate can be reduced by using higher strength splice plates (e.g. temper rolled austenitic plates) [9.3-7]. This decreases the amount of stress in the plates, and consequently, the amount of creep deformation. The results of repeated relaxation tests suggest that repeated retightening of bolts can be used to reduce the loss preload. The same results also showed that the amount of stress relaxation increases with increasing loading speed. Therefore, preloading of bolts should preferably be carried out as slowly as possible. The uniaxial tensile creep testing affects the entire specimen cross-section whereas the stress under a washer in a preloaded connection is not uniformly distributed [9.3-7]. There is also indication that the creep behaviour is different in tensile or compressive state, where the compressive stress state results in less creep [9.3-8]. Thus, the uniaxial tensile creep testing can be used for examining the material behaviour under constant load but may not directly relate to the loss of preload in a preloaded connection.

6.4 Task 5.2 – Relaxation of SS bars and bolts

Introduction

Room temperature stress relaxation testing has been performed on stainless steel. The aim of the testing was to investigate the stress relaxation behaviour of stainless steel bolts in preloaded connections. Bars were chosen over actual bolts due to practical limitations such as availability and ease of testing. The conclusions were that the two tested duplex grades in the “annealed” state had less stress relaxation compared to the tested austenitic grade in the “annealed” state. Cold drawn bars had less stress relaxation compared to bars in the “annealed” state. The cold drawn austenitic bar had less stress relaxation compared to the cold drawn duplex bars. Applying the test results of the bars to preloaded bolt connections, the result indicates that machined bolts are likely to have higher stress relaxation compared to cold forged bolts and that most of the stress relaxation in preloaded bolts occurs within the first hour after the preloading.

The bar materials used were EN 1.4436 (austenitic), EN 1.4162 (lean duplex) and EN 1.4462 (duplex). Three types of bars were used, rebar, annealed bar and cold drawn. Bars were chosen over actual bolts due to practical limitations such as availability and ease of testing. The cold drawn was to represent cold headed bolts with high amount of cold work and rebar/annealed bar to represent

machined bolts with less cold work. The difference between rebar and annealed is that rebar is in condition as-rolled, while annealed is in solution annealed state after rolling. The dimensions were 25 mm diameter rebar for the 1.4436 and 1.4162 and 20 mm annealed bar for the 1.4462. The cold drawn bars were all 12 mm in diameter. The rebar and annealed bars were machined to round tensile specimens with 12.5 mm diameter and 80 mm parallel length in compliance with EN ISO 6892-1. The cold drawn bars were tested as-received.

Experimental technique

The testing system consisted of an electromechanical servo controlled machine. The extensometers used were a macro extensometer for the tensile testing and a clip-on extensometer with 60 mm gauge length for the stress relaxation testing. The tensile testing was based on EN ISO 6892-1:2009 method B11. For the cold drawn bars, no increased strain rate to fracture was used. The tensile properties of the bar material can be seen in Table 6.4-1 together with the tensile properties of cold forged bolts from Bumax (Bumax 88, Bumax 109, Bumax LDX and Bumax DX). The bolts were tested in compliance with ISO 3506-1:1997. For the bar material three tensile tests were performed on each type.

The stress relaxation testing was based on EN 10319-1:2003. The specimens were loaded to an initial stress (σ_0) of 60, 80 or 100 % of the measured $R_{p0.2}$ (Table 9.4-1) and thereafter held at constant strain for 12 h at room temperature conditions and then unloaded. The initial loading rate was 10 MPa/s.

Table 6.4-1: Mean tensile properties of the tested bar material in comparison with cold forged bolts.

Material, EN	Type	$R_{p0.2}$, MPa	$R_{p1.0}$, MPa	R_m , MPa	A_{gt} , %	$R_{p0.2}/R_m$
1.4436	Rebar	357	394	644	33	0.55
1.4162	Rebar	613	683	813	18	0.75
1.4462	Annealed	642	689	787	16	0.82
1.4436	Cold drawn	823	963	966	2	0.85
1.4162	Cold drawn	776	951	974	3	0.80
1.4462	Cold drawn	856	981	988	3	0.87
1.4436	M16-bolt ISO4017 ^a	869		993		0.88
1.4436	M16-bolt ISO4017 ^b	1060		1142		0.93
1.4162	M16-bolt ISO4017	992		1111		0.89
1.4462	M16-bolt ISO4017	1033		1128		0.92
1.4436	M20-bolt ISO4017 ^a	973		1033		0.94
1.4436	M20-bolt ISO4014 ^b	977		1077		0.91
1.4162	M20-bolt ISO4017	1009		1075		0.94
1.4462	M20-bolt ISO4017	1011		1072		0.94

^a BUMAX 88, ^b BUMAX 109

Measured stress relaxation

The initial stress and constant strain for the stress relaxation testing can be seen in Table 6.4-2. The residual (inelastic) strain after 12 h of constant strain is also shown. Two stress relaxation tests were performed for each initial stress level. The stress relaxation was defined as:

$$\sigma_r = \left(1 - \frac{\sigma}{\sigma_0}\right) * 100 \quad (9.4-1)$$

where σ was the measured stress during testing and σ_0 the initial stress.

Table 6.4-2: Mean values for the initial stress (σ_0) and constant strain (ϵ_0) for the 12 h stress relaxation (σ_r) testing together with the standard deviation (SD) of the stress relaxation and the residual inelastic strain (ϵ_{res}) after 12 h.

Material, EN	Type	σ_0 , % of $R_{p0.2}$	σ_0 , MPa	σ_r , %	SD, %	ϵ_0 , %	$\epsilon_{res.}$, %
1.4436	Rebar	60	215	6.9	0.4	0.13	0.02
		80	285	10.6	0.2	0.19	0.05
		97	347	13.7	0.2	0.40	0.22
1.4162	Rebar	60	369	6.3	0.1	0.20	0.02
		80	490	10.4	0.0	0.31	0.07
		99	607	13.6	0.6	0.54	0.24
1.4462	Bar	60	386	4.7	0.1	0.25	0.02
		80	514	8.1	0.1	0.36	0.06
		99	633	13.0	0.2	0.62	0.26
1.4436	Cold drawn	60	495	4.7	0.0	0.33	0.04
		84	690	5.8	0.4	0.50	0.09
		100	821	7.7	0.1	0.69	0.19
1.4162	Cold drawn	60	466	5.7	0.5	0.26	0.02
		80	621	7.4	0.1	0.38	0.06
		100	773	9.5	0.1	0.60	0.18
1.4462	Cold drawn	60	514	4.8	0.0	0.30	0.02
		80	685	7.3	0.2	0.44	0.07
		100	853	9.8	0.2	0.67	0.21

The stress relaxation as a function of time can be seen in Figure 6.4-1. The time was adjusted for removing the difference in time due to different initial loading times. The stress relaxation was high in the beginning but quickly slowed down with increasing time. Most of the stress relaxation occurred within the first minutes of testing.

For the rebar/bar specimens the stress relaxation was similar between the 1.4436 and 1.4162 while 1.4462 showed lower stress relaxation at all stress levels. For the cold drawn bars, the two duplex grades showed similar stress relaxation except at the lowest stress level. The austenitic cold drawn grade showed less stress relaxation compared to two duplex cold drawn grades. The stress relaxation was higher for the rebar/bar compared to the cold drawn bars.

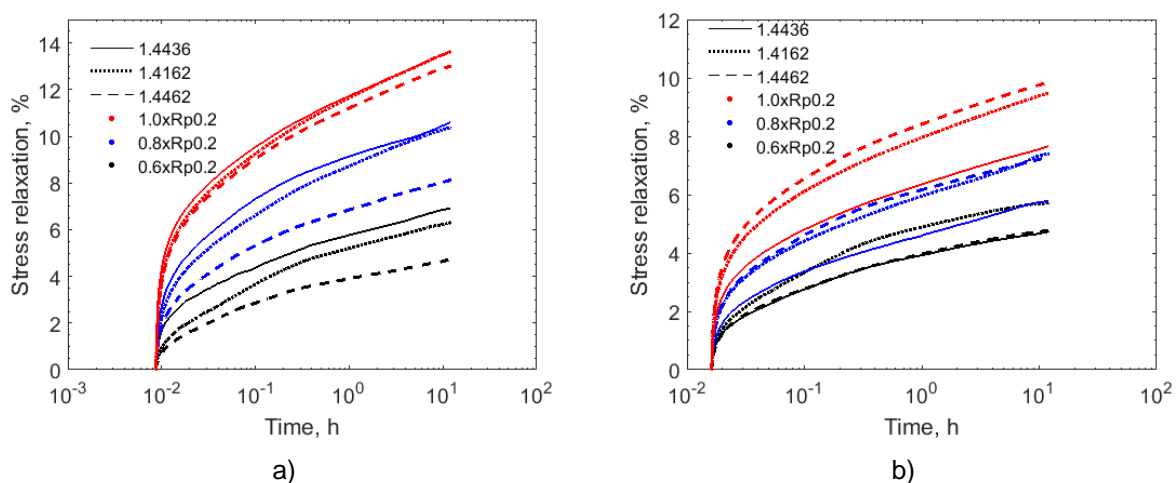


Figure 6.4-1: 12 h stress relaxation of stainless steels, a) rebar or bar, b) cold drawn bar.

Exploitation and impact of research results

It has been found for various metals that the inelastic response (at low homologous temperatures [9.3-1]) can be described by an equation of state [9.3-2, 9.4-1] where the mechanical properties that characterize the material plastic behaviour can be identified by introducing a “hardness state” parameter which is related to the strength of barriers to dislocation motion. For an austenitic stainless steel, Yamada and Li [9.4-4] found out that the inelastic response followed an equation of state of the form:

$$\frac{d\epsilon_{in.}}{dt} = K(\sigma - \sigma^*)^m \quad (9.4-2)$$

where K and m are material parameters, σ the stress and σ^* is the “hardness state” parameter. K is related to the burger vector and mobile dislocation density while m is related to the dislocation velocity-stress exponent [9.3-1]. Equation (9.4-2) has been found to also describe the inelastic

response for duplex and super duplex stainless steel [9.4-2]. It can be shown that equation (9.4-2) can be rearranged in to the following differential equation:

$$(\sigma - \sigma^*)^{-m} d\sigma = -EKdt \quad (9.4-3)$$

By nonlinear curve fitting the measured stress relaxation with equation (9.4-3) by using the nonlinear solver in Excel, it was possible to determine the K, m and σ^* , see Figure 6.4-2. The Young's modulus (E) was assumed to be 200 GPa for all materials.

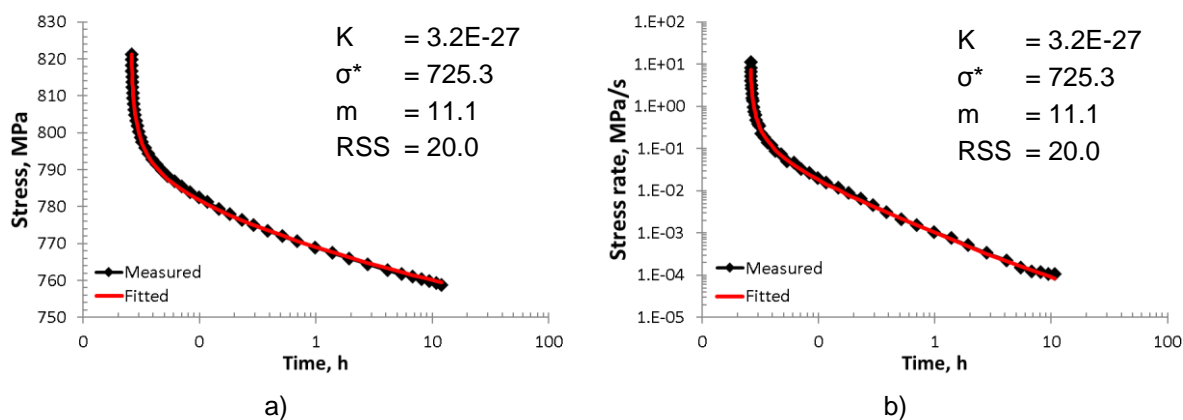


Figure 6.4-2: Fitted parameters according to equation (9.4-3), a) stress relaxation of the 1.4436 cold drawn at $1.0 \times R_{p0.2}$ (48 data points), b) the stress rate. RSS is the lowest residual sum of squares.

However, the number of local minimum in the parameter space of equation (9.4-3) was vast so the following practice was used for determining K, m and σ^* : Hannula et. al [9.3-1] reported no significant dependence between m and strain so K, m and σ^* was first determined for the $1.0 \times R_{p0.2}$ stress level (as these had the “smoothest” curve). The average m of two tests at this stress level was then used for evaluating K and σ^* at the lower stress levels for each type of material. Table 6.4-3 shows the determined values of K, m and σ^* from the nonlinear fitting of the tested bars according to equation (9.4-3).

Table 6.4-3: Found parameter values from solving equation (9.4-3), mean value of two measurements.

Grade, EN	Type	$xR_{p0.2}$	m	K	σ^* , MPa	SD σ^* , MPa	RSS, MPa ²
1.4436	Rebar	0.6	12.1	3.8E-22	191.5	1.6	2.3
		0.8	12.1	1.8E-25	236.9	2.0	11.9
		1.0	12.1	3.2E-27	274.8	2.1	1.7
	CD	0.6	11.2	1.4E-23	456.7	0.4	9.7
		0.8	11.1	2.2E-25	629.5	2.2	18.3
		1.0	11.1	3.2E-27	725.4	0.2	33.4
1.4162	Rebar	0.6	10.3	3.2E-22	331.3	1.4	11.6
		0.8	10.3	1.5E-24	414.8	0.8	16.7
		1.0	10.2	5.7E-26	489.3	7.6	23.4
	CD	0.6	10.3	1.2E-22	422.5	5.1	21.1
		0.8	10.3	3.0E-24	554.7	0.4	17.2
		1.0	10.3	5.3E-26	666.3	0.3	25.6
1.4462	Bar	0.6	10.3	5.0E-21	357.2	1.5	4.8
		0.8	10.3	1.0E-23	452.6	0.8	8.6
		1.0	10.3	5.7E-26	515.6	0.2	10.4
	CD	0.6	10.1	7.2E-22	476.4	0.9	7.4
		0.8	10.1	2.6E-24	610.8	1.7	16.3
		1.0	10.1	5.7E-26	731.3	2.9	15.6

Figure 6.4-3 shows σ^* as a function of initial stress for the tested bars and the σ^* was found to be a linear dependence of the initial stress (which was consistent with the literature [9.4-2], [9.4-3]). For the cold drawn bars, the σ^* as a function of the initial stress was similar for the three tested grades.

It is assumed that the inelastic deformation during stress relaxation testing proceeds only as long as the stress exceeds the threshold determined by the state variable σ^* and that the value of the state variable σ^* characterizes the asymptotic lower bound for the stress in the relaxation experiments (i.e. the stress at infinite time).

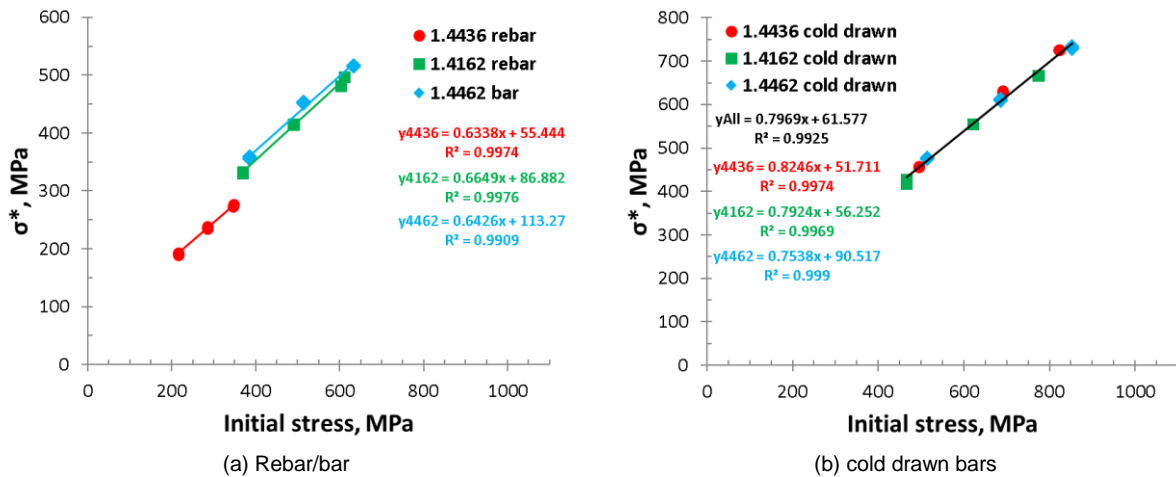


Figure 6.4-3: σ^* as a function of the initial stress

Figure 6.4-4 shows the asymptotic stress relaxation (defined according to equation (9.4-1) where σ^* was used instead of σ) as a function of the initial stress. The relationship between σ^* and the initial stress were the linear dependencies in Figure 6.4-3. The results show that for the tested specimens the duplex grades, in the “annealed” state, has less stress relaxation than the austenitic grade in the “annealed” state at all initial stresses. However, for the cold drawn bars the austenitic grade has less stress relaxation compared to the two duplex grades at higher stresses. Figure 6.4-4 was consistent with Figure 6.4-1. The $F_{p,C}$ corresponds to the estimated stress in the bolts for the used preload levels used in this project (see Task 5.3).

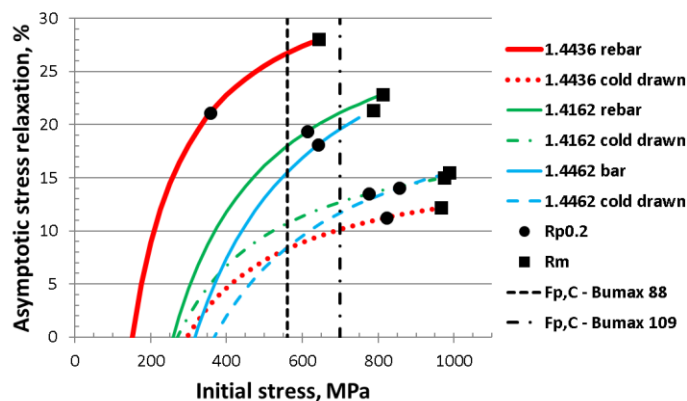


Figure 6.4-4: The asymptotic stress relaxation as a function of the initial stress for the tested bars. $R_{p0.2}$ and R_m were the measured strength of the tested bars, recall Table 9.4-1.

The stress relaxation testing has been performed on bars and as seen in Table 6.4-1 the cold forged bolts have higher proof stress compared to the cold drawn bars. This indicates higher amount of cold work in the bolts compared to the cold drawn bars. The stress relaxation seems to be sensitive to the amount of cold work. One may therefore assume that cold forged bolts will lie below the 1.4436 cold drawn line in Figure 6.4-4 and thus show less stress relaxation than the tested cold drawn bars. One may therefore also assume that machined bolts will show more stress relaxation than cold forged bolts. The stress relaxation testing shows that most of the stress relaxation occurs within minutes of

applying constant strain. Roughly 50 % of the asymptotic stress relaxation occurs within the first hour of testing, see Figure 6.4-5.

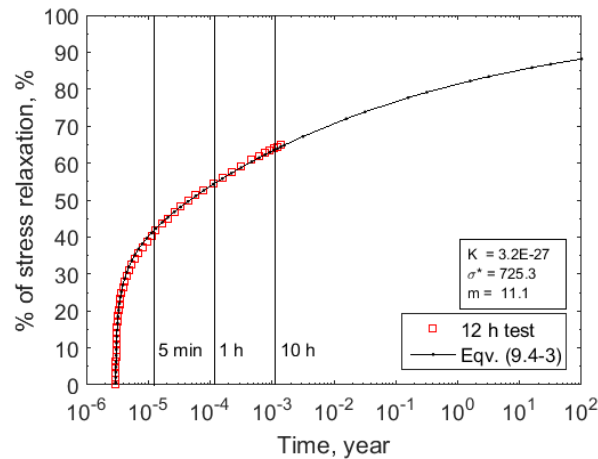


Figure 6.4-5: Comparison between 12 h stress relaxation test and the asymptotic stress relaxation. 5 min, 1 h and 10 h marks the respectively testing time. Cold drawn bar of 1.4436 at the $1.0 \times R_{p0.2}$ stress level.

6.5 Task 5.3 – Preloading and relaxation behaviour of SS bolt assemblies

Tightening tests of stainless steel bolting assemblies

The tightening tests of austenitic and austenitic-ferritic (lean duplex, duplex and super duplex) stainless steel bolting assemblies were performed at the Institute for Metal and Lightweight Structures of the University of Duisburg-Essen (UDE). The objective was to investigate the basic preloading behaviour of stainless steel bolting assemblies and to achieve information regarding the complex interaction behaviour between the applied torque and the achieved preload. Bumax stainless steel bolts (acc. EN ISO 4014 [9.5-1] and EN ISO 4017 [9.5-2]), hexagon nuts (acc. EN ISO 4032 [9.5-3]) and washers (acc. EN ISO 7089 [9.5-4]) were used. As a first step, the used lubrication for Task 5.3 tightening tests was factory provided gleitmo 1952V from Fuchs Lubritech GmbH as a typically dry film lubricant for stainless steel bolts. The bolting assemblies were tightened according to EN 14399-2 [5.7-2] (valid for carbon steel bolts). In absence of existing adequate criteria for preloaded stainless steel bolting assemblies, the evaluation of the tightening tests was referred to EN 14399-3 [5.7-1] and follows for reasons of comparability the requirements and criteria of the HR system.

Test matrix and procedure

The test matrix for tightening tests (STEP 1) of stainless steel bolting assemblies is visualized in Table 6.5-1. The test matrix for tightening tests shows the steel grades and property classes of the bolts. Additionally, tightening tests of bolt dimension M12 and M20 were carried out. Deviating from the technical annex, super duplex steel grade was used for bolt dimension M12 because lean duplex and duplex bolts were not available. The tightening tests of Bumax 88 – M20x100 (bolts manufactured in 2013) showed irregular graphs, so it was decided to stop these tests and repeat all tightening tests with bolts manufactured in 2015.

In total, 12 series and 125 bolting assemblies were tested at UDE-IML using the institute's own tightening torque testing machine which are significantly more than the 80 test specimens prescribed in Task 5.3 technical annex ($80 = 2 \text{ bolt dimensions} \times 4 \text{ steel grades} \times 1 \text{ lubrication} \times 10 \text{ bolts per series}$). All tightening tests carried out according to EN 14399-2 and EN ISO 16047 [5.7-3]. For reasons of comparability and in absence of regulations for stainless steel bolting assemblies, the evaluation of the tested stainless steel bolting assemblies refers to EN 14399-3 for carbon steel bolts. This evaluation is based on criteria for System HR. The test series are labeled according to the following naming convention: BU_Mxx_yyy-zz with

BU:	BUMAX stainless steel bolt	yyy:	strength class respectively duplex steel grade
Mxx:	bolt diameter	zz:	sequential number of bolt

Table 6.5-1: Task 5.3 – Test matrix for stainless steel tightening tests (STEP 1)

Steel grade	Steel standards	Grade	Lubrication	Bolt dimension			
				M12	M16	M20	M24
STEP 1: Tightening tests with standard lubrication							
Bumax 88	bolts: EN 1.4432 nuts: EN 1.4436	Austenitic	gleitmo 1952V ¹⁾	4014 ²⁾	4017 ³⁾	4017	4017
Bumax 109		Austenitic	gleitmo 1952V	4014	4017	4014	-
Bumax LDX	EN 1.4162	Lean Duplex	gleitmo 1952V	-	4017	4017	-
Bumax DX	EN 1.4462	Duplex	gleitmo 1952V	-	4017	4017	-
Bumax SDX	EN 1.4410	Super Duplex	gleitmo 1952V	4017	-	-	-
¹⁾ gleitmo 1952V lubricant from Fuchs Lubritech GmbH ²⁾ 4014: EN ISO 4014 bolt, EN ISO 4032 nut and EN ISO 7089 washer ³⁾ 4017: EN ISO 4017 bolt, EN ISO 4032 nut and EN ISO 7089 washer							

The requirements regarding sufficient ductility of carbon steel HV and HR bolting assemblies are specified in EN 14399-4 and EN 14399-3. HR bolting assemblies are characterised by a longer thread and a higher nut than HV bolting assemblies. Herewith, HR bolts represent more likely the bolting assemblies using EN ISO 4017 bolts and EN ISO 4032 nuts. For this reason and in the absence of existing adequate criteria for preloaded stainless steel bolting assemblies, the following criteria (9.5-1-9.5-5) acc. to EN 14399-2 and EN 14399-3, see Figure 6.5-1 were chosen as a basis for qualification and evaluation of the ductility of preloaded stainless steel bolting assemblies. From these five criteria, only requirements (3) and (5) have to be fulfilled on $F_{p,C}$ -level in the suitability test for preloading acc. to EN 14399-2/3.

$$\square F_{p,C} = 0.7 \cdot f_{ub} \cdot A_s \quad (9.5-1)$$

$F_{p,C}$ specified preloading level acc. to EN 1090-2 [5.3-1]
 f_{ub} nominal tensile strength ($R_{m,nom}$) of the bolt
 A_s nominal stress area of the bolt acc. to EN ISO 898-1 [9.5-5]

$$\square F_{p,C}^* = 0.7 \cdot f_{yb} \cdot A_s \quad (9.5-2)$$

$F_{p,C}^*$ preload level acc. to DIN EN 1993-1-8/NA [5.7-4]
 f_{yb} yield strength of the bolt ($R_{p0.2}$), see EN ISO 898-1
 A_s nominal stress area of the bolt, see EN ISO 898-1

$$\square F_{bi,max} \geq 0.9 \cdot f_{ub} \cdot A_s \quad (9.5-3)$$

$F_{bi,max}$ individual value of the maximum bolt force reached during the test
 f_{ub} nominal tensile strength ($R_{m,nom}$) of the bolt
 A_s nominal stress area of the bolt

$$\square \Delta\Theta_{1i} \geq \Delta\Theta_{1,min} = 90^\circ / 120^\circ / 150^\circ \text{ (depending on the clamp length)} \quad (9.5-4)$$

$\Delta\Theta_{1i}$ individual angle difference of the nut from the first time the preload $F_{p,C}$ is exceeded to the individual value of the maximum bolt force $F_{bi,max}$

$$\square \Delta\Theta_{2i} \geq \Delta\Theta_{2,min} = 210^\circ / 240^\circ / 270^\circ \text{ (depending on the clamp length)} \quad (9.5-5)$$

$\Delta\Theta_{2i}$ individual angle difference of the nut from the first time the preload $F_{p,C}$ is exceeded to the angle when bolt force drops below $F_{p,C}$ again

Mechanical properties of the bolting assemblies

The Bumax 88 correlates to carbon bolts property class 8.8, while Bumax 109 is equal to property class 10.9, with the exception of bolt dimensions larger than M12 (yield strength: 800 MPa). Furthermore, Table 6.5-2 shows the by Bumax suggested combination of bolts, hexagon nuts and washers.

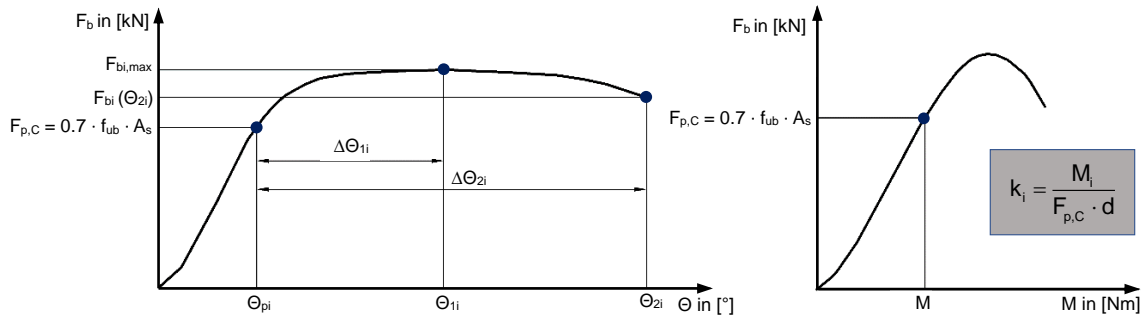


Figure 6.5-1: Schematic bolt force-angle of rotation curve (left) and bolt force-tightening torque curve (right) according to EN 14399-2

Table 6.5-2: Task 5.3 – Nominal mechanical properties of stainless steel bolting assemblies [© BUMAX]

Bolt Steel grade	Bolt type of stainless steel	Tensile strength	Yield strength	Elongation, min	Nut and washer steel grade	Nut and washer type of stainless steel	Nuts – Stress under proof load, min	Washers – Hardness, min
		$R_{m,min}$	$R_{p0.2,min}$				N/mm ²	HV
		N/mm ²	N/mm ²	mm			N/mm ²	
Bumax 88	Austenitic	800	640	0.3 d	Bumax 88	Austenitic	800	200
Bumax 109	Austenitic	1000	900	0.2 d	Bumax 109	Austenitic	1000	300
Bumax LDX	Lean Duplex	1000	900	0.3 d	Bumax 109	Austenitic	1000	300
Bumax DX	Duplex	1000	900	0.3 d	Bumax 109	Austenitic	1000	300
Bumax SDX	Super Duplex	1000	900	0.3 d	Bumax 109	Austenitic	1000	300

Evaluation procedure of tightening parameters

- To complete the evaluation of stainless steel bolting assemblies, it was necessary to determine the additional tightening parameters and check the following criteria as well as the previously defined criteria (1-5) systematically with reference to EN 14399-2/3:
- Individual values of the k-factor (k_i) for k-class K1: $0.10 \leq k_i \leq 0.16$.
- Mean value of the k-factor (k_m) and the coefficient of variation of the k-factor (V_k) for k-class K2: $0.10 \leq k_m \leq 0.23 \wedge V_k \leq 0.06$ (see equations).

$$k_m = \frac{\sum_{i=1}^n k_i}{n}, \quad V_k = \frac{s_k}{k_m}, \quad s_k = \sqrt{\frac{\sum (k_i - k_m)^2}{n-1}}$$

- Additionally in the frame of this research $F_{p,C}^* = 0.7 \cdot f_{yb} \cdot A_s$ as alternate preloading in the context of quantitative improvement of serviceability, where f_{yb} is the nominal yield strength, acc. DIN EN 1993-1-8/NA:2010-10.

Main results and conclusions of tightening tests with gleitmo 1952V lubricants

Table 6.5-3 shows the summary of the evaluation of the tested series after finishing the tightening tests with gleitmo 1952V standard lubrication from Fuchs Lubritech GmbH. In conclusion, it can be figured out that fracture of bolts did not occur and, with the exception of Bumax 109 – M20x140, all tested stainless steel bolting assemblies reached the preload level $F_{p,C}^* = 0.7 \cdot f_{yb} \cdot A_s$ and $F_{p,C} = 0.7 \cdot f_{ub} \cdot A_s$. In contrast, caused by the fact that the bolt force plateaus in the plastic range were less pronounced compared to those of EN 14399-carbon steel bolting assemblies, the criteria of the maximum bolt force $F_{bi,max} \geq 0.9 \cdot f_{ub} \cdot A_s$ was only partially achieved. It can be shown that in total only Bumax 88 – M16x80 series reached $F_{bi,max} \geq 0.9 \cdot f_{ub} \cdot A_s$. Indeed, for the series Bumax 88 – M12x80, Bumax SDX – M12x80 and Bumax 88 – M20x100 (bolts manufactured in 2015) only one bolt failed in

each series. On the contrary, Bumax 88 – M20x100 (2013), Bumax 109 – M20x140, Bumax LDX – M20x100 and Bumax DX – M20x100 test series failed completely. Furthermore, also referred to the less pronounced bolt force plateaus in plastic range, the required angles of nut rotation $\Delta\Theta_{1i,min}$ and $\Delta\Theta_{2i,min}$ are unequally distributed, which can be seen in Table 6.5-3. The analysis of k-values tends to show two groups:

- a narrow range of k-values like Bumax 88 – M16x80 (0.13 to 0.17), Bumax 109 – M20x140 (0.25 to 0.26) and Bumax LDX – M16x100 (0.11 to 0.15),
- a wide range of k-values like Bumax 88 – M12x80 (0.11 to 0.19), Bumax 88 – M24x100 (0.10 to 0.22) and other tested series.

Table 6.5-3: Summary of the evaluation of stainless steel tightening tests according to EN 14399-3 (valid for clamp lengths: $2d \leq \sum t \leq 6d$)

Tested series	n	$F_{p,c}$	$F_{p,c}$	$F_{bi,max}$	$\Delta\Theta_{1i,min}$	$\Delta\Theta_{2i,min}$	k-values	k-class K1	k-class K2		Fracture	Galling
					$\geq 120^\circ$	$\geq 240^\circ$			$0.10 \leq k_1 \leq 0.16$	$0.10 \leq k_m \leq 0.23$		
M12												
Bumax 88 - M12x80	10	100%	100%	90%	70%	80%	0.11 – 0.19	80%	0.149	0.186	0%	100%
Bumax 109 - M12x80	10	100%	100%	40%	70%	60%	0.12 – 0.24	30%	0.183	0.205	0%	100%
Bumax SDX - M12x80	10	100%	100%	90%	60%	90%	0.14 – 0.21	60%	0.138	0.138	0%	100%
M16												
Bumax 88 - M16x80	10	100%	100%	100%	60%	100%	0.13 – 0.17	90%	0.136	0.075	0%	100%
Bumax 109 - M16x100	10	100%	100%	30%	40%	40%	0.11 – 0.22	60%	0.151	0.231	0%	100%
Bumax LDX - M16x100	10	100%	100%	30%	40%	80%	0.11 – 0.15	100%	0.123	0.127	0%	100%
Bumax DX - M16x100	10	100%	100%	20%	20%	30%	0.12 – 0.19	70%	0.150	0.169	0%	100%
M20												
Bumax 88 - M20x100 (2013)	5	100%	100%	0%	0%	0%	0.21 – 0.33	0%	0.239	0.217	0%	20%
Bumax 88 - M20x100 (2015)	10	100%	100%	90%	30%	90%	0.12 – 0.17	80%	0.145	0.118	0%	100%
Bumax 109 - M20x140	10	100%	40%	0%	0%	0%	0.25 – 0.26	0%	0.255	0.023	0%	100%
Bumax LDX - M20x100	10	100%	100%	0%	0%	30%	0.10 – 0.15	100%	0.120	0.148	0%	100%
Bumax DX - M20x100	10	100%	100%	0%	20%	30%	0.10 – 0.15	100%	0.121	0.158	0%	100%
M24												
Bumax 88 - M24x100	10	100%	100%	50%	10%	30%	0.10 – 0.22	60%	0.151	0.235	0%	30%

Consequently, the classification in k-class K1 is also unequally distributed in all tested series and confirming a general high dispersion of all tested values, markedly friction. In addition, all tested stainless steel bolting assemblies did not achieve the criteria for classification to k-class K2, mainly caused by a higher coefficient of variation v_k than 0.06 referring to EN 14399-1. It is noticeable that Bumax 88 – M20x100 (bolts manufactured in 2013) failed as well as Bumax 109 – M20x140 – in most criteria, caused by very high coefficients of friction as a possible evidence for insufficient or ineffective lubrication. In addition, lean duplex and duplex steel grades for bolt dimension M16 and M20 did not achieve $F_{bi,max} \geq 0.9 \cdot f_{ub} \cdot A_s$, and the required angles of nut rotation $\Delta\Theta_{1i,min}$ and $\Delta\Theta_{2i,min}$ were only partially fulfilled. In total, the tested bolting assemblies showed up light to heavy galling in the nut bearing surfaces, when tightened into the plastic range. The damage analysis underlines that all tested bolt assemblies have similar damages at the first (and in some cases second) load-bearing thread turn of the bolt, roughening of paired threads and minimal necking of threaded shanks without bolt or nut fracture. With the exception of Bumax 88 – M20x100 (2013 series) and Bumax 88 – M24x100 series, all tested bolting assemblies showed damages caused by galling, especially in the faying surface between the washer and nut as shown exemplary in Figure 9.5-2. Considering the use of bolting assemblies made of stainless steel as high-strength bolting assembly for preloading, the tightening behaviour had to be investigated by using alternative lubrications to increase the ductility and to avoid galling.



Figure 6.5-2: Galling of the nut bearing surface when tightened into plastic range: bolt (left), nut and washer (middle), and detailed view of washer (right)

The tightening behaviour of EN ISO 4014/4017 stainless steel bolting assemblies compared to System HR and System HV carbon steel bolting assemblies is shown exemplary in Figure 6.5-3. The

tightening curves visualize a comparison between Bumax 88 – M24x100 stainless steel bolting assemblies (black curves) and M24x100 HR 8.8 bolting assemblies (yellow curves), as well as between Bumax 88 – M24x100 stainless steel bolting assemblies (black curves) and M24x100 HV 10.9 bolting assemblies (yellow curves). It has to be noted that these are exemplary curves for presenting the main differences because the shape of the tightening curves is multifactorial influenced (e.g. by lubrication used) and may differ. From beginning of the tightening test to the defined preload level $F_{p,C}^*$ and $F_{p,C}$, stainless steel and carbon steel bolting assemblies show a nearly similar and approximately linear behaviour in the bolt force-angle of rotation curves, differentiated only by the slope of the line. Additionally, in this region, the scattering of the curves in all tested series is negligible. The bolt force plateaus in the plastic range of bolting assemblies made of stainless steel are less pronounced compared to carbon steel bolts, leading to lower angles of rotation $\Delta\Theta_{1i}$ and $\Delta\Theta_{2i}$. Furthermore, the tightening curves of tested stainless steel bolting assemblies show a greater distribution in both axes, meaning scattering of the maximum individual bolt force $F_{bi,max}$ and scattering of the angles of rotation when the bolt force drops to $F_{p,C}$ again. The bolt force-tightening torque curves of HR and HV bolting assemblies tend to display a relatively narrow range of a tightening torque. On the other hand, bolting assemblies made of stainless steel display a wide range of torque for a preload level of $F_{p,C}$. Overall, these circumstances create difficulties in defining predictable, calculable and securely tightening torques for stainless steel bolting assemblies.

Further tightening tests with alternative lubricants are performed in Task 5.4 to investigate the influence of other lubricants on the friction and to optimize the tightening procedure of stainless steel bolts with low deviations and constant, calculable friction coefficients. A detailed comparison between austenitic and austenitic-ferritic bolts and property classes is given in the Deliverable report D5.4 of Task 5.3/5.4. Finally, the evaluation criteria have to be developed for preloaded stainless steel bolting assemblies comparable to those given in EN 14399 for preloaded carbon steel bolting assemblies on the basis of the investigations carried out in this WP (see also Task 5.4 and Deliverable report D5.5). In principle, the preloading of austenitic and lean duplex, duplex and super duplex stainless steel bolting assemblies, property classes 8.8 and 10.9 is possible by choosing a suitable material pairing and lubrication avoiding galling and considering the less pronounced plastic plateau. However, the presented investigations and findings can only provide an initial insight into the tightening behaviour of stainless steel bolting assemblies.

Relaxation tests

Preloaded stainless steel (SS) bolting assemblies relax due to the setting effect of the clamped components surfaces and creep and relaxation of stainless steel material as a result of the applied pretension. As a result of additional relaxing and creeping of the stainless steel bolts and the clamped parts compared to carbon steel, there might be preload losses in the bolts which must be taken into account when defining suitable tightening parameters. Therefore, this task deals with determination of the amount of preload losses resulting from the combined creep and stress relaxation in a preloaded stainless steel bolted connection.

The first step to investigate the relaxation behaviour of the SS bolting assemblies is to find the most reliable method to measure the preload inside the bolt. For this reason, additional creep tests on stainless steel bolts were carried out to investigate the influence of the creeping of the bolt material on the measured preload level. In total ten tests were performed: one test on a carbon steel bolt and nine tests on stainless steel bolts, see Deliverable 5.4. For each type of stainless steel bolts, one creep test was repeated to proof the reusability of the stainless steel bolts. The results show that the accuracy of the instrumented bolts with implanted strain gauges for measuring the preload inside the bolts is acceptable but it has also to be pointed out that already during the preloading process of the stainless steel, creep occurs. These changes in the strain were measured by strain gauges and caused different values in comparison to the real preload level, see Figure 6.5-3. For this reason, it was decided to prepare some small load cells to measure the preload level.

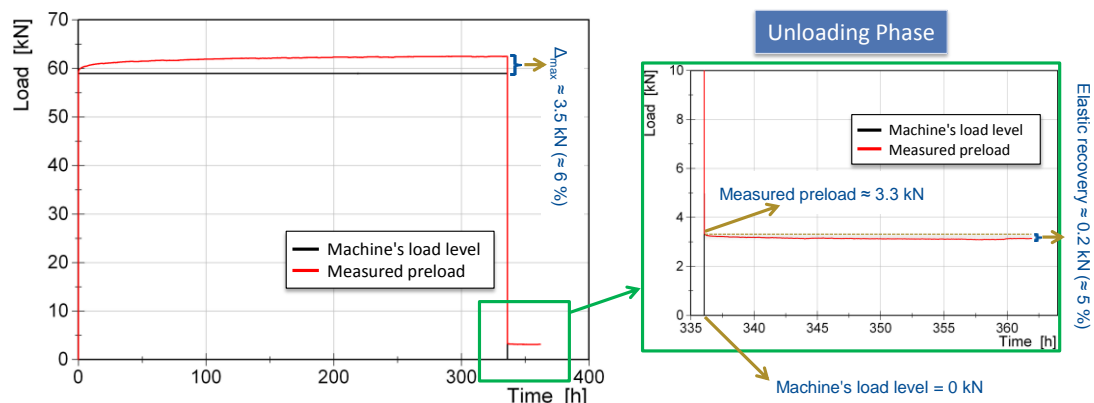


Figure 6.5-3: Exemplary creep test results - M12 super duplex bolting assemblies

The advantage of using load cells is that creep has no influence on the measured preload level. For this purpose, different load cells were prepared by UDE, see Figure 6.5-5. All load cells were calibrated under stepwise tensile loading in a similar way as carried out for instrumented bolts with strain gauges. The combination of the instrumented bolt and load cell was also tested in order to confirm the accuracy of both methods.

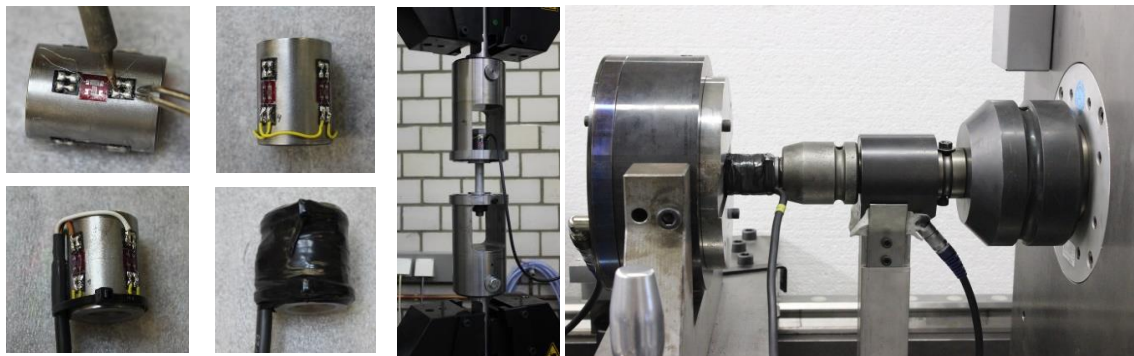


Figure 6.5-4: Production calibration phases of load cells and test setup of relaxation test

In the next step, the additional relaxation tests were carried out in two different groups. In the first group, the preload was measured by instrumented bolts with a clamping length range of $\sum t / d = 2$ in order to take account of the fact that shorter clamping lengths lead to greater preload losses. In the second group, the preload measured with two different methods (instrumented bolts (SG) + load cell (LC)). Using LCs leads to a relatively larger clamping length in comparison to the first group. The results of instrumented bolts and the load cell are comparable. Even though, the load cells provide more reliable test results in the long term relaxation tests.

Relaxation test according to the Technical annex

Within SIROCO, austenitic (1.4404), ferritic (1.4003), duplex (1.4462), and lean duplex (1.4162) stainless steel plates and austenitic (1.4432), duplex (1.4462) and lean duplex (1.4162) stainless steel bolting assemblies according to EN ISO 4017 were used for experimental testing of the loss of preload of stainless steel bolted connections.

All stainless steel plates were used in the “as delivered” 1D surface condition without any further surface treatment, see Figure 6.5-5 (a) and (b). Additionally, further test series were conducted with S355 carbon steel plates (in the “as received” surface condition, see Figure 6.5-5 (c) and (d)) in combination with stainless steel bolts (M16 and M20 austenitic bolts (Bumax 88)) and carbon steel bolts (M16 and M20 HV 10.9 bolts) according to EN 14399-4 and stainless steel plate. These additional tests were carried out in order to be able to separate the creep effect from the stainless steel plates and bolts.

Furthermore, some test series were conducted with carbon steel HV bolts and S355 carbon steel plates in order to be able to compare the preload losses in stainless steel and carbon steel bolting assemblies. The carbon steel plates were only shot blasted to clean the surfaces from rust.

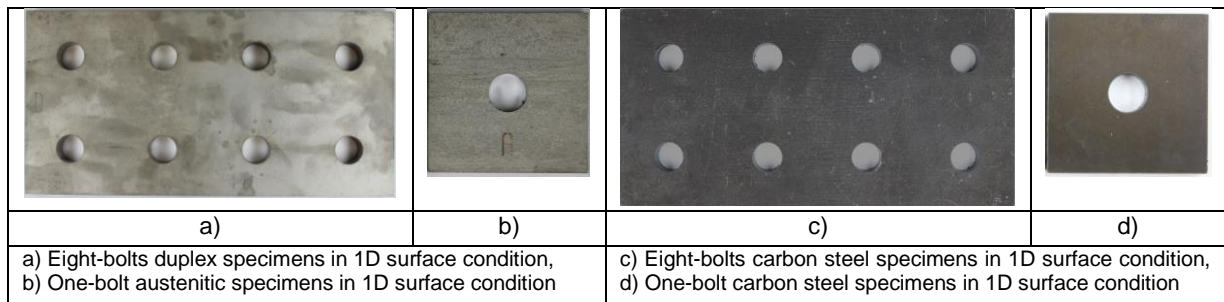


Figure 6.5-5: Exemplary photos for stainless steel and carbon steel test specimens

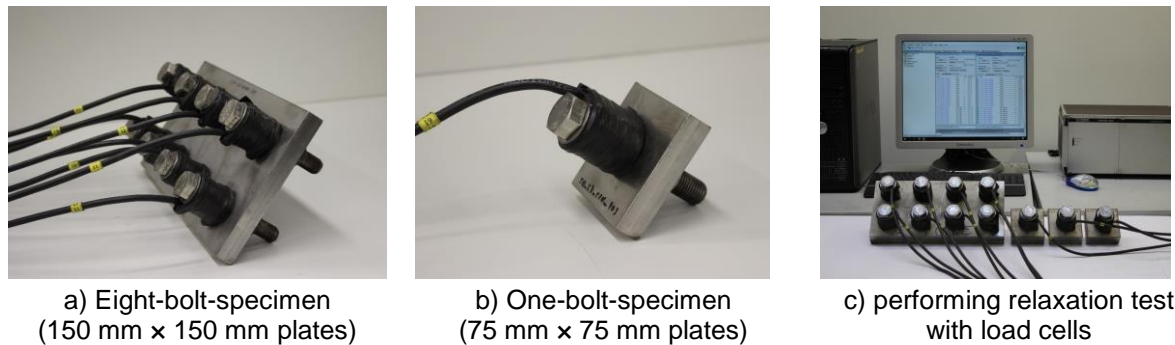


Figure 6.5-6: Test setup

Of great importance is the definition of the starting point for the evaluation of the preload measurement as in the first seconds after tightening of the bolts, a considerable drop in the measured preload level can be observed. The main amount of this instance drop can be explained by turning back of the nut and elastic recovery of the bolt threads when the wrench is removed. By removing the first three seconds and by considering the linear behaviour of the loss of preload in a logarithmic scale, it is possible to derive the exact starting point of the relaxation test. Figure 6.5-8 shows exemplary the preload losses-log (time) diagrams for the austenitic stainless steel SS16 test series with M20 lean Duplex bolts with property class 10.9.

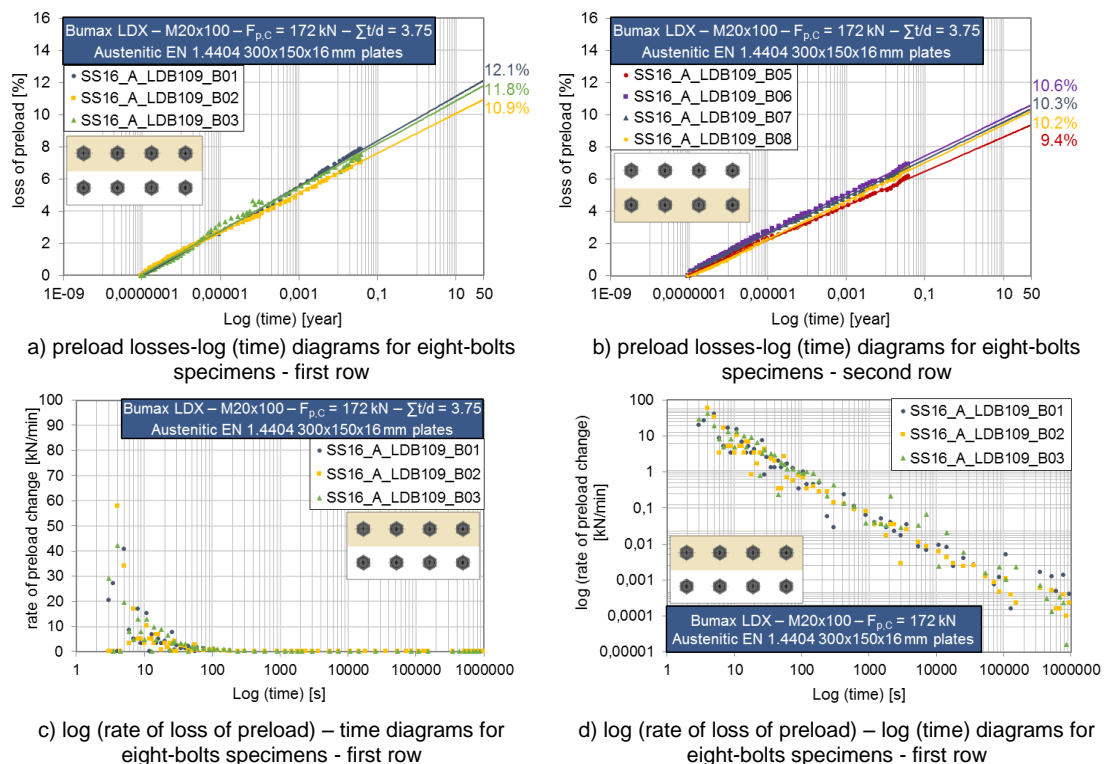


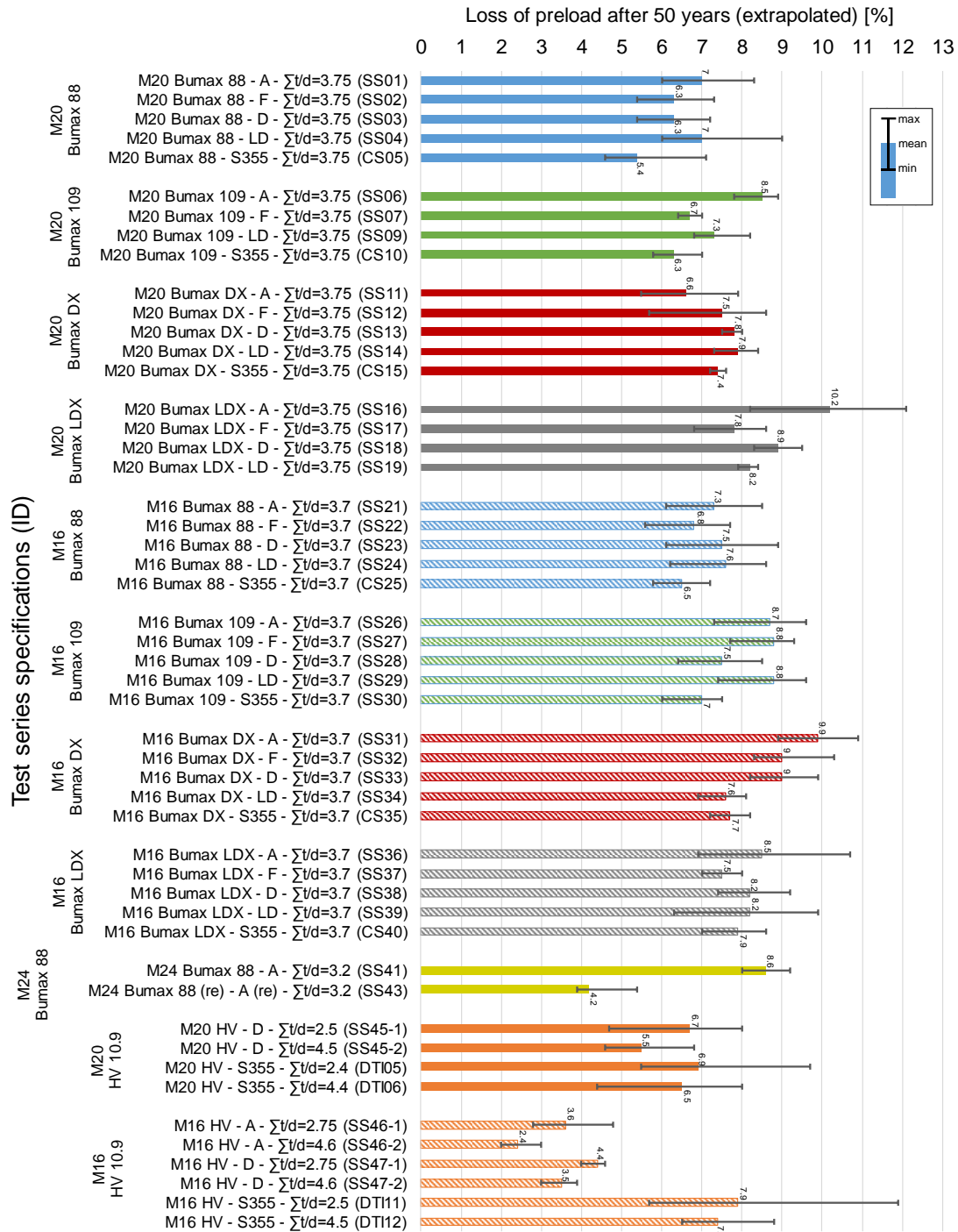
Figure 6.5-7: Exemplary preload losses and rate of loss of preload for SS16 test series (Lean duplex bolts + Austenitic plates)

The loss of preload starts immediately after tightening of the bolts and continues gradually over time. The highest rate can be observed at the beginning of testing, see Figure 6.5-8. The results show that

the highest loss of preload was observed for M20 lean-duplex and M16 duplex bolting assemblies in combination with austenitic plates by about 10 %, see Figure 6.5-8. It can also be seen that the amount of loss of preload between M16, M20 and M24 stainless steel bolting assemblies is comparable for different types of stainless steel with the same clamping length ratio and preload level. As it also can be seen in Figure 6.5-8, a smaller clamping length leads to a higher loss of preload in the preloaded bolted assemblies. This phenomenon can be confirmed for both bolt dimensions (M20 and M16).

Herewith, the conclusion can be drawn that the loss of preload in the preloaded connections investigated in this work was mainly attributed to the embedment/plastic deformation of the clamped component surfaces while the creep in the plates was negligible. The estimated preload losses over 50 years for different grades of stainless steel bolting assemblies (austenitic, duplex and lean-duplex) are similar (between 6 % to 10 %). It is clear that the creep and stress relaxation in the bolt material is detectable but the influence of these parameters on the amount of preload losses is insignificant.

The present relaxation experiments are compared with the results of carbon steel bolted connections from Task 3.3 with approximately the same clamping length ratio and without any DTIs (series names: DTI05, DTI06, DTI11 and DTI12), see Figure 6.5-8. The results show that the loss of preload in preloaded carbon steel bolted connections and preloaded stainless steel bolted connections are comparable as the preload loss for the carbon steel bolted connections yield to approximately the same value of between 7 % to 8 % which is comparable to the values achieved over all stainless steel test samples.



A: Austenitic EN 1.4404 | F: Ferritic EN 1.4003 | D: Duplex EN 1.4462 | LD: Lean Duplex EN 1.4162

Figure 6.5-8: Comparing the loss of preload after 50 years (extrapolated) for different test series

6.6 Task 5.4 – Preloading levels

General

In the context of WP 5 – Preloading levels Task 5.4 and as a continuation of the work undertaken in Task 5.3, tightening tests of stainless steel bolting assemblies with various lubrications as Dow Corning Molykote P-74 paste, Dow Corning Molykote 1000 paste, Dow Corning Molykote 1000 spray and Dow Corning Molykote D-321 spray were performed to identify a suitable, alternative lubrication for stainless steel bolting assemblies. All lubricants are suitable for stainless steels according to the information provided by the producer. These lubrication tests identified Dow Corning Molykote 1000 spray as an alternative lubricant for Fuchs Lubritech gleitmo 1952V standard lubrication (see Task 5.3) and Dow Corning Molykote D-321R spray as a promising alternative under difficult friction conditions. Furthermore, alternative lubricants from Dow Corning were also used in the second step to study the

positive effects as extending the plastic plateau and avoiding galling. In a third step, additionally tightening tests were performed with M20 EN ISO 4017 bolts with the ceramic-based lubricant Interflon® HT1200 spray and paste for austenitic (property classes 8.8 and 10.9) and lean duplex (property class 10.9) bolting assemblies made of stainless steel.

The bolting assemblies were tightened according to EN 14399-2 (valid for carbon steel bolts). In accordance to Task 5.3 and in absence of existing adequate criteria for preloaded stainless steel bolting assemblies, the evaluation of the tightening tests was again referred to EN 14399-3 and follows for reasons of comparability the requirements and the criteria of the HR system (see subchapter 9.5).

Test matrix and procedure

The additional tightening tests (STEP 2 and 3) of stainless steel bolting assemblies are visualized in Table 6.6-1 and Table 6.6-2. The test matrices for tightening tests show the steel grades and property classes of the bolts. Additionally, tightening tests of bolt dimension M12 and M20 were carried out. Deviating from the technical annex, super duplex steel grade was used for bolt dimension M12 because lean duplex and duplex bolts were not available. In total, 24 series and 170 bolting assemblies were tested at UDE-IML using the institute's own tightening torque testing machine (see Figure 6.6-1), which are significantly more than the 80 test specimens prescribed in Task 5.4 technical annex (80 = 2 bolt dimensions x 4 steel grades x 1 lubrication x 10 bolts per series). The test series are named according to the following naming scheme: BU_Mxx_yyy-zz

BU: BUMAX stainless steel bolt yyy: strength class respectively duplex steel grade
Mxx: bolt diameter zz: sequential number of bolt

Table 6.6-1: Task 5.4 – Test matrix for stainless steel tightening tests (STEP 2)

Steel grade	Steel standards	Grade	Lubrication	Bolt dimension			
				M12	M16	M20	M24
STEP 2: Tightening tests with alternative lubrication							
Bumax 88	bolts: EN 1.4432 nuts: EN 1.4436	Austenitic	Molykote 1000 Spray ¹⁾	-	4017 ³⁾	4017	-
			Molykote 1000 Paste ¹⁾	-	-	4017	-
			Molykote P-74 Paste ¹⁾	-	-	4017	-
			Molykote D-321R Spray ¹⁾	-	-	4017	-
Bumax 109		Austenitic	Molykote 1000 Spray	-	4017	4014 ²⁾	-
			Molykote P-74 Paste	-	-	4014	-
	Molykote D-321R Spray		-	4017	4014	-	
Bumax LDX	EN 1.4162	Lean Duplex	Molykote 1000 Spray	-	4017	4017	-
Bumax DX	EN 1.4462	Duplex	Molykote 1000 Spray	-	4017	4017	-
Bumax SDX	EN 1.4410	Super Duplex	Molykote 1000 Spray	4017	-	-	-
¹⁾ Molykote products from DOW Corning ²⁾ 4014: EN ISO 4014 bolt, EN ISO 4032 nut and EN ISO 7089 washer ³⁾ 4017: EN ISO 4017 bolt, EN ISO 4032 nut and EN ISO 7089 washer							

Overview about used types of lubrication

An overview about the used types of lubrication as alternative lubrications for stainless steel bolting assemblies as well as the manufacturer specifications from Dow Corning GmbH are presented in Table 6.6-3. Because Fuchs Lubritech gleitmo 1952V delivered high ranges of μ_{lot} , μ_{th} , and μ_b and is not suitable for calibrated friction coefficients, the main tightening tests were focused on constant and predictable friction coefficients of the paired threads μ_{th} as well as the friction under the head respectively nut bearing surface μ_b for austenitic and austenitic-ferritic series. In addition, the galling behaviour was investigated and compared to the already tested series in Task 5.3. Galling as a form of cold-welding must be avoided in all cases.

Table 6.6-2: Task 5.4 – Test matrix for stainless steel tightening tests (STEP 3)

Steel grade	Steel	Grade	Lubrication	Bolt dimension
-------------	-------	-------	-------------	----------------

	standards			M12	M16	M20	M24
STEP 3: Tightening tests with ceramic based lubrication							
Bumax 88	bolts: EN 1.4432	Austenitic	HT1200 Spray ¹⁾	-	-	4017 ²⁾	-
			HT1200 Paste ¹⁾	-	-	4017	-
Bumax 109	nuts: EN 1.4436	Austenitic	HT1200 Spray	-	-	4017	-
			HT1200 Paste	-	-	4017	-
Bumax LDX	EN 1.4162	Lean Duplex	HT1200 Spray	-	-	4017	-
			HT1200 Paste	-	-	4017	-
¹⁾ HT1200 spray and paste from Interflon ²⁾ 4017: EN ISO 4017 bolt, EN ISO 4032 nut and EN ISO 7089 washer							

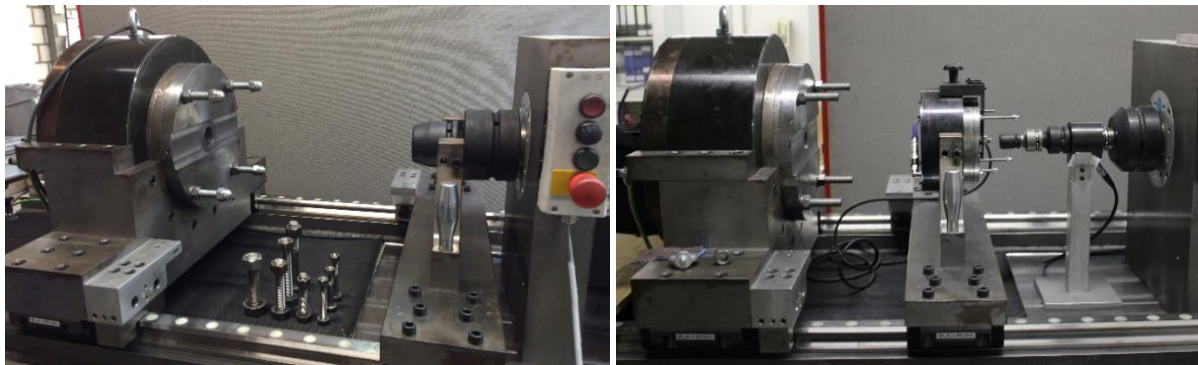


Figure 6.6-1: Tightening torque testing machine at the Institute for Metal and Lightweight Structures of the University of Duisburg-Essen

Table 6.6-3: Overview about used types of lubrication according to manufacturer specifications

			
DOW Corning Molykote P-74 Paste	DOW Corning Molykote 1000 Spray / Paste	DOW Corning Molykote D-321R Spray	Interflon HT1200 Spray / Paste

Results of lubrication tests (STEP 2)

Due to the results of the lubrications tests, Dow Corning Molykote 1000 Spray and Dow Corning Molykote D-321R-Spray were identified as the most promising lubricants for stainless steel bolting assemblies, so that further tightening tests in Task 5.4 have been performed with that sprays. The test results of the lubrication tests are summarized in Table 6.6-4.

Results of tightening tests with alternative lubrication (STEP 2)

As a next step, additional tightening tests of austenitic, lean duplex, duplex and super duplex stainless steel bolting assemblies were performed at the Institute for Metal and Lightweight Structures, University of Duisburg-Essen (UDE-IML).

Table 6.6-4: Task 5.4 – Summary of the evaluation of lubrication tests

Tested series	n [-]	F _{p,c} *	F _{p,c}	F _{bi,max}	ΔΘ _{1,min}	ΔΘ _{2,min}	k-values [-]	k-class K1 0.10 ≤ k _i ≤ 0.16	k-class K2		Fracture	Galling
					≥ 120°	≥ 240°			0.10 ≤ k _m ≤ 0.23	V _k ≤ 0.06		
Bumax 88 - M20x80 EN ISO 4017 bolting assemblies												
Gleitmo 1952V	5	100%	100%	100%	20%	100%	0.12 – 0.13	100%	0.124	0.043	0%	60%
Molykote 1000 spray	5	100%	100%	100%	100%	100%	0.12 – 0.14	100%	0.130	0.094	0%	100%
Molykote 1000 paste	5	100%	100%	100%	80%	100%	0.13 – 0.15	100%	0.136	0.050	0%	100%
Molykote P-74 paste	5	100%	100%	100%	80%	100%	0.14 – 0.17	60%	0.156	0.083	0%	80%
Molykote D-321R spray	5	100%	100%	100%	100%	100%	0.10 – 0.11	100%	0.105	0.047	0%	80%
Bumax 109 - M20x140 EN ISO 4014 bolting assemblies												
Gleitmo 1952V	10	100%	40%	0%	0%	0%	0.25 – 0.26	0%	0.255	0.032	0%	100%
Molykote 1000 paste	5	100%	100%	0%	0%	80%	0.16 – 0.20	40%	0.178	0.105	0%	100%
Molykote P-74 paste	5	100%	100%	0%	0%	20%	0.15 – 0.25	20%	0.187	0.188	0%	80%
Molykote D-321R spray	5	100%	100%	20%	60%	60%	0.11 – 0.13	100%	0.115	0.071	0%	100%

Figure 6.6-5 shows a summary of the additional tested series (using alternative lubrication Molykote 1000 spray and D-321R spray) after finishing the tightening tests for Task 5.4. In conclusion, bolt fractures occurred in three tested series, but only at the end of the test procedure when turning off the nut: Bumax SDX – M12x80 series (lubrication: Molykote 1000 spray), Bumax 88 – M16x100 series (lubrication: Molykote 1000 spray) and Bumax 109 – M16x100 (lubrication: Molykote D-321R spray). All tested stainless steel bolting assemblies achieved the preload level $F_{p,c}^* = 0.7 \cdot f_{yb} \cdot A_s$ and $F_{p,c} = 0.7 \cdot f_{ub} \cdot A_s$. Regarding the criteria of the individual maximum bolt force $F_{bi,max} \geq 0.9 \cdot f_{ub} \cdot A_s$ and sufficient ductility, in particular the required angles of nut rotation $\Delta\Theta_{1,min}$ and $\Delta\Theta_{2,min}$, the test results tend to generate two groups:

- For bolt dimension M16 – austenitic and austenitic-ferritic stainless steel bolting assemblies, the application of alternative lubrication significantly improves the preloading behaviour and expands the plastic plateau and angles of nut rotation $\Delta\Theta_{1,min}$ and $\Delta\Theta_{2,min}$. Furthermore, the tested series show a narrow range of k-values including coefficients of variation less than 8 % (with the exception of Bumax 88 – M16x100 Molykote 1000 series). Consequently, each series achieved criteria for k-class K1 (with exception of Bumax DX – M16x100 series, 8 of 10 bolts achieved k-class K1). Additionally, Bumax 109 – M16x100 (used lubrication: Dow Corning Molykote D-321R spray) and Bumax DX – M16x100 (used lubrication: Dow Corning Molykote 1000 spray) also accomplished k-class K2.
- For bolt dimension M20 – austenitic and austenitic-ferritic stainless steel bolting assemblies, the positive effects of alternative lubrication are relatively small compared to those of M16. The effects on ductility are only weakly defined, especially the criteria of the individual maximum bolt force $F_{bi,max} = 0.9 \cdot f_{ub} \cdot A_s$ is not achieved in Bumax 109 – M20x100 and Bumax LDX – M20x100 series, and only partially achieved (3 of 10 bolts) in Bumax DX – M20x100 series. The k-values show a range between 0.09 – 0.15, but the coefficient of variation is larger than 8 %.

Table 6.6-5: Task 5.4 – Summary of the evaluation of additional stainless steel tightening tests according to EN 14399-3 (used lubrication: Molykote 1000 and Molykote D-321R spray)

Tested series	n [-]	F _{p,c} *	F _{p,c}	F _{bi,max}	ΔΘ _{1,min}	ΔΘ _{2,min}	k-values [-]	k-class K1 0.10 ≤ k _i ≤ 0.16	k-class K2		Fracture	Galling
					≥ 120°	≥ 240°			0.10 ≤ k _m ≤ 0.23	V _k ≤ 0.06		
M12x80												
SDX - Molykote 1000 spray	10	100%	100%	100%	100%	100%	0.12 – 0.16	100%	0.139	0.097	70%	100%
M16x100												
88 - Molykote 1000 spray	10	100%	100%	90%	90%	90%	0.10 – 0.16	100%	0.129	0.150	50%	70%
109 - Molykote 1000 spray	10	100%	100%	100%	100%	100%	0.11 – 0.14	100%	0.130	0.080	0%	100%
109 - Molykote D-321R spray	10	100%	100%	100%	100%	100%	0.10 – 0.12	100%	0.112	0.053	10%	100%
LDX - Molykote 1000 spray	10	100%	100%	90%	100%	100%	0.12 – 0.15	100%	0.133	0.075	0%	100%
DX - Molykote 1000 spray	10	100%	100%	100%	100%	100%	0.14 – 0.17	80%	0.152	0.057	0%	100%
M20x100												
109 - Molykote 1000 spray	10	100%	100%	0%	60%	70%	0.10 – 0.15	100%	0.132	0.128	0%	100%
LDX - Molykote 1000 spray	10	100%	100%	0%	40%	70%	0.10 – 0.13	100%	0.118	0.082	0%	100%
DX - Molykote 1000 spray	10	100%	100%	30%	70%	70%	0.09 – 0.15	90%	0.124	0.128	0%	100%

All tested bolting assemblies showed damages caused by strong pronounced galling, especially in the faying surface between the washer and nut, see Figure 6.6-2.



Figure 6.6-2: Galling of the nut bearing surface when tightened into plastic range: nut (left), washer (middle) and detailed view of washer (right)

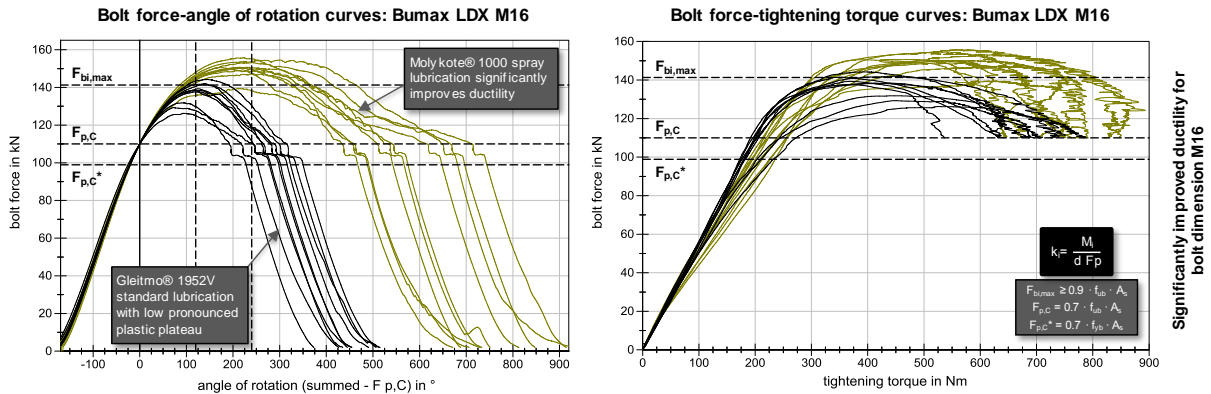


Figure 6.6-3: Comparison of BU_M16_LDX tightening curves between gleitmo 1952V standard lubrication (black curves) and Molykote 1000 spray (yellow curves)

A comparison between gleitmo 1952V standard lubrication and Molykote 1000 spray for Bumax DX – M20x100 ISO 4017 duplex stainless steel bolting assemblies is presented in Figure 6.6-4. Compared to bolt dimension M16, the positive effects of alternative lubrication on the ductility and the plastic plateau, more specifically the maximum individual bolt force and angles of rotation $\Delta\theta_{1i,min}$ and $\Delta\theta_{2i,min}$, are significantly lower. Again, the tightening curves of tested bolts using gleitmo 1952V show less pronounced plastic plateaus and low angles of rotation $\Delta\theta_{1i,min}$ and $\Delta\theta_{2i,min}$. Compared to Bumax LDX – M16x100 gleitmo 1952V series, the bolt force-angle of rotation curves spread more. $F_{p,C}^*$ and $F_{p,C}$ are achieved, but the criteria of the individual maximum bolt force $F_{bi,max} \geq 0.9 \cdot f_{ub} \cdot A_s$ failed. The application of Molykote 1000 spray slightly improved the plastic range as well as the maximum bolt force. The bolt force-tightening torque curves show strong pronounced galling with the use of Molykote 1000 spray, starting at $F_{bi,max}$ when tightened into the plastic range.

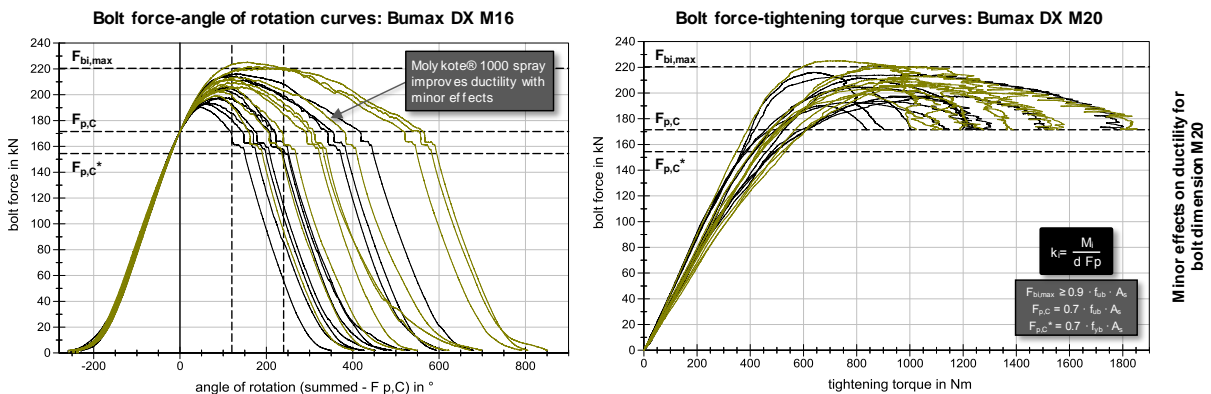


Figure 6.6-4: Comparison of BU_M20_DX tightening curves between gleitmo 1952V standard lubrication (black curves) and Molykote 1000 spray (yellow curves)

Evaluation of tightening tests – Step 3: ceramic-based lubricants

The summary of the evaluation of tightening tests with ceramic-based lubricants Interflon HT1200 spray and paste are shown in Table 6.6-6. Again, all tested bolting assemblies made of stainless steel achieved specified preload levels $F_{p,C}^*$ and $F_{p,C}$ without galling, comparable to DOW Corning Molykote 1000 spray and Molykote D-321R spray. In general, the tightening test results are comparable to the tested series with DOW Corning Molykote 1000 spray. The criteria of $\Delta\theta_{1i,min}$ and $\Delta\theta_{2i,min}$ are again

unequally distributed, k-class K1 was achieved in all tested series with the exception of Bumax LDX – M20x100 HT1200 spray (8 of 10 bolting assemblies achieved k-class K1).

Table 6.6-6: Task 5.4 – Summary of the evaluation of tightening tests with Interflon® HT1200 spray and paste

Tested series	n [-]	F _{p,c} [*]	F _{p,c}	F _{bi,max}	ΔO _{1i,min}	ΔO _{2i,min}	k-values [-]	k-class K1	k-class K2		Fracture	Galling
					≥ 120°	≥ 240°		0.10 ≤ k ₁ ≤ 0.16	0.10 ≤ k _m ≤ 0.23	V _k ≤ 0.06		
Bumax 88 - M20x100 EN ISO 4017 bolting assemblies												
88 - HT1200 spray	5	100%	100%	100%	60%	100%	0.12 – 0.14	100%	0.127	0.065	0%	40%
88 - HT1200 paste	5	100%	100%	100%	60%	100%	0.13 – 0.16	100%	0.139	0.084	0%	40%
Bumax 109 - M20x100 EN ISO 4017 bolting assemblies												
109 - HT1200 spray	5	100%	100%	0%	20%	100%	0.12 – 0.16	100%	0.133	0.148	0%	40%
109 - HT1200 paste	5	100%	100%	0%	40%	100%	0.14 – 0.16	100%	0.147	0.070	0%	60%
Bumax LDX - M20x100 EN ISO 4017 bolting assemblies												
LDX - HT1200 spray	5	100%	100%	0%	20%	20%	0.14 – 0.19	80%	0.162	0.126	0%	60%
LDX - HT1200 paste	5	100%	100%	20%	40%	40%	0.14 – 0.16	100%	0.149	0.047	0%	40%



Figure 6.6-5: Bumax – M20x100 bolting assemblies after tightening with Interflon HT1200 spray (above) and Interflon HT1200 paste (below)

Overall, the use of the ceramic based lubrication Interflon HT1200 spray and paste, see Figure 6.6-5, has nearly similar results to DOW Corning Molykote 1000 spray regarding tightening behaviour and ductility. Further investigations were not performed due to the fact that the tested ceramic-based lubricants react with differing sensitivity to drying times and do not create a homogeneous abrasion-resistant layer in all cases which leads to scattering of friction coefficients μ_{tot} , μ_{th} and μ_b and all related tightening parameters. Figure 6.6-5 shows exemplary Bumax – M20x100 bolting assemblies after tightening with Interflon HT1200 spray and Interflon HT1200 paste.

Preloading levels and design specifications

In principle, the preloading of austenitic and lean duplex, duplex and super duplex stainless steel bolting assemblies, property classes 8.8 and 10.9 is possible by choosing a suitable material pairing and lubrication. For further information see subchapter 9.8: “Task 5.6 – Preloading methods”.

6.7 Task 5.5 – Numerical analysis

Work undertaken

Development of finite element (FE) models

The development and performance optimization of the FE models was a challenging task, because the models have to be solved by ABAQUS/Standard (unlike commonly used ABAQUS/Explicit solver) due to the presence of user-defined yield surfaces in combined hardening material models. In view of the application in parametric study of Task 6.4, the focus was placed on the 3D model with the threaded bolt. The 3D model of the single bolt assembly created by VTT’s plug-in is shown in Figure 6.7-1 (left) and the example of predicted stress distribution over the assembly is presented in Figure 6.7-1 (right). It can be seen that the thread and area under the bolt head undergo plastic deformation while the rest of the assembly remains in the elastic range. A series of 3D models of a single bolt assembly were created by SCI using the VTT plug-in for ABAQUS in order to test out its performance. The work focused on modelling of the contact between the components and on the application of the bolt preload.

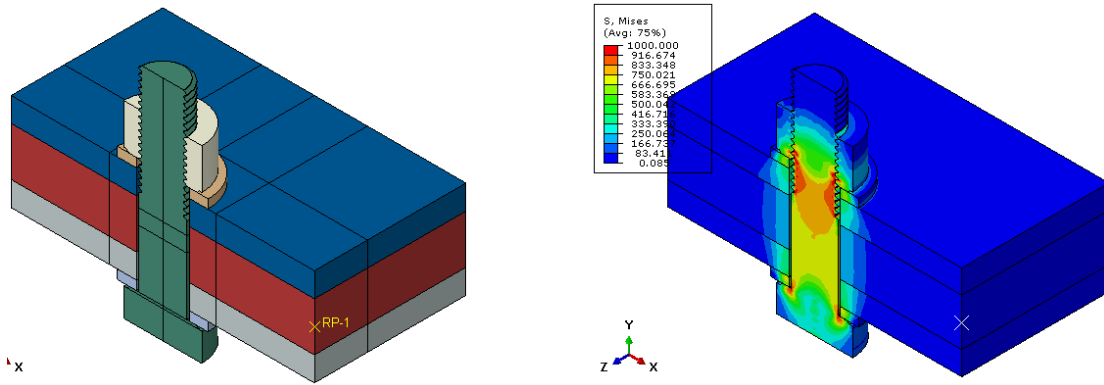


Figure 6.7-1: 3D bolted assembly and the stress distribution under preload

Modelling parametrization and graphical user interface

An automatic script for model generation has been developed by VTT. The script provides the capability of creating both 2D and 3D bolted assemblies subject to a preload force according to the parameters requested by the user. Libraries of pre-defined standard dimensions and material properties were provided for the convenience of the script users. The script was later implemented in the plug-in for ABAQUS/CAE in order to further increase the efficiency of the future calculations in Task 6.4 (see Figure 6.7-2).

Development of material models

The complex viscoplastic model based on Chaboche material was developed by OSOY (see Task 5.1) and implemented in ABAQUS in a form of UHARD subroutine. The model is based on the mixed hardening rule with strain dependent term and in uniaxial tension, it takes form of Eq. (9.7-1) with 11 parameters.

$$\sigma = k + Q[1 - \exp(-b\bar{\epsilon}_p)] + \sum_{i=1}^3 \frac{C_i}{\gamma_i} [1 - \exp(-\gamma_i \bar{\epsilon}_p)] + D(\dot{\bar{\epsilon}}_p)^{\frac{1}{n}} \quad (9.7-1)$$

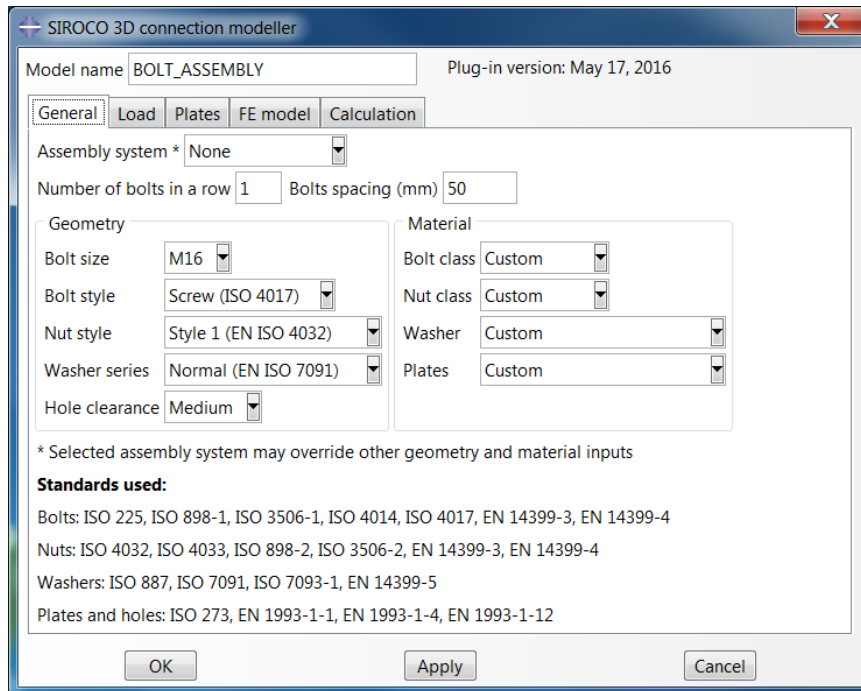


Figure 6.7-2: User interface of the ABAQUS plug-in for 3D bolted connections

The model parameters were calibrated by OSOY to the experiments from Task 5.1 (tensile tests with different loading rates and creep tests) of austenitic plate. Similar model was then provided by SCI for bolts.

Table 6.7-1: Parameters of Chaboche material model

Grade	k (MPa)	D (MPa)	n	Q (MPa)	b	C_1 (MPa)	γ_1	C_2 (MPa)	γ_2	C_3 (MPa)	γ_3
plate EN 1.4404	73	110	15.0	380	2.5	45949	591.4	617031	6765.3	1434	2.5
plate EN 1.4003	106	130	11.0	104	10.8	623733	5855.1	17430	558.6	1680	10.8
plate EN 1.4462	106	313	24.3	723	2.8	947349	11334.6	252038	1222.1	2971	60.0
plate EN 1.4162	109	329	30.2	649	3.5	483769	4875.7	102445	975.3	6766	180.8
bolt EN 1.4436	348.0	200.0	12.0	348.0	1.0	124738.9	320.2	269288.0	2081.2	595.1	1.0
bolt EN 1.4462	248.0	1133.0	5.13	269.7	1.0	124738.9	320.2	379288.0	2081.2	10.0	1.0
bolt EN 1.4162	298.0	290.0	9.67	269.7	1.0	124738.9	320.2	379288.0	2081.2	10.0	1.0

Verification of material models for FE calculations

The material model developed by OSOY was independently verified by VTT in the real FEM simulation of tensile and creep tests and provide very good agreement with the experimental results (examples in Figure 6.7-3 and Figure 6.7-4). Moreover, VTT verified the performance of this model also against relaxation tests from Task 5.1 by VTT on the same material. The agreement was also excellent (Figure 6.7-5), even though these tests were not used in the model calibration. It is concluded that this plate model can describe creep and relaxation of austenitic plates very well.

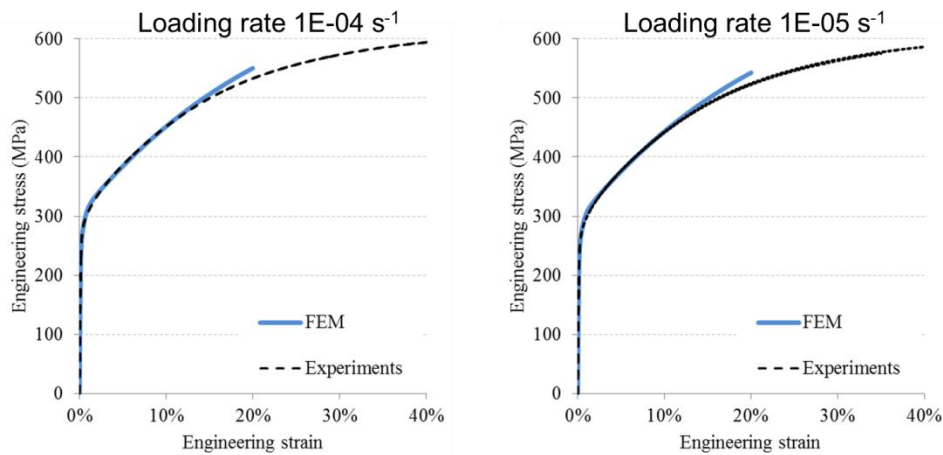


Figure 6.7-3: Examples of FE verification of material model for austenitic plates – tensile tests by OSOY

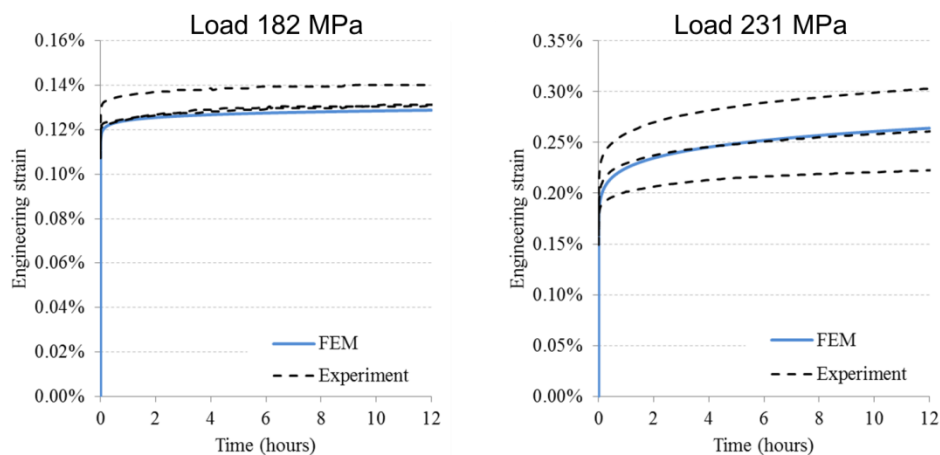


Figure 6.7-4: Examples of FE verification of material model for austenitic plates – creep tests by OSOY

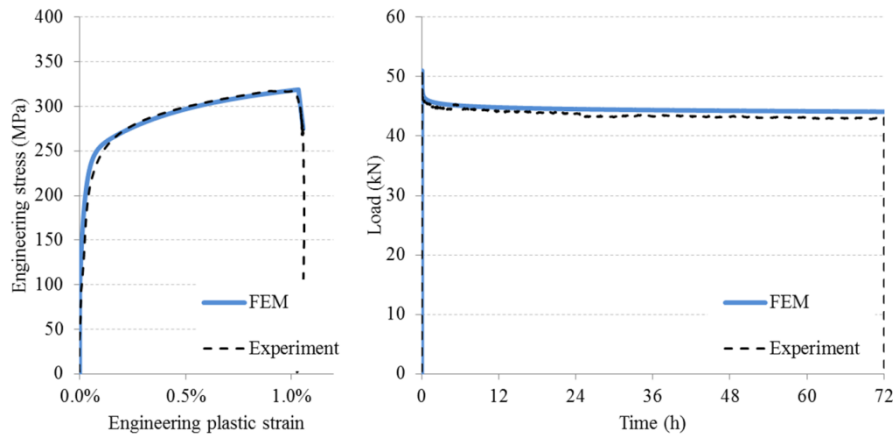


Figure 6.7-5: Examples of FE verification of material model for austenitic plates – relaxation test by VTT at strain level 1.2 %.

Correction actions

Development of FE models

No evidence was observed that the helical thread is more accurate than a simplified parallel thread in axial loading. Therefore, the helical thread option was removed from the plug-in due to the difficulties with mesh optimization and the work continued with the parallel thread exclusively.

Modelling parametrization and graphical user interface

The plug-in was originally developed with a single GUI capable of producing and solving 2D and 3D models. In the course of the project, the 3D modeller was separated from the 2D part to provide easier control over the models in Task 6.4.

Development of material models

Due to the different type of test results for plates (tensile with different loading rates and creep tests) and bolt materials (tensile with single loading rate and relaxation test), different material models were developed in the first phase of the project for plates (Chaboche model with UHARD subroutine) and bolts (exponential model with CREEP subroutine). The Chaboche model for bolts was eventually added in the final phase of the project and proved sufficiently accurate despite the lack of testing data.

Conclusions

FE models are a very convenient way to extend the range of parameters in experimental tests or to predict the behaviour of bolted connections during the whole service life of the structure. One of the most complicated modelling tasks is, however, the simulation of preloaded bolted assemblies made from viscoplastic materials such as stainless steels. Such models need a material definition that provides accurate calculation of plastic strain and associated stress in creep, relaxation and cyclic loading of the material. This task demonstrated that it is possible to successfully implement a comprehensive material model in the FE calculations to carry out the parametric study in Task 6.4. The results of calculations without slip load show that:

- higher preloading speed leads to larger loss of preload,
- it is possible to increase the final clamping force by re-tightening the bolt assembly without over-loading the bolt assembly.

Impact of the research results

Actual applications

The developed FE models can be used to predict the long-term behaviour of bolted connections made of materials included in their library (stainless steels from Table 6.7-1 and standard carbon steels without viscoplasticity).

Technical and economic potential for the use of the results

The developed modelling approach has a potential to be implemented in the sophisticated design software capable of solving FE problems with complex materials. The calibration and testing protocol used to obtain parameters of the material models provides useful guidance for the further extension of the existing material library. Simulated behaviour of the whole service life of the connection can potentially optimize the maintenance costs and improve the reliability of stainless steel bolted assemblies.

6.8 Task 5.6 – Preloading methods

In principle, the preloading of austenitic and lean duplex, duplex and super duplex stainless steel bolting assemblies, property classes 8.8 and 10.9 is possible by choosing a suitable material pairing and lubrication. The higher surface pressures of the EN ISO 4014/4017 systems, resulting from smaller geometrical dimensions than the HR/HV systems, are uncritically up to the preload level $F_{p,C}$ when structural steel is used with yield strength larger than or equal to 355 N/mm^2 .

The presented investigations and findings can only provide an initial insight into the tightening behaviour of stainless steel bolting assemblies. Further investigations are necessary in order to finally determine the tightening procedure including all requirements. It seems, as if a preload level of $F_{p,C}^*$ and also $F_{p,C}$ can be reliably achieved with a suitable lubricant using the torque method. Based on the presented investigations, the most promising lubricants for stainless steel bolting assemblies are DOW Corning Molykote 1000 spray and Molykote D-321R spray. Also, long term relaxation effects must be investigated and systematically considered.

Regarding the preloading levels and design specifications, it is important to note that the tightening procedure and the required preload level are well-matched. For this reason, the suitability test for preloading according to EN 14399-2 must be carried out to check if the bolting assemblies made of stainless steel are in principle suitable for preloading. Subsequently, the boundary conditions regarding the required preload level and tightening procedure as well as the tightening parameters have to be defined in each specific case, so that the test of suitability for preloading for the determination of all functional characteristics and parameters of stainless steel bolting assemblies can be successfully carried out. In addition, the inspection requirements have to be defined depending on the required target level of preloading and the individual and specific boundary conditions.

The process to verify the suitability of the stainless bolting assemblies for preloading and the determination of tightening method and tightening parameters to achieve the required target preload is illustrated in the flow chart shown in Figure 6.8-1.

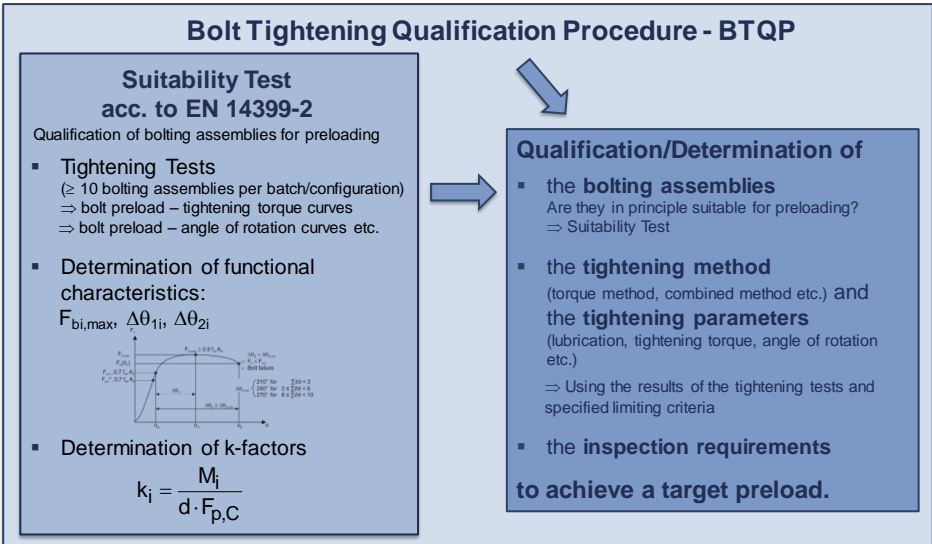


Figure 6.8-1: Flowchart for suitability test and tightening method qualification of stainless steel bolts for preloading

Nonetheless, the complete load-bearing behaviour of a bolted connection should be considered, and for property class 10.9, the unique qualities and benefits of HR and HV bolting assemblies still destine them for use in preloaded applications, which lead to the idea to create a new type of stainless steel

bolting assemblies approaching the geometrical dimensions of carbon steel HV/HR bolting assemblies taking into account the specifics of stainless steel bolting assemblies.

One important finding is that the problem of galling on the bolt head and nut bearing surfaces as well as on the paired threads can be for sure avoided by secure tightening with limitations in the elastic range using a suitable lubricant. With proper lubrication, galling only occurs when the stainless steel bolting assemblies are tightened into the plastic range close to the maximum bolt force $F_{bi,max}$, which must be avoided in all cases.

Figure 6.8-2, Figure 6.8-3 and Figure 6.8-4 show a comparison between Fuchs Gleitmo 1952V standard lubrication, Molykote 1000 spray and Interflon® HT1200 paste at preloading levels $F_{p,C}^*$, $F_{p,C}$ and $F_{bi,max}$ focussing on galling of the washer and nut.

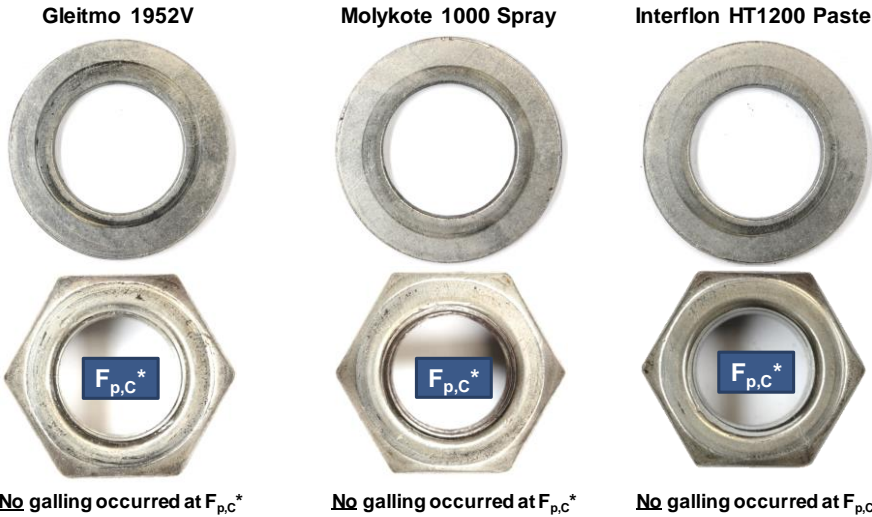


Figure 6.8-2: Inspection of galling of austenitic M20 HV200 washers and M20 Bumax 88 austenitic nuts in property class 8.8 after tightening at specified preload level $F_{p,C}^* = 0.7 \cdot f_{yb} \cdot A_s$

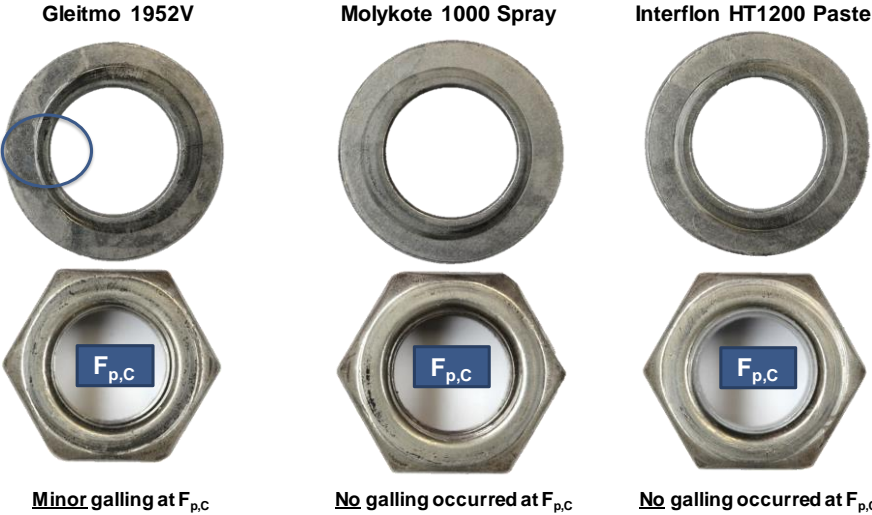


Figure 6.8-3: Inspection of galling of austenitic M20 HV200 washers and M20 Bumax 88 austenitic nuts in property class 8.8 after tightening at specified preload level $F_{p,C} = 0.7 \cdot f_{ub} \cdot A_s$

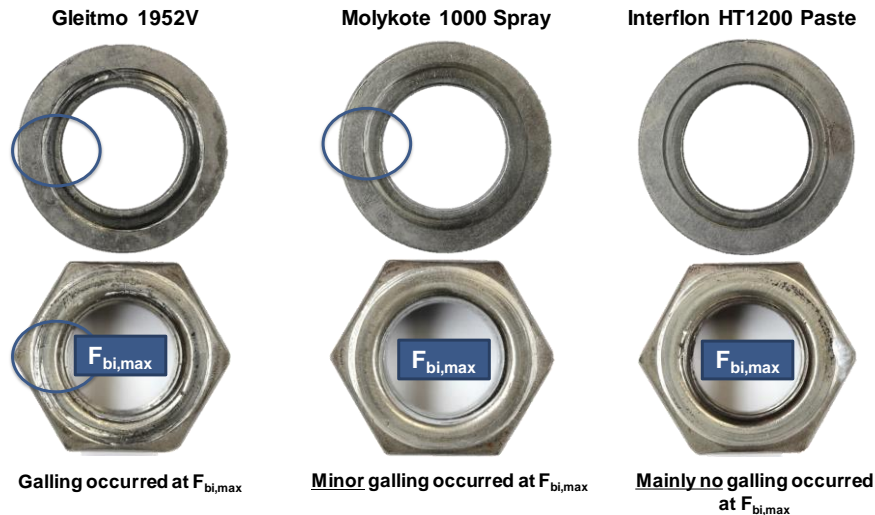


Figure 6.8-4: Inspection of galling of austenitic M20 HV200 washers and M20 Bumax 88 austenitic nuts in property class 8.8 after tightening at specified preload level $F_{bi,max} \geq 0.9 \cdot f_{ub} \cdot A_s$

7 WP 6 – Slip-resistant connections of SS

7.1 Objectives

The main objectives of this WP are as following:

- To provide design parameters (slip factors) of preloaded joints subjected to shear load for slip-resistant connections
- under consideration of various surface preparations and/or coatings of the clamped plates.

7.2 Work undertaken

The tasks undertaken in WP 6:

- 6.1. Surface characterization of stainless steel plates.
- 6.2. Determination of slip factors for typical stainless steel surface finishes.
- 6.3. Determination of slip factors for new types of coatings for stainless steel.
- 6.4. Numerical study.
- 6.5. Design rules for slip-resistant bolted connections made of SS.
- 6.6. Design examples.

The work undertaken for Tasks 6.1 to 6.6 is summarized in Sections 10.3 - 10.8.

Exploitation of the research results of this WP

The research results of this WP were published in nine journal and conference papers: (10), (17), (19), see Chapter 2, Publications. One journal paper is submitted an accepted for publication: (1), see Chapter 2, Publications.

7.3 Task 6.1 – Surface characterization of SS surfaces

Summary

The work in Task 6.1 was decided to focus on surface characterization of the faying surfaces in the bolted joint, rather than on the as-prepared surfaces. The result of the investigation is potential explanations to the differences in slip factor between different surface preparations.

Work undertaken

The included surface preparations were as-delivered 1D surface, shot blasted (SB) and grit blasted (GB) surfaces. Shot blasting and grit blasting were performed by Institut für Korrosionsschutz Dresden GmbH.

The surface roughness of the plates was measured with a mechanical stylus instrument before the tests at University of Duisburg-Essen and at Technical University of Delft. Table 7.3-1 summarizes the

result from University of Duisburg-Essen which coincides well with the results from Technical University of Delft.

Table 7.3-1: Surface roughness of plate surfaces before the slip factor test (results from University of Duisburg-Essen)

Grade	Lap plate		Center Plate	
	Average R_z (μm)	Min Max	Average R_z (μm)	Min Max
1.4404, 1D	54	49 59	49	44 53
1.4404, SB	35	31 42	38	36 40
1.4404 GB	40	37 44	43	40 47
1.4003, GB	45	41 47	47	46 48
1.4462, GB	42	39 49	42	39 46
1.4162, GB	47	39 57	37	36 38

The as-received 1D surface has the highest R_z -values and the shot blasted surfaces the lowest values. The average values of grit blasted surfaces are within the scatter for all grit blasted plates indicating that there are just small differences in roughness between the different grades when grit blasted.

In Figure 7.3-1 the faying surfaces after the slip factor test for the 1D surfaces of 1.4404 are shown. Flat and uniform contact spots (black arrow) can be observed on which sliding has occurred as demonstrated by the scratches on these contact spots (blue arrows). The shot blasted faying surfaces in Figure 7.3-2 are much rougher after sliding and the contact spots are not that evident, probably due to cold welding (red arrow) and associated deep scratches made by the cold welds in the slip test (magenta arrow). The grit blasted faying surfaces in Figure 7.3-3 are even more destroyed by heavy cold welding (red arrow) and associated deep scratches made by the cold welds in the slip test (magenta arrow). As the cold welding spots are caused by the combination of slip and preload, cold welding of the stainless steel surfaces could explain the higher slip factors observed for GB and SB compared to 1D.

A comparison was also made between the different steel grades for grit blasted surfaces. No significant differences between the steel grades was observed, see Figure 7.3-4 to 7.

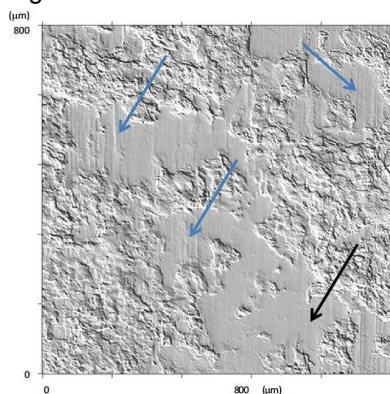


Figure 7.3-1: Faying surfaces for 1.4404 1D

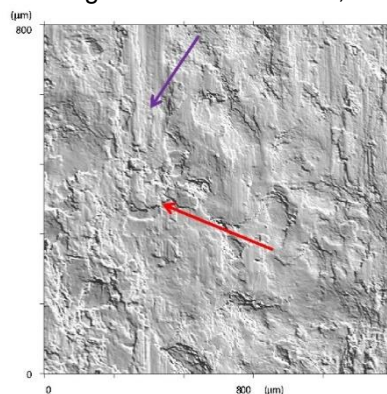


Figure 7.3-2: Faying surfaces for 1.4404 SB

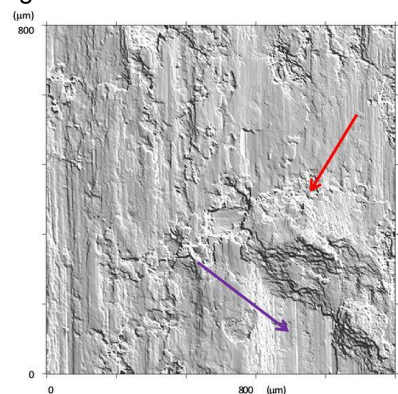


Figure 7.3-3: Faying surfaces for 1.4404 GB

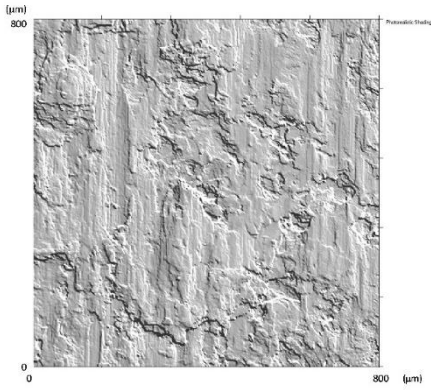


Figure 7.3-4: Faying surfaces for 1.4003 GB

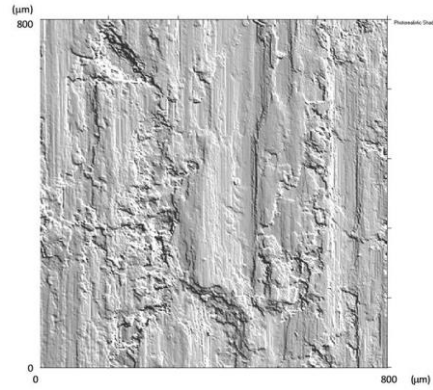


Figure 7.3-5: Faying surfaces for 1.4404 GB

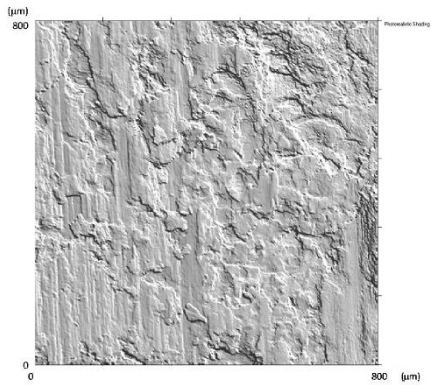


Figure 7.3-6: Faying surfaces for 1.4162 GB

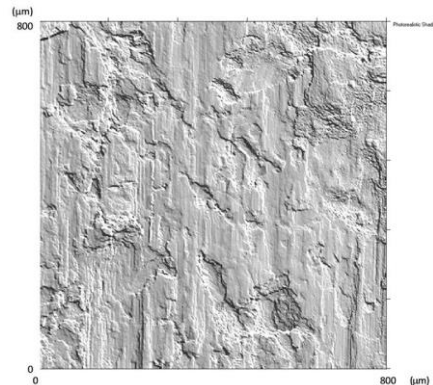


Figure 7.3-7: Faying surfaces for 1.4462 GB

Conclusions

The as-received 1D surface has the highest Rz-values and the shot blasted surfaces the lowest values. The average values of grit blasted surfaces are within the scatter for all grit blasted plates indicating that there are just small differences in roughness between the different grades when grit blasted. After the slip test, the faying surfaces of the as-received 1D surface showed flat and uniform contact spots on which sliding has occurred. The shot blasted faying surfaces were much rougher after sliding and the contact spots were not that evident, probably due to cold welding. The grit blasted faying surfaces were even more destroyed by heavy cold welding.

Impact of the research results

The results can be used to explain the reasons for different slip factors obtained for the different surface preparations. Cold welding at contact asperities explains the high slip factors obtained for the grit blasted surface preparations demonstrated in WP 6.2

7.4 Task 6.2 – Slip factors for SS surface finishes

Existing design codes/standards do not specify slip factors for surface treatments of stainless steel grades, the minimum values of slip factors for common surface treatments/coatings that are specified in EN 1090-2 are exclusively valid for carbon steels. One of the reasons for this is that stainless steel alloys are thought to suffer more than carbon steels from time dependent behaviour creep and relaxation at room temperature. This could lead to higher preload losses and consequently to lower slip factors than used for carbon steels with comparable surface treatment. However, no evidence of this can be found in literature. Creep and relaxation are stress dependant phenomena and the stresses in the components of preloaded bolted connections are locally highly non-uniform. Therefore, slip factors of different stainless steel grades have to be determined by experiments to investigate the effects of time dependant material behaviour. In this investigation, the results of slip factor tests on four stainless steel grades are presented. The influence of surface treatments and the preload level on the slip factor of stainless steel slip-resistant connections is discussed.

Preliminary tests

At the beginning of this task, additional slip factor tests (seven test series) as originally planned according to the Technical Annex were carried out for two different purposes. First purpose was to establish the requirements for the test specimens and to test the most appropriate grades of stainless steel. The second purpose was to the effectivity of the surface treatment methods on the slip factors / friction coefficients of stainless steel plates. Tests were carried out on the stainless steel plates that were used in an earlier phase of the project to preliminary study the slip behaviour of stainless steel with ‘as rolled’ surface treatment (so called 1D surfaces).

The results show that the slip resistant behaviour of both Austenitic and Duplex grades with 1D surfaces is poor (static slip factors of approx. 0.3 was found). The results also show that the effectiveness of grit blasting with Grittal is significant for both Austenitic and Duplex grades and despite lower roughness of the surface, the slip resistance of grit blasted Duplex 1.4462/1.4410 plates is higher than Austenitic 1.4307 plate. The results also show that for Duplex 1.4462 / 1.4410 shot blasting with Chronital is hardly effective, for more information see Deliverable 6.2.

Slip factor test according to Technical Annex

The main focus of this task was on the influence of the different surface treatments on the resulting slip factor for the various stainless steel grades. In the frame of SIROCO, slip factor tests were carried out to determine slip factors for different grades of stainless steel with different surface finishes. Four grades of stainless steel were tested: austenitic (1.4404) (A), duplex (1.4462) (D), lean-duplex (1.4162) (LD) and ferritic (1.4003) (F) stainless steel.

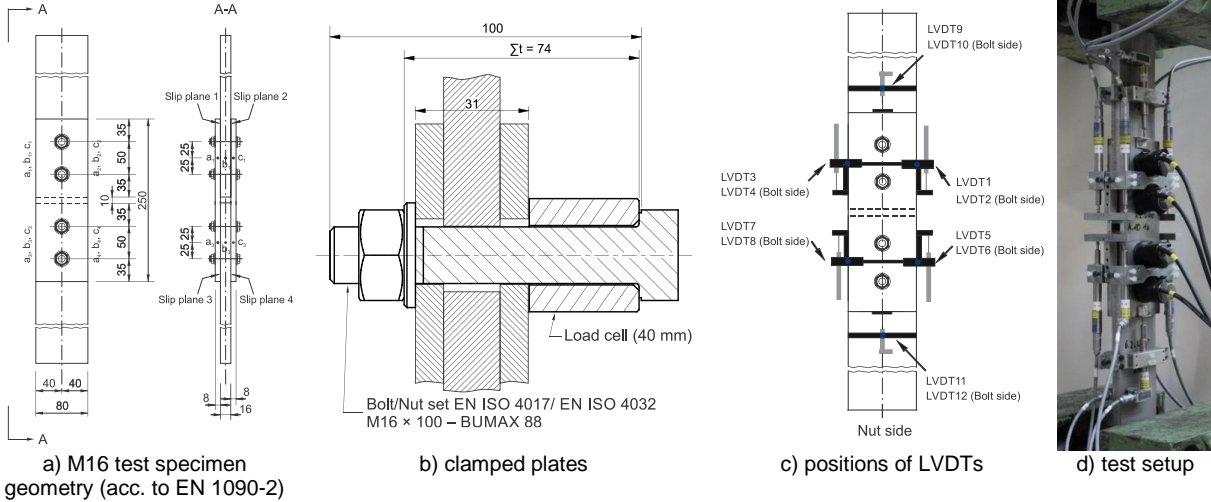


Figure 7.4-1: Test setup, test specimen geometry, positions of displacement transducers (LVDTs) as well as Clamped plates of a bolted connection with bolts with implanted strain gauge

The geometry of the test specimen used was according Annex G of EN 1090-2 for M16 bolts, see Figure 7.4-1 (a). As currently comparable bolting assemblies made of stainless steel are neither standardized nor available on the market, for this investigation austenitic stainless steel bolting assemblies were used consisting of bolts according to EN ISO 4017, nuts according to EN ISO 4032 and washers according to EN ISO 7089. Ten test series were assembled with austenitic bolts M16 A4-88, austenitic nuts M16 A4-88, and washers 17-88, HV 200, A4 (all Bumax 88). For the other ten test series austenitic bolts M16 A4-109, austenitic nuts M16 A4-109 and washers 17-109, HV 300, A4 (all Bumax 109) were used. The Bumax 88 and Bumax 109 bolting assemblies are based on EN ISO 3506-1 and EN ISO 3506-2 but with property classes 8.8 and 10.9 according to EN ISO 898-1 for carbon steel bolts. All bolts were full threaded bolts. The resulting preload levels were $F_{p,C} = 88$ kN for Bumax 88 and $F_{p,C} = 110$ kN for Bumax 109. According to EN 1090-2, the preloads in the bolts have to be measured at the beginning of testing and adjusted to an accuracy of ± 5 %. In case of the presented slip factor tests, the preload in the bolts was measured by self-made small load cells instead of instrumented bolts in order to eliminate the influence of viscoplastic deformation on the measured preload level, see Figure 7.4-1 (b). For more information, check Deliverables 5.4 and 6.2. Like WP1, 2 and 4, the slip factors are evaluated based on the measured slip displacement in CBG position, see Figure 7.4-1 (c) and (d). For each series of the stainless steel grades, firstly, four static tests were conducted in line with Annex G of EN 1090-2. Additionally, one creep test and extended

creep tests were carried out. The mean values of the static slip factors ($\mu_{ini,mean}$ and $\mu_{act,mean}$) and characteristic values ($\mu_{5\%}$ for a passed creep test and μ_{ect} based on a passed extended creep test) are presented in Table 7.4-1.

Table 7.4-1: Test programme, mean slip factors based on static and creep tests ($\mu_{ini,mean}$ and $\mu_{act,mean}$) and characteristic values (final slip factors) calculated as 5%-fractile: $\mu_{5\%}$ or resulting from extended creep tests: μ_{ect}

Series ID	Surface condition Surface finish / Rz ¹⁾ [μm]	Number of tests st/ct/ect ²⁾	$\mu_{ini,mean}$ ³⁾	$\mu_{act,mean}$ ⁴⁾	V (μ_{act}) ⁵⁾	Final slip factor $\mu_{5\%}$ ⁶⁾ / μ_{ect} ⁷⁾ [-]
			st/st+ct [-]	st/st+ct [-]	st/st+ct [%]	
A_1D_B88	1D ⁸⁾ / 24	4/1/2	0.21/0.21	0.21/0.21	4/4	0.2/0.14
A_SB_B88	SB ⁹⁾ / 38	4/1/2	0.29/-	0.30/-	6/-	-/0.2
A_GB_B88	GB ¹⁰⁾ / 45	4/1/1	0.56/0.55	0.60/0.59	6/7	0.49/0.51
D_GB_B88	GB / 47	4/1/1	0.60/0.6	0.63/0.62	6/5	0.54/0.54
LD_GB_B88	GB / 41	4/1/2	0.51/0.51	0.53/0.53	10/9	0.43/0.44
F_GB_B88	GB / 45	4/-/4	0.64/-	0.69/-	3/-	-/0.55
A_1D_B109	1D / 24	4/2/2	0.20/0.20	0.20/0.20	3/3	-/0.16
A_SB_B109	SB / 34	4/2/1	0.32/0.32	0.34/0.34	11/10	-/0.28
A_GB_B109	GB / 41	4/2/1	0.57/0.58	0.65/0.66	9/8	-/0.48
D_GB_B109	GB / 47	4/2/2	0.66/0.66	0.69/0.70	3/4	0.62/0.59
LD_GB_B109	GB / 40	4/2/1	0.62/0.62	0.65/0.64	4/5	0.56/0.49
F_GB_B109	GB / 42	4/2/2	0.68/0.68	0.74/0.75	4/4	0.64/0.59

¹⁾ Rz: roughness | ²⁾ st: static test/ct: creep-ect: extended creep test | ³⁾ $\mu_{ini,mean}$: calculated slip factors as mean values considering the preload at the start of the tests | ⁴⁾ $\mu_{act,mean}$: calculated slip factors as mean values considering the actual preload at 0.15 mm slip | ⁵⁾ V: Coefficient of variation for μ_{act} | ⁶⁾ $\mu_{5\%}$: slip factors as 5%-fractile calculated on the basis of the static tests and the passed creep test | ⁷⁾ μ_{ect} : slip factor as the result from the passed extended creep test | ⁸⁾ 1D surfaces | ⁹⁾ Shot blasted surfaces | ¹⁰⁾ Grit blasted surfaces

Figure 7.4-2 shows typical load - slip displacement curves that resulted from the static slip factor tests for the ten test series with Bumax 88 and Bumax 109 bolts. The figures show that the highest slip load is achieved for the grit blasted ferritic grade, followed by grit blasted duplex, austenitic and lean duplex grades. As it can be seen in Figure 7.4-2 the same results have been achieved for the test series with Bumax 109. With the surface that results from the shot blasting treatment and the as-rolled surface condition only very low slip factors are achieved compared to the grit blasted surfaces. Table 7.4-1 shows that the difference in the surface roughness that is achieved by the grit blasting compared to shot blasting is reflected by the results of the slip factor tests. Table 7.4-1 and Figure 7.4-2 clearly show that the surface roughness plays an important role on the slip behaviour of the specimens. The slip factor can be strongly influenced by the surface treatment of the plates.

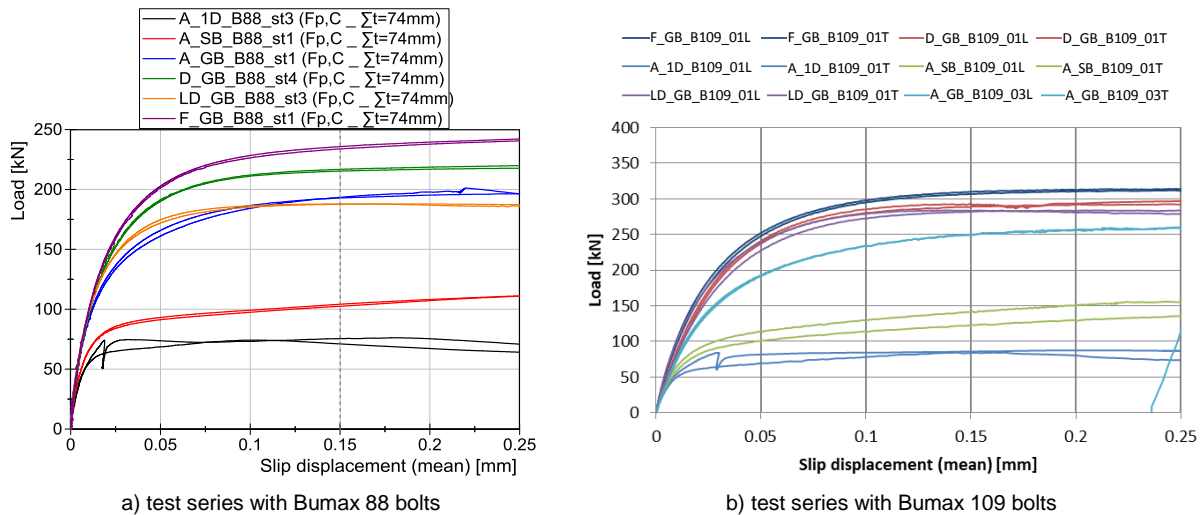


Figure 7.4-2: Typical load-slip-displacement curves for different surface conditions of the test series with bolts Bumax 88 and Bumax 109 - each colour represent the upper and lower section of the specimen

The mean static slip factors were calculated based on 1) the initial preload in the bolts (μ_{ini}), 2) the actual preload at a slip deformation of 0.15 mm (μ_{act}) and 3) the nominal preload in the bolts (μ_{nom}). The achieved static slip factor values for all grit blasted surfaces were greater than 0.5, see Figure 7.4-3. The high static slip factors for grit blasted surfaces in comparison to those of shot blasted specimens can be explained by the topography of the surfaces. The asperity of grit blasted faying

surfaces is sharper than that of the shot blasted surfaces and consequently provides a better mechanical interlocking between the surfaces.

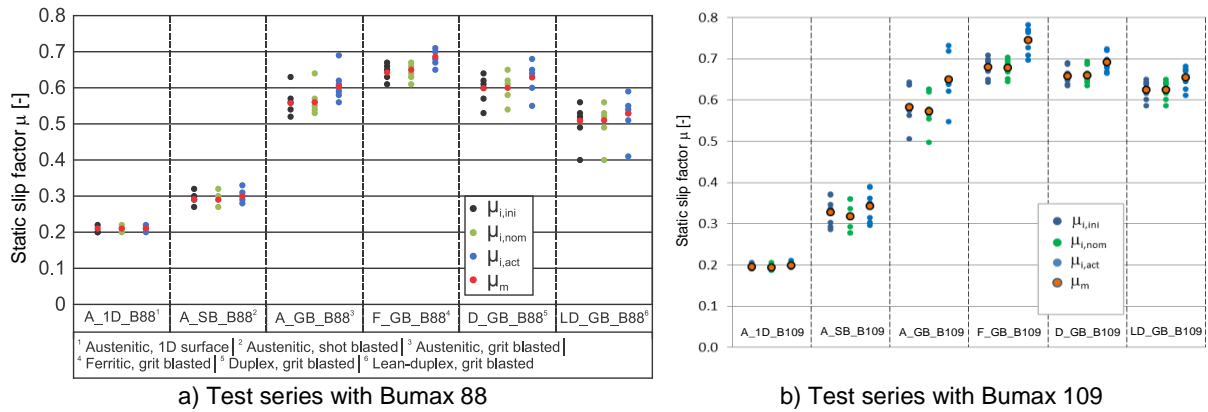


Figure 7.4-3: Influence of different stainless steel surface conditions on the slip factors

For all stainless steel grades that were preloaded with Bumax 88 ($F_{p,C} = 88$ kN) static slip factors were achieved which are equal or lower to those resulting for the higher preload level with Bumax 109 bolts ($F_{p,C} = 110$ kN). A possible explanation for this could be cold welding of the faying surfaces by the combined effect of the preload and slipping of the surfaces, see Task 6.1 (Figure 7.3-1, Figure 7.3-2 and Figure 7.3-3). As the cold welding spots are caused by the combination of slip and preload, cold welding of the stainless steel surfaces could explain the higher slip factors that are found for Bumax 109 (preloaded to 110 kN, so potentially more cold welding spots) compared to Bumax 88 (preloaded to 88 kN).

The creep test was passed for all non-coated Bumax 88-series except for the A_SB_B88. Figure 7.4-4 shows the creep test results for A_GB_B88 and D_GB_B88 test series. All Bumax 109 specimens passed the creep test, except for the A_1D_B109 and A_GB_B109 series. For the A_GB_B109 series the difference between slip that was recorded in 3 hours and the threshold value of $2 \mu\text{m}$ is negligible, so in fact all series with surface treatment can be considered to be non-creep sensitive. Where normally extended creep tests are only carried out on creep sensitive coatings, in this investigation for all test series extended creep tests were conducted although almost all creep tests were passed.

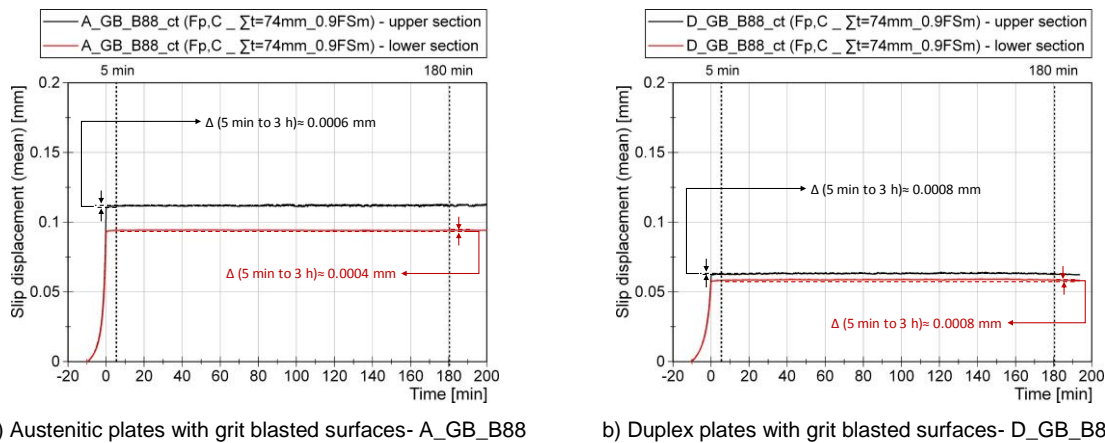


Figure 7.4-4: Exemplary results of creep tests considering different stainless steel grade with GB surfaces

All extended creep tests were conducted with new, unused bolting assemblies in the long-term test rigs in UDE and TUD, see Figure 7.4-5. By this, the combined effect of creep and relaxation of all stainless steel components of the connection could manifest during the tests. As it can be seen from Figure 7.4-6 and Figure 7.4-7, the extended creep tests on the A_GB_B88 and A_GB_B109 series with Bumax 88 and Bumax 109 bolts were passed with constant load level of $0.90 F_{sm}$ and $0.84 F_{sm}$ respectively. The results of final slip factor after extended creep test is presented in Table 7.4-1.

By having a closer look on the final slip factor results, it can be seen in Figure 7.4-8, there is a tendency towards a slightly higher slip factor with higher preload level. This phenomenon can be explained by a better cold welding of the faying surfaces by having higher preload level.

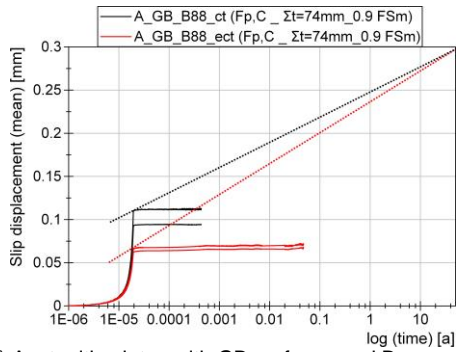


a) test rig for extended creep tests (UDE)

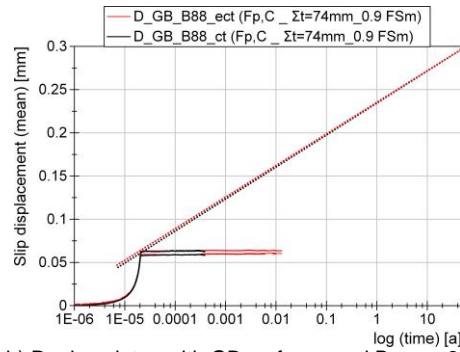


b) test rig for extended creep tests (TUD)

Figure 7.4-5: Test rig for performing the extended creep tests

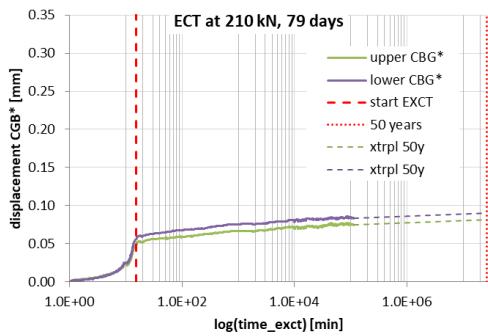


a) Austenitic plates with GB surfaces and Bumax 88

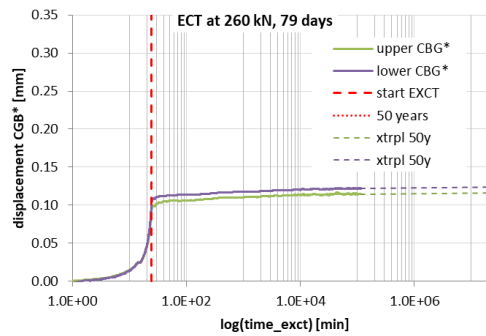


b) Duplex plates with GB surfaces and Bumax 88

Figure 7.4-6: Exemplary results of extended creep tests for test series with Bumax 88 (each colour represents the upper and lower section of the specimen)



a) Austenitic plates with GB surfaces and Bumax 109



b) Duplex plates with GB surface Bumax 109

Figure 7.4-7: Exemplary results of extended creep tests for test series with Bumax 109 (each colour represents the upper and lower section of the specimen)

Conclusions

For the investigated stainless steel plates and bolt sets, the preload losses during slip factor tests caused by viscoplastic deformation of the stainless steel material are not significantly higher than those found for preloaded bolted connections made of carbon steel components.

Grit blasting of stainless steel surfaces result in very high surface roughness and slip factors. For the investigated austenitic, duplex, lean duplex and ferritic stainless steel plates slip factors of about 0.5 and higher could be achieved. Stainless steel plates with untreated (1D) or shot blasted surfaces lead to comparable low slip factors of about 0.16 - 0.28 which might still be enough in some practical applications.

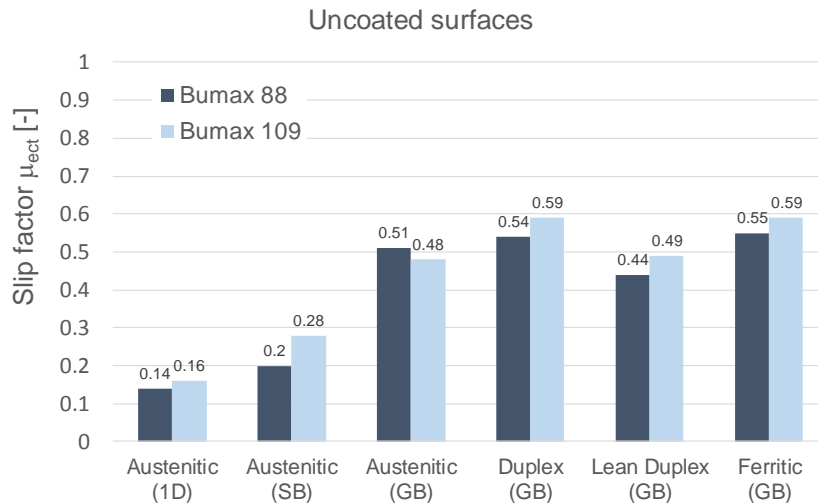


Figure 7.4-8: Final slip factor considering different stainless steel grades and surface treatments with bolts Bumax88 and Bumax109

7.5 Task 6.3 – Slip factors for new types of coatings on SS

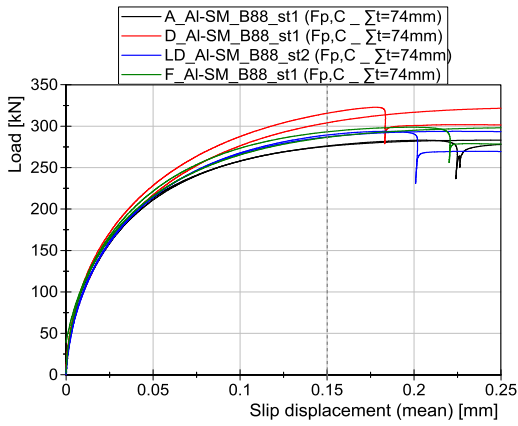
In this task the determination of slip factors for new types of coatings was performed in order to improve the slip resistance. The most promising coating was identified in other tasks. The most suitable coating system was selected from the results of Task 1.1. The Aluminium spray metalized (AI-SM) surfaces showed less creep sensitivity and permissible slip resistant behaviour in compare to other coating systems. For this AI-SM-coating was selected and applied at all stainless steel grades in order to investigate its ability to achieve higher slip-factors. All slip factor testing parameter kept the same as Task 6.2. The geometry of the test specimen used was according Annex G of EN 1090-2 for M16 bolts, see Figure 7.4-1 (a). The preload level was measured by self-made small load cells, see Figure 7.4-1 (b) and the slip displacement was measured at CBG position, see Figure 7.4-1 (c). As shown in Table 7.5-1, eight different test series with two different preload levels were selected with approximately the same clamping length in order to eliminate the effect of clamping length on the loss of preload.

Table 7.5-1: Test programme, mean slip factors based on static and creep tests ($\mu_{ini,mean}$ and $\mu_{act,mean}$) and characteristic values (final slip factors) calculated as 5%-fractile: $\mu_{5\%}$ or resulting from extended creep tests: μ_{ect}

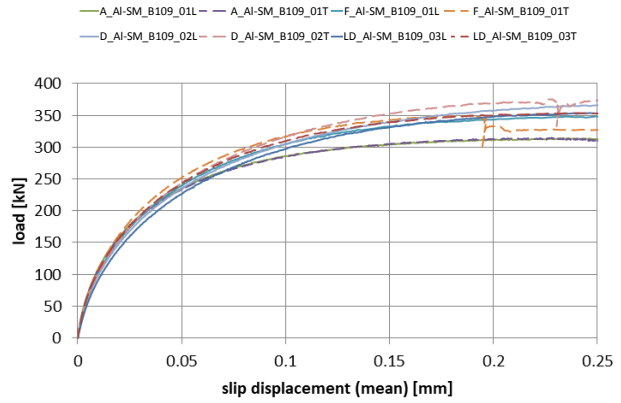
Series ID	Surface condition			Number of tests st/ct/ect ²⁾	$\mu_{ini,mean}$ ³⁾ st/st+ct [-]	$\mu_{act,mean}$ ⁴⁾ st/st+ct [-]	V (μ_{act}) ⁵⁾ st/st+ct [%]	Final slip factor $\mu_{5\%}$ ⁶⁾ / μ_{ect} ⁷⁾
	Surface finish / Rz ¹⁾ [μm]	Type of coating	Coating thickness [μm]					
A_AI-SM_B88	GB ⁸⁾ / 45	AI-SM	100 ⁹⁾	4/1/2	0.78/-	0.94/-	2/	-/0.71
D_AI-SM_B88	GB / 43	AI-SM	116 ¹⁰⁾	4/1/2	0.85/-	0.98/-	2/-	-/0.79
LD_AI-SM_B88	GB / 51	AI-SM	105 ¹⁰⁾	4/1/2	0.79/-	0.89/-	5/-	-/0.72
F_AI-SM_B88	GB / 44	AI-SM	91 ¹⁰⁾	4/1/2	0.81/-	0.93/-	2/-	-/0.74
A_AI-SM_B109	GB / 45	AI-SM	100 ⁹⁾	4/2/1	0.70/-	0.84/-	3/-	-/0.63
D_AI-SM_B109	GB / 43	AI-SM	116 ¹⁰⁾	4/2/1	0.81/-	0.90/-	4/-	-/0.73
LD_AI-SM_B109	GB / 51	AI-SM	105 ¹⁰⁾	4/2/1	0.78/-	0.86/-	4/-	-/0.70
F_AI-SM_B109	GB / 44	AI-SM	91 ¹⁰⁾	4/2/1	0.76/-	0.89/-	2/-	-/0.68

¹⁾ Rz: roughness | ²⁾ st: static test/ct: creep-/ect: extended creep test | ³⁾ $\mu_{ini,mean}$: calculated slip factors as mean values considering the preload at the start of the tests | ⁴⁾ $\mu_{act,mean}$: calculated slip factors as mean values considering the actual preload at 0.15 mm slip | ⁵⁾ V: Coefficient of variation for μ_{act} | ⁶⁾ $\mu_{5\%}$: slip factors as 5%-fractile calculated on the basis of the static tests and the passed creep test | ⁷⁾ μ_{ect} : slip factor as the result from the passed extended creep test | ⁸⁾ Grit blasted surfaces | ⁹⁾ NDFT: nominal dry film thickness | ¹⁰⁾ DFT: dry film thickness (measured value)

Figure 7.5-1 shows typical load - slip displacement curves that resulted from the static slip factor tests for the eight test series with Bumax 88 and Bumax 109 bolts. The results show that the slip factor was significantly improved (greater than 0.7) by aluminium spray metalized coated surfaces for both preload levels in comparison to that of uncoated surfaces, see Table 7.5-1, Figure 7.5-2 and Figure 7.5-3.



a) coated test series with Bumax 88 bolts



b) coated test series with Bumax 109 bolts

Figure 7.5-1: Typical load-slip-displacement curves for different surface conditions of the test series with of Bumax 88 and Bumax 109 bolts - each colour represent the upper and lower section of the specimen

Unlike the uncoated surfaces, the cold welding could not happen for the stainless steel bolted connection with aluminium spray metalized coated surfaces, because the contact surfaces are covered with aluminium and there was no direct contact between stainless steel surfaces. For this reason, like what is known for coated carbon steels by increasing the preload level the slip load increase but slip factor decrease slightly (see Task 1.1), see Figure 7.5-2, Figure 7.5-3 and Table 7.5-1.

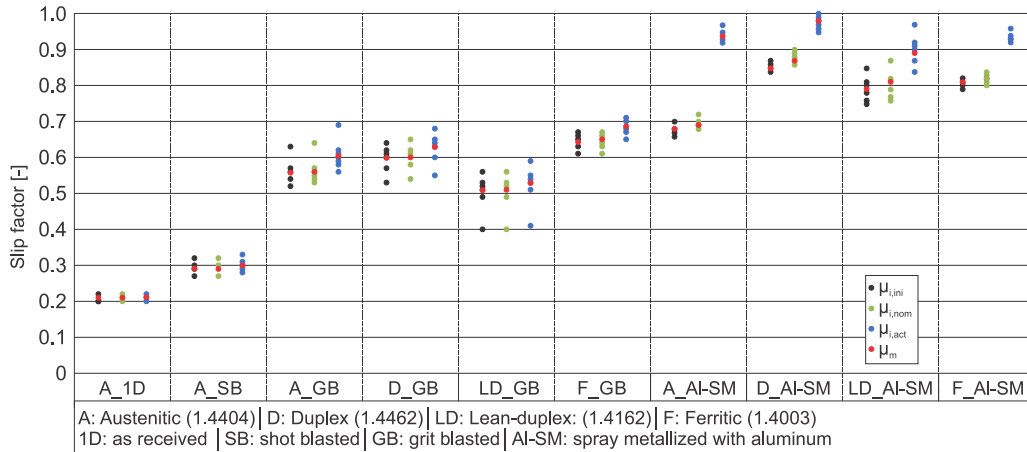


Figure 7.5-2: Influence of different stainless steel surface conditions on the static slip factors – test series with bolts of property class 8.8 (Bumax 88) – compared with the results of Task 6.2

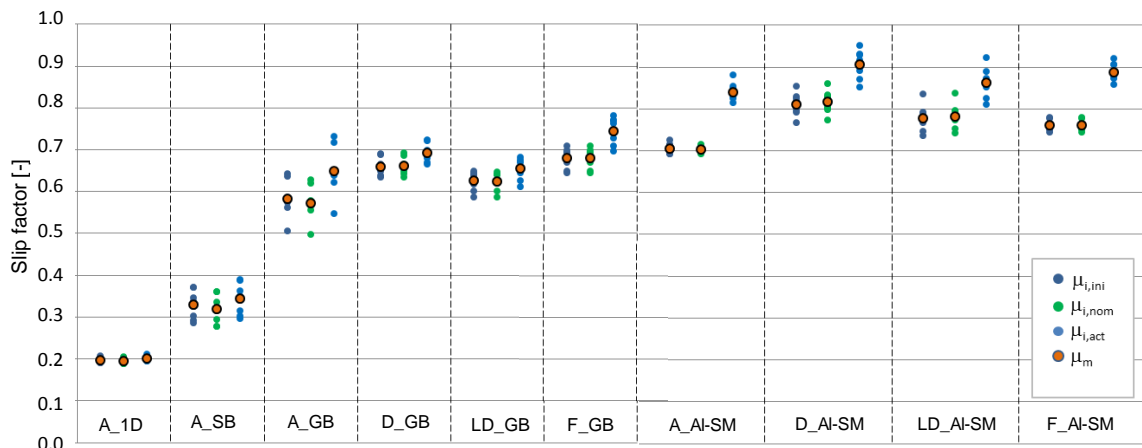


Figure 7.5-3: Influence of different stainless steel surface conditions on the static slip factors – test series with bolts of property class 10.9 (Bumax 109) - compared with the results of Task 6.2

The creep tests were also performed for all series with AI-SM coated surfaces. The results shows that all grades with AI-SM coating behave slightly, but not very creep sensitive according to the creep test criteria, see Figure 7.5-4. The difference between the recorded slip at the end of 5 min and 3 hours after full load application exceeded slightly the limit of 0.002 mm for both parts of the specimen. For

this reason, the creep tests for all Al-SM test series (Bumax 88 and Bumax 109) were failed and consequently extended creep tests were necessary.

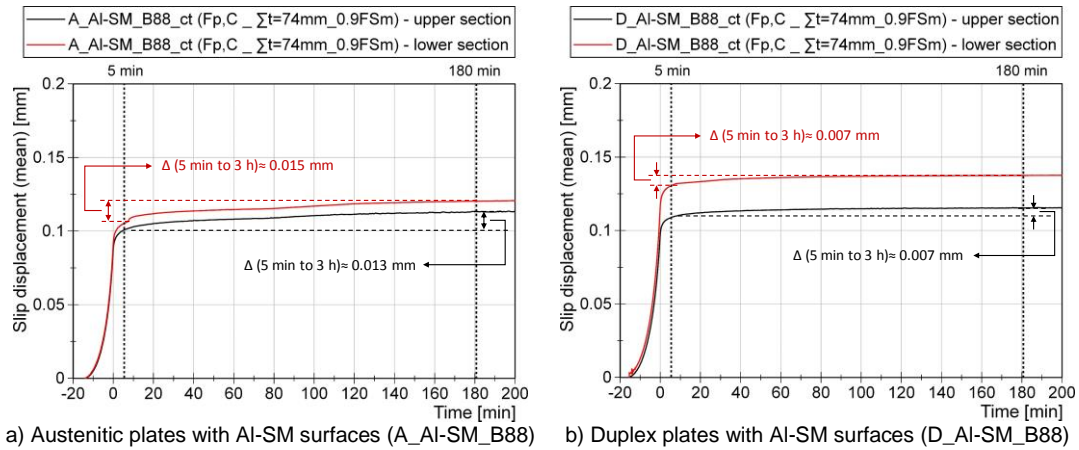


Figure 7.5-4: Exemplary results of creep tests considering different stainless steel grades with aluminium spray metalized surfaces with Bumax 88 bolts

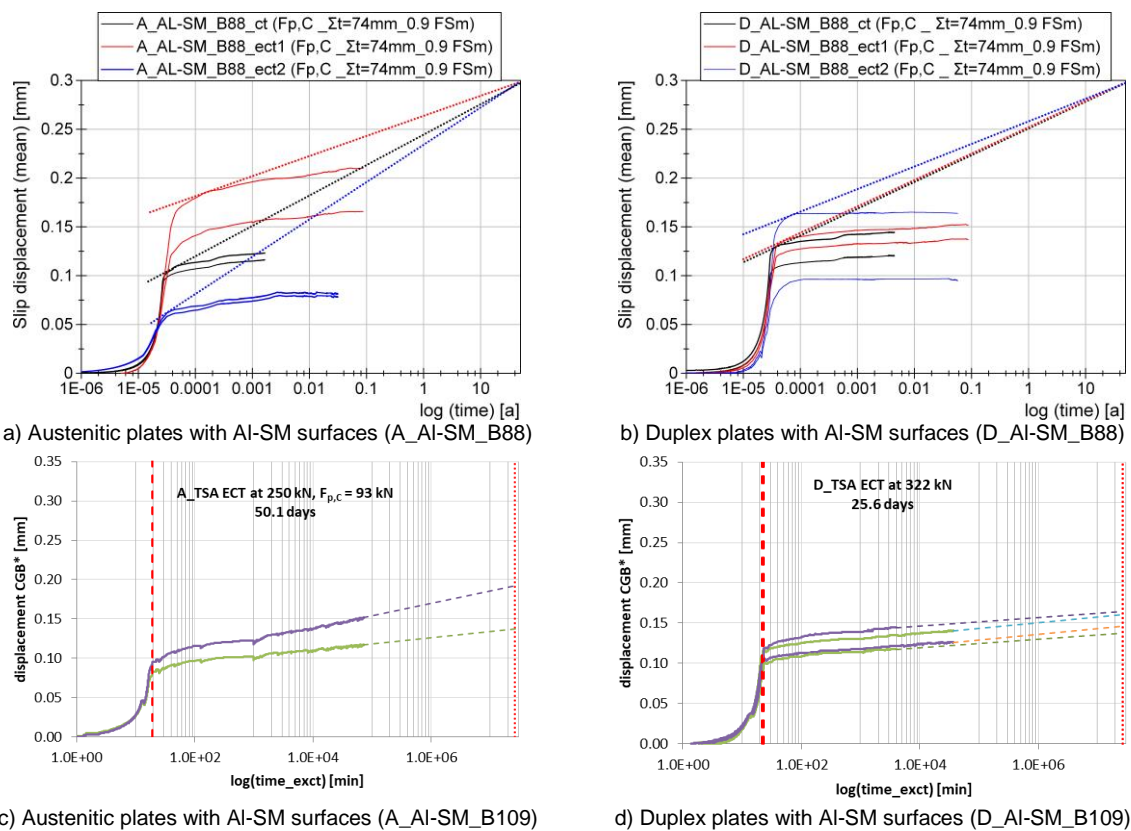


Figure 7.5-5: Results of extended creep tests considering different stainless steel grades coated with Al-SM (each colour represents the upper and lower section of the specimen)

Evaluating the slip displacement – log time curve based on the results of the creep tests for Al-SM test series (on 0.9 F_{Sm} -level) is a valuable way to figure out the creep sensitivity level of the coated surfaces. Unfortunately, the duration of these two extended creep tests is quite short compared to a “normal” extended creep test and extended creep tests are necessary. Nevertheless, this method will help to estimate a more reasonable load level for extended creep tests. For the Al-SM test series, the results show that this type of coating is not very creep sensitive, see Figure 7.5-5 (a) and (b). For this reason, the same load level (0.9 F_{Sm}) was selected for performing the extended creep tests. All extended creep tests were conducted with new/unused bolting assemblies. As it can be seen in Figure 7.5-5, the extended creep tests can be considered as passed tests and the nominal slip factor can be calculated with the same load level (0.9 F_{Sm}). All extended creep tests were also passed with the same load level for test series with Bumax 109. Figure 7.5-6 shows that a higher preload level does not have this positive influence on slip resistance behaviour of the aluminium spray metalized coated surfaces. Because all surfaces are covered with aluminium and there is no contact between the

stainless steel material any more. For this reason, there is no chance to have cold welding effects between the stainless steel faying surfaces. It can be summarized that for all grit blasted surface conditions slip factors of around 0.5 could be achieved. Sometimes even much higher with values of about 0.6 to 0.7 for thermal spray metalized surfaces with aluminium. These are very promising results for carrying out long lasting and cost effective slip-resistant connections made of stainless steel.

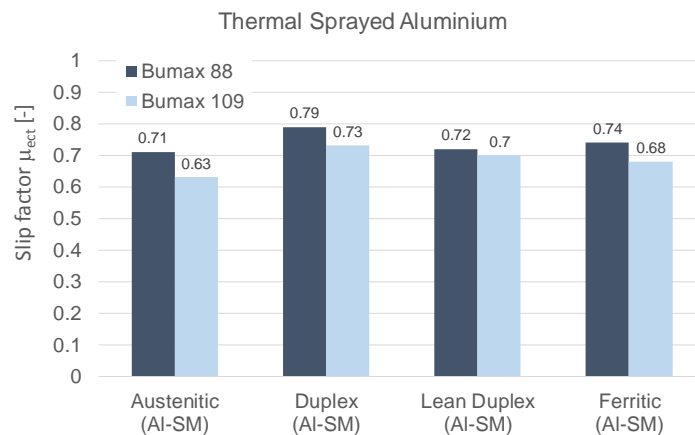


Figure 7.5-6: Final slip factor considering different stainless steel grades and surface treatments with bolts Bumax88 and Bumax109

Conclusions

The results show that the slip factors for different grades of stainless steel with Al-SM-coating with Bumax 109 and Bumax 88 bolts were greater than 0.6 and 0.7 respectively. Opposite to what is known for carbon steels, uncoated slip-resistant connections made of stainless steel plates show with increasing preload levels higher slip factors. On the other hand, increasing the preload level in Al-SM-stainless steel slip-resistant connections lead to increased slip loads but slightly decreased slip factors comparable to the behaviour of coated carbon steel slip-resistant connections.

7.6 Task 6.4 – Numerical study

Work undertaken

The latest work focused on calibration and validation of the previously developed FE model against the slip factor tests and extended creep tests of stainless steel slip resistant connections (Task 6.2). Long term behaviour of the numerical models were also compared with bolt preload relaxation tests. This was aimed to evaluate the performance of the viscoplastic stainless steel material model validated previously (WP5) using material test results. Parametric study was carried out using the validated numerical models to extrapolate the test data and study the response of stainless steel slip resistant connections of different geometry, surface finish and preloading level.

Two types of numerical model have been developed in the project. Figure 7.6-1(a) presents the 2D axisymmetric model developed to study the preload losses of a stainless steel bolted connection. It offers an efficient way to investigate the time-dependent behaviour of stainless steel in a preloaded bolting assembly and validation of the viscoplastic model proposed in WP5. The 3D double symmetric FE model shown in Figure 7.6-1 (b) was developed to study the friction between the faying surfaces under bolt preload for various types of stainless steel plate with typical surface finish.

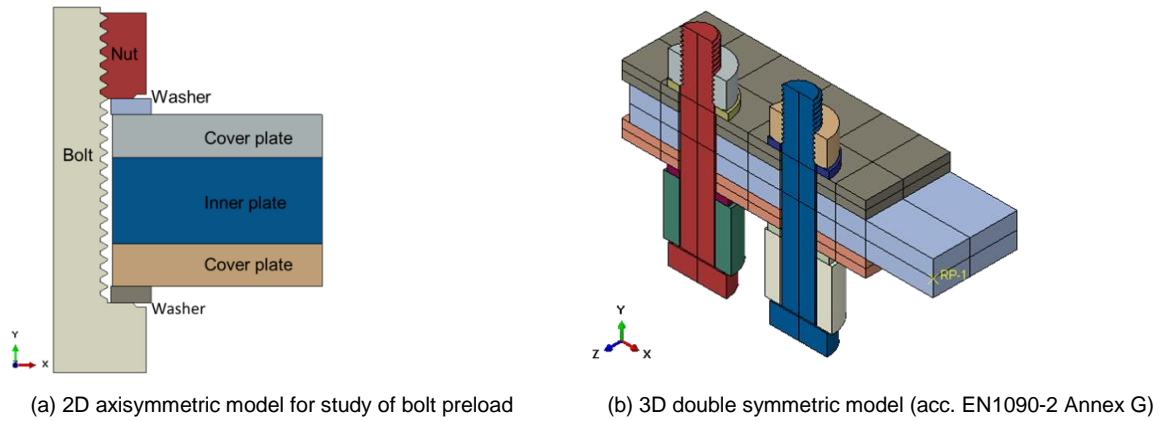


Figure 7.6-1: Numerical models developed in SIROCO

The calibration of the 3D FE model of the stainless steel slip resistant connection is shown in Figure 7.6-2. The value of the friction coefficient μ_{fric} was determined so that the nominal slip factor is the same as that measured in the tests. Figure 7.6-2 presents the calibration of the static coefficient of friction for the connection made of grit blasted austenitic plate with M16 Bumax 109 austenitic bolts. It was found that by assuming $\mu_{\text{fric}} = 0.6$ in the FE model, the slip factor would be the same as the test mean value. The Coulomb friction model is adopted here. The friction is modelled as $\tau = \mu \times p$, where τ is the shear stress on the surface under high contact pressure p and μ is the friction coefficient to be calibrated. It is assumed that the friction coefficient μ is a constant.

It can be observed in Figure 7.6-2 (a) that the slip response of the FE model is in good agreement with the experimental test results, even though the scatter of the experimental data is relatively large. The loss of preload during the tests is compared in Figure 7.6-2 (b). At the slip of 0.15 mm, the residual preloads in the bolts predicted by the FE model were found to be similar to the test measurements.

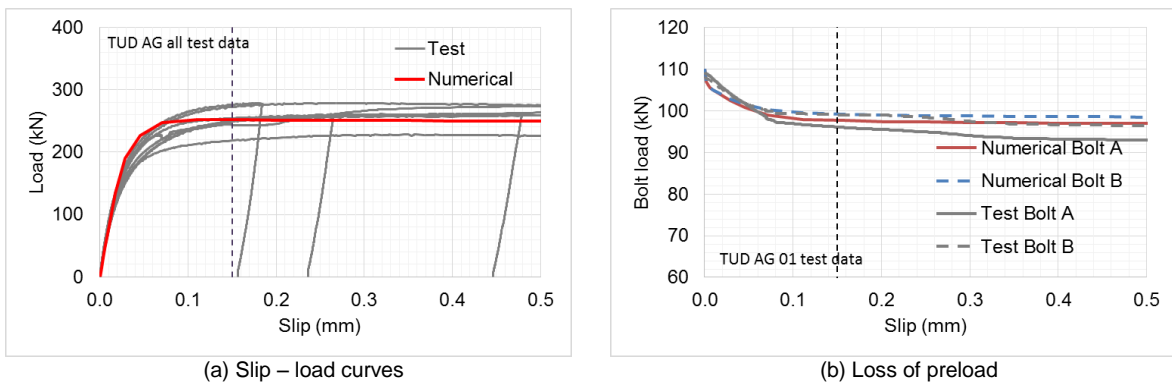


Figure 7.6-2: Calibration results for Austenitic plate with grit blasted surface finish and M16 Bumax 109 bolts (series ID: AG), the static coefficient of friction used for the faying surface was calibrated to be $\mu_{\text{fric}} = 0.60$

Calibrations of the FE models against all available test data provided by UDE and TUD are shown in Table 7.6-1, which presents the calibrated static coefficient of friction for the four grades of stainless steel with typical surface finishes.

Table 7.6-1: Summary of tests results and calibration of numerical model (selected results)

Series ID	Steel grade	Surface finish	$\mu_{\text{ini,mean}}^{4)}$		$\mu_{\text{act,mean}}^{5)}$		$\mu_{\text{nom,mean}}^{6)}$		Loss of preload $LP_{\text{mean}}^{7)}$		FE $\mu_s^{8)}$
			Test	FE	Test	FE	Test	FE	Test	FE	
$\Sigma t = 77 \text{ mm} \mid \Sigma t/d = 4.8 \mid \text{Bumax 109 M16 bolts} \mid F_{p,c} = 110 \text{ kN (TUD)}$											
A_1D	1.4404	1D	0.20	0.19	0.20	0.20	0.19	0.19	1.8%	5.9%	0.2
A_SB		SB	0.33	0.32	0.34	0.34	0.32	0.32	4.1%	6.8%	0.34
A_GB		GB	0.58	0.57	0.65	0.64	0.57	0.57	9.9%	11%	0.64
F_GB	1.4003	GB	0.70	0.68	0.75	0.77	0.68	0.68	8.6%	11.6%	0.77
D_GB	1.4462	GB	0.66	0.66	0.69	0.70	0.66	0.66	5.3%	6.8%	0.705
LD_GB	1.4162	GB	0.63	0.63	0.65	0.68	0.63	0.63	4.6%	6.6%	0.68

¹⁾ as-rolled surface finish | ²⁾ shot blasted surface finish | ³⁾ grit blasted surface finish | ⁴⁾ mean initial slip factor | ⁵⁾ mean actual slip factor | ⁶⁾ mean nominal slip factor | ⁷⁾ mean loss of preload at 0.15 mm slip | ⁸⁾ static coefficient of friction between faying surfaces calibrated for the numerical model

The loss of preload at CBG slip of 0.15 mm predicted by the numerical models generally agreed well with the test measurements.

The initial, actual and nominal slip factors are evaluated as shown in Equation (10.6-1). Since the calibration was based on the nominal slip factors, there were small discrepancies between the initial and actual slip factors produced by the FE model and tests. This discrepancies primarily originated from 1) the initial bolt preload ($F_{p,c,ini}$) achieved at the start of the slip factor tests were always slightly different from the specified value due to uncertainties in the pre-tightening process, and 2) the numerical actual bolt preload ($F_{p,c,act}$) at slip of 0.15 mm also differs from the test measurements. These are also the reasons that the nominal slip factor was used for calibration as the only parameter needs to be varied is the slip load (F_{si}).

$$\mu_{i,ini} = \frac{F_{si}}{4F_{p,c,ini}}, \mu_{i,act} = \frac{F_{si}}{4F_{p,c,act}}, \mu_{i,nom} = \frac{F_{si}}{4F_{p,c,nom}} \quad (10.6-1)$$

It can be observed that the static coefficient of friction calibrated for plates with Bumax 109 bolts are in general greater than for Bumax 88 bolts. The higher clamping force introduced by the Bumax 109 bolts is probably a contributing factor, which suggests that, at these contact pressure levels, friction depends on bearing pressure.

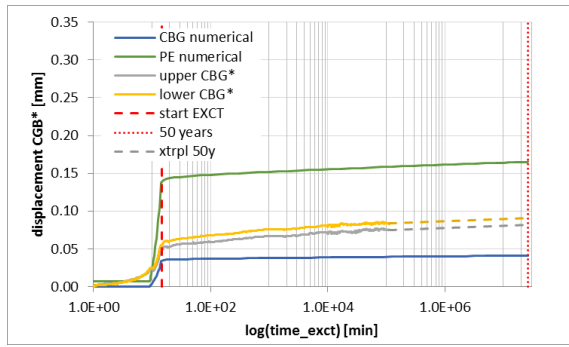
The viscoplastic material model calibrated in WP 5 for various grades of stainless steel were based on material tests. It is beneficial to evaluate the time-dependent performance of stainless steel in actual bolting assembly. The preload relaxation test programme (WP5) provided a good opportunity to examine the validity of the previously proposed viscoplastic stainless steel material model in a more realistic environment, i.e. in a preloaded bolt assembly as opposed to simple material model simulation. The 2D axisymmetric model shown in Figure 7.6-1(a) was used in the numerical investigation and compared with the extrapolated results at the end of 50 years. It can be seen from Table 7.6-2 that the loss of preload predicted by the numerical 2D model compares favourably with test results. It is worth pointing out that more than one test was carried out for each specimen so the maximum and minimum values were tabulated for discussion of the results. The good agreement proved that the calibrated material model is working accurately in predicting the viscoplastic behaviour of stainless steel.

Table 7.6-2: Predicted loss of preload in bolted assemblies made of stainless steel and comparison with FE results (selected cases)

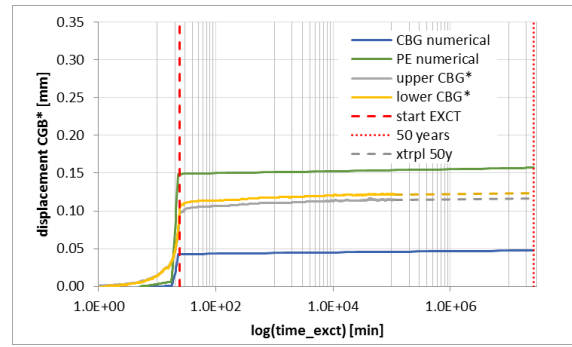
Specimen ID ¹⁾	Σt [mm] ²⁾	$\Sigma t/d$ ³⁾	Bolt material	Plate material	Loss of preload after 50 years [%]	
					Test (extrapolated) min/max	FE
SS01	75	3.75	Bumax 88 M20	Austenitic 1.4404	6.0/8.3	7.3
SS02				Ferritic 1.4003	5.4/7.3	7.1
SS03				Duplex 1.4462	5.4/7.2	6.9
SS04				Lean Duplex 1.4162	6.0/9.0	6.8
CS	48	2.4	M20 HV-bolt class 10.9	Carbon Steel	7.8/10.5	-

¹⁾ all bolts were preloaded to the $F_{p,c}$ level | ²⁾ clamping length | ³⁾ clamping length to bolt diameter ratio

A further evaluation was done by comparing the 3D FE model with extended creep tests. In these tests, the slip load was hold constant at $0.9 F_{sm}$ (which is the mean value of the slip load determined from the slip factor tests). Two typical comparisons are shown in Figure 7.6-3 below.



(a) Austenitic plates with grit blasted surface (AG)



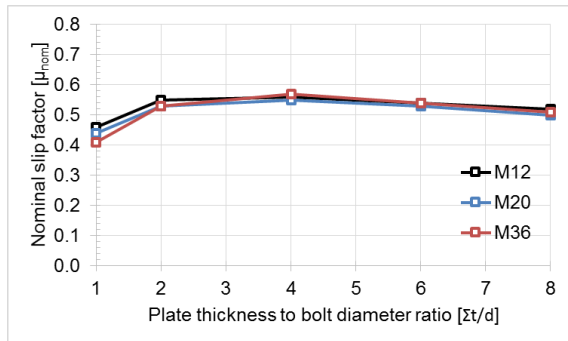
(b) Duplex plates with grit blasted surface (DG)

Figure 7.6-3: Comparison of numerical model with extended creep test results

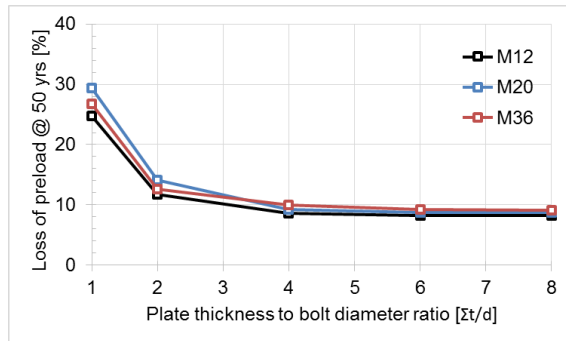
It can be seen that the slip displacement at the CBG position after 50 years predicted by the FE models are smaller than the test data. This may suggest that most of the slip occurred at the frictional surface due to high contact stress induced by viscoplastic deformation. The stainless steel plate and bolt material do not suffer from any significant creep/stress relaxation and therefore do not contribute to the development of slip over the long term. The FE model of the extended creep test assumed a constant frictional coefficient and was only able to predict the long term creep/stress relaxation occurring in the plate and bolt material.

The validated 3D slip test model was then used in parametric study to extrapolate the test results. Parameters included the clamped plate thickness, bolt size, surface friction coefficient and preload level.

The effect of plate thickness to bolt diameter ratio on the slip factor achieved and loss of preload can be observed in Figure 7.6-4. For the same plate surface finishes (AG) the achieved slip factor decreases when the thickness to bolt size ratio is less than 2. This is mainly due to the large loss of preload at low thickness to bolt size ratio. Beyond ratio of 2 there is no significant effect on the slip factor and loss of preload after 50 years.



(a) Nominal slip factors



(b) Loss of preload after 50 years

Figure 7.6-4: Effect of plate thickness to bolt size ratio on the behaviour of stainless steel slip resistant connections (bolt: A88 M20, plate: A_GB)

The effect of plate thickness to bolt size ratio on the slip factor achieved and loss of preload can be observed in Figure 7.6-5. Plate thickness to bolt size ratio of 2 and 6 were selected in the analysis. It is shown that the size of bolts did not have any meaningful influence over the nominal factor achieved by the stainless steel slip resistant connection models. Slightly higher loss of preload can be observed at larger bolt sizes.

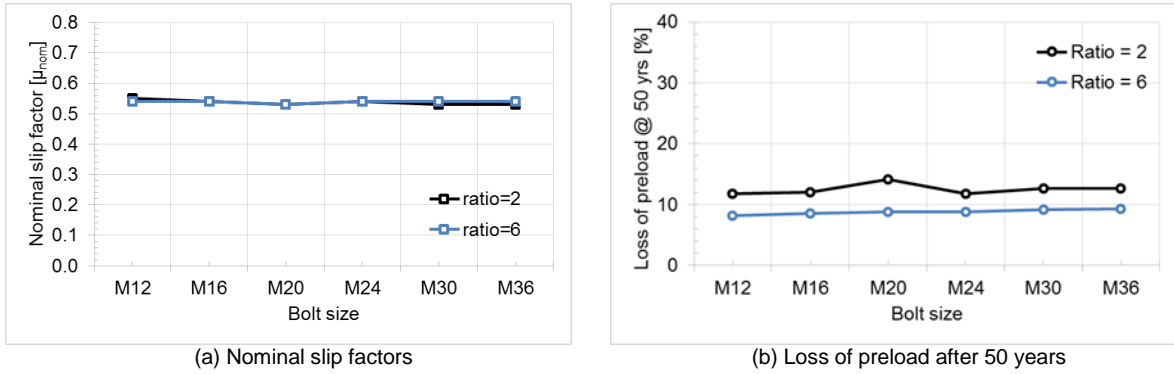


Figure 7.6-5: Effect of bolt size on the long term behaviour of a stainless steel slip resistant connection (bolt: A88, plate: A_GB, $\sum t/d=2$ & 6)

Surface roughness can be generally related to the friction coefficient of a surface. Eight friction coefficients were included in the study. Both the plates and bolts were assumed to be austenitic. The size and property class of the bolt are M20 and 8.8. The surface finish of the plate was not specified since the friction coefficient was the variable in the parametric study. The effect of friction coefficient on the response of preloaded bolted connections are presented in Figure 7.6-6. As illustrated, higher friction coefficient undoubtedly results in higher nominal slip factors and higher loss of preload at slip.

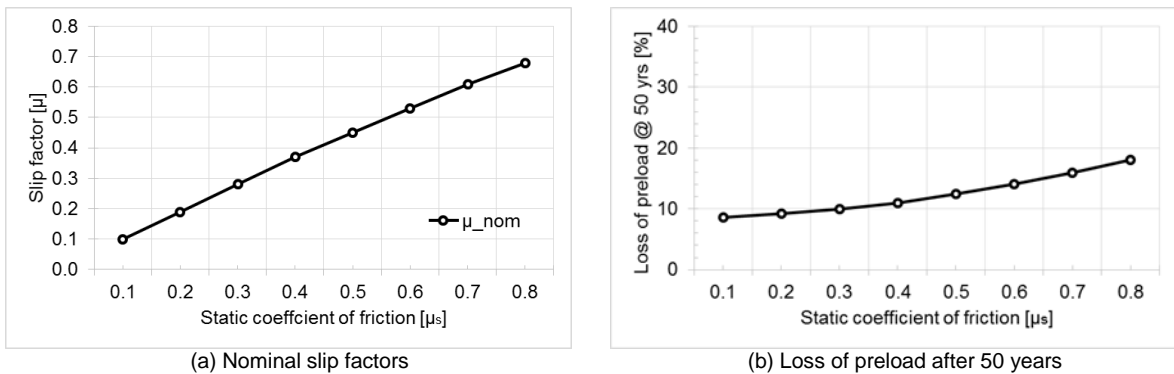


Figure 7.6-6: Effect of friction coefficient on the behaviour of a stainless steel slip resistant connection (bolt: A88 M20, plate: A, $\sum t/d=2$)

The effect of bolt preload on the slip factor and loss of preload are shown in Figure 7.6-7. It can be seen that the nominal slip factors were not affected significantly by the reduction of the bolt preload level, but the loss of preload reduced slightly when lower preload was used. It can be seen that there is a small increase in the nominal slip factor as the preload was reduced. This is mainly because the friction coefficient in the current modelling study was fixed but in reality it is dependent on the contact pressure. The lower friction coefficient as a result of smaller preload would keep the slip factor roughly constant between the four preload levels.

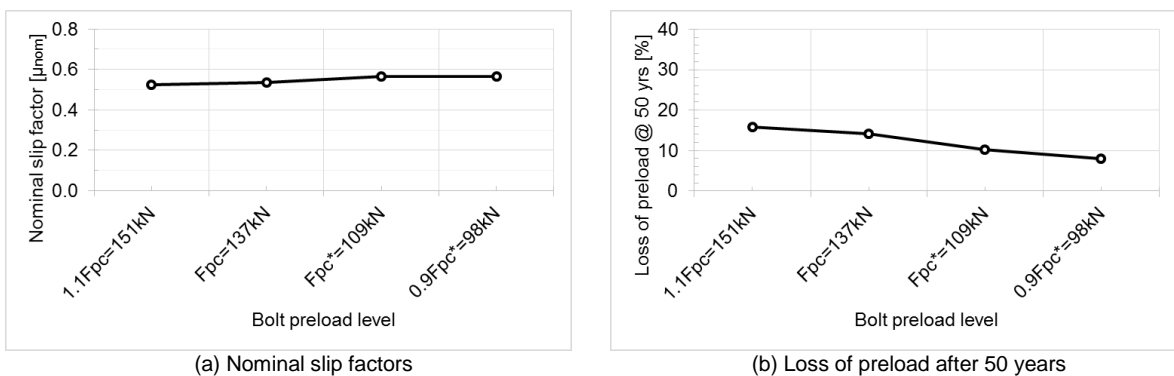


Figure 7.6-7: Effect of bolt preload on the behaviour of a stainless steel slip resistant connection (bolt: A88 M20, plate: A_GB, $\sum t/d=2$)

Conclusions

The numerical model developed in previous work package was extended with a surface friction model and calibrated against slip factor tests of stainless steel preloaded bolted connections in this current work package. The slip response and long term behaviour of the numerical models has been also evaluated by comparison against relaxation and extended creep tests of bolted assemblies. It was shown that the numerical model is able to accurately predict both short and long term behaviour of stainless steel slip resistant connections. The validated numerical models have been subsequently used in parametric studies to extrapolate the test results. The parametric studies focused on different geometric and material parameters, surface friction coefficient and bolt preload levels. The numerical results were presented and discussed in this report. Based on the numerical study, some observations and recommendations can be made for the design and use of stainless steel slip resistant connections:

- Preload loss was around 10% or less as found out in the parametric study. Due to the relatively high loading speed of 10 RPM the loss of preload would be higher than in practice.
- Plate thickness to bolt diameter ratio should be between 2 – 4 to achieve the desired slip factors, although a longer clamping length would reduce the loss of preload.
- Bolt size does not affect the slip resistance of the connection, but in order to minimise long term creep, smaller bolts should be used.
- Reducing the preload level does not lead to lower nominal slip factors. However, as the friction is dependent on the bearing pressure between the faying plates, it is recommended to use the slip factor which has been determined by the same level of preload in the slip factor test. As a result, the recommended slip factors from this project should only be used for preload level of $F_{p,C}$.

The numerical model presented in the current study assumed a constant friction coefficient between the faying surfaces. It would be beneficial in future work to use a more complicated friction model which can be made dependent on contact pressure and time. This should improve the accuracy of the numerical model for predicting both the short and long term behaviour of stainless steel slip resistant connections.

7.7 Task 6.5 – Design rules for slip-resistant connections

Summary

Stainless steel bolts are covered by EN ISO 3506, *Corrosion-resistant stainless steel fasteners* [10.7-1, 10.7-2]. The specification give chemical compositions and mechanical properties for austenitic, martensitic, ferritic and duplex fasteners. In EN ISO 3506, bolt and nut materials are classified by a letter: “A” for austenitic, “F” for ferritic, “C” for martensitic and “D” for duplex. It is recommended that austenitic or duplex bolts are used in structural applications. The letter is followed by a number (1, 2, 3, 4, 5, 6 or 8) which reflects the corrosion resistance; 1 representing the least durable and 8 the most durable. The corrosion resistance of a stainless steel fastener should be at least equivalent to the material being joined.

Design rule and guidelines were proposed based on the research results obtained in the research project SIROCO. Furthermore, recommendations are given on how to carry out tests to ensure a stainless steel slip resistant connection is installed correctly to a defined preload level and to determine slip factors for scenarios not covered in these guidelines.

In the absence of a specific product standard for stainless steel bolting assemblies for preloading applications, the following combination of bolts, nuts and washers were used for testing purposes, supplied by one producer of bolting assemblies:

- Bolts: EN ISO 4014 Hexagon head bolts — Product grades A & B [9.5-1]
- Bolts: EN ISO 4017 Fasteners – Hexagon head screws — Product grades A & B [9.5-2]
- Nuts: EN ISO 4032 Hexagon regular nuts (style 1) — Product grades A & B [9.5-3]
- Washers: EN ISO 7089 Plain washers — Normal series, Product grade A [9.5-4]

Austenitic stainless steel components in accordance with the above standards are widely available; duplex components are also available. However, there is no product standard for preloaded stainless steel bolting assemblies comparable to the series of EN 14399 for high-strength carbon steel structural bolting assemblies. Therefore, bolt tightening qualification procedure (BTQP) tests have to

be carried out for each configuration and batch of bolting assemblies made of stainless steel in order to specify the relevant tightening parameters and preloading method.

This BTQP consists of:

- (a) suitability test for preloading on the basis of EN 14399-2 [5.7-1];
EN 14399 requires this test for each batch of bolting assemblies to be used for preloading; usually it is carried out by the bolt producer. The k-class is determined by this test. This test has to be carried out for both carbon steel and stainless steel bolts.
- (b) definition of tightening parameters based on a statistical evaluation according to EN 1990.

Care is needed over the choice of lubricant because stainless steel preloaded assemblies are susceptible to galling if loaded into the plastic range. The assembly must be sufficiently well lubricated to enable the bolt to be loaded up to the required preload level using the chosen tightening procedure, without the occurrence of galling.

The guidelines are based on investigations for bolting assemblies consisting of EN ISO 4014/4017 bolts in property classes 8.8 and 10.9 with EN ISO 4032 nuts and EN ISO 7089 washers. These bolts have a smaller head and nut bearing surface than the carbon steel HV or HR systems according to EN 14399-3/-4 which were especially developed with optimised geometries for preloading. Furthermore, stainless steel bolting assemblies are not available on the market with calibrated lubrication needed for applying a specified preload level.

Tightening of stainless steel bolting assemblies is possible using various tightening procedures, e. g. torque method, combined method or using direct tension indicator (DTI) in accordance with EN 1090-2. It is important that the tightening procedure and the required preload level are well-matched. The process to qualify stainless bolting assemblies for preloading and the tightening method to achieved target preload is outlined in the flow chart shown in Figure 7.7-1.

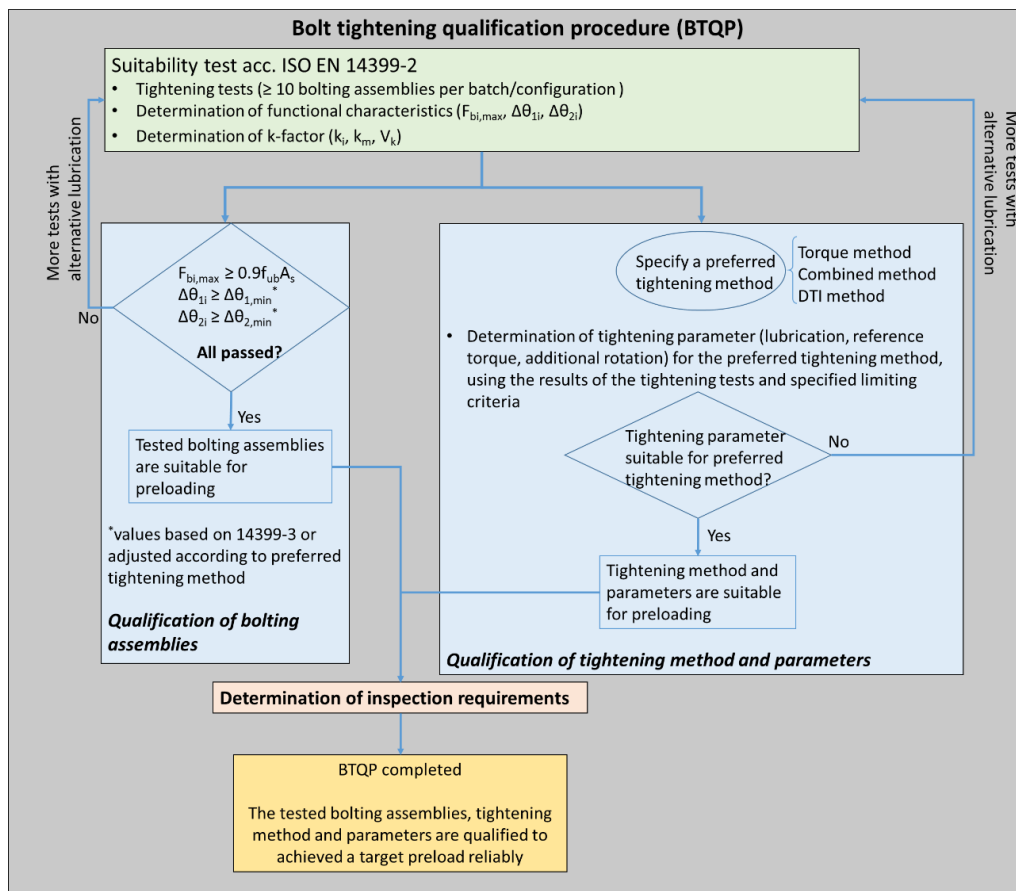


Figure 7.7-1:Flowchart for bolt tightening qualification procedure (BTQP)

The suitability for preloading of stainless steel bolting assemblies has to be assessed in accordance with EN 14399-2. It is a bolt force-torque tightening test. If all test specimens passed the maximum strength and ductility requirement, the bolting assembly is considered to be suitable for preloading.

Otherwise, additional suitability tests with different lubrication should be carried out until all specimens in a series can satisfy all criteria.

A preloading method is subsequently selected once the stainless steel bolting assemblies are deemed suitable for preloading. The k-class-concept introduced in EN 1090-2 is not specified for stainless steel bolting assemblies. Therefore, it is necessary to qualify the tightening method according to the general requirements of EN 1090-2 and to determine the tightening parameters to achieve a reliable preload level for the preferred tightening method. Limiting criteria for the determination of tightening parameters were proposed. These criteria are used to check that the required preload load can be reliably achieved and that it is smaller than the maximum allowable bolt load considering simultaneous tensile and torsional stress in the bolt. Inspection requirements should be in accordance with EN 1090-2, clause 12.5.2.

The preload losses due to viscoplastic deformation (creep and relaxation) in stainless steel preloaded bolted assemblies are not significantly higher than those for equivalent connections made of carbon steel. Hence, the design rules for carbon steel slip-resistant connections are applicable to stainless steel slip-resistant connections, provided the slip factors for stainless steel are used.

The following design rules apply to stainless steel bolted assemblies using bolts of property classes 80 and 100, in accordance with EN ISO 3506. Alternatively, if the bolts are property class 8.8 or 10.9 in accordance with EN ISO 898-1, then they must fulfil the requirements of EN 15048 [10.7-3].

Design of stainless steel slip resistant connections

Slip resistance

In applications where disassembly is unlikely to be necessary, stainless steel bolts can be preloaded to $F_{p,C}$ and the design slip resistance is given by:

$$F_{s,Rd} = \frac{k_s n \mu}{\gamma_{M3}} F_{p,C} \quad \text{Slip resistance at ULS (Category C)} \quad (7.7-1)$$

$$F_{s,Rd,ser} = \frac{k_s n \mu}{\gamma_{M3,ser}} F_{p,C} \quad \text{Slip resistance at SLS (Category B)} \quad (7.7-2)$$

where

k_s is given in Table 3.6 EN 1993-1-8:2005

n is the number of friction planes;

μ is the slip factor obtained either by specific tests for the friction surface in accordance with EN 1090-2 or when relevant as given in **Combined tension and shear**

Table 7.7-1 Slip factor, μ , for preloaded stainless steel bolted connections

Class of friction surfaces	Stainless steel grade	Surface condition		Slip factor μ
		Surface finish	Rz [μm]	
A++	Duplex 1.4462/ Lean Duplex 1.4162	Aluminium spray metallized (measured dry film thickness (DFT) = $100 \mu\text{m} \pm 20 \mu\text{m}$)	≥ 40 (before coating application)	0.7
A+	Austenitic 1.4404/ Ferritic 1.4003			0.6
A	Duplex 1.4462	Surfaces blasted with grit	≥ 50	0.5
	Ferritic 1.4003		≥ 45	
B	Austenitic 1.4404	Surfaces blasted with grit	≥ 45	0.4
	Lean Duplex 1.4162		≥ 40	
C	-	-	-	0.3
D	Austenitic 1.4404	Surfaces blasted with shot	≥ 35	0.2
E	Austenitic 1.4404	Surfaces as rolled	≥ 25	0.15

Note: Care is needed during grit and shot blasting processes to ensure there is no detrimental effect on the corrosion resistance.

The recommended values for γ_{M3} and $\gamma_{M3,ser}$ are 1.25 and 1,1 respectively. Note that these values need to be verified for stainless steel slip resistant connections by a reliability assessment in accordance with EN 1990 Annex D.

For other surface conditions, the slip factor can be determined according to the slip factor test of Annex G, EN 1090-2. Unlike for coated carbon steel slip-resistant connections, the influence of the preload level on the resulting slip factor is negligible for stainless steel slip-resistant connections. For

bolts of property classes 80 and 100, conforming with EN ISO 4014 or EN ISO 4107, and installed with controlled tightening in accordance with EN 1090-2, the preloading force $F_{p,C}$ to be used in equations (7.7-1) and (7.7-2) should be taken as:

$$F_{p,C} = 0.7f_{ub}A_s \quad (7.7-3)$$

Nevertheless, a lower preload level can be used as long as the bolting assemblies, the tightening method, the tightening parameters and the inspection requirements are specified and the lower preload level is consequently considered in the design and execution process. In applications where easy fastener removal is important, in order to avoid any possibility of galling, stainless steel bolts should be only preloaded into the elastic range and the design slip resistance may be taken as:

$$F_{s,Rd} = \frac{k_s n \mu}{\gamma_{M3}} F_{p,C}^* \quad \text{Slip resistance at ULS (Category C)} \quad (7.7-4)$$

$$F_{s,Rd,ser} = \frac{k_s n \mu}{\gamma_{M3,ser}} F_{p,C}^* \quad \text{Slip resistance at SLS (Category B)} \quad (7.7-5)$$

For bolts of property classes 80 and 100, conforming with EN ISO 4014 or EN ISO 4107, and installed with controlled tightening in accordance with EN 1090-2, the preloading force $F_{p,C}^*$ according to DIN EN 1993-1-8/NA to be used in equations (7.7-4) and (7.7-5) may be taken as:

$$F_{p,C}^* = 0.7f_{yb}A_s \quad (7.7-6)$$

Combined tension and shear

If a slip-resistant connection is subjected to an applied tensile force, $F_{t,Ed}$ or $F_{t,Ed,ser}$, in addition to the shear force, $F_{v,Ed}$ or $F_{v,Ed,ser}$, tending to produce slip, the design slip resistance per bolt should be taken as follows:

$$\text{for a category B connection:} \quad F_{s,Rd,ser} = \frac{k_s n \mu (F_{p,C} - 0.8 F_{t,Ed,ser})}{\gamma_{M3,ser}} \quad (7.7-7)$$

$$\text{for a category C connection:} \quad F_{s,Rd} = \frac{k_s n \mu (F_{p,C} - 0.8 F_{t,Ed})}{\gamma_{M3}} \quad (7.7-8)$$

If in a moment connection, a contact force on the compression side balances the applied tensile force, no reduction in the slip resistance is required.

Conclusions

Based on the tests conducted, it is evident that stainless steel bolting assemblies are suitable for preloading, provided a suitable lubricant is identified and the functional characteristics and tightening criteria can be satisfied. In the absence of a product standard for preloaded stainless steel bolting assemblies, a bolt tightening qualification procedure has to be carried out to ensure the suitability for preloading of the bolt assemblies, determine the tightening parameters and confirm the reliability of the tightening method to achieve the design preload. Finally, design equations are proposed and slip factors for four grades of stainless steel with typical surface finishes provided for calculation of slip resistance of preloaded stainless steel bolted connections.

7.8 Task 6.6 – Design examples

Two worked examples are provided to illustrating the application of design equations and slip factors for design of stainless steel slip-resistant connections. Austenitic bolts (BUMAX 88) and duplex plate material with grit blasted surface finish were used throughout in the examples, see Annex A:

Example – 1: Connection of Tensile Bracing Members,

Example – 2: Main girder splice.

8 WP 7 – Guidelines and exploitation activities

8.1 Objectives

This WP will enable effective dissemination of major project deliverables by:

- Preparing guidelines on the design and execution of slip-resistant connections separately for carbon and stainless steel connections;
- Preparing amendments to EN 1090-2 regarding the slip-test procedure and enhanced slip factors considering modern surface treatments and alternative coatings for connections made of carbon and stainless steel;
- Preparing amendments to EN 1993-1-8 for better use of slip-resistant connections considering different load levels guaranteeing sufficient reliability;
- Preparing amendments to EN 1993-1-8 for connections with injection bolts and to EN 1090-2 for testing and execution of connections with non-preloaded and preloaded injection bolts;
- Preparing amendments to EN 1090-2 for the application of lock bolts and direct tension indicators;
- Preparing amendments to EN 1993-1-4 for including design rules for preloading of stainless steel bolts.

8.2 Work undertaken

The tasks undertaken in WP 7:

- 7.1. Guidelines on the design and execution of slip-resistant connections made of carbon steel.
- 7.2. Guidelines on the design and execution of slip resistant connections made of stainless steel plates and bolts.
- 7.3. Other dissemination activities.
- 7.4. Contribution to standardization and regulation process.

The work undertaken for Tasks 7.1 to 7.4 is summarized in Sections 11.3 - 11.6.

8.3 Task 7.1 – Guidelines for carbon steel

Annex G of EN 1090-2 prescribes a generalized experimental procedure to obtain the slip factor. This slip factor test procedure has been thoroughly investigated in the frame of SIROCO with the aim not only to clarify it but also to optimize it. The basics of the test procedure have not been changed in SIROCO. The clarification and optimization which could be achieved from the research results cover essentially

- the type of preload measurement,
- definition of the slip planes,
- the test speed, the position of slip measurement,
- the clamping length,
- the preload level,
- the evaluation of critical slip load and
- the performance of the extended creep test to cover creep effects.

The slip factor test consists of a three step test procedure, see Figure 8.3-1. Four static tests shall be conducted at “normal speed”, followed by a creep test and in case the creep test is not passed, at least three extended creep tests have to be performed.

The test duration has no influence on the scatter of the test results neither on the determination of the sensitivity of the investigated coating to creep.

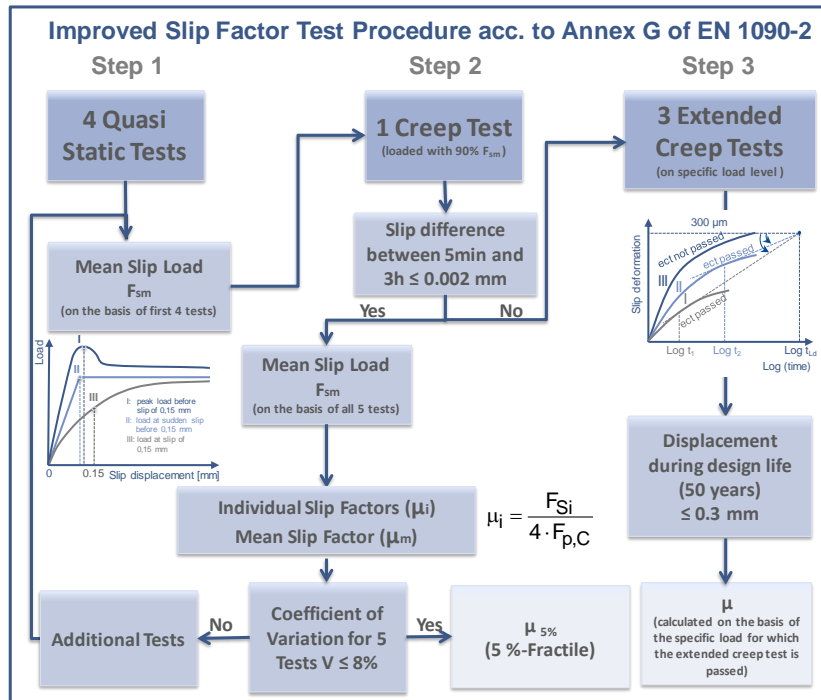


Figure 8.3-1: Improved three step test procedure of the slip factor test acc. to Annex G of EN 1090-2

The slip has to be measured in the direction of the applied load as the relative displacement between specific points on the inner (b) and cover plates (a and c), as shown in Figure 8.3-2. The slip shall be measured in eight different positions for each end and each side of the specimen separately at points a, b and c in the centre of the upper and lower bolt group. Two slip values have to be determined based on eight measured displacements by considering the type of failure mode which can be a combination of slip in the faying slip planes (1 and 2) or (3 and 4) or diagonal in the slip planes (1 and 4) or (2 and 3).

Various possibilities exist to measure the preload in the bolts continuously during the testing time. It is recommended to use either

- instrumented bolts with implanted and calibrated strain gauges in the bolts or
- stiff calibrated load cells.

The maximum allowable slip deformation is defined to 0.15 mm. If a peak load occurs below a slip deformation of 0.15 mm, the peak load can be chosen as the slip load. Does a sudden slip occur below a slip deformation of 0.15 mm, the load at sudden slip has to be chosen. In all other cases, the load at a slip deformation of 0.15 mm defines the slip load.

In the frame of SIROCO, a procedure with two different approaches was developed for evaluating the load level for a successful extended creep test when the creep test was not passed and extended creep tests are necessary. Both approaches are applicable to obtain an initial load level for testing the creep sensitivity of a coating system with the extended creep test. At the obtained load level, the extended creep test will (most probably) pass, according to the requirements of Annex G of EN 1090-2.

The fundamentals of the load level that result from the new procedure are

- (1) the mean slip load F_{Sm} (the result of the 4 static slip factor tests) and

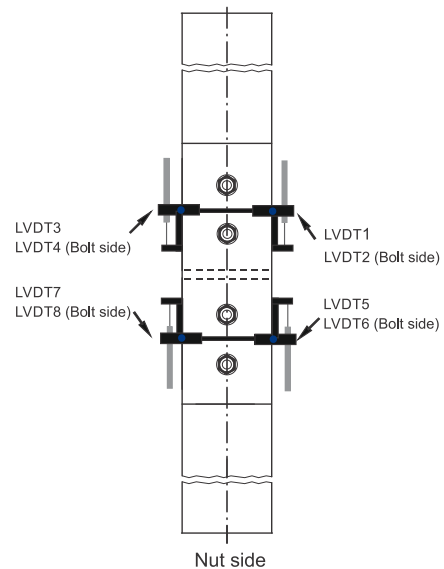


Figure 8.3-2: Positions of measurement of the slip

- (2) a test procedure in which the load is increased stepwise and kept constant over a relatively short period.

The new test procedure is a short-term stepwise loading test and denoted as “step test”.

The surface condition has a great influence on the slip factor. The creep sensitivity is directly linked to the surface condition. Grit blasted surfaces are not creep sensitive at all whereas coated surfaces are usually creep sensitive. In general, it can be stated, that this leads to higher slip factors for grit blasted surfaces and lower slip factors for coated surfaces.

Table 8.4-1 comprises the finally resulting slip factors for carbon steel slip-resistant connections achieved in SIROCO in comparison to those of FprEN 1090-2. It can be seen that especially for grit blasted surfaces alkali-zinc silicate coating (ASI) and thermally sprayed with aluminium (Al-SM) surfaces higher slip factors can be achieved than given in EN 1090-2.

It can be concluded that in special cases it might be of interest to determine the slip factor by testing in order to achieve higher slip factors than tabulated in EN 1090-2.

8.4 Task 7.2 – Guidelines for stainless steel

The preload losses due to viscoplastic deformation (creep and relaxation) in stainless steel preloaded bolted assemblies are not significantly higher than those for equivalent connections made of carbon steel. Hence, the design rules for carbon steel slip-resistant connections are applicable to stainless steel slip-resistant connections, provided the slip factors for stainless steel are used. Design rules of stainless steel slip resistant connections and typical slip factors have been proposed in Task 6.5.

Table 8.4-1 Slip factors for various surface treatments achieved in SIROCO and compared to FprEN 1090-2

Surface Treatment	Class ^a	Slip Factor μ	Slip Factor μ
	FprEN 1090-2	SIROCO	
Grit blasted, Sa 2½ / Rz = 80 μ m, $F_{p,C}$	A	0.5	0.75
Alkali-zinc silicate coating (ASI), Sa 2½ / Rz = 80 μ m, 60 μ m DFT, $F_{p,C}$	B	0.4	0.56
Alkali-zinc silicate coating (ASI), Sa 2½ / Rz = 80 μ m, 60 μ m DFT, $F_{p,C}^*$	-	-	0.63
Thermally sprayed with aluminium (Al-SM), 250 μ m DFT, $F_{p,C}$	B	0.4 (NDFT \leq 80 μ m)	0.58
Thermally sprayed with zinc (Zn-SM), Sa 3 / Rz = 100 μ m, 140 μ m DFT, $F_{p,C}$	B		0.44
Thermally sprayed with zinc (Zn-SM), Sa 3 / Rz = 100 μ m, 164 μ m DFT, $F_{p,C}^*$ and 0.9 $F_{p,C}^*$	-	-	0.48
Combination ASI – ZnSM, Sa 2½ / Rz = 100 μ m, 55 μ m / 170 μ m DFT, $F_{p,C}$	-	-	0.44
Combination ASI – ZnSM, Sa 3 / Rz = 100 μ m, 55 μ m / 170 μ m DFT, 0.9 $F_{p,C}^*$	-	-	0.55

In the absence of a product standard for preloaded stainless steel bolting assemblies, a bolt tightening qualification procedure is required for each configuration of stainless steel bolted connection. This procedure ensures the suitability for preloading of the designed bolting assemblies, determines the tightening parameters and confirms the reliability of the tightening method to achieve the design preload.

The test results showed that it is possible to preload stainless steel bolting assemblies within the elastic range to $F_{p,C}^*$ and also up to $F_{p,C}$. With a suitable lubricant, the functional characteristics can be successfully achieved and tightening parameters determined. Appropriate lubrication extends the plastic plateau of the bolt preload – angle rotation curve. The ability to satisfy the functional characteristics is highly dependent on the type of lubricant used. The suitability for preloading tests in SIROCO indicated that DOW Corning Molykote 1000 spray and Molykote D-321R spray were

appropriate lubricants for preloading of stainless steel bolting assemblies. Other lubricants might also be appropriate and need to be validated by suitability tests.

In the tests carried out under SIROCO, galling only occurred with certain lubricants when the bolts were tightened into the plastic zone, i.e. at preload levels near to $F_{bi,max}$ and far exceeding $F_{p,C}$. Galling generally occurs on the interface between the washer and the nut, but may also occur between the paired threads. Galling can be avoided by a combination of the use of an appropriate lubricant and the use of a tightening procedure which avoids overtightening (i.e. not tightening too far beyond the required preload level $F_{p,C}$.)

Slip factor tests according to EN 1090-2 Annex G shall be carried out for stainless steel plate and bolt assemblies not covered in this project. The measurement of the preload in the bolting assemblies has to be carried out in such a way that creep in the stainless steel bolt material does not influence the measured preloads. A relatively rigid load cell should be used, calibrated for linear strain-load behaviour. Implanted strain gauges are not suitable.

8.5 Task 7.3 – Dissemination

In total 20 peer-reviewed papers have been published in journals (14 papers) and conferences (9 papers). The November-2017-issue of the journal *Steel Construction* was dedicated to SIROCO publishing in total 8 papers presenting results from SIROCO.

8.6 Task 7.4 – Contribution to standardization

Carbon Steel

An amendment to EN 1993-1-8 is proposed to explicitly open the design of preloaded bolted connections also lower preload levels than $F_{p,C}$, EN 1090-2 already allows lower preload levels than $F_{p,C}$. Furthermore, in some applications the re-use of components of the bolting assemblies might be necessary, e. g. bearings. Furthermore, for stainless steel bolting assemblies, see below, a lower preload level than $F_{p,C}$ is of great interest as well. For these reasons, it should be possible to apply lower preload levels than $F_{p,C}$, which can also be used for preloaded tension connections. EN 1090-2 already allows lower preload levels than $F_{p,C}$. Some findings of SIROCO have already been implemented in the latest draft of Annex G of FprEN 1090-2:2017 which will be published in 2018. These are:

- Clarification of wording,
- Defining of the slip planes,
- Determination of the slip load F_{Si} ,
- Positioning of the displacement measurement.

Further amendments to EN 1090-2 include, see also Table 8.4-1,

- Enhancement of the slip factor for grit blasted surfaces,
- Enhancement of slip factors for thermally sprayed with aluminium (Al-SM) surfaces,
- Additional slip factors for surface treatments not covered yet, e. g. combinations as alkali-zinc silicate coating and thermally sprayed with zinc (ASI – Zn-SM),
- Implementing the step test in order to be able to assume a load level for extended creep tests.

Stainless Steel

The SIROCO research project has made a useful contribution to the application of stainless steel bolts in preloaded bolted connections. Amendments to Clause 2.2.2 of EN 1993-1-4 have been proposed. This allows preloaded stainless steel bolts to be used in structural applications. Amendments to EN 1090-2 include a new table of slip factors for different surface classifications that may be assumed for the friction surface between stainless steel plates. The amendments also recommend preparation of contact surfaces in stainless steel slip resistant connections and requires a bolt tightening qualification procedure for each configuration of stainless steel bolting assemblies.

9 List of figures

Figure 2.3-1: M20-Bolts with implanted strain gauges	15
Figure 2.3-2: Calibration of bolt and load cell at TUD and UDE.....	16
Figure 2.3-3: Results for the use of customary small load cells.....	16
Figure 2.3-4: Test setup for comparative studies	17
Figure 2.3-5: Influence of positioning the LVDTs (the different colours represent the upper and lower sections of the specimen)	17
Figure 2.3-6: Comparison of preload measurements considering LC and SG for GB-I.....	18
Figure 2.3-7: Comparison of preload measurements considering LC and SG for ASI-I.....	18
Figure 2.3-8: Comparison of preload measurements considering LC and SG for HDG-I.....	18
Figure 2.3-9: Influence of different surface conditions on the slip-load behaviour.....	18
Figure 2.4-1: Graphical representation of the experimental results of Task 1.2	23
Figure 2.5-1: Influence of the coating system on the faying surfaces from specimens in Task 1.1 (LVDTs A3, B3, C3, D3 were not used for calculation of the mean displacement).....	24
Figure 2.5-2: Criteria for the evaluation of the slip load	25
Figure 2.6-1: Slip load tests of Zn-SM from Task 1.1.....	27
Figure 2.6-2: Results of long-term step test for Zn-SM specimen	27
Figure 2.6-3: Load-time-displacement diagram of an EXC (top: 80 % of the load, bottom: 75 % of the load)	28
Figure 2.6-4: <i>Long-term step test</i> of HDG specimen (left); <i>Short-term step-test</i> of Zn-SM specimen (right).....	28
Figure 2.6-5: Extended creep test with 70 % and 65 % load for Zn-SM specimens.....	28
Figure 2.6-6: Extended creep test with 60 % for Zn-SM specimen (450 d test duration)	29
Figure 2.6-7: Autarkic test rigs for the investigations of the creep behaviour for the coating systems .	29
Figure 2.6-8: Summary of the observations of the creep behaviour for the coating systems	29
Figure 2.7-1: Task 1.5 – Types of lubrication	30
Figure 2.7-2: Tightening curves and criteria of evaluation acc. EN 14399-2 [5.7-2].....	31
Figure 2.7-3: Comparison between HR M24x100 8.8 – factory provided (black) and Molykote 1000 (yellow).....	33
Figure 2.7-4: Comparison between HR M36x160 10.9 – factory provided (black) and Molykote 1000 (yellow).....	33
Figure 2.7-5: Achieved preloads of HR bolting assemblies in property class 8.8 and 10.9	35
Figure 3.3-1: Combined results of SSWL and extended creep test.....	39
Figure 3.3-2: Illustration of intended use of SSWL test result for new coatings.....	39
Figure 3.4-1: Test setup, test specimen geometry, positions of displacement transducers (LVDTs) as well as clamped plates of a bolted connection with bolts with implanted strain gauge	41
Figure 3.4-2: Influence of different preload levels for ASI-surface condition	41
Figure 3.4-3: Influence of different preload level on the static slip factors	42
Figure 3.4-4: Influence of different preload levels for Zn-SM-surface condition	42
Figure 3.4-5: Influence of different preload levels for ASI-Zn-SM-surface condition	42
Figure 3.4-6: Influence of different preload levels and surface pressures	43
Figure 3.4-7: Exemplary results of creep tests considering different coating surfaces.....	43
Figure 3.4-8: Test rig for extended creep tests	43
Figure 3.4-9: Results of the extended creep tests for different test series.....	44
Figure 3.5-1: Hexagonal die used to (1) centre and (2) keep the drill parallel to the bolt axis.....	46

Figure 3.5-2: Strain gauge installed in bolt and connected to terminal. Bolt is placed in Skidmore-Wilhelm instrument.	46
Figure 3.5-3: Instrumented bolts in the beam flange friction grip connection in the Middachterbrug (1974).....	47
Figure 3.5-4: Longitudinal strain distribution along the bolt centreline (CL) for $F_{p,C} = 247$ kN	49
Figure 4.3-1: Alternative high-strength bolting systems, H360® and Bobtail Lockbolts for preloaded joints and preloaded specimen (acc. to EN 1090-2, Annex G, Figure G.1, Type a)	51
Figure 4.3-2: Preload-time diagram of the tightening process of Lockbolts, H360® and HV-Bolts	52
Figure 4.3-3: Test setup for experimental investigation according to EN 1090-2, Annex G, specimen type a)	53
Figure 4.3-4: Characteristic slip load – displacement curves of Lockbolts, H360® and HV bolts with different prepared faying surfaces (grit-blasted – GB, aluminium spray metallised Al-SM, hot-dip galvanised – HDG).....	53
Figure 4.3-5: Left: Test bench for torque/clamp force testing acc. to DIN EN ISO 16047:2013-01, right: Forming effect of the nut by tightening up to the nominal torque H360® size M20	54
Figure 4.3-6: left - points of analysis for torque/clamp force test, right – evaluation points	55
Figure 4.4-1: Injection bolt in a double lap joint.....	57
Figure 4.4-2: Specimen with instrumentation, test machine and test procedure	58
Figure 4.4-3: Initial test results: a) load–displacement curves, b) displacement–time curves	58
Figure 4.4-4: a) load procedure, b) & c) curing temperature results, d) overload behaviour	59
Figure 4.4-5: loading procedures for Edilon Dex-R2K and RenGel (Araldite)	60
Figure 4.4-6: Loading procedures for long-duration tests – effect of using slotted holes	60
Figure 4.4-7: Long-term test results for a RenGel specimen with slotted holes with 6 mm clearance – $F_{max} = 70$ kN.....	61
Figure 4.4-8: Long-term test results for a Dex-R2K specimen with normal round holes with 2 mm clearance – $F_{max} = 56$ kN	61
Figure 4.4-9: Large bolt test results: a) load–displacement curves, b) stress–displacement curves....	61
Figure 4.4-10: Long bolt tests: a) loading procedure, b) specimen in test rig, c) test results	62
Figure 4.4-11: a) Reinforced resin with spherical steel particles (shots) and b) unit cell with body-centred cubic arrangement for c) derivation of an analytical material model for the reinforced resin	62
Figure 4.5-1: Use of a feeler gauge to check the gap	63
Figure 4.5-2: Compression test acc. to EN 14399-9 and gap - compression load diagram for each DTI	64
Figure 4.5-3: Tightening curves of test specimen M16-HN-2.....	65
Figure 4.5-4: Test specimen geometry for the relaxation tests of the bolted connections (test specimens for M16 and M20 bolts).....	65
Figure 4.5-5: Exemplary test setup for M16 bolted connection without DTIs (left) and for M20 bolted connection with DTIs (right)	65
Figure 4.5-6: The achieved preload level for different DTIs bolted assemblies configurations (under the bolt head and under the nut) – results of eight-bolts-specimens.....	66
Figure 4.5-7: Exemplary preload losses and rate of loss of preload for DTI01 test series	67
Figure 4.5-8: Extrapolated loss of preload at a service life of 50 years	67
Figure 5.3-1: Blast-cleaned surface of variations	69
Figure 5.3-2: Application of pretension using air driven torque tool; mounting of LVDT brackets on cover plates.....	70
Figure 5.3-3: Typical load – slip displacement diagram for series A and B	71

Figure 5.3-4: Metallographic cross-sections of different roughness profiles	73
Figure 5.4-1: Test setup, test specimen geometry, positions of displacement transducers (LVDTs) as well as clamped plates of a bolted connection with bolts with implanted strain gauge	75
Figure 5.4-2: Influence of different surface treatment/preparation on the slip-load behaviour and initial slip factors	75
Figure 5.4-3: Influence of different post treatments on the static slip factors.....	76
Figure 5.4-4: Results of creep tests considering different post treatment for galvanized specimens...	76
Figure 5.4-5: Evaluating the slip displacement – log time curves	76
Figure 5.4-6: Test specimen geometry for the relaxation tests of the bolted connections.....	77
Figure 5.4-7: Preload losses for HDG-Ref (preload level: $F_{p,C} = 0.7 \cdot f_{ub} \cdot A_s = 172$ kN)	78
Figure 5.4-8: Extrapolated loss of preload at a service life of 50 years	78
Figure 5.4-9: Rate of loss of preload for HDG-Ref (preload level $F_{p,C} = 172$ kN)	78
Figure 5.5-1: M20-test specimen according to Annex G of EN 1090-2 [5.3-1] and LVDT position	81
Figure 5.5-2: Left: Slip load-displacement curves of test series A-ESI-3-n, Right: Faying surfaces of specimen with the coating system A-ESI-3-n	81
Figure 5.5-3: Left: Load-time-displacement curve of the step test of specimen with A-ESI-3-n, Right: Extended creep test (ECT) with 81.3 % load of F_{Sm} for the specimen A-ESI-3-n	82
Figure 5.5-4: Slip load-displacement curves of the test series B-ESI-1-o and C-ESI-1-n	82
Figure 5.5-5: Left: Load-time-displacement curve of step test (B-ESI-1-o), Right: Load-log-time-displacement of the extended creep test (ECT) with 80 % load of F_{Sm} (B-ESI-1-o).....	83
Figure 5.5-6: Left: Load-log time-displacement of the extended creep test (ECT) with 85 % load of F_{Sm} for specimen B-ESI-1-o, Right: Comparison of the slip load-mean displacement curves of the three test series A-ESI-3-n, B-ESI-1-o and C-ESI-1-n	83
Figure 6.3-1: Repeated 4 x 3 h relaxation test for grade 1.4404 plate material. The stress relaxation curve measured on continuous 12h loading is shown as reference. The loading speed was 0.5 MPa/s and the load level corresponds to the 82.5 % of the 0.2 % proof stress of the material. ..	87
Figure 6.3-2: Uniaxial tensile creep results at room temperature condition.....	87
Figure 6.3-3: The creep rate, a) logarithmic creep behaviour in region III, b) influence of the initial loading rate, c) influence of the load level, d) similar creep behaviour for 1.4462.	88
Figure 6.4-1: 12 h stress relaxation of stainless steels, a) rebar or bar, b) cold drawn bar.	93
Figure 6.4-2: Fitted parameters according to equation (9.4-3), a) stress relaxation of the 1.4436 cold drawn at $1.0 \times R_{p0.2}$ (48 data points), b) the stress rate. RSS is the lowest residual sum of squares.	93
Figure 6.4-3: σ^* as a function of the initial stress	94
Figure 6.4-4: The asymptotic stress relaxation as a function of the initial stress for the tested bars. $R_{p0.2}$ and R_m were the measured strength of the tested bars, recall Table 9.4-1	95
Figure 6.4-5: Comparison between 12 h stress relaxation test and the asymptotic stress relaxation. 5 min, 1 h and 10 h marks the respectively testing time. Cold drawn bar of 1.4436 at the $1.0 \times R_{p0.2}$ stress level.	95
Figure 6.5-1: Schematic bolt force-angle of rotation curve (left) and bolt force-tightening torque curve (right) according to EN 14399-2.....	97
Figure 6.5-2: Galling of the nut bearing surface when tightened into plastic range: bolt (left), nut and washer (middle), and detailed view of washer (right)	99
Figure 6.5-3: Exemplary creep test results - M12 super duplex bolting assemblies.....	100
Figure 6.5-4: Production calibration phases of load cells and test setup of relaxation test	100
Figure 6.5-5: Exemplary photos for stainless steel and carbon steel test specimens	101
Figure 6.5-6: Test setup	101

Figure 6.5-7: Exemplary preload losses and rate of loss of preload for SS16 test series	102
Figure 6.5-8: Comparing the loss of preload after 50 years (extrapolated) for different test series....	103
Figure 6.6-1: Tightening torque testing machine at the Institute for Metal and Lightweight Structures of the University of Duisburg-Essen	105
Figure 6.6-2: Galling of the nut bearing surface when tightened into plastic range: nut (left), washer (middle) and detailed view of washer (right)	107
Figure 6.6-3: Comparison of BU_M16_LDX tightening curves between gleitmo 1952V standard lubrication (black curves) and Molykote 1000 spray (yellow curves)	107
Figure 6.6-4: Comparison of BU_M20_DX tightening curves between gleitmo [®] 1952V standard lubrication (black curves) and Molykote [®] 1000 spray (yellow curves).....	107
Figure 6.6-5: Bumax – M20x100 bolting assemblies after tightening with Interflon HT1200 spray (above) and Interflon HT1200 paste (below)	108
Figure 6.7-1: 3D bolted assembly and the stress distribution under preload	109
Figure 6.7-2: User interface of the ABAQUS plug-in for 3D bolted connections.....	109
Figure 6.7-3: Examples of FE verification of material model for austenitic plates – tensile tests by OSOY	110
Figure 6.7-4: Examples of FE verification of material model for austenitic plates – creep tests by OSOY	110
Figure 6.7-5: Examples of FE verification of material model for austenitic plates – relaxation test by VTT at strain level 1.2 %.....	111
Figure 6.8-1: Flowchart for suitability test and tightening method qualification of stainless steel bolts for preloading	112
Figure 6.8-2: Inspection of galling of austenitic M20 HV200 washers and M20 Bumax 88 austenitic nuts in property class 8.8 after tightening at specified preload level $F_{p,C}^* = 0.7 \cdot f_{yb} \cdot A_s$	113
Figure 6.8-3: Inspection of galling of austenitic M20 HV200 washers and M20 Bumax 88 austenitic nuts in property class 8.8 after tightening at specified preload level $F_{p,C} = 0.7 \cdot f_{ub} \cdot A_s$	113
Figure 6.8-4: Inspection of galling of austenitic M20 HV200 washers and M20 Bumax 88 austenitic nuts in property class 8.8 after tightening at specified preload level $F_{bi,max} \geq 0.9 \cdot f_{ub} \cdot A_s$	114
Figure 7.3-1: Faying surfaces for 1.4404 1D.....	115
Figure 7.3-2: Faying surfaces for 1.4404 SB.....	115
Figure 7.3-3: Faying surfaces for 1.4404 GB	115
Figure 7.3-4: Faying surfaces for 1.4003 GB	116
Figure 7.3-5: Faying surfaces for 1.4404 GB	116
Figure 7.3-6: Faying surfaces for 1.4162 GB	116
Figure 7.3-7: Faying surfaces for 1.4462 GB	116
Figure 7.4-1: Test setup, test specimen geometry, positions of displacement transducers (LVDTs) as well as Clamped plates of a bolted connection with bolts with implanted strain gauge	117
Figure 7.4-2: Typical load-slip-displacement curves for different surface conditions of the test series with bolts Bumax 88 and Bumax 109 - each colour represent the upper and lower section of the specimen.....	118
Figure 7.4-3: Influence of different stainless steel surface conditions on the slip factors	119
Figure 7.4-4: Exemplary results of creep tests considering different stainless steel grade with GB surfaces	119
Figure 7.4-5: Test rig for performing the extended creep tests	120
Figure 7.4-6: Exemplary results of extended creep tests for test series with Bumax 88	120
Figure 7.4-7: Exemplary results of extended creep tests for test series with Bumax 109	120

Figure 7.4-8: Final slip factor considering different stainless steel grades and surface treatments with bolts Bumax88 and Bumax109	121
Figure 7.5-1: Typical load-slip-displacement curves for different surface conditions of the test series with of Bumax 88 and Bumax 109 bolts - each colour represent the upper and lower section of the specimen.....	122
Figure 7.5-2: Influence of different stainless steel surface conditions on the static slip factors – test series with bolts of property class 8.8 (Bumax 88) – compared with the results of Task 6.2.....	122
Figure 7.5-3: Influence of different stainless steel surface conditions on the static slip factors – test series with bolts of property class 10.9 (Bumax 109) - compared with the results of Task 6.2..	122
Figure 7.5-4: Exemplary results of creep tests considering different stainless steel grades with aluminium spray metalized surfaces with Bumax 88 bolts	123
Figure 7.5-5: Results of extended creep tests considering different stainless steel grades coated with Al-SM (each colour represents the upper and lower section of the specimen)	123
Figure 7.5-6: Final slip factor considering different stainless steel grades and surface treatments with bolts Bumax88 and Bumax109.....	124
Figure 7.6-1: Numerical models developed in SIROCO	125
Figure 7.6-2: Calibration results for Austenitic plate with grit blasted surface finish and M16 Bumax 109 bolts (series ID: AG), the static coefficient of friction used for the faying surface was calibrated to be $\mu_{fric} = 0.60$	125
Figure 7.6-3: Comparison of numerical model with extended creep test results	127
Figure 7.6-4: Effect of plate thickness to bolt size ratio on the behaviour of stainless steel slip resistant connections (bolt: A88 M20, plate: A_GB)	127
Figure 7.6-5: Effect of bolt size on the long term behaviour of a stainless steel slip resistant connection (bolt: A88, plate: A_GB, $\sum t/d=2$ & 6).....	128
Figure 7.6-6: Effect of friction coefficient on the behaviour of a stainless steel slip resistant connection (bolt: A88 M20, plate: A, $\sum t/d=2$)	128
Figure 7.6-7: Effect of bolt preload on the behaviour of a stainless steel slip resistant connection (bolt: A88 M20, plate: A_GB, $\sum t/d=2$)	128
Figure 7.7-1:Flowchart for bolt tightening qualification procedure (BTQP)	130
Figure 8.3-1: Improved three step test procedure of the slip factor test acc. to Annex G of EN 1090-2	134
Figure 8.3-2: Positions of measurement of the slip.....	134

10 List of tables

Table 2.3-1: Test programme of Task 1.1, mean slip factors based on static and creep tests only ($\mu_{ini,mean}$ and $\mu_{act,mean}$) with LVDTs 1–8 (CBG position).....	15
Table 2.3-2: Mean static slip factor results based on LVDTs 9-12 (PE position).....	18
Table 2.4-1: Test specimens and surface conditions for slip tests in Task 1.2.....	20
Table 2.4-2: Results of Task 1.2 - influence of the test duration on the slip factor	23
Table 2.5-1: Compared results for Task 1.3, achieved from Task 1.1	25
Table 2.6-1: Overview of test campaign in Task 1.4	26
Table 2.7-1: Task 1.5 – Test matrix for System HR and HV bolting assemblies	30
Table 2.7-2: Summary of the evaluation of tightening tests acc. to EN 14399-3 and EN 14399-4.....	31
Table 2.7-3: Summary of the evaluation of the modified torque method and modified combined method acc. to DIN EN 1993-1-8/NA for all tested carbon steel HR/HV bolting assemblies	33
Table 3.3-1: Test specimens and surface conditions.....	37
Table 3.3-2: Results quasi static slip factor tests	37

Table 3.3-3: Influence of preload on long term slip factor	38
Table 3.4-1: Mean slip factors based on static and creep tests only ($\mu_{ini,mean}$ and $\mu_{act,mean}$) as well as final slip factors calculated as 5% fractile or determined in the extended creep test ($\mu_{5\%}$ or μ_{ect})	40
Table 3.5-1: Calibration factors	47
Table 3.5-2: Actual preload levels obtained in the testing programme	48
Table 4.3-1: Test matrix with specimen acc. EN 1090-2 (4 bolts [preload values] per test)	51
Table 4.3-2: Results for the preloads obtained over all tests includes different faying surfaces	52
Table 4.3-3: Results of the slip load tests	53
Table 4.3-4: Description of test sections	54
Table 4.3-5: Description of points of analysis.....	54
Table 4.3-6: Results of torque/clamp load tests with washers from company FUCHS.....	55
Table 4.4-1: Summary of test planned and performed.....	56
Table 4.4-2: Experimental parameters for double shear connections with injection bolts	57
Table 4.5-1: Proper thickness of the feeler gauge	63
Table 4.5-2: Results of compression tests	64
Table 5.3-1: Coating systems with different surface preparations	68
Table 5.3-2: Material properties of steel plates in Task 4.1	69
Table 5.3-3: Test matrix ethyl silicate zinc series (series A)	69
Table 5.3-4: Test matrix epoxy series (series B).....	69
Table 5.3-5: Results of slip factor tests series A: Ethyl Silicate Zinc coating	71
Table 5.3-6: Results of creep tests.....	71
Table 5.3-7: Results corrosion protection tests series A	72
Table 5.3-8: Results corrosion protection tests series B	73
Table 5.4-1: Test programme, mean slip factors based on static and creep tests only ($\mu_{ini,mean}$ and $\mu_{act,mean}$) as well as final slip factors calculated as 5 % fractile or determined in the extended creep test ($\mu_{5\%}$ or μ_{ect})	74
Table 5.4-2: Relaxation test matrix/results	77
Table 5.5-1: Coating systems for examinations in regard to corrosion protection	79
Table 5.5-2: Test matrix.....	79
Table 5.5-3: Results of corrosion protection tests for System A and N	79
Table 5.5-4: Results on slip load test of test series A-ESI-3-n.....	82
Table 5.5-5: Results of slip load test of test series B-ESI-1-o and C-ESI-1-n.....	83
Table 6.3-1: Mean mechanical properties of the investigated materials.	85
Table 6.3-2: Loading levels used for room temperature constant load creep tests.	85
Table 6.3-3: Load levels and loading rates used in the repeated relaxation tests. Continuous 12-hour relaxation tests also were conducted for comparison purposes.....	86
Table 6.3-4: Chaboche model parameters for the plate materials.	89
Table 6.3-5: Measured and extrapolated loss of preload (mean values) from instrumented preloaded connections (reused bolts) (Task 5.3).	90
Table 6.4-1: Mean tensile properties of the tested bar material in comparison with cold forged bolts.	91
Table 6.4-2: Mean values for the initial stress (σ_0) and constant strain (ϵ_0) for the 12 h stress relaxation (σ_r) testing together with the standard deviation (SD) of the stress relaxation and the residual inelastic strain ($\epsilon_{res.}$) after 12 h.	92
Table 6.4-3: Found parameter values from solving equation (9.4-3), mean value of two measurements.	94
Table 6.5-1: Task 5.3 – Test matrix for stainless steel tightening tests (STEP 1)	96

Table 6.5-2: Task 5.3 – Nominal mechanical properties of stainless steel bolting assemblies [© BUMAX]	97
Table 6.5-3: Summary of the evaluation of stainless steel tightening tests according to EN 14399-3 (valid for clamp lengths: $2d \leq \sum t \leq 6d$)	98
Table 6.6-1: Task 5.4 – Test matrix for stainless steel tightening tests (STEP 2)	104
Table 6.6-2: Task 5.4 – Test matrix for stainless steel tightening tests (STEP 3)	104
Table 6.6-3: Overview about used types of lubrication according to manufacturer specifications	105
Table 6.6-4: Task 5.4 – Summary of the evaluation of lubrication tests	105
Table 6.6-5: Task 5.4 – Summary of the evaluation of additional stainless steel tightening tests according to EN 14399-3 (used lubrication: Molykote 1000 and Molykote D-321R spray)	106
Table 6.6-6: Task 5.4 – Summary of the evaluation of tightening tests with Interflon [®] HT1200 spray and paste	108
Table 6.7-1: Parameters of Chaboche material model	109
Table 7.3-1: Surface roughness of plate surfaces before the slip factor test (results from University of Duisburg-Essen)	115
Table 7.4-1: Test programme, mean slip factors based on static and creep tests ($\mu_{ini,mean}$ and $\mu_{act,mean}$) and characteristic values (final slip factors) calculated as 5%-fractile: $\mu_{5\%}$ or resulting from extended creep tests: μ_{ect}	118
Table 7.5-1: Test programme, mean slip factors based on static and creep tests ($\mu_{ini,mean}$ and $\mu_{act,mean}$) and characteristic values (final slip factors) calculated as 5%-fractile: $\mu_{5\%}$ or resulting from extended creep tests: μ_{ect}	121
Table 7.6-1: Summary of tests results and calibration of numerical model (selected results)	125
Table 7.6-2: Predicted loss of preload in bolted assemblies made of stainless steel and comparison with FE results (selected cases)	126
Table 7.7-1 Slip factor, μ , for preloaded stainless steel bolted connections	131
Table 8.4-1 Slip factors for various surface treatments achieved in SIROCO and compared to FprEN 1090-2	135

11 List of acronyms

$(CF)_{act,\mu}$	Mean observed calibration factor
$(CF)_{ch}$	Characteristic calibration factor (95% exceedance prob.)
1D	The as-received hot rolled surface
α	Parameter used for describing the logarithmic creep
α_A	Tightening factor (VDI 2230)
β	Parameter used for describing the logarithmic creep
Δ_{max}	Maximum difference between measured preload and constant tensile load
$\Delta\theta_{1i}$	The angle difference is defined as $(\theta_{1i} - \theta_{pi})$ and corresponds to the point at which the maximum bolt force $F_{bi,max}$ has been reached
$\Delta\theta_{2i}$	The angle difference is defined as $(\theta_{2i} - \theta_{pi})$ and corresponds to the point at which the test has been stopped
ϵ	Strain
ϵ_0	Initial strain at the start of stress relaxation test
ϵ_{res}	Residual inelastic strain after stress relaxation test (unloaded)
$\dot{\epsilon}$	Strain rate
θ_{1i}	The angle of nut rotation at which the bolt force reaches its maximum value $F_{bi,max}$
θ_{2i}	The angle of nut rotation at which the tightening test is stopped
θ_{pi}	The angle of nut rotation at which the bolt force first reaches the value of $F_{p,c}$
μ	Slip factor

$\mu_{5\%}$	Slip factors as 5 % fractile calculated on the basis of the static tests and the creep test passed
$\mu_{act,mean}$	Calculated slip factors as mean values considering the actual preload at slip
μ_b	Coefficient of friction in the head bearing area
$\mu_{b, 0.75F_p}$	Friction coefficient of the bolt thread at proof load F_p (DIN 898-1)
$\mu_{b, F_p,C}$	Friction coefficient of the bolt thread at preload $F_{p,C}$
μ_{b, F_p,C^*}	Friction coefficient of the bolt thread at preload F_{p,C^*}
$\mu_{b, F_p,C,H360}$	Friction coefficient of the bolt thread at preload $F_{p,C,H360}$
μ_{ect}	Slip factor resulting from the extended creep test passed
μ_{ini}	Initial Slip factor
$\mu_{ini,mean}$	Calculated slip factors as mean values considering the initial preload when the tests started
$\mu_{nom,exp}$	Nominal preload level form experimental investigation
μ_{th}	Coefficient of friction in the thread
μ_{tot}	Total coefficient of friction
σ	Stress or Standard deviation
σ_0	Initial stress at the start of stress relaxation test
σ_i	Measured stress in relaxation test
σ_r	Amount of stress relaxation during stress relaxation testing
σ_{relax}	Stress relaxation
σ^*	Internal state variable describing the strength of dislocation substructures in the material in Hart's model
$\Sigma t / d$	Clamping length ratio
Σt	Clamping length
A	Bolt area (actual or nominal) or Fracture elongation (calculated proportional length)
A_{gt}	Total uniform elongation
Al-SM	Aluminium spray metallized (coating)
ARP	ARUP
A_s	Stress cross section of the bolt thread
ASi-Zn/ ASI	Alkali-zinc silicate (coating)
BUMAX	BUMAX AB
CBG	Centre bolts group
CF	Actual calibration factor
CL	Clam packet length
COV	Coefficient of variation
CS	Carbon Steel
ct	Creep
DFT	Dry Film Thickness (coating thickness)
DTI	Direct Tension Indicators
E	Young's Modulus (actual or nominal)
ECT	Extended Creep Test
ect	Extended creep test
EGGA	European General Galvanizers Association
ER	Elastic recovery of the bolt when the specimen is unloaded
ESI	Ethyl-silicate-zinc (coating)
EXCT/ ect	Extended creep test acc. to EN 1090-2, Annex G.5
$F_{0.4} / F_{p,C}$	Relative load at gap of 0.4 mm
$F_{0.4}$	Compression load at gap of 0.4 mm
FAGP	Fraunhofer AGP
$f_{b, resin}$	Bearing strength of an injection bolt

$F_{bi,max}$	Maximum individual bolt force within a tightening test
FE	Finite element
F_{max}	Maximum compression load
F_p	Proof load according to DIN 898-1
$F_{p,C}$	Preload level = $0.7 \times f_{ub} \times A_s$
$F_{p,C}^*$	Preload level = $0.7 \times f_{yb} \times A_s$
$F_{p,C,H360}$	Nominal preload for H360 given by the manufacturer Arconic
$F_{p,C,nom}$	Nominal preload level
F_{Sm}	Mean value of the slip load
$F_{Sm(150\mu m)}$	Equal to F_{Sm} slip load at $\delta_{mean} = 150 \mu m$
$F_{Sm,max}$	Maximum load of the slip load test
f_{ub}	Nominal tensile strength of the bolt
F_{yield}	Load at yield point in torque/clamp test
GB	Grit blasted surface
GUI	Graphical user interface
H	Mean value correction factor
HDG	Hot-dip Galvanized (coating)
HSFG	High strength friction grip
IKS	Institute for Corrosion Protection Dresden GmbH
K	Coefficient of friction or Parameter used for describing the inelastic response during stress relaxation testing
k	Parameter used for describing the logarithmic creep rate
LB	Lockbolt
LC	Load Cell
LVDT	Linear Variable Differential Transformer
m	Parameter used for describing the logarithmic creep rate
M	Parameter used for describing the inelastic response during stress relaxation testing
M_A	Torque (tightening)
n	Number of test results
$n_{refusal}$	Number of feeler gauge refusals
OSAB	Outokumpu Stainless AB
OSOY	Outokumpu Stainless OY
PE	Plate edges
R_m	Tensile strength
$R_{p0.2}$	Proof stress at 0.2 % plastic strain
$R_{p1.0}$	Proof stress at 1.0 % plastic strain
RSS	Residual sum of squares
R_z	Average distance between the highest peak and lowest valley in the surface
Sa	Blast-cleaning grade of surface preparation
SB	Shot blasted surface
SCI	The Steel Construction Institute
SD	Standard deviation
SG	Strain Gauge
sp	Step test
SS	Stainless Steel
SSWL	Short Step Wise Loading
st	Static test
t	Time
$T_{0.75 Fp}$	Torque at 75 % of proof load F_p (DIN 898-1)

$T_{F_p,C}$	Torque at preload $F_{p,C}$
T_{F_p,C^*}	Torque at preload F_{p,C^*}
T_{H360}	required torque for H360 to reach the nominal preload $F_{p,C,H360}$ (defined by the manufacturer Arconic)
TUD	Delft University of Technology
T_{yield}	Torque at yield point in torque/clamp test
UDE	University of Duisburg-Essen, Institute for Metal and Lightweight Structures
UTM	Universal Testing Machine
$V(\mu_{act})$	Coefficient of variation for μ_{act}
v_F	Testing rate
VTT	VTT, Technical Research Centre of Finland, Ltd.
V_x	Coefficient of variation (deviation s / mean value m)
Zn-SM	Zinc spray metallized (coating)

12 List of references

- 5.3-1 EN 1090-2:2008+A1:2011 (2011). "Execution of steel structures and aluminium structures – Part 2: Technical requirements for steel structures".
- 5.3-2 EN 14399-4:2015: High-strength structural bolting assemblies for preloading – Part 4: System HV – Hexagon bolt and nut assemblies.
- 5.3-3 EN 14399-6:2015: High-strength structural bolting assemblies for preloading – Part 6: Plain chamfered washers.
- 5.3-4 Cruz, A.; Simões, R.; Alves, R.: Slip factor in slip resistant joints with high strength steel. *Journal of Constructional Steel Research* 70 (2012), No. 3, pp. 280–288.
- 5.4-1 RCSC 2014, Specification for Structural Joints Using High-Strength Bolts, August 1, 2014 (includes April 2015 Errata), RESEARCH COUNCIL ON STRUCTURAL CONNECTIONS, Chicago, Illinois, USA.
- 5.7-1 EN 14399-3:2015: High-strength structural bolting assemblies for preloading – Part 3: System HR – Hexagon bolt and nut assemblies.
- 5.7-2 EN 14399-2:2015: High-strength structural bolting assemblies for preloading - Part 2: Suitability for preloading
- 5.7-3 EN ISO 16047:2013-01, Fasteners — Torque/clamp force testing (ISO 16047:2005 + Amd 1:2012)
- 5.7-4 DIN EN 1993-1-8/NA:2010-12, National Annex – Nationally determined parameters – Eurocode 3: Design of steel structures – Part 1-8: Design of joints.
- 6.5-1 Wang, T., Song, G., Liu, S., Li, Y., Xiao, H.: Review of Bolted Connection Monitoring. *International Journal of Distributed Sensor Networks* 9 (2013), Nr. 12, S. 871213. Review of Bolted connection monitoring (November. 2013). *International Journal of Distributed Sensor Networks*, Volume 2013, Article 871213.
- 6.5-2 Liu, S., Li, Y., Wang, T., Luo, Y.: A piezoelectric active sensing method for detection of bolt load loss. *Sensor Review* 34 (2014), Nr. 4, S. 337-342.
- 6.5-3 Mohammadi, S.R.S., Matos, R., Rebelo, C.: Bobtail Bolt Preload Loss in Wind Turbine Tower Prototype: Hammerstein-Wiener Identification Model. *Eurosteel Conference 2017*. Copenhagen: Ernst & Sohn, 2017.
- 6.5-4 NEN Normcommissie 104. Voorlopige richtlijnen voor het ontwerpen en de uitvoering van verbindingen met voorspanbouten in staalconstructies. Delft: Nederlands Normalisatie Instituut, 1968.
- 6.5-5 Rijkswaterstaat: Richtlijnen ontwerpen kunstwerken (ROK 1.3). Utrecht: Ministerie van Infrastructuur en Milieu, 2015.
- 6.5-6 Kulak, G.L., Fisher, J.W., Struik, J.H.A.: *Guide to Design Criteria for Bolted and Riveted Joints*. Chicago: American Institute of Steel Construction, 2001.
- 6.5-7 de Vries, P., Nijgh, M., Veljkovic, M.: Determining the preload in preloaded bolt assemblies in existing steel structures. *Steel Construction* 10 (2017), Issue 4, p. 282-286.
- 7.3-1 VDI 2230 Blatt 1:2015-11: Systematische Berechnung hochbeanspruchter Schraubenverbindungen - Zylindrische Einschraubenverbindungen.
- 7.3-2 DIN EN ISO 16047:2013-01: Verbindungselemente - Drehmoment/Vorspannkraft-Versuch (ISO 16047:2005 + Amd 1:2012); Deutsche Fassung EN ISO 16047:2005 + A1:2012.
- 7.4-1 M. P. Nijgh, M. v. Arnim, M. Pavlovic und M. Veljkovic, „Preliminary assessment of a composite flooring system for reuse,“ in 8th International Conference on Composite Construction in Steel and Concrete , Jackson, 2017.
- 7.4-2 A. M. P. De Jesus, J. F. N. Da Silva, M. V. Figueiredo, A. S. Ribeiro, A. A. Fernandes, J. A. F. O. Correia, A. L. L. Da Silva and J. M. C. Maeiro, "Fatigue behaviour of resin-injected bolts – An experimental approach,“ in Iberian Conference on Fracture and Structural Integrity, 2010.
- 7.4-3 J. A. F. O. Correia, A. M. P. De Jesus, C. Rebelo and L. S. Da Silva, "Fatigue behaviour of single and double shear connections with resin-injected preloaded bolts.,“ in 19th Congress of IABSE, Stockholm, 2016.
- 7.4-4 A. M. Gresnigt and P. De Vries, "Injection bolts update on research and applications,“ 2016.
- 7.4-5 EN1993-1-8 - Eurocode 3: Design of steel structures – Part 1-8: Design of Joints, Delft: NEN, 2005.
- 7.4-6 A. M. Gresnigt and D. Beg, "Design bearing stresses for injection bolts with short and long duration high loads,“ *Research and Applications in Structural Engineering, Mechanics and Computation* , 2013.
- 7.4-7 ECCS, European recommendations for bolted connections with injection bolts, ECCS pub. No. 79, Brussels: ECCS, 1994.
- 7.4-8 M. P. Nijgh, "New materials for injected bolted connections – A feasibility study for demountable connections,“ Delft, 2017.
- 7.5-1 EN 14399-9:2009: High-strength structural bolting assemblies for preloading – Part 9: System HR or HV – Direct tension indicators for bolt and nut assemblies.

- 7.5-2 EN 10025-2:2004, Hot rolled products of structural steels - Part 2: Technical delivery conditions for non-alloy structural steels.
- 7.5-3 EN ISO 4287:2010-07: Geometrical Product Specifications (GPS) - Surface texture: Profile method - Terms, definitions and surface texture parameters (ISO 4287:1997 + Cor 1:1998 + Cor 2:2005 + Amd 1:2009); German version EN ISO 4287:1998 + AC:2008 + A1:2009.
- 8.3-1 EN ISO 12944-4:1998-07: Paints and varnishes - Corrosion protection of steel structures by protective paint systems - Part 4: Types of surface and surface preparation (ISO 12944-4:1998); German version EN ISO 12944-4:1998
- 8.3-2 ISO 9227:2017-07. Corrosion tests in artificial atmospheres - Salt spray tests; German version EN ISO 9227:2017.
- 8.3-3 ISO 6270-1:2017-11. Paints and varnishes - Determination of resistance to humidity - Part 1: Condensation (single-sided exposure).
- 8.3-4 EN ISO 2409:2013-06: Paints and varnishes - Cross-cut test (ISO 2409:2013); German version EN ISO 2409:2013
- 8.3-5 ISO 4624:2016-08. Paints and varnishes - Pull-off test for adhesion; German version EN ISO 4624:2016
- 8.5-1 ISO 2808:2007-05. Paints and varnishes- Determination of film thickness; German version EN ISO 2808:2007
- 9.3-1 S.P. Hannula, C.Y. Li, Repeated load relaxations of type 316 austenitic stainless steel, Scripta Metallurgica, volume 18, issue 3, March 1984, 225-229.
- 9.3-2 E.W. Hart, C.-Y. Li, H. Yamada, G.L. Wire, Phenomenological theory: a guide to constitutive relations and fundamental deformation properties, Constitutive Equations in Plasticity. 171 (1975) 149–197.
- 9.3-3 M. E. Kassner, K. Smith, Low temperature creep plasticity, Journal of materials research and technology, 3(3), 2014, pp. 280-288.
- 9.3-4 J.L. Chaboche, G. Rousselier, On the plastic and viscoplastic constitutive equations - Part I: Rules developed with internal state variable concept, Journal of Pressure Vessel Technology. 105 (1983) 153–158.
- 9.3-5 J.L. Chaboche, G. Rousselier, On the plastic and viscoplastic constitutive equations - Part II : Application of the internal state variable rules to the 316 stainless steel, Journal of Pressure Vessel Technology. 105 (1983) 159–163.
- 9.3-6 J. Lemaitre, J.-L. Chaboche, Mechanics of solid materials, Cambridge university press, 1994.
- 9.3-7 M. Tendo, Y. Shimura, Stress relaxation behavior at high-tension bolted connections of stainless-steel plates, Journal of engineering materials and technology, vol. 123, April 2001, pp. 198-202.
- 9.3-8 W. Schmidt, H. Dietrich, Einfluss einer kaltverformung auf den zusammenhang zwischen raumtemperaturekriechen und Bauschinger-effekt, Thyssen Edelst. Techn. Ber., 7. Band, 1981, Heft 1, pp. 41-54.
- 9.4-1 E.W. Hart, Constitutive relations for the nonelastic deformation of metals, Journal of Engineering Materials and Technology. 98 (1976) 193–202.
- 9.4-2 M. Boniardi, G. M. La Vecchia, R. Roberti, Stress relaxation behaviour in duplex and super duplex stainless steels, Duplex stainless steels, Glasgow, Scotland, 13-16, November 1994, paper 110.
- 9.4-3 S.P. Hannula, M. A. Korhonen, C.Y. Li, Strain aging and load relaxation behavior of type 316 stainless steel at room temperature, Metallurgical and Materials Transactions A, 17 (1986), 1757-1767.
- 9.4-4 H. Yamada, C.-Y. Li, Stress relaxation and mechanical equation of state in austenitic stainless steels, Metallurgical Transactions. 4 (1973) 2133–2136.
- 9.5-1 EN ISO 4014:2011, Hexagon head bolts — Product grades A and B (ISO 4014:2011)
- 9.5-2 EN ISO 4017:2014, Fasteners – Hexagon head screws — Product grades A and B (ISO 4017:2014)
- 9.5-3 EN ISO 4032:2013-04, Hexagon regular nuts (style 1) — Product grades A and B (ISO 4032:2012)
- 9.5-4 EN ISO 7089:2000-11, Plain washers — Normal series, Product grade A (ISO 7089:2000)
- 9.5-5 EN ISO 898-1:2013, Mechanical properties of fasteners made of carbon steel and alloy steel – Part 1: Bolts, screws and studs with specified property classes – Coarse thread and fine pitch thread (ISO 898-1:2013).
- 10.7-1 EN ISO 3506-1:2009, Mechanical properties of corrosion-resistant stainless steel fasteners – Part 1, Bolt, screws and studs (ISO 3506-1:2009)
- 10.7-2 EN ISO 3506-2:2009, Mechanical properties of corrosion-resistant stainless steel fasteners – Part 2, Nuts (ISO 3506-2:2009)
- 10.7-3 EN 15048-1:2016: Non-preloaded structural bolting assemblies - Part 1: General requirements; German version EN 15048-1:2016

Appendix A – Design Example

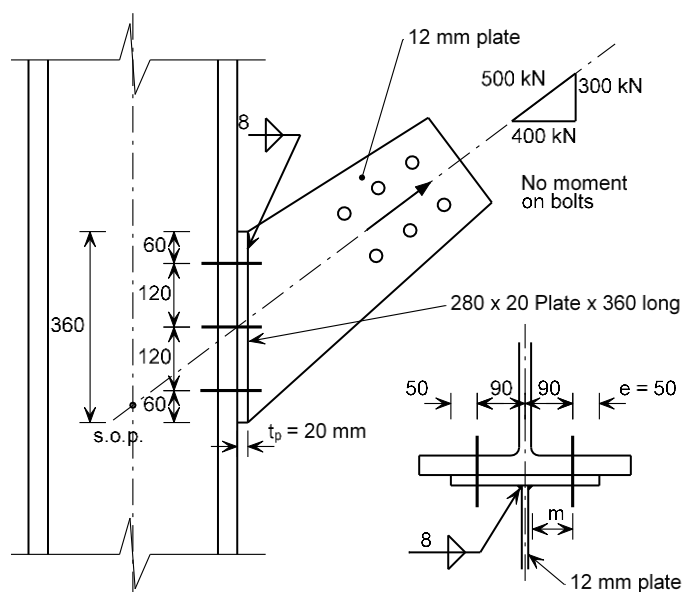
Two worked examples are provided to illustrating the application of design equations and slip factors for design of stainless steel slip-resistant connections.

1 Design Example 1 – Connection of Tensile Bracing Member

Check the slip resistant connection of a diagonal stainless steel bracing member to a stainless steel fabricated column, in accordance with EN 1993-1-8 and EN 1993-1-4. (It is based on Example 6 of The Steel Construction Institute's publication P324 Tension Control Bolts¹.)

1.1 Structure

The connection is shown below:



356 x 406 x 287 fabricated section

All material Duplex 1.4462

6 M24 preloaded Bumax 88 austenitic stainless steel bolts

NOTE

Loading = 500 kN tension ULS

Grit blasted finish to the faying surface

Stainless steel bolts are in accordance with EN ISO 4017 (full threaded bolts).

1.2 Action

Permanent and variable actions result in a vertical design shear force and a design tension force equal to:

$$V_{Ed} = 300 \text{ kN}$$

$$F_{Ed} = 400 \text{ kN}$$

1.3 Geometric properties

$$t_p = 20 \text{ mm (end plate thickness)}$$

$$m = 90 - 12/2 - 8 = 76 \text{ mm (distance from bolt centre to toe of weld)}$$

$$e = e_{min} = 50 \text{ mm (edge distance)}$$

EN 1993-1-8,

Figure 6.2

¹ Tension Control Bolts, Grade S10T, in Friction Grip Connections, P324, The Steel Construction Institute, Ascot, 2004

$A_s = 353 \text{ mm}^2$ (M24 bolt tensile stress area)

1.4 Material properties

Duplex plate 1.4462 ($13.5 \text{ mm} \leq t \leq 75 \text{ mm}$)

EN 10088-4

$$f_{yp} = 460 \text{ N/mm}^2 \quad f_{up} = 640 \text{ N/mm}^2$$

Bumax 88 austenitic bolt (equivalent to carbon steel bolt of class property 8.8)

$$f_{yb} = 640 \text{ N/mm}^2 \quad f_{ub} = 800 \text{ N/mm}^2$$

1.4.1.1 Slip factor

$\mu = 0.5$ for duplex grit blasted surface²

1.5 Design resistance – Plate and bolts

Resistance of end plate

EN 1993-1-8,

Basic requirement:

Clause 6.2.4.1(6)

$$F_{Ed} \leq \min(F_{T,1,Rd}; F_{T,2,Rd}; F_{T,3,Rd})$$

where $F_{T,Rd}$ is the design tension resistance of a T-stub flange

1.5.1.1 Mode 1

$$F_{T,1,Rd} = \frac{(8n - 2e_w) M_{pl,Rd}}{2mn - e_w(m + n)}$$

EN 1993-1-8,
Table 6.2

The effective length of the equivalent T-stub $\Sigma l_{eff} = 360 \text{ mm}$

EN 1993-1-8,
Figure 6.2

$$M_{pl,Rd} = \frac{0.25 \Sigma l_{eff} t_p^2 f_{yp}}{\gamma_{M0}} = \frac{0.25 \times 360 \times 20^2 \times 460}{1.1} \times 10^{-6} = 15.1 \text{ kNm}$$

where $\gamma_{M0} = 1.1$ for stainless steel

EN 1993-1-4,
Table 5.1

Assuming no washer is used, from EN ISO 4017 for M24 setscrews $d_w = 33.25 \text{ mm}$

EN ISO 4017

$$e_w = \frac{d_w}{4} = \frac{33.25}{4} = 8.31 \text{ mm}$$

$n = e_{min}$ but $\leq 1.25m$

$n = e_{min} = e_2 = 50 \text{ mm}$; $1.25m = 1.25 \times 76 = 95 \text{ mm}$

$n = 50 \text{ mm}$

$$F_{T,1,Rd} = \frac{(8 \times 50 - 2 \times 8.31) \times 15.1 \times 10^3}{2 \times 76 \times 50 - 8.31 \times (76 + 50)} = 883 \text{ kN}$$

1.5.1.2 Mode 2

$$F_{T,2,Rd} = \frac{2M_{pl,Rd} + n \Sigma F_{t,Rd}}{m + n}$$

EN 1993-1-8,
Table 6.2

$$F_{t,Rd} = \frac{k_2 f_{ub} A_s}{\gamma_{M2}} = \frac{0.9 \times 800 \times 353}{1.25} \times 10^{-3} = 203 \text{ kN}$$

EN 1993-1-8,
Table 3.4

² Execution and reliability of slip-resistant connections for steel structures using CS and SS (SIROCO), RFCS research project, Deliverable 7.2 Guidelines for design and execution 2018

$$F_{T,2,Rd} = \frac{2 \times 15.1 \times 10^3 + 50 \times 6 \times 203 \times 10^3}{76 + 50} \times 10^3 = 484 \text{ kN}$$

1.5.1.3 Mode 3

$$F_{T,3,Rd} = \Sigma F_{t,Rd} = 6 \times 203 = 1218 \text{ kN}$$

EN 1993-1-8,
Table 6.2

$$\min(F_{T,1,Rd}; F_{T,2,Rd}; F_{T,3,Rd}) = \min(883; 484; 1218) = 484 \text{ kN}$$

$$F_{Ed} = 400 \text{ kN} \leq 484 \text{ kN}$$

∴ **OK**

Note: In accordance with EN 1993-1-8 Table 3.2, the punching shear resistance $B_{p,Rd}$ should also be checked for tension connections.

1.6 Resistance of bolts under combined shear and tension

EN 1993-1-8,
Table 3.4, Clause
3.6

Basic requirement:

$$\frac{F_{v,Ed}}{F_{v,Rd}} + \frac{F_{t,Ed}}{1.4F_{t,Rd}} \leq 1.0$$

Shear resistance of stainless steel bolt:

EN 1993-1-4,
Clause 6.2

$$F_{v,Rd} = \frac{\alpha f_{ub} A}{\gamma_{M2}}$$

$\alpha = 0.5$ and $A = A_s$ since fully threaded bolt (EN ISO 4017) are assumed to be used

$\gamma_{M2} = 1.25$ for stainless steel

EN 1993-1-4,
Table 5.1

$$F_{v,Rd} = \frac{\alpha f_{ub} A_s}{\gamma_{M2}} = \frac{0.5 \times 800 \times 353}{1.25} \times 10^{-3} = 113 \text{ kN}$$

$$F_{t,Rd} = \frac{k_2 f_{ub} A_s}{\gamma_{M2}} = \frac{0.9 \times 800 \times 353}{1.25} \times 10^{-3} = 203 \text{ kN}$$

$$F_{v,Ed} = \frac{V_{Ed}}{6} = \frac{300}{6} = 50 \text{ kN} \text{ and } F_{t,Ed} = \frac{F_{Ed}}{6} = \frac{400}{6} = 66.7 \text{ kN}$$

$$\frac{F_{v,Ed}}{F_{v,Rd}} + \frac{F_{t,Ed}}{1.4F_{t,Rd}} = \frac{50}{113} + \frac{66.7}{1.4 \times 203} = 0.68 \leq 1.0$$

∴ **OK**

1.7 Slip resistance of preloaded bolts

Basic requirement for slip-resistance at ultimate (Category C):

EN 1993-1-8,
Table 3.2

$$F_{v,Ed} \leq F_{s,Rd}$$

Slip resistance for combined tension and shear:

$$F_{s,Rd} = \frac{k_s n \mu (F_{p,C} - 0.8F_{t,Ed})}{\gamma_{M3}}$$

k_s is 1.0 for bolts in normal holes

n is the number of friction planes = 1

Slip factor $\mu = 0.5$ for duplex plate with grit blasted surface finish

$$\gamma_{M3} = 1.25$$

$$F_{p,C} = 0.7f_{ub}A_s = 0.7 \times 800 \times 353 \times 10^{-3} = 197.7 \text{ kN}$$

$$F_{s,Rd} = \frac{1.0 \times 1 \times 0.5 \times (197.7 - 0.8 \times 66.7)}{1.25} = 57.7 \text{ kN}$$

$$F_{v,Ed} = 50 \text{ kN} \leq F_{s,Rd} = 57.7 \text{ kN}$$

EN 1993-1-8,
Clause 3.9.2(1)
and SIROCO
D7.2³

EN 1993-1-8,
Table 3.6

∴ **OK**

Thus the slip resistant connection has adequate resistance to the member axial load.

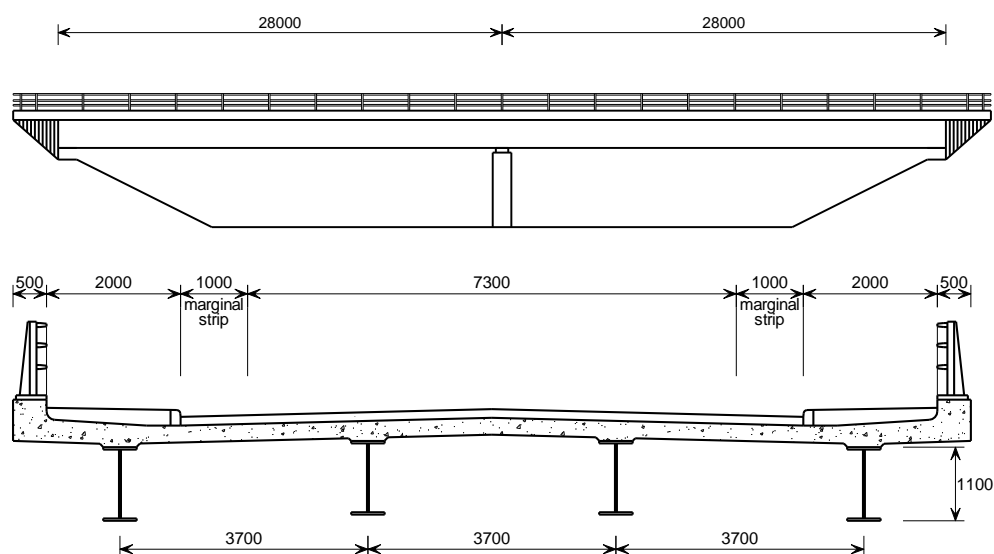
Note: In accordance with EN 1993-1-8 Table 3.2 for Category C connections, the bearing resistance $F_{b,Rd}$ should be checked (EN 1993-1-8 Table 3.4) and the net section resistance $N_{net,Rd}$ should be checked (EN 1993-1-1 clause 6.2.3).

³ Execution and reliability of slip-resistant connections for steel structures using CS and SS (SIROCO), RFCS research project, Deliverable 7.2 Guidelines for design and execution, 2018

2 Design Example 2 – Main girder splice

This example demonstrates the design of a main girder splice in a bridge carrying a 2-single carriageway rural road over another road. Duplex structural stainless steel (1.4462) and austenitic preloaded bolts (BUMAX 88) are assumed to be used in the design. The surface finish of the splice connection is assumed to be grit blasted.

A four-girder arrangement has been chosen for this bridge and the complete design is available in P357 *Composite Highway Bridge Design: Worked Examples*⁴. The structural arrangement of the bridge is shown below. The configuration and dimensions of the main girder splice is presented in Section 2.2.2.



The fabricated stainless steel girders are 1100 mm in depth. The size of the girder plates are presented in the table below.

	21.7 m span girder		12.6 m pier girder	21.7 m span girder	
Top flange	500 × 40		500 × 40	500 × 40	
Web	12	10	14	10	12
Bottom flange	500 × 40		600 × 60	500 × 40	

2.1 Force and moment

Design values of the effects of the combined actions for the design situations are given in P357. The following calculations present the force and moments at the splice position.

The hogging moment and shear will be considered here, because the maximum sagging moment is smaller than the maximum hogging moment.

P357, Page 25
Example 1

Design force for top flange splice

$$F_{\text{tf,Ed}} = 1226 \text{ kN at ULS}$$

⁴ Composite Highway Bridge Design: Worked Examples, P357, The Steel Construction Institute, Ascot, 2014

This is the design force calculated for the construction stage. It is more onerous than in the final situation, where the stresses are of similar magnitude but the flange is restrained against buckling and no amplification is needed.

Design force for bottom flange splice

$$F_{bf,Ed} = -3960 \text{ kN at ULS}$$

$$F_{bf,Ed,ser} = -3168 \text{ kN at SLS}$$

Design force for web splice

Design shear force, horizontal force and moment at ULS:

$$\text{Shear force at the web } V_{Ed} = 834 \text{ kN}$$

$$\text{Longitudinal force on the outer bolts in hogging } F_{L,Ed} = 609 \text{ kN}$$

$$\text{Total moment acting on the outer bolts in hogging } M_{Ed} = 201 \text{ kNm}$$

Design resultant force on the bolts at the web position due to total horizontal and vertical force

$$F_{b,Ed} = 169 \text{ kN at ULS}$$

$$F_{b,Ed,ser} = 134 \text{ kN at SLS}$$

2.2 Geometry and dimension

Bumax 88 M24 bolts in accordance with EN ISO 4017, in double shear in normal clearance holes:

$$d = 24 \text{ mm (nominal diameter)}$$

$$d_0 = 26 \text{ mm (hole diameter)}$$

$$A_s = 353 \text{ mm}^2 \text{ (tensile stress area)}$$

2.2.1 Bolt spacing and edge distance

Limiting spacings for M24 bolts, for strength:

EN 1993-1-8,
Table 3.3

$$\text{End and edge distances: } 1.2d_0 = 1.2 \times 26 = 31.2 \text{ mm}$$

$$\text{Spacing in direction of force: } 2.2d_0 = 2.2 \times 26 = 57.2 \text{ mm}$$

$$\text{Spacing perpendicular to force } 2.4d_0 = 2.4 \times 26 = 62.4 \text{ mm}$$

Limiting spacings for M24 bolts, for fatigue classification:

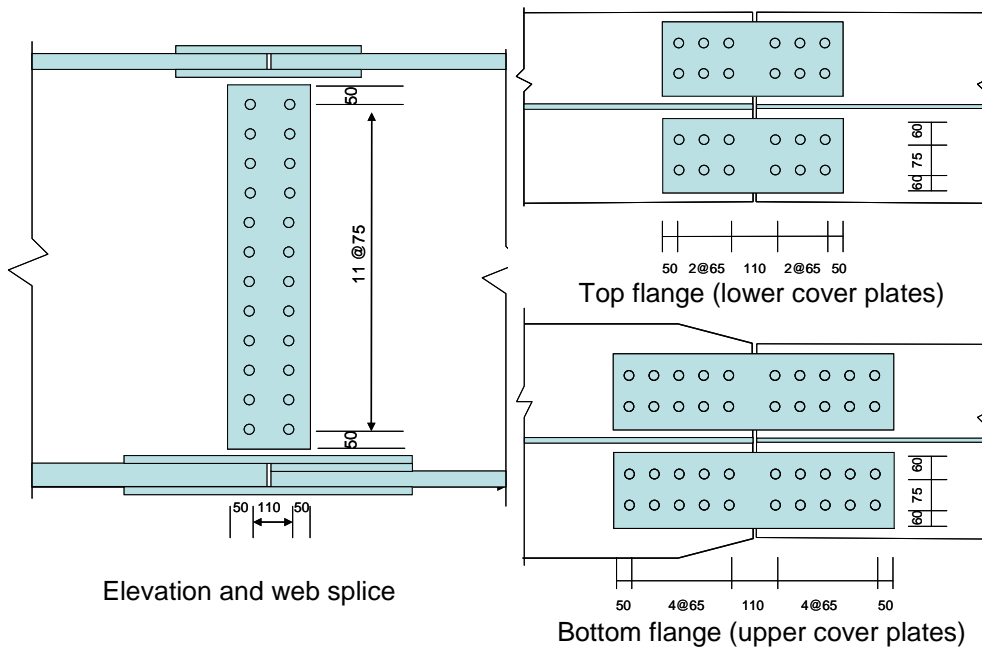
EN 1991-1-9,
Table 8.1

$$\text{End and edge distances: } 1.5d = 1.5 \times 26 = 39 \text{ mm}$$

$$\text{Spacing: } 2.5d = 2.5 \times 24 = 60 \text{ mm}$$

2.2.2 Splice configuration

Consider the following splice configuration:



Top flange splice

(Dimensions for lower covers)

Bolt spacing:

In line of force: $e_1 = 50 \text{ mm}$, $p_1 = 65 \text{ mm}$

Perpendicular to force: $e_2 = 60 \text{ mm}$, $p_2 = 75 \text{ mm}$

Overall dimension $470 \times 195 \text{ mm}$. Thickness 10 mm

Bottom flange splice

(Dimensions for upper covers)

Bolt spacing:

In line of force: $e_1 = 50 \text{ mm}$, $p_1 = 65 \text{ mm}$

Perpendicular to force: $e_2 = 60 \text{ mm}$, $p_2 = 75 \text{ mm}$

Overall dimension $730 \times 195 \text{ mm}$. Thickness 20 mm

Web splice

Bolt spacing:

In line of force: $e_1 = 50 \text{ mm}$, $p_1 = 110 \text{ mm}$

Perpendicular to force: $e_2 = 50 \text{ mm}$, $p_2 = 75 \text{ mm}$

Overall dimension $210 \times 925 \text{ mm}$. Thickness 10 mm

Minimum spacing, end and edge distance are satisfied.

EN 1993-1-8,
Table 3.3

2.3 Material properties

Duplex plate 1.4462

$f_{yp} = 460 \text{ N/mm}^2$ $f_{up} = 640 \text{ N/mm}^2$

EN 10088-4

$E = 200000 \text{ N/mm}^2$

EN 1993-1-4,
Clause 2.1.3

Bumax 88 austenitic bolt (equivalent to carbon steel bolt of class property 8.8)

$f_{yb} = 640 \text{ N/mm}^2$ $f_{ub} = 800 \text{ N/mm}^2$

Slip factor

$\mu = 0.5$ for duplex grit blasted surface⁵

SIROCO D7.2¹

2.4 Verification of connection resistance

Slip resistance of bolt

$$F_{s,Rd} = \frac{k_s n \mu}{\gamma_{M3}} F_{p,C}$$

SIROCO D7.2¹
EN 1993-1-8,
Clause 3.9.1

$$F_{s,Rd,ser} = \frac{k_s n \mu}{\gamma_{M3,ser}} F_{p,C}$$

$k_s = 1.0$ assuming normal round holes

$n = 2$ for two friction surfaces in double shear

$\mu = 0.5$ for duplex stainless steel plates with grit blasted surface finish

SIROCO D7.2¹

$\gamma_{M3} = 1.25$ and $\gamma_{M3,ser} = 1.1$

$$F_{p,C} = 0.7 f_{ub} A_s = 0.7 \times 800 \times 353 \times 10^{-3} = 198 \text{ kN}$$

$$F_{s,Rd} = \frac{k_s n \mu}{\gamma_{M3}} F_{p,C} = \frac{1.0 \times 2 \times 0.5}{1.25} \times 198 = 158 \text{ kN}$$

$$F_{s,Rd,ser} = \frac{k_s n \mu}{\gamma_{M3,ser}} F_{p,C} = \frac{1.0 \times 2 \times 0.5}{1.1} \times 198 = 180 \text{ kN}$$

Shear resistance of bolts

At ULS

$$F_{v,Rd} = \frac{\alpha f_{ub} A}{\gamma_{M2}}$$

$$\gamma_{M2} = 1.25$$

EN 1993-1-4,
Equation 6.2
EN 1993-1-4,
Clause 5.1

$\alpha = 0.5$ and $A = A_s$ since bolts are in accordance with EN ISO 4017 (fully threaded)

$$F_{v,Rd} = \frac{\alpha f_{ub} A}{\gamma_{M2}} = \frac{0.5 \times 800 \times 353}{1.25} = 113 \text{ kN}$$

In double shear $F_{v,Rd} = 226 \text{ kN}$

2.4.1 Top flange splice

There are 3 rows of bolts, with 4 bolts per row across the flange

A category C connection is required (the design situation is for resistance against buckling of the beam during construction)

Slip resistance at ULS

$$\Sigma F_{s,Rd} = 3 \times 4 \times F_{s,Rd} = 12 \times 158 \text{ kN} = 1896 \text{ kN} > F_{tf,Ed} = 1226 \text{ kN}$$

⁵ Execution and reliability of slip-resistant connections for steel structures using CS and SS (SIROCO), RFCS research project, Deliverable 7.2 Guidelines for design and execution, 2018

Note: In accordance with EN 1993-1-8 Clause 3.10.2, a block shear check should also be carried out.

2.4.2 Bottom flange splice

There are 5 row of bolts, with 4 bolts per row across the flange

A category B connection is required (the design situation is for resistance against compression in the flange in service)

Slip resistance at ULS

$$\Sigma F_{s,Rd} = 5 \times 4 \times F_{s,Rd} = 20 \times 158 \text{ kN} = 3160 \text{ kN} < F_{bf,Ed} = 3960 \text{ kN}$$

So the splice will slip into bearing at ULS

Bolt shear resistance at ULS

$$\Sigma F_{v,Rd} = 5 \times 4 \times F_{v,Rd} = 20 \times 226 \text{ kN} = 4520 \text{ kN} > F_{bf,Ed} = 3960 \text{ kN} \quad \therefore \text{OK}$$

Bolt bearing resistance at ULS

Bearing resistance per bolt at ULS is

$$F_{b,Rd} = \frac{k_1 \alpha_b f_{u,red} d t}{\gamma_{M2}} \quad \begin{array}{l} \text{EN 1993-1-8,} \\ \text{Table 3.4} \end{array}$$

$$f_{u,red} = 0.5f_y + 0.6f_u = 0.5 \times 460 + 0.6 \times 640 = 614 \text{ N/mm}^2 \quad \begin{array}{l} \text{EN 1993-1-4,} \\ \text{Clause 6.2(1)} \end{array}$$

$$f_{u,red} < f_{up} = 640 \text{ N/mm}^2$$

$$\gamma_{M2} = 1.25 \quad \begin{array}{l} \text{EN 1993-1-4,} \\ \text{Clause 5.1} \end{array}$$

Bolt spacings, for determination of factors k_1 and α_b

In line of force: $e_1 = 50 \text{ mm}$, $p_1 = 65 \text{ mm}$

Perpendicular to force: $e_2 = 60 \text{ mm}$, $p_2 = 75 \text{ mm}$

Since $f_{ub} > f_u$, $\alpha_b = \alpha_d$ (but ≤ 1) EN 1993-1-8,
Table 3.4

For end bolts: $\alpha_d = e_1/3d_0 = 50/(3 \times 26) = 0.64$

For inner bolts:

$$\alpha_d = \frac{p_1}{3d_0} - \frac{1}{4} = \frac{65}{3 \times 26} - \frac{1}{4} = 0.58$$

For edge bolts, k_1 is the smaller of:

$$\left[2.8 \frac{e_2}{d_0} - 1.7, \quad 1.4 \frac{p_2}{d_0} - 1.7, \quad 2.5 \right]$$

$$k_1 = \min(4.76, 2.34, 2.5) = 2.34$$

In the upper cover plates there is no 'inner' line of bolts (in the direction of force) and for the flange and lower cover, the mean value of p_2 that would apply is sufficient to ensure that $k_1 = 2.34$

$$F_{b,Rd} = \frac{k_1 \alpha_b f_u d t}{\gamma_{M2}} = \frac{2.34 \times 0.58 \times 614 \times 24 \times 20}{1.25} = 320 \text{ kN}$$

Bearing resistance of bolt group, with double covers $\Sigma F_{b,Rd} = 20 \times 2 \times 320 = 12800 \text{ kN} > F_{bf,Ed} = 3960 \text{ kN}$ **∴ OK**

Slip resistance at SLS

$\Sigma F_{s,Rd,ser} = 20 \times F_{s,Rd,ser} = 20 \times 180 \text{ kN} = 3600 \text{ kN} > F_{bf,Ed,ser} = 3168 \text{ kN}$ **∴ OK**

2.4.3 Web splice

Note: The directions of the resultant forces are not parallel to a plate edge. Resistance is determined assuming the force is in the horizontal direction.

For end bolts (there is only a single row, transverse to the force): EN 1993-1-8, Table 3.4
 $\alpha_b = \alpha_d = e_1/3d_0 = 50/(3 \times 26) = 0.64$

For edge bolts, k_1 is the smaller of:

$$\left[2.8 \frac{e_2}{d_0} - 1.7, \quad 1.4 \frac{p_2}{d_0} - 1.7, \quad 2.5 \right]$$

$$k_1 = \min(4.76, 2.34, 2.5) = 2.34$$

For inner bolts, k_1 is the smaller of:

$$\left[1.4 \frac{p_2}{d_0} - 1.7, \quad 2.5 \right]$$

$$k_1 = \min(2.34, 2.5) = 2.34$$

$$F_{b,Rd} = \frac{k_1 \alpha_b f_{u,red} d t}{\gamma_{M2}} = \frac{2.34 \times 0.64 \times 614 \times 24 \times 14}{1.25} = 247 \text{ kN}$$
 EN 1993-1-4, Clause 6.2(1)

where t is the minimum of the girder web thickness (14 mm) and the total cover plate thickness (20 mm).

The bearing resistance is greater than the resistance of the bolt in double shear (226 kN) so bolt double shear governs.

At ULS: $F_{s,Rd} = 158 \text{ kN} < F_{b,Ed} = 169 \text{ kN}$
 but $F_{v,Rd} = 226 \text{ kN} > F_{b,Ed} = 169 \text{ kN}$ **∴ OK**

At SLS: $F_{s,Rd,ser} = 180 \text{ kN} > F_{b,Ed,ser} = 134 \text{ kN}$, there no slip at service limit **∴ OK**

Note: In accordance with EN 1993-1-8 Clause 3.10.2, a block shear check should also be carried out.

2.5 Resistance of cover plate

The cover plates are verified as members in tension or compression, in accordance with EN 1993-1-4.

2.5.1 Top flange

The covers are in tension. Assume half of the load is carried in the lower cover plates. The force per cover plate thus $F_{Ed} = 1226/4 = 307 \text{ kN}$

$$\text{Area of gross cross section (A)} = 195 \times 10 = 1950 \text{ mm}^2$$

$$\text{Area of net section (A}_{net}) = 1950 - 2 \times 26 \times 10 = 1430 \text{ mm}^2$$

This is a Category C slip resistant connection, therefore the design tension resistance is given by:

$$N_{net,Rd} = \frac{A_{net}f_y}{\gamma_{M0}}$$

EN 1993-1-1,
Clause 6.2.3(4)
EN 1993-1-4,
Clause 5.1

$$\gamma_{M0} = 1.1$$

$$N_{net,Rd} = \frac{A_{net}f_y}{\gamma_{M0}} = \frac{1430 \times 460}{1.1} \times 10^{-3} = 598 \text{ kN} > F_{Ed} = 307 \text{ kN}$$

The maximum spacing of bolts is 110 mm and the limiting spacing is given by Table 3.3 as the smaller of $14t$ ($= 140$ mm) and 200 mm. The spacing is satisfactory.

EN 1993-1-8,
Table 3.3

2.5.2 Bottom flange

The covers are in compression. Assume half of the load is carried in the upper cover plates. The force per cover plate is $F_{Ed} = 3960/4 = 990$ kN.

$$\varepsilon = 0.698 \text{ for duplex 1.4462}$$

$$c/t = 195/20 = 9.75 \text{ which is less than } 14\varepsilon = 9.77 \text{ and greater than } 9\varepsilon = 6.3$$

EN 1993-1-4,
Table 5.2

The cover plate section is Class 3 and for Class 1,2 or 3 cross-sections:

$$N_{c,Rd} = \frac{Af_y}{\gamma_{M0}}$$

EN 1993-1-1,
Clause 6.2.4

$$A = 1950 \times 20 = 3900 \text{ mm}^2$$

$$\gamma_{M0} = 1.1$$

EN 1993-1-4,
Clause 5.1

$$N_{c,Rd} = \frac{Af_y}{\gamma_{M0}} = \frac{3900 \times 460}{1.1} \times 10^{-3} = 1631 \text{ kN} > F_{Ed} = 990 \text{ kN}$$

2.5.3 Web

Consider the stress in the cover plate on a line through the vertical row of bolts.

$$\text{The shear force } V_{Ed} = 834/2 = 417 \text{ kN}$$

$$\text{The axial force } F_{L,Ed} = 609/2 = 305 \text{ kN}$$

$$M_{Ed} = 201/2 = 101 \text{ kNm}$$

The stress at the bottom of the cover plate is thus

$$\frac{My}{I} + \frac{F}{A} = \frac{101 \times 10^6}{\frac{10 \times 925^2}{6}} + \frac{305 \times 10^3}{925 \times 10} = 104 \text{ N/mm}^2$$

The value of $p_1/t = 110/10 = 11$, which is greater than $9\varepsilon = 6.3$ so buckling must be checked.

EN 1993-1-8,
Table 3.3

Using a buckling length of $0.6p_1 = 66$ mm, $i = 10/\sqrt{12} = 2.89$ mm and

$$\lambda_1 = \pi/\sqrt{E/f_y} = 65.5, \text{ the slenderness is}$$

$$\bar{\lambda} = \frac{L_{cr}}{i\lambda_1} = \frac{66}{2.89 \times 65.5} = 0.35$$

EN 1993-1-1,
Clause 6.3.1.3(1)

Using $\alpha = 0.49$ and $\bar{\lambda}_0 = 0.2$, the reduction factor $\chi = 0.92$, so the limiting stress is $0.92 \times 460/1.1 = 385 \text{ N/mm}^2$ which is greater than the design effect of 104 N/mm^2 .

EN 1993-1-4,
Clause 5.7(2)

∴ OK

The shear stress is $417 \times 10^3 / (10 \times 925) = 45 \text{ N/mm}^2$

This is satisfactory and is low enough that the resistance to direct stress does not need to be reduced.

∴ OK

Getting in touch with the EU

In person

All over the European Union there are hundreds of Europe Direct information centres. You can find the address

of the centre nearest you at: https://europa.eu/european-union/contact_en

On the phone or by email

Europe Direct is a service that answers your questions about the European Union. You can contact this service:

- by freephone: 00 800 6 7 8 9 10 11 (certain operators may charge for these calls),
- at the following standard number: +32 22999696 or
- by email via: https://europa.eu/european-union/contact_en

Finding information about the EU

Online

Information about the European Union in all the official languages of the EU is available on the Europa website

at: https://europa.eu/european-union/index_en

EU publications

You can download or order free and priced EU publications at:

<https://publications.europa.eu/en/publications>. Multiple copies of free publications may be obtained by contacting Europe Direct or your local information centre (see https://europa.eu/european-union/contact_en).

EU law and related documents

For access to legal information from the EU, including all EU law since 1952 in all the official language versions,

go to EUR-Lex at: <http://eur-lex.europa.eu>

Open data from the EU

The EU Open Data Portal (<http://data.europa.eu/euodp/en>) provides access to datasets from the EU.

Data can be downloaded and reused for free, for both commercial and non-commercial purposes.

SIROCO investigated the slip-resistant behaviour of carbon and stainless steel preloaded connections as well as the preloading behaviour of stainless steel bolting assemblies in principle.

The slip factor test procedure according to Annex G of EN 1090-2 was investigated regarding the influence of the test speed, preload level, tightening method, criteria for the slip load and load level for extended creep tests, different bolting assemblies and surface conditions (grit blasted, hot-dip galvanized, alkali/ethyl zinc silicate coating, thermally sprayed with aluminium/zinc and combinations). Improvements regarding the slip factor test procedure have been formulated which have already partly been implemented in the revision of EN 1090-2. Enhanced slip factors allow more economic slip-resistant connections.

The use of stainless steel bolting assemblies in preloaded bolted slip-resistant connections joining stainless steel plates was studied through investigations into the creep/relaxation behaviour with regard to potential preload losses, the tightening and slip resistance behaviour for austenitic, duplex, lean duplex and super duplex stainless steels. Preload losses due to the viscoplastic deformation behaviour in preloaded stainless steel bolting assemblies lie in the same range as those for carbon steel. Stainless steel bolting assemblies are in principle preloadable and galling can be avoided using suitable lubricants and tightening methods. Slip factors for stainless steel slip-resistant connections show high values for grit blasted surfaces whereas even 1D and shot blasted surfaces demonstrated slip factors for practical use.

Recommendations for design and execution of slip-resistant connections and amendments to EN 1993 1-4, EN 1993-1-8 and EN 1090-2 are formulated.

Studies and reports

